

Conjugated carbonyl molecules for lithium ion batteries.

by

Jagadish Dhanaji Aher

10CC17J26045

A thesis submitted to the
Academy of Scientific & Innovative Research
for the award of the degree of
DOCTOR OF PHILOSOPHY
in
SCIENCE

Under the supervision of

Dr. K. Krishnamoorthy



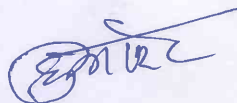
CSIR- National Chemical Laboratory, Pune



Academy of Scientific and Innovative Research
AcSIR Headquarters, CSIR-HRDC campus
Sector 19, Kamla Nehru Nagar,
Ghaziabad, U.P. – 201 002, India
June-2022

Certificate

This is to certify that the work incorporated in this Ph.D. thesis entitled, "Conjugated carbonyl molecules for lithium ion batteries.", submitted by Mr. Jagadish Dhanaji Aher to the Academy of Scientific and Innovative Research (AcSIR), in partial fulfillment of the requirements for the award of the Degree of Doctor of Philosophy in Science, embodies original research work carried-out by the student. We, further certify that this work has not been submitted to any other University or Institution in part or full for the award of any degree or diploma. Research material(s) obtained from other source (s) and used in this research work has/have been duly acknowledged in the thesis. Image(s), illustration(s), figure(s), table(s), *etc.*, used in the thesis from other sources (s), have also been duly cited and acknowledged.



Mr. Jagadish Dhanaji Aher

Research Student

Date: 20/06/2022



Dr. K. Krishnamoorthy

Research Supervisor

Date: 20/06/2022

STATEMENTS OF ACADEMIC INTEGRITY

I **Mr. Jagadish Dhanaji Aher**, a Ph.D. student of the Academy of Scientific and Innovative Research (AcSIR) with Registration No. **10CC17J26045** hereby undertake that, the thesis entitled " Conjugated carbonyl molecules for lithium ion batteries. " has been prepared by me and that the document reports original work carried out by me and is free of any plagiarism in compliance with the UGC Regulations on "*Promotion of Academic Integrity and Prevention of Plagiarism in Higher Educational Institutions (2018)*" and the CSIR Guidelines for "*Ethics in Research and in Governance (2020)*".

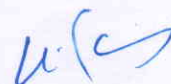


Signature of the Student

Date :20/06/2022

Place : Pune

It is hereby certified that the work done by the student, under my/our supervision, is plagiarism-free in accordance with the UGC Regulations on "*Promotion of Academic Integrity and Prevention of Plagiarism in Higher Educational Institutions (2018)*" and the CSIR Guidelines for "*Ethics in Research and in Governance (2020)*".



Signature of the Supervisor

Name : Dr. K.Krishnamoorthy

Date : 20/06/2022

Place : Pune

Dedicated to
My Beloved Parents

Shri. Dhanajirao G. Aher
Smt. Taramati D. Aher

ACKNOWLEDGEMENT

First and foremost, I would like to thank God for his never-ending grace and mercy during the toughest time of my life. with the divine grace of almighty God, I would be able to complete the work that was initiated years ago. Although Ph.D. is awarded to the individual, in reality, it's the hidden effort of so many people who contributed to the cause. at this juncture, I have many people to thank with open arms for their help and probably words will fall short.

I would like to express my sincere gratitude and thanks to my research supervisor Dr. K. Krishnamoorthy for the continuous support that he provided to my Ph.D. study for his patience, motivation, and immense knowledge. His guidance helped me throughout the period of research and writing of manuscripts. He was always with me during the tough phase of my research and personal life. Working with him was really a great pleasure and fetched me a lot of learning experience. I could not have imagined having a better advisor and mentor for my Ph.D. study. Sir, my family and I will always be thankful to you forever.

I want to extend my sincere gratitude to Dr. J. Nithyanandhan (CSIR-NCL, Pune) not only for being my DAC member but also for his valuable suggestions during a group meeting that has been very helpful for this study. His soft, kind-hearted, caring and his welcoming nature found a solution for many scientific or personal problems.

I owe special thanks to my DAC members Dr. Santhosh babu Dr. J. Nithyanandhan, Dr. Balaraman (Former DAC member) Dr. M.J. Kulkarni for their timely discussion, valuable suggestions, and encouragement during my DAC sessions.

I would like to acknowledge Dr. Ashish Lele (Director, CSIR-NCL), Dr. Ashwini Kumar Nangia, (Former Director, CSIR-NCL) for providing world-class infrastructure and adequate instrumentation facilities.

I would like to take this opportunity to express my gratitude, especially towards Dr. Manjusha Shelke (CSIR-NCL Pune) for providing an electrode cutter and electrode pressing facility. The students from their Labs, Vikas, Apurva, Tripurari, Dr. Ashwini, and Kundan, for their help during electrode cutting and making the facility available for use.

Acknowledgement

I extend my thanks to the Council of Scientific and Industrial Research (CSIR), New Delhi, for the prestigious UGC-JRF and SRF fellowship and financial aid. I extend my appreciation to Student Academic Office (SAO) staff for their persistent and prompt co-operation during the entire tenure.

I would like to acknowledge Mr. Shamal K Menon, Mr. Ramkrishna Gholap, Mrs. Poorvi Purohit, Mrs. Santhakumari, Mrs. Sangeeta hambire, and Mrs. Sheetal for helping me immensely with various characterization techniques.

I am grateful to all seniors Dr. Satej Dharmapurikar, Dr. Mirmoy Chini, Dr. Arulrajalkashmir Dr. Manik Bhosale, Dr. Anup Singh. Dr. Somya singh, Dr. Chayanika Das, Dr. Sudhakar Nesan, Mr. chitravel, Dr. Sharad Parawe, and Dr. Nagnath Patil for everything that I learned from them. I appreciate their time, co-operation, and support. I wish to thank my labmates from CSIR-NCL, Kumar, Gitanjali, Bharath, Dr. Gunavant, Radhakisan, Sarika, and Satish for their help and support.

I extend my warmest appreciation to my roommates Avinash, Gorakh, Jaydeep, and Praful for a lot of fun, IPL matches. They always make me feel like I am with my extended family.

“A friend is someone who understands your past, believes in your future and accepts you just the way you are.” I am honored and blessed to have Dr. Shrikant, Dr. Gunwant, Vijay Nirgude, Sandip, Dr. Prabhanjan, Yogesh, Sarang, Swapnil, Akshay, Praful, Viajy kalbande, Avinash Muley, Madan, Santosh, Gajanan markande and Gopal as my friends. I never felt the difficulties that difficult because the support I got from them was always on dominating side. When I count the things, I should be grateful for, our friendship is at the top. I extend my gratitude towards Sachin, Narugopal, Prashant, Nitin, Bhupendraa, Chetan (FE-SEM) Dr. Ambarish, Indrajeet, Kiran, Shivadeep, Amreeta, Navanth, Arayan, Ganesh, Mahendra (Pawar and Wagh), and Pratiksh, for their endless support and motivation.

I express my deep sense of gratitude to my family for their continuous support love and affection. I find no word to express my feeling for my mother (Taramati D. Aher) and father (Dhanaji G. Aher), Their unconditional love and sacrifices are a huge source of inspiration and courage for me. My mother is a strong and gentle soul who thought me to trust in God and believe in hard work. My father for earning, an honest living for us and standing to support us like a mountain in every bad situation. Their enormous support in every decision I took allowed my kite to fly in an open sky. I also would like to express a profound sense of gratitude towards my brother Shri. Gajanan D. Aher, Santhosh Aher, Akshay Aher, and sister-in-law Mrs. Sangeeta G. Aher for their support. My nieces Siddhi and nephew Om,

Acknowledgement

Pawan, and Raju is a source of joy. Their pure smile dissolves all the sorrows in life. I would like to extend my gratitude to my uncle late. Arjun Aher, Uttamrao Aher, my sister Mrs. Sunita S. Gote, Mrs. Nanda S. Mule, Dr. Rupali Aher, and my brother-in-law Shri. Sharad Gote for their unconditional love and blessings.

At the Near end of my Ph.D. one more family being a part of my life that is the Kale family. I would like to express my deepest thanks to my wife Dr. Rajshree J. Aher (Kale) for being a part of my life and supporting me in every difficulty. I would like to express my sincere thanks to Dr. Sureshrao Kale (father-in-law) and Dr. Sarita Kale (Mother-In-law), Dr. Sanket Kale and Dr. Pallavi S. kale, and the entire kale family for believing and supporting to me.

I would like to express my gratitude to all teachers and professors from my school to my Postgraduate. Because all respected teachers and professors play a massive role in shaping my career.

Last but not least, I am thankful to unknown reviewers of the thesis for investing their precious time and knowledge in reviewing the work.

-Jagadish D. Aher

ABBREVIATIONS AND SYMBOLS

Å	Angstrom
AQ	Anthraquinone
AAQ	2-aminoanthraquinone
ACN	Acetonitrile
Ar	Argon
BQ	Benzoquinone
BTs	Batteries
CV	Cyclic voltammetry
C-Polys	Conducting polymers
COF	Covalent organic framework
CNT	Carbon nanotube
DCM	Dichloromethane
2,5-DBQ	2,5-dihydroxy-1,4-benzoquinone
DCA	dichloroisocyanuric acid (DCA)
DMSO	Dimethyl sulfoxide
CO ₂	Carbon dioxide
CO	Carbon monoxide
CVD	Chemical vapour deposition
DMF	N, N,-dimethylformamide
EC	Electrochemical
e.g.	For example
EES	Electrical energy storage
EIS	Electrochemical impedance spectroscopy

EVs	Electric vehicles
eV	Electron Volt
FE-SEM	Field emission scanning electron microscopy
FCs	Fuel cell
FET	Field effect transistor
FT-IR	Fourier transform infrared spectroscopy
g	Gram
HEVs	Hybrid electric vehicle
h	Hour
HR-TEM	High resolution transmission electron microscopy
HPLC	High-performance liquid chromatography
KBr	Potassium bromide
LED	Light emitting diode
LIBs	Lithium-ion batteries
Li-Ion	Lithium Ion
Li-derivative	Lithiated derivative
MWCNT	Multi wall carbon nano tube
Mg	Milligram
μ L	Microlitre
mL	Millilitre
μ m	Micrometre
mol	Mole
mmol	Millimole
nm	Nanometre
NHBQ	Nonylbenzo-hexaquinone

NMP	N-Methyl-2-Pyrrolidone
NO ₂	Nitrogen Dioxide
NDA	1,4,5,8-naphthalene tetracarboxylic dianhydride
NMR	Nuclear magnetic resonance
OLBs	Organic lithium-ion batteries
PTVE	poly (2,2,6,6- tetramethyl piperidinyloxy-4-yl vinyl ether)
PTEO	(Poly (2,2,5,5-tetramethylpyrrolidine-1-oxyl-3-yl ethylene oxide)
PVAQ	Poly (vinyl anthraquinone)
PAQS	Poly-(anthraquinonyl sulfide)
Pac	Polyacetylene
PAn	Polyaniline
PPP	Polyparaphenylene
PPy	Polypyrrole
PTh	Polythiophene
PDA	Perylene-3,4,9,10-tetracarboxylic dianhydride
PDI	Perylene diimide
ppm	Parts per million
PMDA	pyromellitic dianhydride
PMDI	Pyromellitic diimide
PVDF	Polyvinylidene fluoride
Redox	Reduction-Oxidation
Rs	Electrolytic resistance
Rct	Charge transfer resistance
RI	Rylene Imides
RT	Room temperature

SEM	Scanning electron microscopy
SCs	Supercapacitors
SO ₂	Sulphur Dioxide
SIBs	Sodium-ion batteries
TEM	Transmission electron microscopy
TETD	tetraethyl thiuram disulfide
TGA	Thermogravimetric analysis
THF	Tetrahydrofuran
TLC	Thin-layer chromatography
UV-Vis	Ultraviolet-Visible
V	Voltage
Wh/kg	Watt-hours per kilogram
Wh/L	Watt-hours per liter
W/kg	Watt per kilogram
W/L	Watt per liter
W	Warburg impedance
λ	wavelength

SYNOPSIS

1 Introduction

Humanity has powered itself for the last 200 years in science and advanced technologies: we, the witness to such an enormous amount of development and progress. The development came with the consumption of a large amount of energy. The energy demand is high because of the massive outbreak of population and their modified standard of living. Now a day trend of portable electric devices, the electric vehicle market is the most demanding area of energy, with more than 90% of energy requirements filled by fossil fuels such as oil, coal, and natural gas. Though it's available today, its sources are depleting day by day. The problem associated with such energy sources is that it releases carbon monoxide, nitrogen oxides, sulfur dioxide, and carbon dioxide when burned. These gasses are responsible for warming up the earth, rising sea level, oil spills, and acid rain.¹ To avoid these issues without compromising the energy demand, we need to use clean and environmentally friendly renewable energy sources such as solar, wave, and wind power.² The problem with such energy sources is that they might not be produced when needed. The energy creation from such sources depends on the environmental condition because windy nature might not always be available to use wind energy, and the sun does not shine at night. Such challenges can be overcome by using suitable energy storage devices, which are more sustainable and environmentally friendly. As we know, if we transit toward hybrid electric vehicles (HEVs) and electric vehicles (EVs), it will have great potential to reduce fossil fuel use, which ultimately solves the problem of global warming, which we all are facing for the 20 years. Nowadays, electric vehicles are started running on the road but for large applications and to convert almost all cars to the electric-based device, which require high energy density, high power density, long cycle life, and safer battery devices. For such large applications recently, the scientific community is making a great effort to improve the performance of energy storage devices. However, rechargeable lithium-ion batteries were one of the leading energy storage devices for next-generation technologies.

2 Statements of the problem

To a large extent, the improvement of lithium-ion energy density depends upon the characteristics of cathode material present in LIBs batteries.³ Recently, widely used inorganic cathode materials such as LiCoO_2 , LiNiO_2 , LiMn_2O_4 , and LiFePO_4 ^{4,5} have some

apparent disadvantages. However, some of these materials can achieve only half of the capacity compared to their theoretical capacity. At the same time, elements used in some of the materials are not naturally abundant. Therefore, it impacts the price increase, and large-scale production and use of these transition metals are somewhat unsustainable due to serious environmental issues. On the other hand, large-scale production and mining require high energy. Industrial waste from such materials contains a high amount of heavy metal, seriously impacting the environment. So, compared to inorganic cathode materials, organic cathode materials have the advantages of high theoretical specific capacities, flexible structural designability, environmental friendliness, increased safety, and natural abundance. On the other hand, it's a promising class of energy storage materials with broad application prospects. But it has also been full of challenges in the research and commercialization of organic conjugated carbonyl electrode materials. The challenges associated with materials are soluble in the electrolyte, responsible for fading specific capacity. Even such material has low mass density, and low discharge potential and the aggregation of the material leads to hindered lithium-ion transport. We have synthesized different molecule sets to overcome these problems to address these issues.

3 Objectives of the thesis

- ✚ Synthesis and characterizations (NMR, IR, FESEM) of conjugated carbonyl Rylene imide derivatives (substituted with TPA-triphenylamine, naphthalic anhydride, and anthraquinone)
- ✚ Fabrication of Synthesized organic compound as an active cathode electrode
- ✚ Preparation of pouch and coin cell for electrochemical study.
- ✚ Electrochemical performance study of all sets of the molecule [charge-discharge study at different C rates and CV (cyclic Voltammetry) EIS (Electrochemical impedance spectroscopy)]
- ✚ Comparative study concerning change in electrochemical performance of rylene imide derivatives with substitution.
- ✚ Synthesis and characterization (NMR, IR, FESEM, EDAX) of star shape conjugated carbonyl molecule
- ✚ Electrochemical performance study of all of the molecule [charge-discharge study at different C rates and CV (cyclic Voltammetry) EIS (Electrochemical impedance spectroscopy)]

Significant outcomes from the individual thesis chapters

Chapter 2: Effect of Aromatic Ring and Substituent on The Performance of Lithium-Ion Batteries with Rylene Imide Cathode.

The simple and cost-effective organic molecule synthesis for lithium-ion batteries is a necessity. Generally, Rylene imides (RIs) are attractive organic battery materials because of the inherent modularity of the molecules. While strong aggregation of RIs is disadvantageous for fast lithium-ion transport in the active organic material, decreasing the solubility of the RIs in battery electrolytes is essential to avoid performance fading. Therefore, the design and synthesis of RIs for lithium batteries is a non-trivial task that must, among other considerations, balance lithium-ion transport in the solid material vs. low

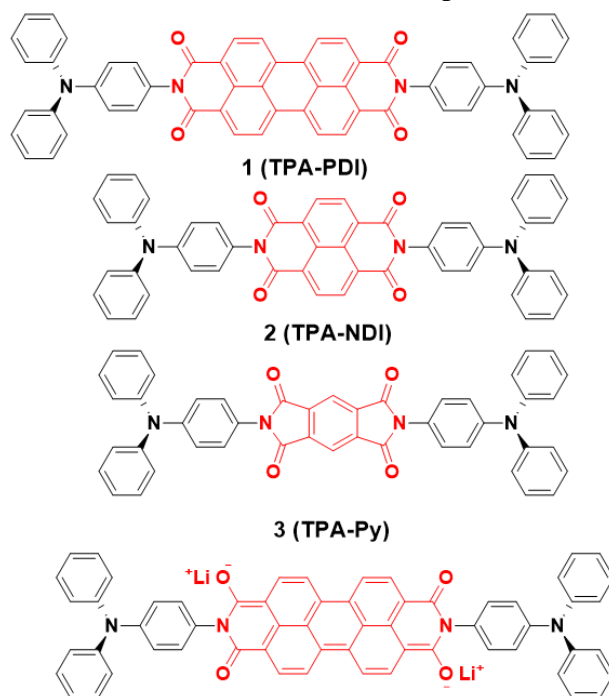


Figure 1: TPA Substituted Rylene imide derivatives

solubility by controlling aggregation. We have chosen triphenylamine (TPA) as a substituent that disrupts the aggregation but maintains a low solubility due to the increased aromaticity of TPA. We have synthesized three RIs (Figure 1) with one, two, and four aromatic units in the core. All of them showed stable specific capacity over 300 charge-discharge cycles. The batteries also showed specific capacities close to their theoretical capacities with 97–99 % coulombic efficiency. The three molecules chosen from the RIs family have different

aromatic units. The theoretical capacity of the RIs is expected to decrease with the number of aromatic rings in the rylene imides core of the molecule. Contrary to this, the experimental specific capacities varied with the number of aromatic units in the sequence $1 < 4 < 2$. Thus, decreasing the molecular weight alone does not impart improvement in battery performance. From this, we could conclude that TPA acts as an effective moiety to disrupt the aggregation of RIs without causing solubility of the molecule in battery electrolytes.

Chapter 3: An Insoluble Naphthalic Anhydride Based Rylene Imide Derivatives Cathode for Lithium-ion Batteries.

A bulky substitution over rylene imide dyes increases their molecular weight, which decreases the theoretical specific capacity of the material. However, without substitution,

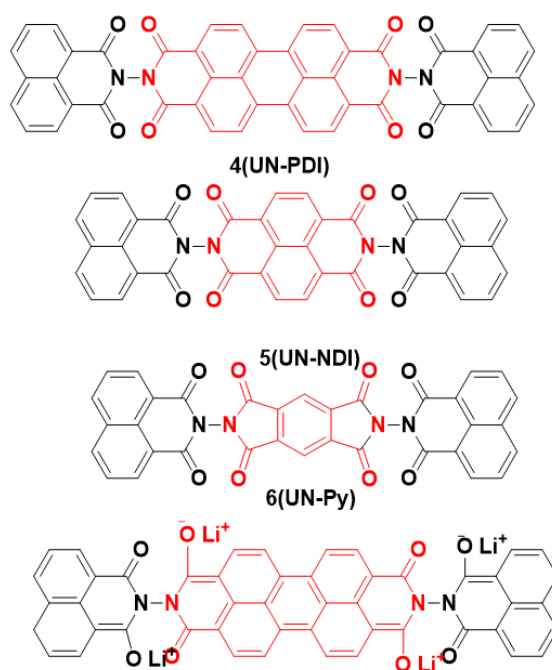


Figure 2: Naphthalic anhydride Substituted Rylene imide derivatives

the RIs are aggregated strongly, which restricts the transport of lithium. However, improper substitution leads to a severe solubility of compounds in electrolytes. In this chapter, we have synthesized three naphthalic anhydrides substituted rylene imide (Figure 2) derivatives. We kept the compound's molecular weight nearly the same as the previous chapter's molecule. However, a Naphthalic anhydride contained an aromatic conjugated carbonyl structure in which the carbonyl group is Responsible for an increase in electron count in electrochemical performance. In contrast, the perpendicular substitution of the entire

naphthalic anhydride over rylene dyes helps it disturb aggregation and decrease the solubility in the electrolyte. All set of the molecule has been shown the stable specific capacity up to 200 cycles, having a 97-100 % coulombic efficiency at a 0.2 C rate. The sequence of long cycle stability as UN-PDI>UN-NDI>UN-Py, which follows the previous set of molecules.

Chapter 4: An Anthraquinone Based Rylene Imide Derivatives Cathode for Organic Lithium-ion Batteries.

Searching for high-performance electrode materials in organic rechargeable batteries remains a crucial challenge. An anthraquinone (AQ) has a high theoretical specific capacity of 257 mAh /g and a charge/discharge voltage of 2.2–2.3 V. Although it has a high theoretical capacity, the bare anthraquinone electrode is highly soluble in the electrolyte, which leads to capacity fading. In this chapter, we synthesized three molecules (Figure 3) containing anthraquinone substituted rylene imide derivatives to obtain a high and stable specific capacity. Anthraquinone is possible to increase the number of bound Li atoms. Its arrangement over rylene dyes may disturb the aggregation of rylene dyes, which is helpful for fast reaction kinetics and high lithium-ion diffusion, whereas rylene dyes' robust structure and conjugation provide stability to the molecule for a long cycle. All molecule

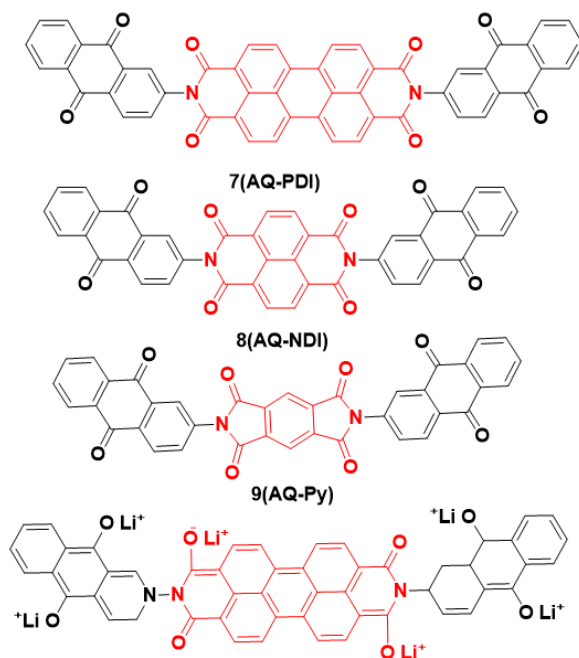


Figure 3: Anthraquinone Based Rylene Imide Derivative.

has been used as active cathode electrode material for lithium-ion batteries. The effect of anthraquinone substituent over rylene imide was studied comparatively at different C rates and long cycle stability.

All molecules showed stable capacity up to 150 cycles at a 0.2 C rate. Among the series, an AQ-PDI molecule shows a high stable specific capacity of 120 mA h/g at 0.2C, which is a 40% decrease from its theoretical capacity.

Chapter 5: A Star-Shaped Conjugated Carbonyl Imide cathode for Lithium-Ion Batteries

A rigid group containing molecules having extended conjugation helps decrease their solubility in electrolytes and may increase their initial discharge potential. Herein we have synthesized two star-shaped molecules, UN-4 and NDI-4 (Figure 4), in which a four naphthalic group connected to benzoquinone forms a rigid structure. At the same time, a π -electron delocalization over four naphthalic groups may lower the energy of the lowest unoccupied molecular orbital (LUMO), providing more active carbonyls sites with an extended conjugated structure. Therefore, UN-4 shows a first discharge potential near 2.9 V, which is relatively high for organic molecules, with an initial discharge capacity of 200 mAh/g, further decreasing to 77 after 150 cycles. Whereas the electrochemical performance NDI-4 is too low compared to UN-4 due to the molecule's solubility in the electrolyte.

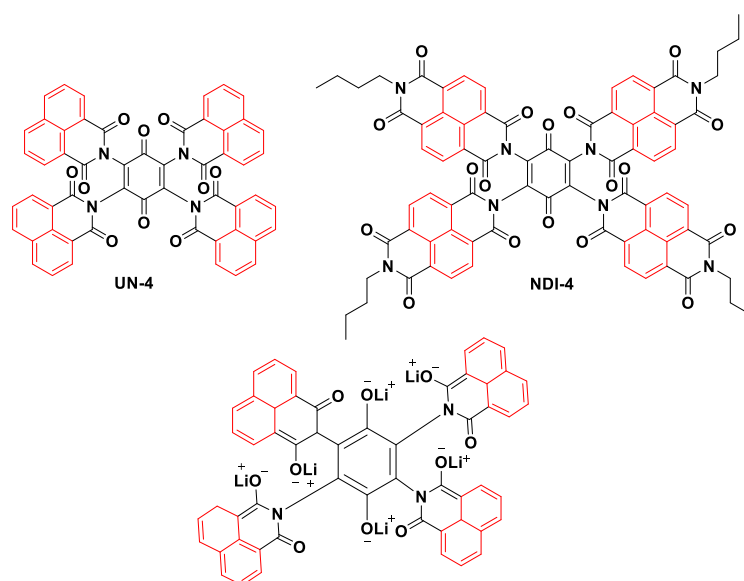


Figure 4: A Star Shaped Conjugated Carbonyl Imide

Summary

This thesis focuses on developing carbonyl molecules, specifically rylene dye derivatives, as active cathode material for lithium-ion battery applications. Various sets of molecules were synthesized, and their electrochemical performance was studied successfully. In the **second chapter**, we successfully explored the effect of substituent over rylene dyes and found out which parameter is needed to disturb the aggregation and solubility in the electrolyte and how it will affect the electrochemical performance. In the **third chapter**, we have extended the analogy of the substituent effect over rylene dyes here we have synthesized naphthalene-based rylene imide, and naphthalic-based substituent successfully participates in electrochemical performance and its perpendicular arrangement facilitates lithium transport and decreases the solubility in the electrolyte. In the **fourth chapter**, we have synthesized anthraquinone-based rylene dyes for achieving a high capacity, whereas among the series AQ-PDI molecule shows the highest stable specific capacity up to 150 cycles. The increase in capacity was achieved by an increase in electron count by anthraquinone while keeping the molecular weight the same as the previous set of molecules. In the **fifth chapter**, we have synthesized robust star-shaped conjugated molecules for an increase in electrochemical performance as well as an increase in discharge potential. The extended delocalization over four naphthalic groups was responsible for the increase in discharge potential of UN-4.

References

- 1) G. Jeong, Y. U. Kim, H. Kim, Y. J. Kim, H. J. Sohn, *Energy Environ. Sci*, 2011, **4**, 1986-2002
- 2) M. Armand, J.- M Tarascon, *Nature*, 2008, **451**, 652-657.
- 3) C. Hu, S. Qiu, G. Lu, H. Cao, H. Lv, S. Guo, J. Liu, *RSC Adv.* 2015, **5**, 70749-70757.
- 4) M. Okubo, E. Hosono, J. Kim, M. Enomoto, N. Kojima, T. Kudo, H. Zhou, I. Honma, *J. Am. Chem. Soc*, 2007, **129**, 7444-7452
- 5) X. Zuo, C. Fan, X. Xiao, J. Liu, J. Nan, *J. Power Sources*, 2012, **219**, 94-99

List of publications

- **Jagdish Aher**, Alexander Graefenstein, Gunvant Deshmukh, Kumar Subramani, Bastian Krueger, Mareike Haensch, Julian Schwenzel, Kothandam Krishnamoorthy

and Gunther Wittstock. Effect of Aromatic Rings and Substituent on the Performance of Lithium Batteries with Rylene Imide Cathodes. *ChemElectroChem* **2020**, *7*, 1160–1165.

- **Jagadish D. Aher**, Krishnamoorthy K. An Insoluble Naphthalic Anhydride Based Rylene Imide Derivatives Cathode for Lithium-ion Batteries. (*Manuscript under preparation*)
- **Jagadish D. Aher**, Krishnamoorthy K. An Anthraquinone Based Rylene Imide Derivative for Organic Lithium-Ion Batteries (*Manuscript under preparation*)
- Kanetkar, M. V., **J. D. Aher**, Kakde, G. K, Puyad, A., Kalalawe, V. G., Dharmapurikar, S. Synthesis and characterization of urethane side chain substituted Diketopyrrolopyrrole, *J. Sci. Res.* **2021**, *13*, 635-642.

Table of Content

	Content	Page No
	Acknowledgment	i
	Abbreviations and symbols	iv
	Synopsis	viii

CHAPTER 1

General Introduction and Literature

1.1	Need for green renewable energy storage technologies	1
1.2	Type of electrochemical energy storage devices	1
1.3	Lithium-ion batteries (LIBs)	3
1.3.1	Brief history of lithium-ion batteries development	3
1.3.2	Working principle of lithium-ion batteries	5
1.4	Need of organic cathode materials for LIBs	6
1.4.1	Organic electrode materials for LIBs	7
1.4.2	Structure and redox mechanism	9
1.4.3	Advantages	10
1.4.3.1	High energy density	10
1.4.3.2	High power density	10
1.4.3.3	Structural diversity	11
1.4.3.4	Flexibility	11
1.4.3.5	Sustainability	11
1.4.4	Challenges	11
1.4.4.1	Low mass density	11
1.4.4.2	Low electronic conductivity	12
1.4.4.3	Dissolutions	12
1.4.5	Requirement for electrochemical performance	12

1.4.5.1	Reaction reversibility	13
1.4.5.2	Redox potential	13
1.4.5.3	Theoretical specific capacity	14
1.4.5.4	Synthesis and cost	14
1.5	A brief history of organic electrode materials	15
1.5.1	Conducting polymer (1981)	15
1.5.2	Organodisulfided (1988)	17
1.5.2.1	Dimeric organodisulfided	17
1.5.2.2	Polymeric organodisulfided with S-S bond in the main chain	18
1.5.2.3	Polymeric organo-disulfide with S-S bond present in the side chain	18
1.5.3	Thioether (2007)	19
1.5.4	Nitroxyl radical polymer (2002)	20
1.5.5	Conjugated carbonyl compound (1969)	21
1.5.5.1	Small organic molecules	23
1.5.5.2	Organic conjugated carbonyl polymer	25
1.5.5.3	Organic conjugated carbonyl compound salt (2008)	27
1.6	Aim of the thesis	29
1.7	References	31

CHAPTER 2

Effect of Aromatic Rings and Substituent on the Performance of Lithium Batteries with Rylene Imide Cathodes.

2.1	Introduction	43
2.2	Experimental section	44
2.2.1	Chemical and materials	44
2.2.2	General experimental method and instrumentation	44
2.2.3	Synthesis and characterization	45

a)	Synthesis of TPA-NO ₂	46
b)	Synthesis of TPA-NH ₂	47
c)	Synthesis of TPA-PDI	48
d)	Synthesis of TPA-NDI	49
e)	Synthesis of TPA-Py	50
f)	Synthesis of PH-PDI	51
2.3	Result and discussion	52
2.3.1	UV-Visible absorption spectroscopy	52
2.3.2	Morphological study of molecule	52
2.3.2.1	Scanning electron microscopy	52
2.3.2.2	Transmission electron microscopy	53
2.3.3	Electrochemical performance of molecules.	54
2.3.3.1	Cyclic voltammetry	54
2.3.3.2	Proposed electrochemical mechanism	54
2.3.3.3	Galvanostatic charge/discharge experiments	55
2.3.3.4	Electrochemical impedance spectroscopy (EIS)	57
2.3.4	Effect of TPA substituent on solubility in electrolyte	60
2.3.4.1	Morphological study of molecules by SEM before and after batteries cycling	60
2.3.4.2	UV-Visible absorption spectroscopy	60
2.4	Conclusion	62
2.5	References	63

CHAPTER 3

An Insoluble Naphthalic Anhydride Based Rylene Imide Derivatives Cathode for Lithium-ion Batteries.

3.1	Introduction	67
3.2	Experimental section	68

3.2.1	Chemical and materials	68
3.2.2	Instrumentation and general experimental method	69
3.2.3	Synthesis and characterization	70
a)	Synthesis of UN-NH ₂	70
b)	Synthesis of UN-PDI	72
c)	Synthesis of UN-NDI	72
d)	Synthesis of UN-Py	73
3.3	Result and discussion	74
3.3.1	UV-Visible absorption spectroscopy	74
3.3.2	Fourier transform infrared spectroscopy (FT-IR)	74
3.3.3	Morphological study of molecules before and after battery cycling by field emission scanning electron microscopy FE-SEM	76
3.3.4	Thermogravimetric analysis (TGA)	78
3.3.5	Electrochemical performance of molecules.	78
3.3.5.1	Cyclic voltammetry (CV)	78
3.3.5.2	Electrochemical impedance spectroscopy (EIS) study	79
3.3.5.3	Proposed electrochemical redox mechanism of molecules	81
3.3.5.4	Galvanostatic charge/discharge experiments	81
3.3.6	Solubility study of molecules in liquid electrolyte	84
3.3.6.1	Electrode soaking experiments	84
3.3.6.2	UV-Visible absorption spectroscopy after 200 th cycle	85
3.4	Conclusion	86
3.5	References	87

CHAPTER 4

An Anthraquinone Based Rylene Imide Derivatives Cathode for Organic Lithium-ion Batteries.

4.1	Introduction	91
4.2	Experimental section	92

4.2.1	Chemical and materials	92
4.2.2	Instrumentation and general experimental method	92
4.2.3	Synthesis and characterization	93
a)	Synthesis of AQ-PDI	94
b)	Synthesis of AQ-NDI	95
c)	Synthesis of AQ-Py	96
4.3	Result and discussion	97
4.3.1	Fourier transform infrared spectroscopy (FT-IR)	97
4.3.2	UV-Visible absorption spectroscopy	97
4.3.3	A Morphological study of molecules by field emission scanning electron microscopy (FE-SEM) before and after battery cycling	99
4.3.4	Thermogravimetric analysis (TGA)	101
4.3.5	Electrochemical performance of molecules.	101
4.3.5.1	Cyclic voltammetry (CV)	101
4.3.5.2	Electrochemical impedance spectroscopy (EIS) study	102
4.3.5.3	Proposed electrochemical redox mechanism of molecules	103
4.3.5.4	Galvanostatic charge/discharge experiments	104
4.3.6	Solubility study of molecules in liquid electrolyte	107
4.3.6.1	UV-Visible absorption spectroscopy after 150 th cycle	107
4.3.6.2	Electrode soaking experiment	108
4.4	Conclusions	109
4.5	References	110

CHAPTER 5

A Star-Shaped Conjugated Carbonyl Imides Cathode for Lithium-ion Batteries.

5.1	Introduction	114
5.2	Experimental section	115
5.2.1	Chemical and materials	115

5.2.2	Instrumentation and general experimental method	115
5.2.3	Synthesis and characterizations	116
a)	Synthesis of NDI-BA	116
b)	Synthesis of tetra(phthalimido)-benzoquinone (BQ-TM)	118
c)	Synthesis of 2,3,5,6-tetraaminocyclohexa-2,5-diene-1,4-dione (BQ-NH ₂ -4)	119
d)	Synthesis of NDI-4	121
e)	Synthesis of UN-4	121
5.3	Result and discussion	122
5.3.1	Fourier transform infrared spectroscopy (FT-IR)	122
5.3.2	UV-Visible absorption spectroscopy	123
5.3.3	Morphological study by field emission scanning electron microscopy (FE-SEM) before and after battery cycling	124
5.3.4	Thermogravimetric analysis (TGA)	126
5.3.5	Electrochemical performance of molecules.	126
5.3.5.1	Cyclic voltammetry (CV)	126
5.3.5.2	Galvanostatic charge/discharge experiments	127
5.4	Conclusion	130
5.5	References	131

CHAPTER 6

CONCLUSION AND FUTURE PERSPECTIVES

6.1	Conclusion	134
6.2	Future Perspective	135
	Abstract for indexing	137
	List of Publications and Patents	138
	List of posters	139
	About the author	141

Copy of SCI Publications

Erratum

CHAPTER 1

General Introduction and Literature

Outline of introduction

1.1 Need for green renewable energy storage technologies.

Energy consumption is growing across many countries globally, with a substantially increasing population and increased quality of living. Recently, Science and advanced technologies, such as portable equipment and electric automobiles, are the top demanding sector for energy. We, the witness to such an enormous development and progress. The development story came with the consumption of a large amount of energy. Among all sectors of energy requirement, 90% of energy requirements are filled by fossil fuels, including natural oil, black coal, and natural gas. Though it's available today, its sources are depleting day by day. However, excess consumption of such fuel leads to serious environmental issues. The burnt fossil releases CO, NO₂, SO₂, and CO₂; these gasses are responsible for warming the earth, rising sea level, oil spills, and acid rain.¹ In the last few years, the more severe impact was seen in the entire range, from wildfire to flooding to extreme heat and draft. These impacts become worsen if we don't overcome the problem. To avoid these issues without compromising the energy demand, we need to use clean and environmentally friendly energy originating from solar, wave, and wind power.² The problem with such energy sources is that they might not be produced when it is most needed. The energy created from such sources depends on the environmental condition because windy nature might not always be available to use wind energy, and the sun does not shine at night. Such challenges can be overcome by using impactful energy storage devices, which are more sustainable and environmentally friendly.

1.2 Type of Electrochemical Energy Storage Devices.

The stockpile of energy could be a possible variety of ways, mainly three electrochemical energy storage and transformation devices available: fuel cells, (FCs) batteries (BTs), and supercapacitors (SCs). However, in these three-system, energy storage and conversion mechanisms are different, but this system has an "electrochemical similarity." In all these systems, the energy creation process occurs at the phase border of the electrode/electrolyte crossing,³ where electronic and ionic transportation gets isolated. However, the BTs, FCs, and SCs be made of two electrodes in contact with a liquid electrolyte. In BTs and FCs, the redox reaction at the anode and cathode is responsible for chemical energy change to electric energy. An observed difference between BTs and FCs is the location of energy storage and transformation. However, BTs are closed devices in which the positive and negative

electrodes are the charge-carrying medium and take an operational role in a redox reaction. Whereas FCs are open devices consisting of anode and cathode are just charge-carrying mediums, actual active materials that participate in the energy conversion process are provided from external sources. Instead, in an electrochemical supercapacitor, the redox reaction may not be responsible for energy production. Due to that, the coined terms anode and cathode may not be suitable here, but we use them commonly. In this system, the energy delivering process occurs by physical absorption of electrolyte ion on electrode/electrolyte interface and release of ion which result in a movement of electron through an external circuit.

As compared to SCs and FCs, batteries are, till now, have found far much better applications in terms of their unique properties, such as their energy storage and delivery process. More scientifically, we can compare in terms of “specific energy” (defined in Wh/kg) and “energy density” (defined in Wh/L). However, “specific power” (defined in W/kg) and “power density” (defined in W/L), on the other hand, are expressed as the “gravimetric” (kilogram) and “volumetric” (litter) this parameter coined for comparing the energy capability of the system. A simplified Ragone plot or diagram (figure 1.1) was used to compare specific energy and specific power of energy storage devices. This plot discloses that the specific energy of FCs is considered high, whereas the specific power of the electrochemical SCs is seemed to be high. The battery system was found to be intermediate between FCs and electrochemical SCs in terms of their energy and power characteristics. We can simplify it as the FCs have a very high specific energy but less specific power, which means the FCs can store a large amount of energy. But it delivers these energies very slowly, restricting it for high-power applications. On the other hand, the electrochemical SCs have low specific energy but the highest specific power, which means that the capacitor can quickly deliver the stored energy. These unique properties of energy storage devices are used for a particular application. Batteries show intermediate characteristics. It has higher specific energy than the supercapacitor. Still, it is lower than the fuel cell, and it offers higher specific power than the specific power of a fuel cell but is lower than the supercapacitor. One of the main reasons for today’s global warming issue is fossil fuel combustion in transport and industries. However, in today’s energy technology, none of the devices have fully developed to effectively replace today’s combustion engine technology. As we know, if we transit toward hybrid electric vehicles (HEVs) as well as electric vehicles (EVs), these would have sizable potential to reduce fossil fuel use, which ultimately solves the problem

of global warming, which we all have been facing for the last many decades. Nowadays, electric vehicles are started running on the road, but for large applications and to convert almost all

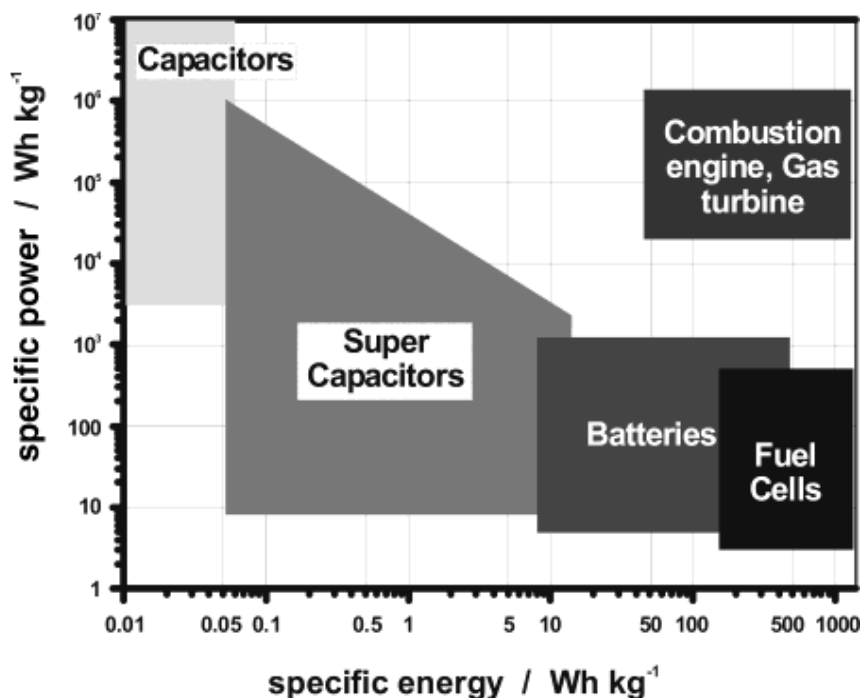


Figure 1.1: A Ragone plot of the energy storage domain for different electrochemical energy conversion and storage devices with compared to turbines, internal combustion engines, and turbines and conventional capacitors.³

Vehicles with electric-based devices require high energy density (HED), high power density (HPD), safer battery devices, and long-term cycle life,⁴ For such extensive applications recently, the scientific community is making a great effort to improve the performance of energy storage devices. However, rechargeable lithium-ion batteries (LIBs) were found to be one of the leading energy storage systems for future applications due to the presence of all the characteristics mentioned above.

1.3 Lithium-ion batteries. (LIBs)

1.3.1 Brief history of LIBs development.

The batteries are a source of electric power, in which stored chemical energy can be convertible to electric energy when it is needed for powering various applications. Three types of batteries are available based on their use i) Primary batteries. It is not rechargeable;

once it discharges, then it must be discarded. ii) Secondary batteries. It is rechargeable, and we can repeatedly discharge and charge it over a long period. iii) And specialty BTs are developed and constructed to satisfy specific applications. Lithium batteries come across a type of primary battery, whereas LIBs are categorized as secondary batteries. Lithium batteries were invented before LIBs. Since it's not repeatedly useful due to safety or cannot be efficiently recharged. Due to the inherent drawbacks of lithium batteries, the scientific community was motivated to come up with a reliable solution, i.e., rechargeable lithium-ion batteries.

Arfwedson.⁵ and Berzelius⁶ in 1817 discovered lithium "lithion/lithina" by scrutinizing petalite ore ($\text{LiAlSi}_4\text{O}_{10}$); however, the extraction of the metals was done by Brande and Davy in 1821⁷ through electrolysis of lithium oxide. Just a decade later, Lewis started to inspect the electrochemical behavior of elements.⁸ However, based on physical properties, such as its high specific capacity (3861 mAh/g), less density (0.534 g cm^{-3}), and significantly less redox potential (-3.0 V), it was realized that lithium could be the best material as a battery anode. One step toward practical use of primary LIBs had seemed when Harris⁹ started studying the dissolution of lithium in several non-aqueous electrolytes. This work was begun in early 1958. The electrolyte used for examining the solubility was cyclic esters, molten salts, inorganic lithiated salt (LiClO_4), and solutions in propylene carbonate (PC). They found that direct chemical reactions between electrolytes and lithium could be prevented by forming a passivation layer without disturbing the ionic transformation through the electrolyte. However, the development of rechargeable batteries started more than a century before. Physicist Gaston contrived lead-acid batteries in 1859.¹⁰ In the same era; nickel hydride batteries came to light being replacements for lead-acid batteries. However, until the 1990s, an appropriate battery for portable electronic equipment, including mobile phones, laptop flashlights, video cameras, and radios, was used as nickel-cadmium batteries.¹¹ The work on lithium batteries started explored in 1912; the first commercial break got in the 1970s, as LIBs were made utilized for military applications, but further implementation failed due to safety issues.

However, in the middle of the 1970s, the heavy oil crisis prompted the development of solar and wind energy as potential sources of electric power. Thus, the empowerment battery system also comes into the picture to use such non-renewable sources. An English chemist named Stanley Whittingham has started working on the concept of rechargeable LIBs as desired energy storage devices. He endeavors to use lithium metal and titanium disulfide as the electrodes, but it had raised a safety issue due to the short circuit that caught fire.¹² After

that, the work was extended by scientist John Goodenough; in the 1980s, he decided to use LiCoO_2 as the cathode by doubling the energy potential.¹² After that, Japanese scientist Akira Yoshino has shown that batteries can significantly be safer without lithium metal. Instead of lithium metal, he started an experiment using a carbonaceous material, petroleum coke. This pioneering work was the beginning of LIBs development. After enormous pioneering research, the first practical use LIBs were launched by Sony in 1991.¹³

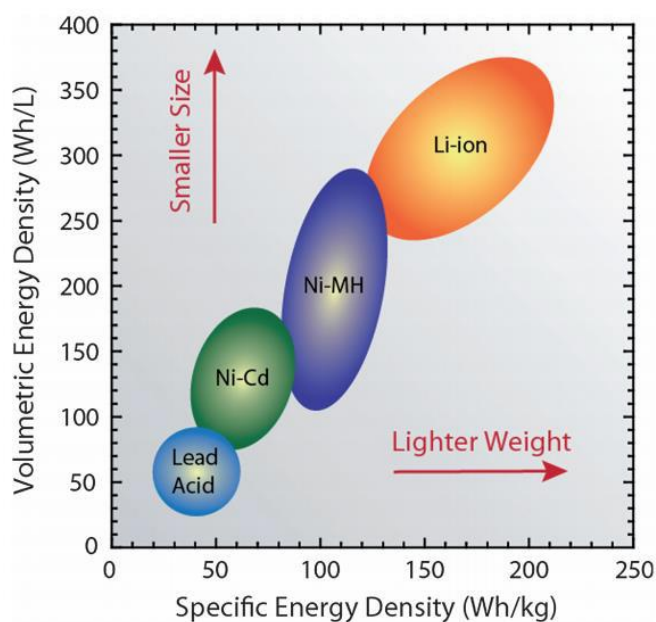


Figure 1.2: Specific energy and specific power of rechargeable battery technologies.⁵⁵

Among all battery systems, the energy density of LIBs is recorded to be high than that of other rechargeable batteries. (Figure 1.2) Rechargeable LIBs influenced the portable electronics business compared to all battery systems by considering their high energy and power density.^{2,14} whereas LIBs are strongly contenders for huge-scale energy storage equipment for EVs and smart grids.^{15,16}

1.3.2 Working principle of lithium-ion batteries.

A typical rechargeable LIBs be made of an anode, a cathode, and an electrolyte for ionic conductivity. (Figure 1.3) The anode and cathode are set apart using a porous membrane to avoid a short circuit. The working principle and cell contraction of today's lithium-ion batteries are the same as those cells Sony commercialized the first time. During charging, an external source voltage is implemented for pulling electrons from the cathode and moving through the external circuit to the anode. Subsequently, Li-ions move towards the anode from the cathode throughout the electrolyte. During discharge, the processes are exactly

reversed: An external load pulls back the electron from the anode. It moves to the cathode and simultaneously transports Li-ions through electrolytes in the same direction. This is called the “shuttle chair” effect, where the Li-ion shuttle between the anode and cathode in the course of the charge/discharge cycle.¹⁷ The simplified graphics of the working principle of LIBs is shown in (Figure 1.3)

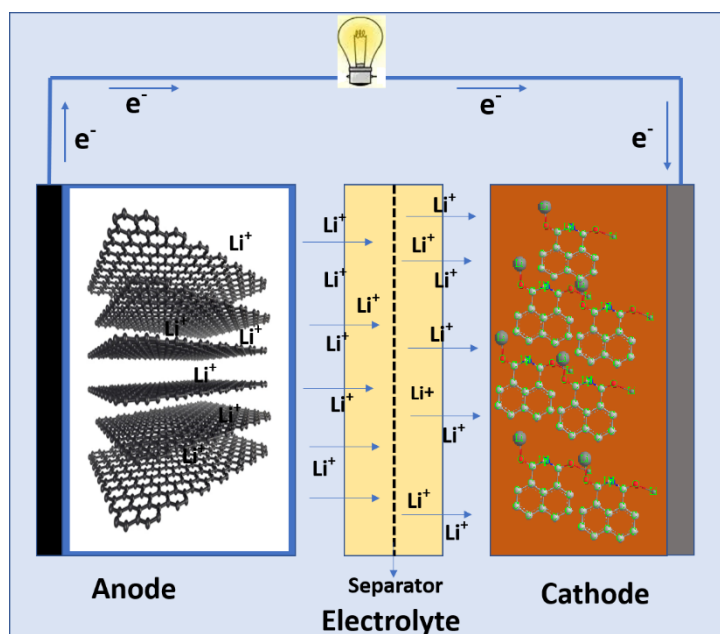


Figure 1.3: Schematic representation of lithium-ion batteries.

A conventional lithium-ion battery consists of the following material.

Cathode: - LiCoO_2 , LiNiO_2 , LiMn_2O_4 and LiFePO_4

Anode: Hard carbon graphite

Electrolyte: - LiPF_6 in carbonyl solvent

Separator: - polyethylene (PE) Polypropylene (PP)

Remarkably, the advancement of lithium-ion energy density depends upon the properties of cathode material present in LIBs .¹⁸⁻²⁰ Even the cost of the batteries very much depends upon the cathode materials.

1.4 Need for organic cathode material for LIBs.

Recently, widely used inorganic cathode materials such as LiCoO_2 ,^{21,22} LiNiO_2 ,^{23,24} LiMn_2O_4 ,^{25,26} and LiFePO_4 ²⁷⁻²⁹ but all have some apparent disadvantageous. Among them, Lithium cobalt dioxide is extensively used as cathode material in conventional LIBs. Assuming complete extraction of Li^+ , The theoretical capacity of LiCoO_2 is 274 mAh/g ³⁰ but the practically observed capacity is only 130 mAh/g at $4.0 \text{ V vs. Li/Li}^+$. This means that

only half a mole of Li^+ was extracted from the such materials. Complete extraction of Li^+ exhibit highly unstable CoO_2 , and evolution of O_2 take place.^{30,31} To achieve high stability, only half of the lithium-ion deintercalated from the cathode. Though LiCoO_2 has good electrochemical performance, it has increased production costs, and pollution issues create problems for large production.^{32,33} However, LiNO_2 exhibits high capacity and high-power density compared to lithium cobalt dioxide. Even so, not much useful due to its high expensiveness and cycling Instability.³⁴⁻³⁶ A LiMn_2O_4 can adequately reduce cost price and pollution issues, but it has a critical capacity feeding as well as reversibility problem.³⁷⁻³⁹ The researcher is attracted to a group of polyanion cathode materials such as LiFePO_4 ^{40,28} and $\text{Li}_2\text{FeSiO}_4$ ⁴¹ due to their safer and cheapest feature. But regrettably, these materials exhibit bad ionic and electronic conductivity, which ensue a poor rate performance.⁴²⁻⁴⁴ a few decades before, it was expected that multi-element cathode material could account for a high capacity and energy density for LIBs. Still, it was also suffering sizable initial irreversible capacity and less cycling at high rates.⁴⁵⁻⁴⁸ However, the above discussion reveals that inorganic material has their limitation. Part of these materials could reach just half the capacity compared to their theoretical capacity, whereas elements used in some materials are not naturally abundant. Therefore, it impacts the increase in price. Even large-scale manufacturing of transition metals is somewhat inappropriate due to serious environmental issues. On the other hand, large-scale production and mining require a high amount of industrial waste from such materials containing a high amount of heavy metal, which seriously impacts the environment. Due to structural changes in the material throughout fast charging/discharging, these material shows deficient cyclability and power densities. Even the biggest challenge of inorganic electrode materials is that it is difficult to improve their energy densities. Therefore, it is one of the challenges for the scientific community to find advances in cathode materials in case of higher capacity, safety, plenty of available precursors, and environment friendly.⁴⁹⁻⁵² As compared to inorganic cathode materials, the organic cathode has merits like excessive theoretical capacities, flexibility, structural diversity, environmental-safe, increased safety, and natural abundance. However, it will be a favorable energy storage material with a wide application view.^{53,54} Thus, researchers are looking for alternative organic cathode material for LIBs.

1.4.1 Organic electrode material for LIBs.

In the long term, organic electrode material has encountered significantly less recognition than inorganic electrode material, owing to their moderate electrochemical performance and appreciable outcome for inorganic material from the market point of view. But with time,

the vast requirement of energy and environmental issues associated with inorganic materials make them restricted for further use. However, throughout the last few years, attention toward organic electrodes has increased. Several organic structured and redox processes (table 1.1) were attempted to enhance electrochemical performance and tried to overcome inorganic material. Many researchers reveal that organic material offers several advantages compared to inorganic material. However, the organic compound consists of carbon, nitrogen, oxygen, and sulfur; all are abundant and inexpensive. The structural changes in an organic molecule (table 1.1)

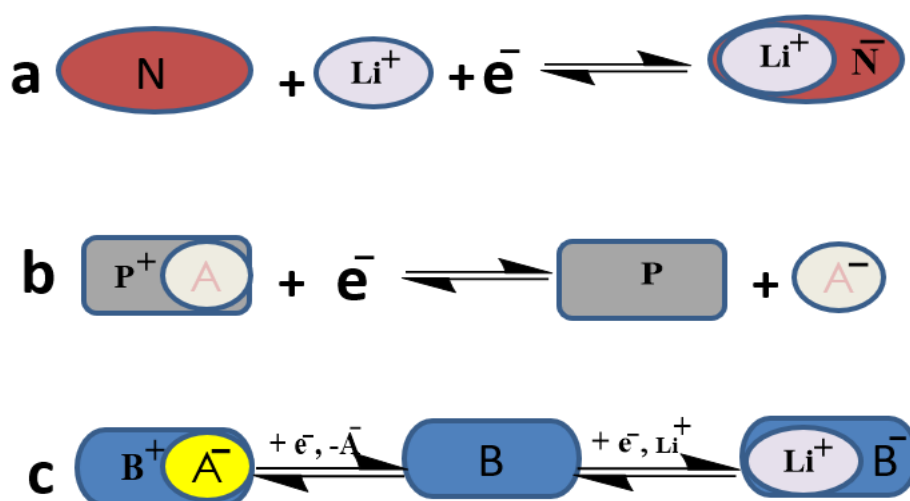


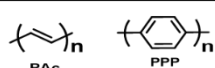
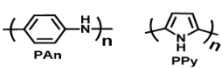
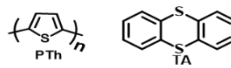
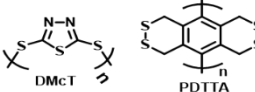
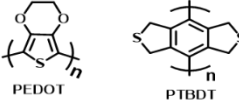
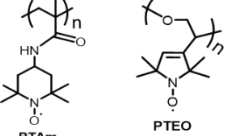
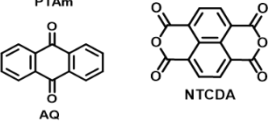
Figure 1.4: The redox reaction of three types of electroactive organics: (a) n-type; (b) p-type; (c) bipolar. (A^- means anion of the electrolyte and Li^+ can be replaceable cation by other metal ion⁵⁵)

During charging and discharging are almost omitted because of the amorphous nature of the material. The redox process is delivered by inorganic material by changing the valency of transition metal. In contrast, for organic material, the redox reaction depends upon in the charge state of the electroactive group. On the basis of the distinct redox process, we can divide all organic material into three types: p-type organics, n-type organics, and bipolar organics.⁵⁵ (Figure 1.4) When the neutral form (M) accepts electron and forms negatively charged (M^-) thus, the interaction between neutral (M) and (M^-) is called n-type organics; in the case of p-type organics, the positively charged form (R^+) interacts with the neutral form (R). However, in the case of bipolar organics, in that the neutral state (E) may undergo reduction to get a negatively ionic form (E^-) or either oxidized into a positively ionic form (E^+). That could also be considered as either M or R due to most times; only half cell reaction

takes place at a particular electrode. In a full electrochemical cell, M undergoes reduction to M^- and R undergoes oxidation to R^+ for neutralization of these charges; there is always a need for cation Li^+ for M^- and anion D^- for R^+ . In the case of a reverse oxidation/reduction process, a Li^+ or D^- would move reverse via an electrode to the electrolyte. In n-type organic, Li^+ is replaceable with another positively charged ion such as Na^+ , K^+ , and indeed H^+ , where it may not effectively change the material's electrochemical process. On the other hand, it's remarkably different than inorganic intercalation material, which is significantly shows sensation toward cation radius. In the case of p-type organics, D^- consists of ClO_4^- , PF_6^- , and TFSI in a nonaqueous and $-Cl^-$ and $-NO_3^-$ in the aqueous electrolyte.

1.4.2 Structure and redox mechanism.

Table 1.1: The structure and redox mechanism of seven different types of organic electrode materials.⁵⁵

Name	Redox Mechanisms	Example
Conjugated hydrocarbon	$(R)^{X^+} \longleftrightarrow (R)_n \longleftrightarrow (R)^{Y^-}$	
Conjugated amine	$R-N^+-R \longleftrightarrow R-NH-R$	
Conjugated thioether	$R-S^+-R \longleftrightarrow R-S-R$	
Orgnodisulfide	$R-S-S-R \longleftrightarrow R-S^- + S^-R$	
Thioether (4e)	$R-S(=O)-R \longleftrightarrow R-S(=O)-R \longleftrightarrow R-S-R$	
Nitroxyl radical	$R-N^+-R \longleftrightarrow R-N^{\cdot}-R \longleftrightarrow R-N^--R$	
Conjugated carbonyl	$R-C(=O)-R \longleftrightarrow R-C(O^{\cdot})-R$	

The above conversation reveals the oxidation/reduction reactions of unlike electroactive organic, but obviously, it is still insufficient for us to seek a variety of organic electrode compounds. Thus, we must solve which type of organic compounds and oxidation/reduction process could be put on for organic electrodes.

Generally, organic materials are broadly categorized into seven types (Table 1.1),⁵⁵ which differentiate most research on organic electrodes in past decades. Out of seven kinds of structure, organo-disulfide and conjugated carbonyl compound belongs to an n-type organic, conjugated thioether and amine persist in a p-type organic. Whereas hydrocarbon, as well as nitroxyl radicals, are categorized into bipolar organics. A listing of thioether (4e) as one kind may be controversial due to the redox mechanism being unable to match any kind in figure 1.4 and has not been understandably demonstrated. However, we still take it into the board by considering of multi-electron reaction at an electrode. Despite nitroxyl radicals being bipolar, they are usually estimated as p-type organics materials for experimental purposes in order to get a balance electrochemical performance.

1.4.3 Advantages.

In the past few years, we found that many conventional inorganic photoelectronic devices material are successfully replaced by organic materials, and it already comes to applications in devices, for example, organic compounds OLEDs, photovoltaic (PV) devices, organic OFETs, and organic solar cell devices (OSC).^{56,57} This is because the organic material shows comparable performance and some cases, even superior to conventional inorganics. Even organic material has some incomparable advantages over inorganics materials. Like other devices, many organic materials exhibit good electrochemical performance in batteries because of the following inherent benefits of the material.

1.4.3.1 High energy density.

Despite the fact that, relative to inorganic materials, organic cathode materials have a lower oxidation/ reduction potential. But yet, it is practically feasible to offset high energy density due to the presence of much excessive theoretical capacity. For example, benzoquinone (BQ).⁵⁸ consists of a theoretical energy density of nearly 1400 W h/kg, that can be evaluated from its theoretical capacity of 496 mAh/g and redox voltage of 2.8 V. However, the commercial LiCoO₂ has shown an energy density of only 550 W h/kg, which is very much less than benzoquinone.

1.4.3.2 High power density.

If the reaction kinetics of materials is high, then the power density will be increased; organic material has fast reaction kinetics. Therefore, it shows high power density than inorganic intercalation compounds. Such as, a polymer of nitroxyl-radical poly (PTVE) has been able to keep 97% of its theoretical capacity discharge at 60 C and charge at 1200 C in an aqueous electrolyte.⁵⁹ Just about all organic electrochemically active compounds provide a high-rate performance, excluding some compounds, organoidisulfides, and organic-thioethers.

1.4.3.3 Structural diversity.

Even though inorganic cathode material has been studied much compared to organics electrode material, but it was almost emphasized only on fewer materials. In recent days, it has become difficult to find newer inorganic materials and make an advanced development in battery performance. However, for organics compounds electrodes, there was plenty of probability in both the diverse structures and their properties prospective. Rather than the electrochemically active compounds listed in table 1.1, many other combinations of compounds and redox mechanisms could still be expected and are yet to be discovered.

1.4.3.4 Flexibility.

Inorganic materials are easily breakable and weighty, so constructing and fabricating electrodes is too tricky. Nowadays, there is a need to make devices thinner, smaller, flexible, and wearable. Thus, organic material has immanently presented all these properties compared to inorganics. Rather than ordinary electrode preparation, there are various methods available such as vapor deposition, printing, casting, etc. It is possible due to their characteristic's solubility, film-forming ability, and sublimability.

1.4.3.5 Sustainability.

Due to limited transition metal sources, environmental issues associated with such metal, and significantly high utilization of energy for synthesis and recycling. Thus, making an electrode from such metal for energy conversion and storage for large-scale applications is unsuitable. On the other hand, organic materials can be extracted.^{60,61} or synthesized^{62,63} from carbon dioxide cycling and biomass. The whole process is much more environmentally benign because, with respect to no added CO₂ generated, significantly less energy is utilized throughout the chemical synthesis and recycling.

1.4.4 Challenges.

In the preceding discussion, we come across the critical significance of organic electrode material. Even though it is not left without drawbacks, most of them have not been noticed at present. However, from still research and commercialization points of view, organic electrode materials face plenty of problems. The challenges associated with such material are summarized below.

1.4.4.1 low mass density.

Due to the presence of non-metal elements carbon, oxygen, nitrogen, and sulfur, organic material usually has a much lower mass density as compared to inorganic material. When It's concerned about only gravimetric energy density, it seems acceptable. But the batteries performed in phones, laptops, and EVs, such as LIBs, in that case, we have to consider even

about volumetric energy density. This is a big drawback, which increases the volume of this device. Thus, the unique organics with significantly higher gravimetric energy density are useful for such applications.

1.4.4.2 Low electronic conductivity.

In most organics molecules, high-rate performance and full utilization of active electrode material are impossible because the active organic material is an electric insulator except conducting polymer. The inorganic materials are found to be sufficiently good conductive than organics. Thus, to overcome this problem, we generally mix a sufficient amount of conductive carbon by adapting a genuine method for crucially improving the electron conduction in the electrode, and it would also help a high implementation percentage of the active material. However, due to the utilization of plenty amount of conductive carbon, the active masses of materials in an entire electrode are just 20–70% which significantly reduces the actual capacity observed in previous research. This drawback control by synthesizing compounds with a large aromatic conjugated backbone containing an electrochemically active group or electrochemically active compounds with excellent conductive CNT or graphene at the molecular stage itself.

1.4.4.3 Dissolution.

An unnecessary solubility of active compounds in the conventional liquid electrolyte is a significant drawback shown by organic electrode materials that have been observed over a long period. However, the dissolution is very noticeable for many organic small molecules, and the shuttle effect results in the cell being unchargeable. A design and synthesis of organic polymer containing stable Skelton and highly electroactive moiety are one of the solutions for this problem afterward; they are usually insoluble conventional in electrolytes of batteries. Synthesis of the coordinated polymer by forming a coordination bond between electroactive moieties and metal is the strategic way to solve the dissolution problem. But still, essentially unable to avoid this problem. However, such a giant polymeric structure increases electrochemical polarization and disturbs Li-ion transport, resulting in decreasing the theoretical capacity and discharge potential. Using small organic molecules with extended conjugated carbonyl group structure can be an efficient way to resolve this drawback.

1.4.5 Requirements for electrochemical performance.

A practical and possible candidate electrode material for energy storage, either polymer or small molecules, must undergo a reversible redox reaction.⁶⁴ Due to the presence of plenty of diversity shown in table 1.1, we can synthesize a library of organic molecules. Here we

will discuss the elementary requirement for this organic material, preferentially related to electrochemical performance.

1.4.5.1 Reaction reversibility.

When we talk about reaction reversibility, it's not just concerned about chemical reversibility but deals with thermodynamic reversibility too. Such factor is very much necessary for regulating the electrochemical polarization and rate of the electrochemical reaction. Reaction kinetics of various organic materials vary from material to material. For example, organosulphide and thioether material have slow reaction kinetics due to the high activation energy required for bond breaking/making of the S-S or S=O. On the other hand, other categories of a compound, i.e., a nitroxyl radical and aromatic conjugated carbonyl compounds, show fast reaction kinetics. Thus, high rates of electrochemical performance are possible for such compounds.

1.4.5.2 Redox potential.

Same as reaction reversibility, this parameter is also usually governed by the electroactive organic group. The potential of cathode and anode decided the potential of batteries. The obtaining batteries with high potential, the cathode and anode must behave with a high potential difference.⁶⁵ when introducing organic material as an electrode in batteries, cathode redox potential should be higher, and anode redox potential should be lower. In comparison, it is found that organics favor being performed as cathode over the anode due to its oxidation/reduction potentials generally falling in the range 2.0 and 4.0 V vs. Li/ Li⁺, which is significantly less than inorganic intercalated cathodes. However, compared to P-type organics compounds, n-type organics consist of lower redox potential. For example, nitroxyl radical (TEMPO) and conducting polymer usually exhibit a similar average voltage of nearly 3.5 V. In contrast, organodisulde and many carbonyl compounds, consisting of dianhydrides and quinones, detected oxidation/reduction potentials less than 3.0 V. However, the redox potential of organic electrode material tunable by an introduction of electron-withdrawing (Cl, CN, and NO₂) and electron-donating (OCH₃, NH₂, and OH) group which elevated and lowered the redox potential of compound respectively.^{66,67} however, such substituent doesn't show active participation in the electrochemical reaction, but it directly increases the molecular weight of the compound resulting in to decrease in theoretical capacity. While testing the electrochemical performance of any respective material, the role of electrolyte also plays a crucial part. Thus, to use an electrolyte in the given potential window, the redox potential of the cathode must be less than the LUMO of the electrolyte to prevent electrolytic decomposition by reduction. On the other hand, the

redox potential of anode material must be more than the HOMO of the electrolyte to circumvent electrolytic decomposition by Oxidation.

1.4.5.3 Theoretical specific capacity.

A theoretical capacity of an organic compound as an electrode could be evaluated by using the following formula:

$$\begin{aligned}C_t (mAhg^{-1}) &= \frac{nF(C mol^{-1})}{Mw(g mol^{-1})} = n \times \frac{96485(C)}{M_w(g)} \\ &= n \times \frac{96485(C)}{M_w(g)} \\ &= n \times 96485 \times \frac{1000}{3600(mAh)} \\ &= n \times 96485 \times \frac{3600(mAh)}{M_w(g)} \\ C_t mAhg^{-1} &= \frac{n \times 26801 \times (mAh)}{M_w(g)}\end{aligned}$$

In this formula, C_t , n , F , and M_w stand for,

C_t - theoretical specific capacity.

n - the transferred electron number in each structural unit.

F - faradays constant.

M_w - molecular weight of the structural unit.

By following the above formula, it is revealed that the theoretical capacities of the organic electrode are directly and universally proportional to the number of electrons transferred (n) and molecular weight, respectively. So, the theoretical specific capacity for the organic electrode can be increased in two ways: the first is by acquiring multielectron reactions, and the second is by reducing the structural unit's molecular weight.

1.4.5.4 Synthesis and cost.

The molecular design of an organic electrode is often a more straightforward task than synthesizing it. Some organic with optimal structures are very lengthy and impossible to synthesize. So, sometimes we have to compromise between structural optimization and a simplified synthesis method. However, the development of organic electrode material is in its preliminary step. Thus, we generally ignore cost and raw material, and synthesis, but in the future, if they come to the application, then cost must be the important parameter. As a consequence, simple synthesis methods and cheap synthetic materials are very important.^{78,79} A conjugated carbonyl compounds fulfill almost all these requirements, so

these materials are considered to be a favorable electrode material for next-era rechargeable batteries, mainly for LIBs and NIBs.

1.5 A brief history of organic electrode material.

We came across a detailed and elementary knowledge of organic electrode material, but still, there was a need to study different types of organic material elaborately. However, depending on the redox mechanism and organic structure, as shown in table 1.1. they have been split up into seven types. The progress is approximately by considering this classification and roughly in chronological arrangement. Here, we should account for the first three compounds (Table 1.1) containing hydrocarbons, amines, and thioethers; these are categorized as conducting polymers and prefer to persist in these categories due to exhibiting many alike properties. One more thing needs to note; the chronological order follows an era when one category of organic-electrode materials was extensively explored. It can be much suitable to acknowledge their evolutionary history and working properties. We are paying more attention to the conjugated carbonyl compound in section 1.5.5 because it is the earliest type of organic and the more appealing and demanding research field.

1.5.1 conducting polymers. (C-Polys) (1981)

The conducting polymer has been used as an electrode material since its discovery by MacDiarmid, Shirakawa, and Heeger in 1977.⁷⁰ Its use in electrode material is successful because of its unique properties that as electronic conductivity as well as redox activity. Since 1981 a lot of research has appeared where C-Polys are used as an electrode for batteries.⁷¹ Among the library of C-Polys explored in the last few years, there are a few representatives, consisting of polyacetylene (PAC),^{71,72} polyparaphenylene (PPP),^{72,73} polyaniline (PAn),^{74,75} polypyrrole (PPy)^{76,77} and polythiophene. (PTh)^{78,79} (Table 1.2) Even though table 1.1 assign them three categories of structures, they actually exhibit most close electrochemically similar properties. Out of it, PAn, PPy, and PTh were utilized as p-type, while PAC and PPP were utilized as bipolar organics. PAC and PPP act as p-type organics when we use them as cathode, whereas a C-Polys always exists as a p-doping form instead of the electroneutralization state. An electroneutral polymer can show improved electronic conductivity only when it is doped. Otherwise, it is an absolute insulator; this was the first discovery in conducting polymer.⁷⁰ Rather than PAC, other C-Polys are immaculately present as p-doped form, usually synthesized by method chemical⁷⁵ and electrochemical⁸⁰ Oxidation polymerization. The theoretical capacity of these C-Polys depends upon doping degree or doping level. The ratio of all structural units to the doped unit is demonstrated as the doping degree. The doping degree represented in a x as $(p^{x+} \cdot xA^{-})_n$ ($0 \leq x \leq 1$). Where p

represents a structural unit in C-Polys. This cathode material's open-circuit voltage dynamically follows the doping degree; (Table 1.2). It is found that PAc, PPP, PPy, and PTh consist of a lower theoretical capacity of 150 mAh/g because of their low doping level, and even significantly lower experimental capacity was observed than their theoretical capacity. In table 1.2 mentions that conducting polymers have a redox potential of average at 3.0V, and among them, PPP (4.0–4.5 V) has an even highest redox potential compared to many inorganic electrode materials. Due to much less specific capacity, the energy density of C-Polys never becomes compatible with inorganics materials. They show unstable cycling, remarkably when enhanced with a cut-off voltage for increasing capacity. That is mostly observed owing to the more structural unit getting deactivated throughout the redox cycle. It happens due to an irreversible over-oxidation reaction at high voltage. Again, the two noticeable negative factors are less coulombic efficiency and self-discharge, which hinders the practical application of C-Polys in rechargeable LIBs. Instead of the disadvantage mentioned above, the conducting polymer has one of the greatest strengths: high electronic conductivity. The most suitable use of such polymer is a positive electrode in energy storage in supercapacitors^{81,82} or a conductive additive in the composite cathode material.⁸³ However, most pristinely, PAn and PPa are used for this application because of their easy preparation method, elevated energy density, and good cyclability. Due to the fast redox mechanism in the mass of the material, the pseudocapacitor formed by the C-Polys cathode obtained much higher capacitance than the ordinary double-layer capacitor consisting of a

Table 1.2: Conducting polymer with some electrochemical parameters.

Name	Structure	Doping Level	Theoretical Capacity mAh/g	Redox Potential V vs Li ⁺ /Li
Polyacetylene (PAc)		0.07	144	0–2.0 (n) 3.5–4.0 (p)
Polyparaphenylene (PPP)		0.4	141	0–1.0 (n) 4.0–4.5 (p)
Polyaniline (PAn)		1.0	295	3.0–4.0
Polypyrrole (PPy)		0.33	136	3.0–4.0
Polythiophene (PTh)		0.25	82	3.0–4.2

carbon electrode.⁸² However, its electrochemical performance could assist by enhancing electronic conductivity, ionic conductivity, and surface area. Nowadays, most researchers focus on synthesizing nanostructured polymer^{84,85}, even nanocomposite of conducting polymer with CNT⁸⁶ or Graphene⁸⁷ is also helpful to improve the electrochemical performance.

1.5.2 Organodisulfid (1988)

As we know, the reversible broken and rebuilt nature of the S-S bond and two-electron redox reaction could furnish the relatively higher capacity compared to a doping/undoing reaction of C-Polys. Hence, much research has been put forward on organodisulfide cathode material since 1988.⁸⁸ Among which most of the research conducted by Visco et al.⁸⁸⁻⁹¹ and Oyama et al.⁹²⁻⁹⁷ for understanding and elaborately studying the precise history of the electrochemical behavior of organodisulfide material is categorized into three stages.

1.5.2.1 Dimeric organodisulfide.

S. J. Visco et al. in 1988, firstly used tetraethyl thiuram disulfide (TETD) as cathode material for high-temperature SIBs.⁸⁸ After that, they focused on some other dimeric

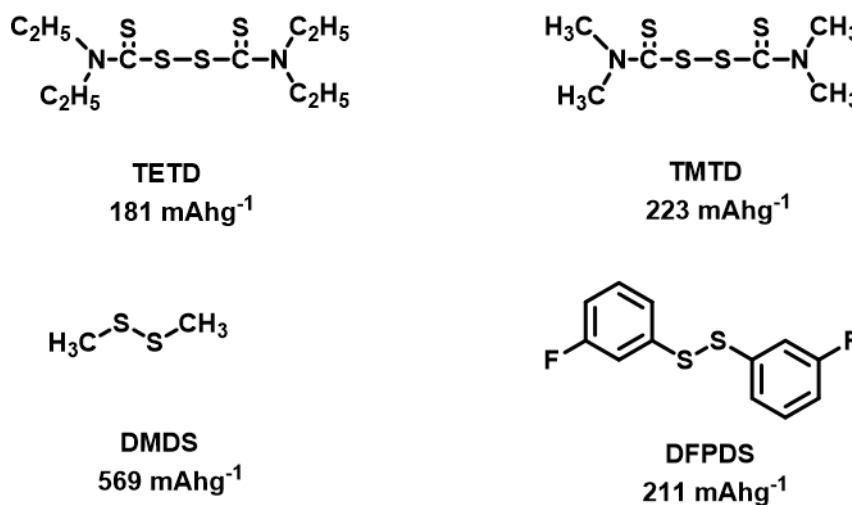


Figure 1.5: Dimeric organosulfide with their theoretical capacity

organodisulfide such as tetramethyl thiuram disulfide (TMTD), dimethyl disulfide (DMDS), and difluorophenyl disulfide (DFPDS) (Figure 1.5) and used electrodes in LIBs and their reaction kinetics of $\text{RSSR}/2\text{RS}^-$ studied.⁸⁹ However, and electrochemical performance of this material was abysmal because of the high solubility in organic electrolytes. Thus, this organodisulfide is unlikely to be applied to rechargeable LIBs

1.5.2.2 Polymeric organodisulfides with S-S bonds in the main chain.

This type of polymer is preferentially prepared from di-mercaptan and multi-mercaptan by adopting a method of oxidation polymerization.^{90,91} The example of such Organodisulfide polymers is PDMcT, PTTED, poly (trithiocyanuric acid), and poly (dithiopiperazine)⁹²⁻⁹⁷. (Figure 1.6) Due to the optimum theoretical specific capacity and energy storage process formed by the reversible two-electron reaction in the disulfide (S-S) bond.⁸⁸ these polymers

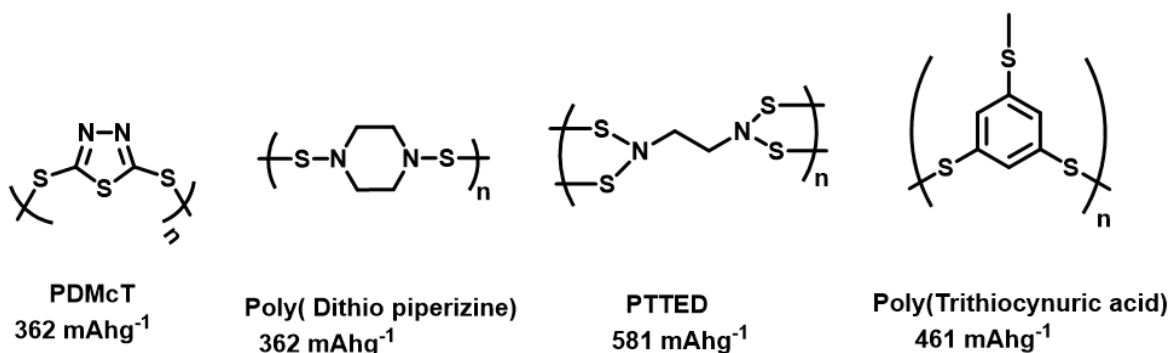


Figure 1.6: Polymeric organodisulfides with their theoretical capacity

Were practiced thoroughly as an energy storage material for LIBs. But, the reduction product of this kind of polymeric organodisulfide has become a small molecule that shows extensive solubility in organic electrolytes. For example, although a PDMcT in an oxidized state is a polymer in a discharged state, DMcT²⁻ is a small molecule. Thus, DMcT also can act as an active electrode in its reduced form. However, such a small organic molecule will show profound dissolution in organic electrolytes. Therefore, the cycling stability of such polymeric cathodes seems very poor. Another noticeable problem is that an S-S bond had very slow reaction kinetics, leading to low active material utilization at ambient temperature. The Electrocatalytic influence of PAn on the oxidation/reduction reaction of DMcT was discovered by N. Oyama et al. in 1995.⁹³ After that, they also studied DMcT performance could be enhanced further by that the addition of Cu²⁺ because of its electrocatalytic and stability effect.⁹⁴ Further, much research focused on DMcT/PAn and DMcT/Cu (II) composition material.⁹⁵⁻⁹⁷ But due to intrinsic dissolution and slow reaction kinetics associated with such polymer, batteries' practical use is still far away.

1.5.2.3 Polymeric organo-disulphide with S-S bonds present in the side chain.

In this type of polymer consisting an S-S bond in the side-chain, whereas conducting polymeric chain is in the main backbone. Two classic examples are PDTDA⁹⁸ and PDTTA.⁹⁹ (Figure 1.7). Despite the presence of insoluble and electro-conductive centered polymeric backbone in PDTDA, the cyclability of this polymeric organodisulfide is still

very poor. However, a dissolution of the two-center backbone after reduction also restricts from the reconstruction of the S-S bond. To overcome this problem, researchers are focused on one more category of polymer PDTTA. This synthesized polymer may be expected to resolve both the solubility and displacement problems. However, the electrochemical performance of PDTTA wasn't found enough, which is mostly because of the slow reaction kinetics. It is concluded from the above discussion that in the 1990s, organodisulfide was considered a promising organic cathode material for a rechargeable lithium-ion battery. The scientist has made even a considerable effort to optimize the polymer structure and incorporate electrolytic additives to solve the issue of solubility and sluggish reaction kinetics of material. But still, the electrochemical performance of organodisulfide is unable to achieve the desired stage of commercial use. This is because of the inherent difficulty, which is very pathetic to overcome. Thus, at present, research on this topic has nearly slowed down.

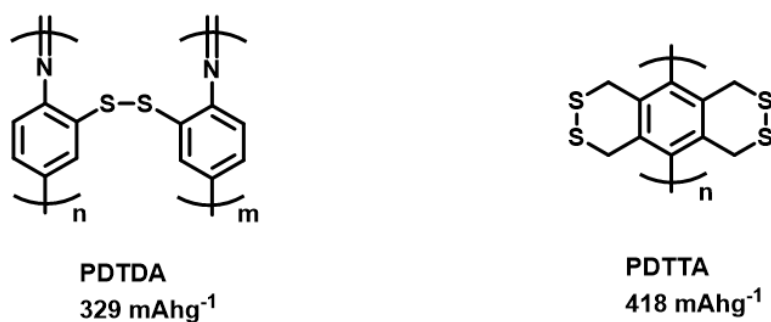


Figure 1.7: Polymeric organodisulfides (Side S-S bond) with their theoretical capacity

1.5.3 Thioether (2007)

Zhan et al.¹⁰⁰⁻¹⁰³ discovered while researching organodisulfide cathode material, occasionally, the material could exhibit a significantly enhanced specific capacity compared to its calculated theoretical capacity while using specific electrolytes were used (LiTFSI/DOL + DME), and an end charge voltage of >4.2 V was implemented. In this case, they hypothesize that it could possibly be due to a four-electron reaction of “thioether–sulfoxide–sulphone” (Table 1.1). To conclude, they tested plenty of thioethers as positive electrode materials, consisting of conjugated^{101,102} or unconjugated.^{100,103} For example, PEDOT¹⁰² and PDBDT¹⁰³ (Figure 1.8) can gain a discharge capacity in the range of 500–800 mAh/g while sweeping potential between 1.5 and 2.5 V. Even though the presence of significant energy density, cycling performance was still unstable due to high reaction polarization. Even there was not any surprise when the cells get dead only after the initial few

charge/discharge cycles. Because of the uncommon reaction mechanism in which electrolyte may be the source of O atoms during the sulphoxide and sulphone group formation. However, to date, there is no detailed reaction mechanism available, and the poor cycle stability performance of the material is not at all expected for commercial use. Thus, this type of thioether cathode material does not carry any sense of practical use except only showing the number of possibilities of organics with multi-electron reactions.



Figure 1.8: Thioether with their theoretical capacity

1.5.4 Nitroxyl Radical polymers (2002)

The first stabilized nitroxyl radical polymer, specifically PTMA introduced by K. Nakahara et al.¹⁰⁴ in 2002 as a positive electrode for LIBs. Because of its stable polymer structure and rapid reaction kinetics, PTMA exhibits a high-rate performance and good cyclability. After that, they focused on photo crosslinked 2,2,6,6-tetramethylpiperidine-1-oxyl (TEMPO)-substituted polynorbornene (PTN).¹⁰⁵ (Figure 1.9) as cathode material. This polymer has shown some characteristic changes, such as increasing mechanical toughness, improving flexibility, and allowing patterning on the device, in spite of the specific capacity found to be 106 mAh/g and tunable solubility. However, A TEMPO-substituted polyacrylamide (PTAm)¹⁰⁶ was used as cathode material, showing high charge-discharge and good cycle performance in an aqueous electrolyte. PTEO¹⁰⁷ Exhibits a specific capacity of 147 mAh/g with long-term cyclability 1000, and high-rate capability possible. Usually, nitroxyl-radical polymers have a fast electron transport rate constant which is the more significant aspect of high-rate performance in rechargeable batteries. But it has a less theoretical capacity.

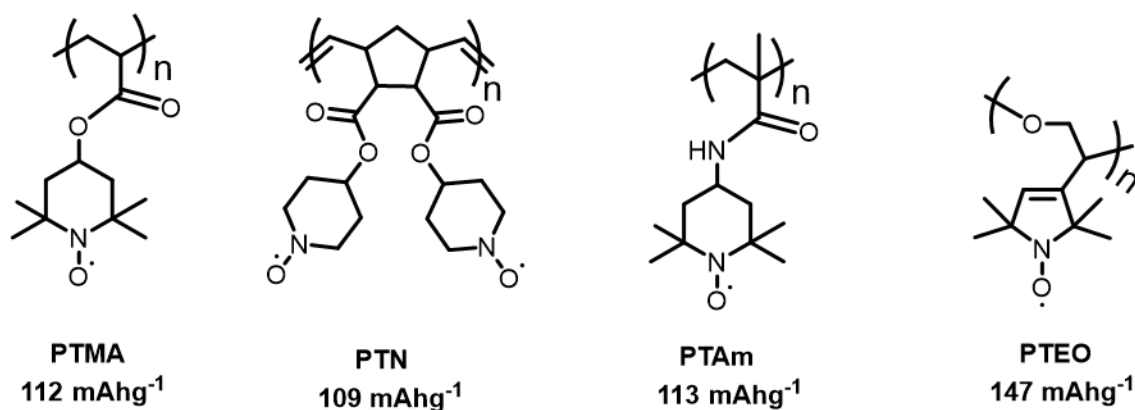


Figure 1.9: Nitroxyl radical polymers with their theoretical capacity.

1.5.5 Conjugated carbonyl compounds (1969)

Several classes of organic compounds consist of the carbonyl group, having part of many larger compound groups and displays redox features. Nearly all carbonyl compounds are n-type, which could be transport a minimum of two electrons throughout the redox cycle. However, n-type organics go through reduction, resulting in the formation of a negatively charged anion (Enolate) that is further stabilized by an appropriate counterion generated from electrolyte salt. A carbonyl's reversible oxidation and reduction process at anode and cathode count as a charge/discharge cycle. The oxidation and reduction reaction mechanism occurred by intercalation and deintercalation of Li⁺ ion. Carbonyl compounds get reduced during discharge, and every carbonyl compound interacts with Li⁺ ion to form lithium enolate. During the charging process, the deintercalation Li⁺ ion occurred in which the carbonyl group undergoes oxidation. However, an enolization is a primely significant reaction of the carbonyl double bond, which is stabilized with the conjugation of the carbonyl compound.¹⁰⁸

Depending on Functional group differences, carbonyl compound electrodes were assorted into three types (Figure 1.10)¹⁰⁹ Structurally quinones, conjugated carboxylates, and imides, which are like anhydrides. A carbonyl group of quinone is attached with a conjugated aromatic ring. Most of the time, it is present at the ortho or para position over rings; during reduction, it will form additional aromatic rings. Quinone is expected to become a next-generation organic cathode material owing to the presence of high energy density and theoretical capacity.¹⁰⁹ In the case of conjugated

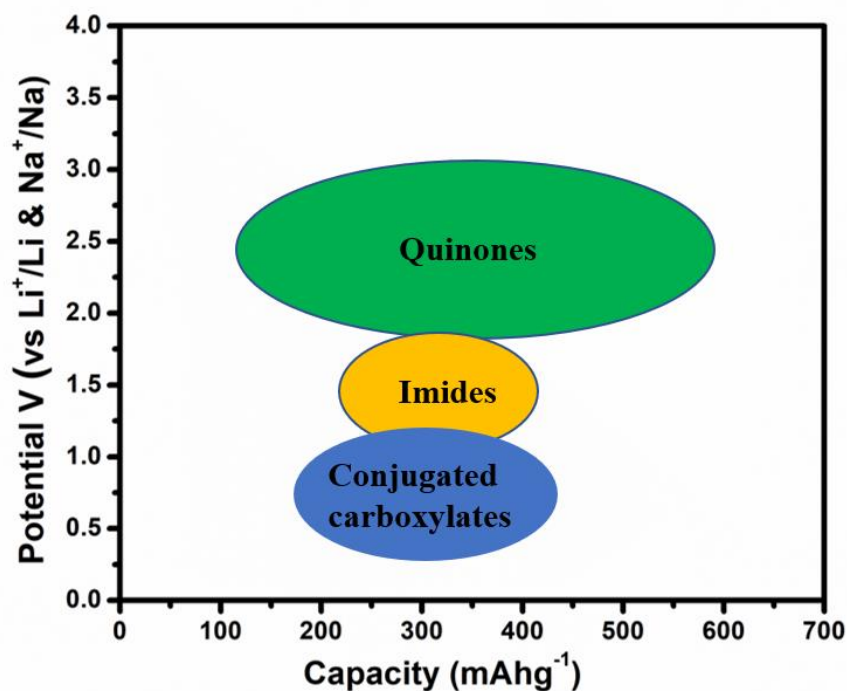


Figure 1.10: Comparison of the discharge potential and the theoretical capacity of the major organic carbonyl materials.¹⁰⁹

Carboxylates, a conjugated system, can be generated by direct attachment of the carboxylate group to the aromatic ring.¹¹⁰ Its best used as an anode material because of an electron-donating group $-OM$ ($M = Li, Na, K$) connected to carbonyl groups.¹¹¹ imides were categorized in the organic compound in which nitrogen is directly attached with aromatic conjugated carbonyl group to form conjugated imide linkage ($O=C-N$).¹¹² imides usually have a large aromatics plane containing four electrochemically active carbonyl groups. However, only two carbonyl groups participate in the enolate formation mechanism to avoid repulsion of charge and irreversible structure distribution.

The enolate formation mechanism of three types of carbonyl compounds is shown in figure 1.11. As we have seen in the above equation for measuring the theoretical capacity of the material, an increase in electron transport will increase the theoretical capacity will seem for the cathode. However, if all carbonyl undergoes reduction, then theoretical capacity may increase. But in ideal conditions seems operose to this approach; all carbonyl moieties of a carbonyl compound only reduce unless, at a less potential. During redox reactions, electron transfer and redox potential are also important; however, for practical application, there is

necessary to increase the reduction potential of the cathode and the oxidation potential of the anode. When we consider enhancing cyclability and the rate of the carbonyl compound, the main noticeable problem is dissolution in electrolytes. Which adversely affects the electrochemical activity. Even another point, for example, observed side reactions between anion and electrolyte, anion instability, electrolyte suitability, and conductive additive for improving active material's conductivity also need to be considered. However, to resolve this problem, considerable efforts need to take to enhance the electrochemical activity of carbonyl compounds for their utilization in batteries. Compared to other organics, organic carbonyl compounds are desired as auspicious electrodes due to their unique properties,

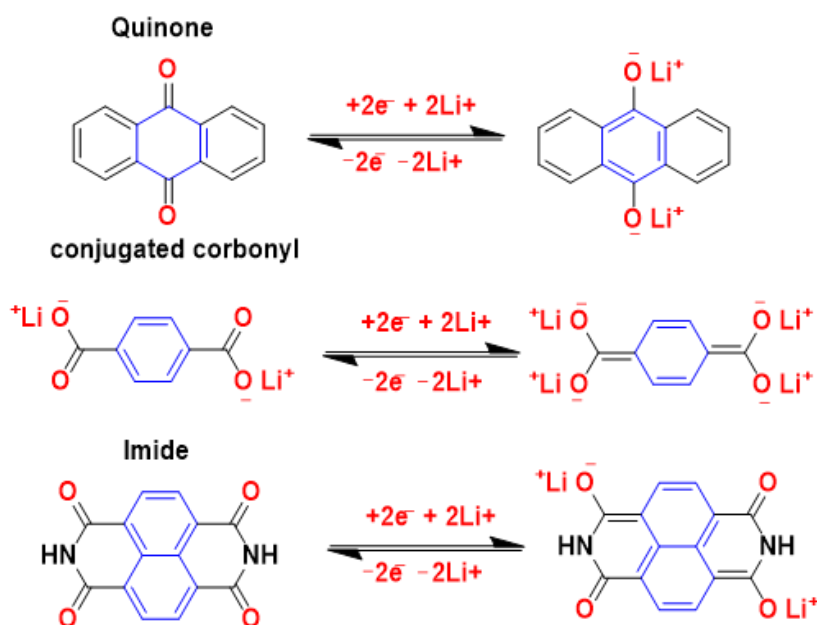


Figure 1.11: Three Categories of a carbonyl compound with their electrochemical mechanism.

Such as high theoretical capacity, high reaction kinetics, structural diversity, and stable cyclability. To acknowledge clearly, their progress and electrochemical behavior, we have categorized them into three steps, which are subsequently summarized below.

1.5.5.1 Small organic molecules.

Over the last few decades, many attempts have been made to modify small organic molecules, mainly because of unacceptable solubility and less conductivity. Additionally, anode to cathode quick dispatch of dissolved materials through electrolyte leads to a shuttle effect, which ultimately affects the cycle stability. However, those organic compounds are

inherently conducting, which decreases the quick reaction kinetics of organic electrode material.

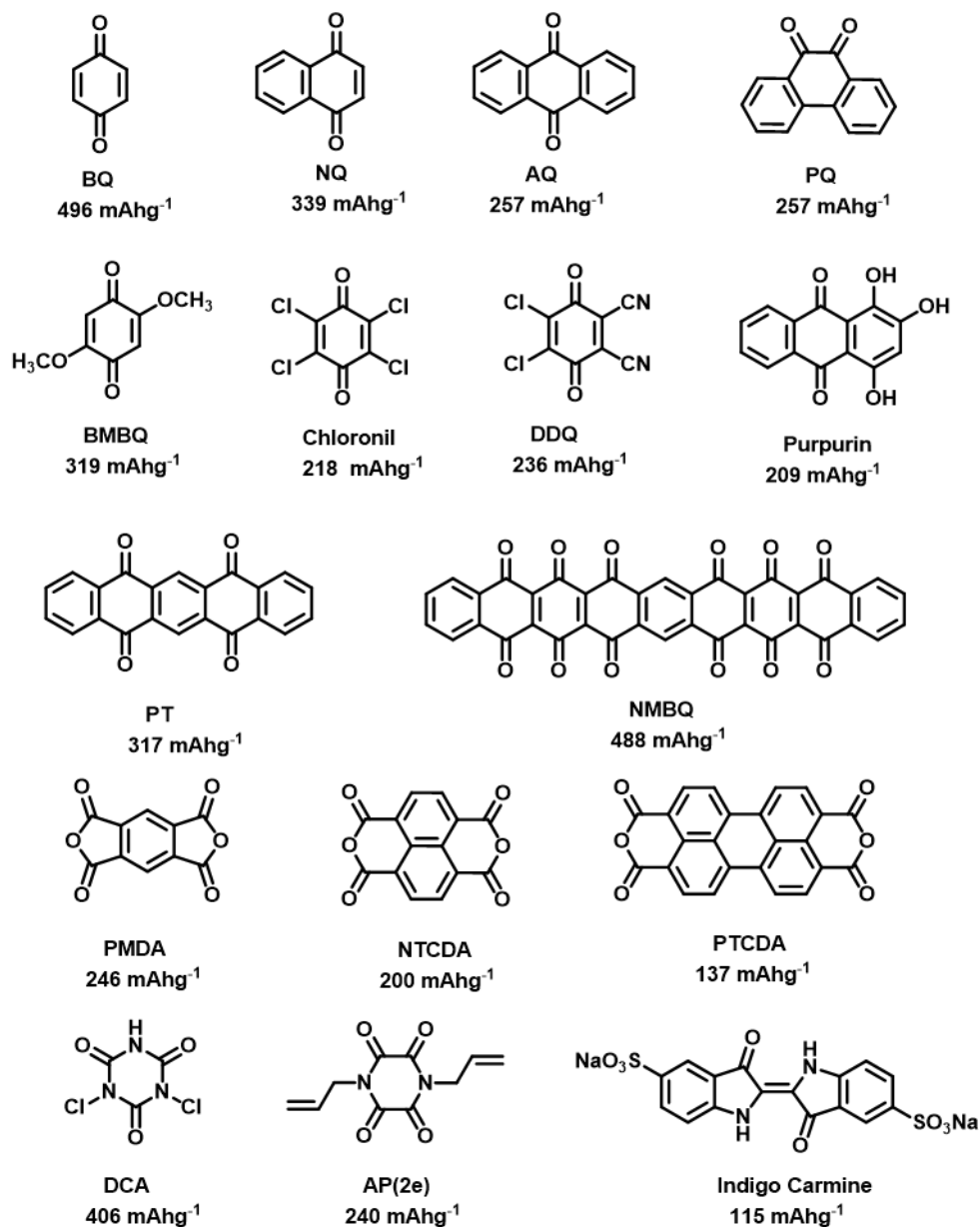


Figure 1.12: Small organic conjugated carbonyl molecule with theoretical capacity.

For the first time, a primary lithium battery was constructed using DCA as a cathode in 1969 by Williams et al.¹¹³ This probably be the first report on organic electrode material. Alt et al.¹¹⁴ successfully explored chloranil as electrode LIBs. Afterward, the people attended to construct small organic compounds as cathodes for assembling LIBs using the non-aqueous electrolyte. Figure 1.12 listed molecules' typical structure and theoretical capacity, primarily considering different quinones and dianhydride. Even though most of them can gain high

energy density and elevated discharge capacity, they still suffer from severe dissolution problems. Hence, they are unable to attend desirable cycling performances. To resolve the solubility problem, researchers have attempted to increase the percentage of conducting carbon.¹¹⁵ or incorporate mesoporous carbon.¹¹⁶ which can prevent active material from dissolving by stretching immobilization. An immobilization approach was used by Genorio et al.¹¹⁷ to solve the solubility problem. They implant Calix [4] arene (CQ) over top of nanosized silica containing a large surface area and carbon black. Even the immobilization method is also unable to crucially avoid the dissolving of active material and thus eventually reduce the capacity of the whole electrode. On the other hand, to solve the dissolution problem, Boschi et al.¹¹⁸ designed and synthesized giant conjugated carbonyls, e.g., NBHQ, having the planer structure, with a 489 mAh/g theoretical specific capacity. But still, it has only delivered 127 mAh/g specific capacity, which is only 25 % of its theoretical capacity. Another crucial way to avoid dissolution is using solid (LISICON)¹¹⁹ or polymer electrolyte (LiTFSI/ PEO).¹²⁰ still, there were no agreeable results appeared yet. A problem associated with solid electrolytes or polymer electrolyte is that at room temperature shows less ionic conductivity and high interface resistance. However, by adapting liquid¹¹⁹ or quasi-solid¹²⁰ the electrode is can lessen the interface resistance, but it much lower the energy density of LIBs. The early report conveys the dissolution of polysulfide in Li-S batteries.¹²¹ can be inhibited using a high salt concentration; we can use the same strategy for organic electrode material. The effective way to solve this problem is to design and synthesize highly conjugated carbonyl molecules containing perfect substituent and active functional groups.

1.5.5.2 Organic conjugated carbonyl polymers.

Many small organic molecules go through unwanted solubility in a liquid electrolyte, bringing severe capacity feeding. Rather than constructing salts and composite materials, polymers synthesis containing redox active group is also an effective strategy to overcome this problem. A benefit of polymers is that it's wholly insoluble or slightly soluble to some extent. Generally, without any severe environmental pollution, the synthesis is feasible. Specifically, polyamide and poly-quinones (PQ) was major appealing polymer because of the presence of higher redox-active feature of the carbonyl, significant redox potential, and large capacity. A PQ was attempted to synthesize from electrochemically synthesized poly(1,4-dimethoxybenzene) by J. S. Foos et al.¹²² in 1986. They have evaluated its electrochemical feature by preparing cathode electrodes for LIBs. PQ was primarily looked the ideal design for polymer cathode depending on their conjugated carbonyl, even large voltage, high theoretical capacity, and insolubility in a liquid electrolyte, still,

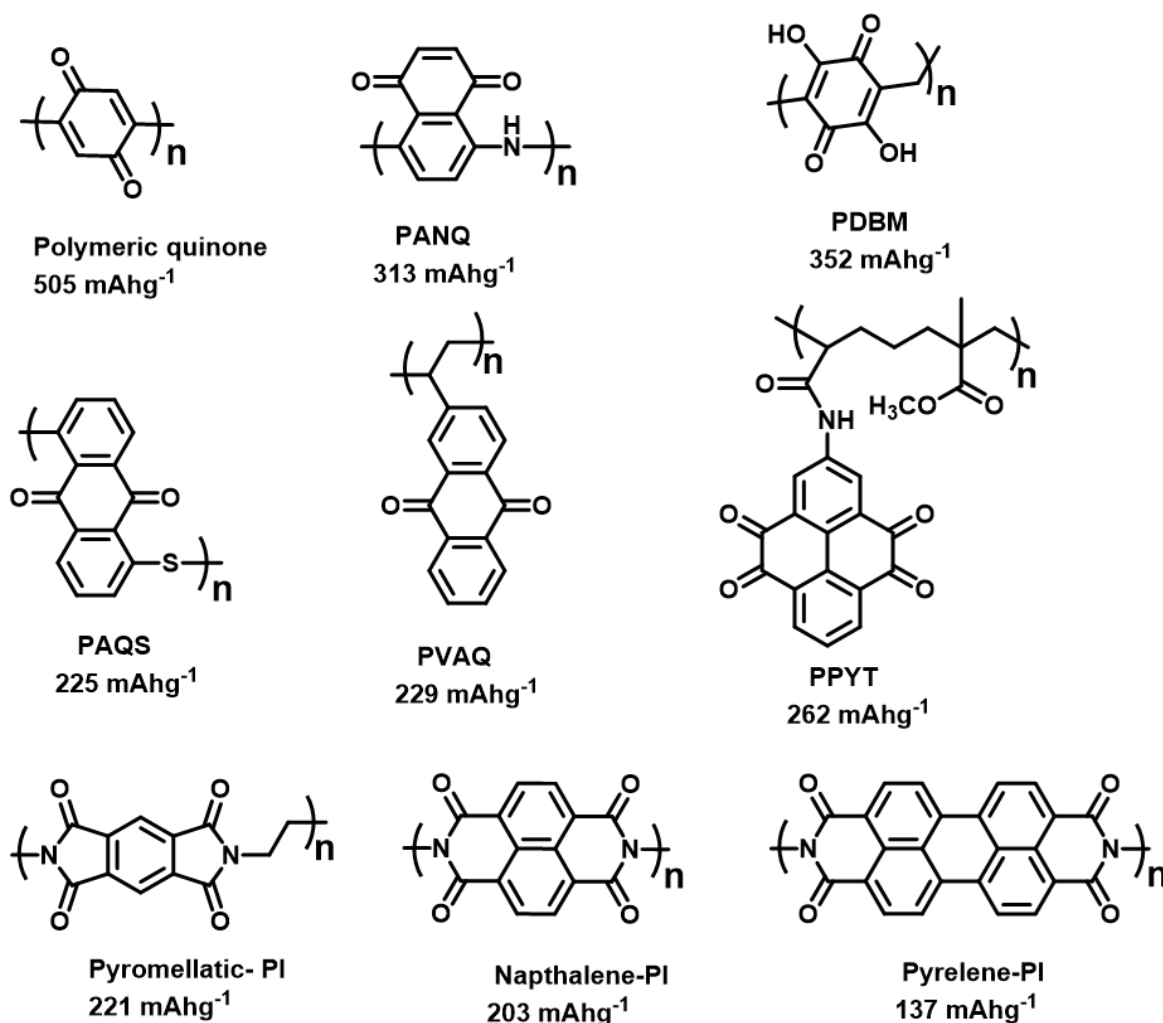


Figure 1.13: conjugated carbonyl polymers with their theoretical capacity

the experimental capacity obtained just one-fourth of its theoretical capacity and was poor cycling performance. This unfortunate result may be due to the defect in the synthesis and unoptimized electrode construction. In 1999 researchers attempted to synthesize and test more polymer electrodes depending on quinone and dianhydride. (Figure 1.13).¹²³⁻¹³¹ However, in recent years, many polymers such as PAQS,¹²⁶ PVAQ,¹²⁸ PPYT¹²⁹, and Naphthalene-PI¹³⁰ exhibited outstanding electrochemical activity than the preceding outcome. PPYT can be gain 90 % of capacity at 30 C and 83 % of its initial capacity after 500 cycles at 1C.¹²⁹ PAQS¹²⁶ successfully synthesized and recorded their electrochemical activity for rechargeable LIBs as a cathode electrode material. An observed capacity was 198 mAh/g with good cyclability. After that, PVAQ¹²⁸ was applied as anode material to polymer air batteries, exhibiting 214 mAh/g capacity, 93% of its theoretical capacity. First-time polyimide was used as cathode material by Song et al. In 2010 due to its high

mechanical and thermal strength. The polymer was always seemed insoluble in electrolytes than its parental monomer. Thus, better way to use a highly electroactive group and stable skeleton containing polymer electrodes to escape from the solubility problem. But it will also consist of many demerits such as reduced discharge potentials, formation of electrochemical polarization, and hindered ionic transportation in the electrode. One of the significant problems associated with polymer is less electronic conductivity due to mostly such polymer insulators. Thus, for full utilization of active masses, a large amount of conductive carbon (30-60 %) needs to add at the time of electrode construction. We can overcome this problem by adapting in situ polymerisation¹³¹ with graphene or MWCNT. If the electrode is constructed efficiently, a conjugated carbonyl polymer can achieve high-rate performance because of high reaction kinetics.

1.5.5.3 Organic conjugated carbonyl compound salts (2008)

A dissolution problem of the organic electrode in the electrolyte seems to be a prime obstacle. Scientists have synthesized metal salts (Na, Li) of the corresponding conjugated dicarboxylates¹³²⁻¹³⁷ hydroxyl quinone,^{137,138,139} and dianhydride derivatives¹⁴⁰⁻¹⁴² to solve this problem. (Figure 1.14) In this field, most of the work was done by three eminent scientists, namely Armand, Poizot, and Tarascon, in 2008.^{132,136,137,140-141} A benefit of these organics molecules is the presence of coordinated bonds, e.g., O-Li-O can be attached to organic compounds to form a lithiated salt which partially solves the solubility problem. Thus, it can achieve better cycling stability than its parent compound; However, it is still undesirable for long-term cyclability. Even though these organics previously consisted of Li ions, even they were used as n-type organics because the -C=O- group attached to lithium was not helpful in capacity contribution unless there will be a breaking of crystal structure irreversibly, showing poor cycling activity. The existence -C=O- group in enolate form results in repulsion charges that will reduce the discharge potential of the materials. For example, molecules $\text{Li}_2\text{C}_6\text{H}_2\text{O}_4$ ¹³⁹ and $\text{Li}_2\text{C}_{14}\text{H}_6\text{O}_4$ ¹³⁸ exhibit much lower voltage than their parent molecules BQ and AQ, respectively. As compared to other conjugated carbonyl compounds Specifically, conjugated carboxylate¹³²⁻¹³⁶ always shows less redox potential (e.g., 0.5–1.5 V vs. Li^+/Li). Thus, they act as rare organics anode materials for rechargeable LIBs and SIBs.

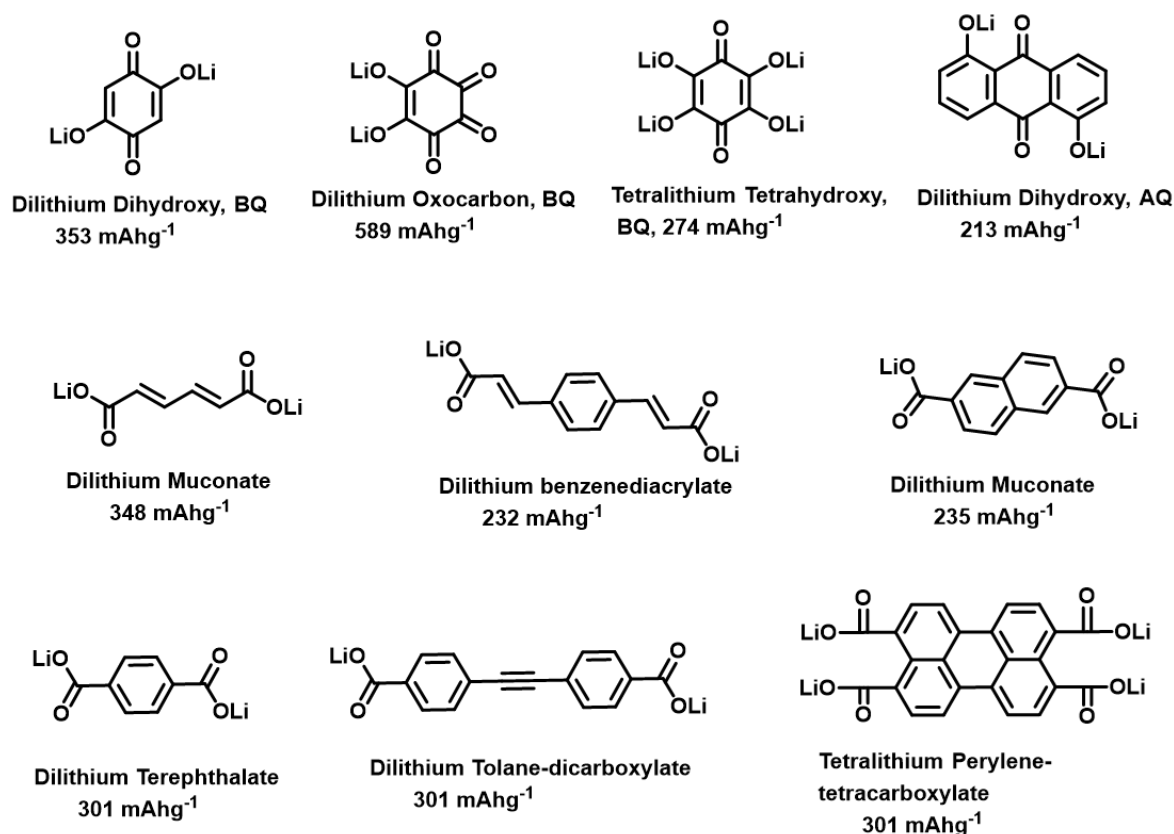


Figure 1.14: Organic conjugated carbonyl compound salts with theoretical capacity

The first time this concept was introduced to LIBs by Xiang et al. to reduce the dissolution of a small organic molecule in electrolyte and successfully synthesized and evaluated the electrochemical activity of lithiated 2,5-DBQ.¹³⁹; however, a 23 % capacity fading was observed for the first ten cycles. Later, Tarascon used modified dilithiated oxocarbon that showed a specific capacity and energy density at 580 mAh/g and a specific energy density of 1300 Wh/kg⁶²; respectively; just after 25 cycles 43% capacity decrease was observed after 25 cycles due to solubility. Thus, they conclude multi-charge formation is key to decreasing solubility. Anyway, a cycle's stability can increase additional charge formation, but it is responsible for decreases in the theoretical capacity and reduction potential. However, a Li-derivative of AQ shows 213 mAh/g theoretical capacity and 2.25 V potential, whereas AQ shows a theoretical capacity of 258 mAh/g at 1.8 V working potential. But, a Li-derivative of AQ shows good cyclic performance compared to AQ.¹³⁸ Piozot In 2011, attempted to synthesize PMDI dilithium salt as electrode materials. However, there was nothing drastic decrease in theoretical capacity because H⁺ and Li⁺ have a minimal difference in formula weight. Still, a decrease in working potential was observed by 0.38 V compared to their parent diimide.¹⁴¹

Tarascon et al. successfully prepared and recorded the electrochemical activity of lithiated trans-muconate as a cathode for LIBs.¹³² They observed that lithium muconate showed a specific capacity of 205 mAh/g, which was reduced to 125 mAh/g after 80 cycles at a 0.1 C rate. However, LIBs constructed by using dilithium terephthalate exhibit a capacity of 301 mAh/g, which is equal to the theoretical capacity and decreases to 234 mAh/g after 50 cycles, around 78% retention of capacity observed after 50 cycles. Due to a significant decrease in working potential after the salt formation of organic molecules, these molecules can act as quality anode material for LIBs. Even though the anode materials' improved capacity is observed by adopting this approach, considerably low cost and electrochemically superior anode materials are already present in the market. However, organics cathode materials research is much lag behind, so there has been a need for more emphasis on organic cathode materials in recent day.

1.6 Aim of the thesis

After coming across through brief review about different kinds of organic electrode material availability, their use as active electrode materials in LIBs, the working mechanism of organic electrodes for LIBs, and the method of design and synthesis of environmentally benign, simple, cost-effective, scalable electrode materials. Although many organic molecules are currently available, many have their own apparent problem. There is still a race to make an ideal organic molecule electrode for LIBs. This thesis emphasized the designing and synthesizing a different derivative of rylene imides dyes (conjugated carbonyl molecules), and it is used as active cathode materials for LIBs. Here we have chosen rylene dyes for study due to the cheaper and readily available starting materials. another crucial aspect of these dyes is the easy, scalable synthesis of substituted different aromatic conjugated structures containing redox-active carbonyl group, which helps make robust insoluble molecules in an electrolyte that is highly beneficial for developing LIBs. The key manifest of this thesis work is highlighted below.

1. Design and synthesis of a library of substituted rylene imide derivative (conjugated carbonyl molecule) consisting of high theoretical capacity.
2. Use of synthesized molecules as a cathode electrode material for LIBs.
3. To study the electrochemical performance of synthesized molecules.
4. To monitor the effect of substituent and conjugation on the solubility of molecules in the electrolyte
5. To study the effect of substituent and conjugation on the electrochemical performance of synthesized conjugated carbonyl molecules.
6. To study the reaction kinetics of the different substituted molecules.

7. To study the effect of conjugated carbonyl delocalized structure on the redox potentials of lithium batteries.

1.7 REFERENCES.

- (1) Jeong, G.; Kim, Y. U.; Kim, H.; Kim, Y. J.; Sohn, H. J. Prospective materials and applications for Li secondary batteries. *Energy Environ. Sci.* **2011**, *4*, 1986-2002.
- (2) Armand, M.; Tarascon, J. M. Building better batteries. *nature.* **2008**, *451*, 652-657.
- (3) Winter, M.; Brodd, R. J. What are batteries, fuel cells, and supercapacitors?. *Chem. Rev.* **2004**, *104*, 4245-4270.
- (4) Cericola, D.; Kötz, R. Hybridization of rechargeable batteries and electrochemical capacitors: Principles and limits. *Electrochim. Acta.* **2012**, *72*, 1-17.
- (5) Arfwedson, A. Untersuchung einiger bei der Eisen-Grube von Utö vorkommenden Fossilien und von einem darin gefundenen neuen feuerfesten Alkali. *J. Chem. Phys.* **1818**, *22*, 93-117.
- (6) Berzelius, J. J. Ein neues mineralisches Alkali und ein neues Metall. *J. Chem. Phys.* **1817**, *21*, 44-48.
- (7) Brande, W.T. A Manual of Chemistry, 2nd ed.; John Murray: London, UK, **1821**, *2*, 57-58.
- (8) Lewis, G. N.; Keyes, F. G. The Potential of The Lithium Electrode. *J. Am. Chem. Soc.* **1913**, *35*, 340-344.
- (9) Harris, W. S. University of California Radiation Laboratory. *Electrochemical studies in cyclic esters.* **1958**, 8381.
- (10) Salkind, A. J.; Cannone, A. G.; Trumburey, F. A. Handbook of Batteries, ed. Linden, D.; Reddy, T. B., **2002**, 3rd edn, 23.1-23.8.
- (11) Liang, Y.; Zhao, C. Z.; Yuan, H. A review of rechargeable batteries for portable electronic devices. *InfoMat.* **2019**, *1*, 6-32
- (12) Goodenough, J.B. How we made the Li-ion rechargeable battery?. *Nat. Electron* **2018**, *1*, 204.
- (13) Nagaura, T. Lithium ion rechargeable battery. *Pro. Batteries Sol. Cells.* **1990**, *9*, 209.
- (14) Cheng, F.; Liang, J.; Tao, Z.; Chen, J. Functional materials for rechargeable batteries. *Adv. Mater.* **2011**, *23*, 1695-1715.
- (15) Yang, Z.; Zhang, J.; Kintner-Meyer, M. C.; Lu, X.; Choi, D.; Lemmon, J. P.; Liu, J. Electrochemical energy storage for green grid. *Che. Rev.* **2011**, *111*, 3577-3613.
- (16) Dunn, B.; Kamath, H.; Tarascon, J. M. Electrical energy storage for the grid: a battery of choices. *Science.* **2011**, *334*, 928-935.
- (17) Deng, D. Li-ion batteries: basics, progress, and challenges. *Energy Sci. Eng.* **2015**, *3*, 385-418.

- (18) Manthiram, A. Materials challenges and opportunities of lithium ion batteries. *J. Phys. Chem. Lett.* **2011**, *2*, 176-184.
- (19) Chu, S.; Majumdar, A. Opportunities and challenges for a sustainable energy future. *Nature*, **2012**, *488*, 294-303.
- (20) Hu, C.; Qiu, S.; Lu, G.; Cao, H.; Lv, H.; Guo, S.; Liu, J. Enhanced electrochemical performance of barium hexaferrite nanoplates by Zn²⁺ doping serving as anode materials. *RSC adv.* **2015**, *5*, 70749-70757.
- (21) Okubo, M.; Hosono, E.; Kim, J.; Enomoto, M.; Kojima, N.; Kudo, T.; Honma, I. Nanosize effect on high-rate Li-ion intercalation in LiCoO₂ electrode. *J. Am. Chem. Soc.* **2007**, *129*, 7444-7452.
- (22) Zuo, X.; Fan, C.; Xiao, X.; Liu, J.; Nan, J. High-voltage performance of LiCoO₂/graphite batteries with methylene methanedisulfonate as electrolyte additive. *J. Power Sources.* **2012**, *219*, 94-99.
- (23) Kalyani, P.; Kalaiselvi, N. Various aspects of LiNiO₂ chemistry. *Sci. Technol. Adv. Mater.* **2005**, *6*, 689.
- (24) Kang, K.; Meng, Y. S.; Breger, J.; Grey, C. P.; Ceder, G. Electrodes with high power and high capacity for rechargeable lithium batteries. *Science*, **2006**, *311*, 977-980.
- (25) Bruce, P.; Robert Armstrong, A.; Gitzendanner, R. New intercalation compounds for lithium batteries: layered LiMnO₂. *J. Mater. Chem.* **1999**, *9*, 193-198.
- (26) Wang, R.; He, X.; He, L.; Wang, F.; Xiao, R.; Gu, L.; Chen, L. Atomic structure of Li₂MnO₃ after partial delithiation and re-lithiation. *Adv. Energy Mater.* **2013**, *3*, 1358-1367.
- (27) Delacourt, C.; Poizot, P.; Levasseur, S.; Masquelier, C. Size effects on carbon-free LiFePO₄ powders: The key to superior energy density. *Electrochem. Solid-State Lett.* **2006**, *9*, A352.
- (28) Huang, X.; Yao, Y.; Liang, F.; Dai, Y. Concentration-controlled morphology of LiFePO₄ crystals with an exposed (100) facet and their enhanced performance for use in lithium-ion batteries. *J. Alloys Compd.* **2018**, *743*, 763-772.
- (29) Madec, L.; Robert, D.; Moreau, P.; Bayle-Guillemaud, P.; Guyomard, D.; Gaubicher, J. Synergistic effect in carbon coated LiFePO₄ for high yield spontaneous grafting of diazonium salt. Structural examination at the grain agglomerate scale. *J. Am. Chem. Soc.* **2013**, *135*, 11614-11622.
- (30) Koksang, R.; Barker, J.; Shi, H.; Saidi, M. Y. Cathode materials for lithium rocking chair batteries. *Solid State Ion.* **1996**, *84*, 1-21.

- (31) Delmas, C. Alkali metal intercalation in layered oxides. *J. Mater. Sci. eng. B.* **1989**, *3*, 97-101.
- (32) Teranishi, T.; Yoshikawa, Y.; Sakuma, R.; Hashimoto, H.; Hayashi, H.; Kishimoto, A.; Fujii, T. High-rate performance of ferroelectric BaTiO₃-coated LiCoO₂ for Li-ion batteries. *Appl. Phys. Lett.* **2014**, *105*, 143904.
- (33) Reddy, M. V.; Jie, T. W.; Jafta, C. J.; Ozoemena, K. I.; Mathe, M. K.; Nair, A. S.; Chowdari, B. V. R. Studies on bare and Mg-doped LiCoO₂ as a cathode material for lithium ion batteries. *Electrochim. Acta.* **2014**, *128*, 192-197.
- (34) Cho, Y.; Oh, P.; Cho, J. A new type of protective surface layer for high-capacity Ni-based cathode materials: nanoscaled surface pillaring layer. *Nano Lett.* **2013**, *13*, 1145-1152.
- (35) Qiu, S.; Lyu, H.; Liu, J.; Liu, Y.; Wu, N.; Liu, W. Facile synthesis of porous nickel/carbon composite microspheres with enhanced electromagnetic wave absorption by magnetic and dielectric losses. *ACS Appl. Mater. Interfaces.* **2016**, *8*, 20258-20266.
- (36) Geng, L.; Liu, J.; Wood III, D. L.; Qin, Y.; Lu, W.; Jafta, C. J.; Belharouak, I. Probing Thermal Stability of Li-Ion Battery Ni-Rich Layered Oxide Cathodes by Means of Operando Gas Analysis and Neutron Diffraction. *ACS Appl. Energy Mater.* **2020**, *3*, 7058-7065.
- (37) Choi, W.; Manthiram, A. Comparison of metal ion dissolutions from lithium ion battery cathodes. *J. Electrochem. Soc.* **2006**, *153*, A1760.
- (38) Zhu, W.; Liu, W.; Li, T.; Yue, X.; Liu, T.; Zhang, W.; Wang, J. Facile green synthesis of graphene-Au nanorod nanoassembly for on-line extraction and sensitive stripping analysis of methyl parathion. *Electrochim. Acta.* **2014**, *146*, 419-428.
- (39) Nkosi, F. P.; Jafta, C. J.; Kebede, M.; le Roux, L.; Matheb, M. K.; Ozoemena, K. I. Microwave-assisted optimization of the manganese redox states for enhanced capacity and capacity retention of LiAl_xMn_{2-2x}O₄ (x = 0 and 0.3) spinel materials. *RSC. Adv.* **2015**, *5*, 32256-32262.
- (40) Mohamed, N.; Allam, N. K. Recent advances in the design of cathode materials for Li-ion batteries. *RSC Adv.* **2020**, *10*, 21662-21685.
- (41) Ensling, D.; Stjerndahl, M.; Nyttén, A.; Gustafsson, T.; Thomas, J. O. A comparative XPS surface study of Li₂FeSiO₄/C cycled with LiTFSI- and LiPF₆-based electrolytes. *J. Mater. Chem.* **2009**, *19*, 82-88.

- (42) Xie, J.; Imanishi, N.; Zhang, T.; Hirano, A.; Takeda, Y.; Yamamoto, O. Li-ion diffusion kinetics in LiFePO₄ thin film prepared by radio frequency magnetron sputtering. *Electrochim. Acta.* **2009**, *54*, 4631-4637.
- (43) Lepage, D.; Michot, C.; Liang, G.; Gauthier, M.; Schougaard, S. B. A soft chemistry approach to coating of LiFePO₄ with a conducting polymer. Int. Ed. *Angew. Chem.* **2011**, *50*, 6884-6887.
- (44) Kim, J.; Kim, H.; Park, I.; Park, Y. U.; Yoo, J. K.; Park, K. Y.; Kang, K. LiFePO₄ with an alluaudite crystal structure for lithium ion batteries. *Energy Environ. Sci.* **2013**, *6*, 830-834.
- (45) Jafta, C. J.; Ozoemena, K. I.; Mathe, M. K.; Roos, W. D. Synthesis, characterisation and electrochemical intercalation kinetics of nanostructured aluminium-doped Li [Li_{0.2}Mn_{0.5}Ni_{0.13}Co_{0.13}] O₂ cathode material for lithium ion battery. *Electrochim. Acta.* **2012**, *85*, 411-422.
- (46) Li, J.; Downie, L. E.; Ma, L.; Qiu, W.; Dahn, J. R. Study of the failure mechanisms of LiNi_{0.8}Mn_{0.1}Co_{0.1}O₂ cathode material for lithium ion batteries. *J. Electrochem. Soc.* **2015**, *162*, A1401.
- (47) Mohanty, D.; Dahlberg, K.; King, D. M.; David, L. A.; Sefat, A. S.; Wood, D. L.; Albano, F. Modification of Ni-Rich FCG NMC and NCA Cathodes by Atomic Layer Deposition: Preventing Surface Phase Transitions for High-Voltage Lithium-Ion Batteries. *Sci. Rep.* **2016**, *6*, 26532.
- (48) Lyu, H.; Li, Y.; Jafta, C. J.; Bridges, C. A.; Meyer III, H. M.; Borisevich, A.; Sun, X. G. Bis (trimethylsilyl) 2-fluoromalonate derivatives as electrolyte additives for high voltage lithium ion batteries. *J. Power Sources.* **2019**, *412*, 527-535.
- (49) Hu, C.; Cao, H.; Wang, S.; Wu, N.; Qiu, S.; Lyu, H.; Liu, J. Synthesis of strontium hexaferrite nanoplates and the enhancement of their electrochemical performance by Zn²⁺ doping for high-rate and long-life lithium-ion batteries. *New J. Chem.* **2017**, *41*, 6427-6435.
- (50) Lu, X.; Zhang, N.; Jahn, M.; Pflöging, W.; Seifert, H. J. Improved capacity retention of SiO₂-coated LiNi_{0.6}Mn_{0.2}Co_{0.2}O₂ cathode material for lithium-ion batteries. *Appl. Sci.* **2019**, *9*, 3671.
- (51) Kebede, M. A.; Kunjuzwa, N.; Jafta, C. J.; Mathe, M. K.; Ozoemena, K. I. Solution-combustion synthesized nickel-substituted spinel cathode materials (LiNi_xMn_{2-x}O₄; 0 ≤ x ≤ 0.2) for lithium ion battery: enhancing energy storage, capacity retention, and lithium ion transport. *Electrochim. Acta.* **2014**, *128*, 172-177.

- (52) Jafta, C. J.; Mathe, M. K.; Manyala, N.; Roos, W. D.; Ozoemena, K. I. Microwave-assisted synthesis of high-voltage nanostructured LiMn_{1.5}Ni_{0.5}O₄ spinel: tuning the Mn³⁺ content and electrochemical performance. *ACS Appl. Mater. Interfaces*. **2013**, *5*, 7592-7598.
- (53) Lu, Y.; Chen, J. Prospects of organic electrode materials for practical lithium batteries. *Nat. Rev. Chem.* **2020**, *4*, 127-142.
- (54) Liang, Y.; Tao, Z.; Chen, J. Organic electrode materials for rechargeable lithium batteries. *Adv. Energy Mater.* **2012**, *2*, 742-769.
- (55) Song, Z.; Zhou, H. Towards sustainable and versatile energy storage devices: an overview of organic electrode materials. *Energy Environ. Sci.* **2013**, *6*, 2280-2301.
- (56) Dong, H.; Zhu, H.; Meng, Q.; Gong, X.; Hu, W. Organic photoresponse materials and devices. *Chem. Soc. Rev.* **2012**, *41*, 1754-1808.
- (57) Wang, C.; Dong, H.; Hu, W.; Liu, Y.; Zhu, D. Semiconducting π -conjugated systems in field-effect transistors: a material odyssey of organic electronics. *Chem. Rev.* **2012**, *112*, 2208-2267.
- (58) Senoh, H.; Yao, M.; Sakaebe, H.; Yasuda, K.; Siroma, Z. A two-compartment cell for using soluble benzoquinone derivatives as active materials in lithium secondary batteries. *Electrochim. Acta.* **2011**, *56*, 10145-10150.
- (59) Koshika, K.; Sano, N.; Oyaizu, K.; Nishide, H. An ultrafast chargeable polymer electrode based on the combination of nitroxide radical and aqueous electrolyte. *Chem. Commun.* **2009**, 836-838.
- (60) Milczarek, G.; Inganäs, O. Renewable cathode materials from biopolymer/conjugated polymer interpenetrating networks. *Science*, **2012**, *335*, 1468-1471.
- (61) Reddy, A. L. M.; Nagarajan, S.; Chumyim, P.; Gowda, S. R.; Pradhan, P.; Jadhav, S. R.; Ajayan, P. M. Lithium storage mechanisms in purpurin based organic lithium ion battery electrodes. *Sci. Rep.* **2012**, *2*, 1-5.
- (62) Chen, H.; Armand, M.; Demailly, G.; Dolhem, F.; Poizot, P.; Tarascon, J. M. From biomass to a renewable Li_xC₆O₆ organic electrode for sustainable Li-ion batteries. *ChemSusChem.* **2008**, *1*, 348-355.
- (63) Tarascon, J. M. Towards sustainable and renewable systems for electrochemical energy storage. *ChemSusChem.* **2008**, *1*, 777-779.
- (64) Muench, S.; Wild, A.; Friebe, C.; Häupler, B.; Janoschka, T.; Schubert, U. S. Polymer-based organic batteries. *Chem. Rev.* **2016**, *116*, 9438-9484.

- (65) Goodenough, J. B.; & Kim, Y. Challenges for rechargeable Li batteries. *Chem. Mater.* **2009**, *22*, 587-603.
- (66) Namazian, M.; Almodarresieh, H. A. Computational electrochemistry: aqueous two-electron reduction potentials for substituted quinones. *J. Mol. Struct. THEOCHEM.* **2004**, *686*, 97-102.
- (67) Alizadeh, K.; Shamsipur, M. Calculation of the two-step reduction potentials of some quinones in acetonitrile. *J. Mol. Struct. THEOCHEM.* **2008**, *862*, 39-43.
- (68) Deng, W.; Liang, X.; Wu, X.; Qian, J.; Cao, Y.; Ai, X.; Yang, H. A low cost, all-organic Na-ion battery based on polymeric cathode and anode. *Sci. Rep.* **2013**, *3*, 1-6.
- (69) Dieterich, V.; Milshtein, J. D.; Barton, J. L.; Carney, T. J.; Darling, R. M.; Brushett, F. R. Estimating the cost of organic battery active materials: a case study on anthraquinone disulfonic acid. *Transl. Mater. Res.* **2018**, *5*, 034001.
- (70) Shirakawa, H.; Louis, E. J.; MacDiarmid, A. G.; Chiang, C. K.; Heeger, A. J. Synthesis of electrically conducting organic polymers: halogen derivatives of polyacetylene, (CH)_x. *J. Chem. Soc. Chem. Commun.* **1977**, 578-580.
- (71) Nigrey, P. J.; MacInnes, D.; Nairns, D. P.; MacDiarmid, A. G.; Heeger, A. J. Lightweight rechargeable storage batteries using polyacetylene,(CH)_x as the cathode-active material. *J. Electrochem. Soc.* **1981**, *128*, 1651.
- (72) Shacklette, L. W.; Toth, J. E.; Murthy, N. S.; Baughman, R. H. Polyacetylene and polyphenylene as anode materials for nonaqueous secondary batteries. *J. Electrochem. Soc.* **1985**, *132*, 1529.
- (73) Zhu, L. M.; Lei, A. W.; Cao, Y. L.; Ai, X. P.; Yang, H. X. An all-organic rechargeable battery using bipolar polyparaphenylene as a redox-active cathode and anode. *Chem. Commun.* **2013**, *49*, 567-569.
- (74) MacDiarmid, A. G.; Yang, L. S.; Huang, W. S.; Humphrey, B. D. Polyaniline: Electrochemistry and application to rechargeable batteries. *Synth. Met.* **1987**, *18*, 393-398.
- (75) Gospodinova, N.; Terlemezyan, L. Conducting polymers prepared by oxidative polymerization: polyaniline. *Prog. polym. sci.* **1998**, *23*, 1443-1484.
- (76) Mermilliod, N.; Tanguy, J.; Petiot, F. A study of chemically synthesized polypyrrole as electrode material for battery applications. *J. Electrochem. Soc.* **1986**, *133*, 1073.

- (77) Zhou, M.; Qian, J.; Ai, X.; Yang, H. Redox-active Fe (CN) 64--doped conducting polymers with greatly enhanced capacity as cathode materials for Li-ion batteries. *Adv. Mater.* **2011**, *23*, 4913-4917.
- (78) Kaneto, K.; Yoshino, K.; Inuishi, Y. Characteristics of polythiophene battery. *Jpn. J. Appl. Phys.* **1983**, *22*, L567.
- (79) Liu, L.; Tian, F.; Wang, X.; Yang, Z.; Zhou, M.; Wang, X. Porous polythiophene as a cathode material for lithium batteries with high capacity and good cycling stability. *React. Funct. Polym.* **2012**, *72*, 45-49.
- (80) Gurunathan, K.; Murugan, A. V.; Marimuthu, R.; Mulik, U. P.; Amalnerkar, D. P. Electrochemically synthesised conducting polymeric materials for applications towards technology in electronics, optoelectronics and energy storage devices. *Mater. Chem. Phys.* **1999**, *61*, 173-191.
- (81) Rudge, A.; Davey, J.; Raistrick, I.; Gottesfeld, S.; Ferraris, J. P. Conducting polymers as active materials in electrochemical capacitors. *J. Power Sources.* **1994**, *47*, 89-107.
- (82) Snook, G. A.; Kao, P.; Best, A. S. Conducting-polymer-based supercapacitor devices and electrodes. *J. Power Sources*, **2011**, *196*, 1-12.
- (83) Gomez-Romero, P. Hybrid organic-inorganic materials—in search of synergic activity. *Adv. Mater.* **2001**, *13*, 163-174.
- (84) Cho, S. I.; Lee, S. B. Fast electrochemistry of conductive polymer nanotubes: synthesis, mechanism, and application. *Acc. Chem. Res.* **2008**, *41*, 699-707.
- (85) Yin, Z.; Zheng, Q. Controlled synthesis and energy applications of one-dimensional conducting polymer nanostructures: an overview. *Adv. Energy Mater.* **2012**, *2*, 179-218.
- (86) Salvatierra, R. V.; Oliveira, M. M.; Zarbin, A. J. One-pot synthesis and processing of transparent, conducting, and freestanding carbon nanotubes/polyaniline composite films. *Chem. Mater.* **2010**, *22*, 5222-5234.
- (87) Wang, D. W.; Li, F.; Zhao, J.; Ren, W.; Chen, Z. G.; Tan, J.; Cheng, H. M. Fabrication of graphene/polyaniline composite paper via in situ anodic electropolymerization for high-performance flexible electrode. *ACS Nano.* **2009**, *3*, 1745-1752.
- (88) Visco, S. J.; DeJonghe, L. C. Ionic conductivity of organosulfur melts for advanced storage electrodes. *J. Electrochem. Soc.* **1988**, *135*, 2905.

- (89) Liu, M.; Visco, S. J.; De Jonghe, L. C. Electrode kinetics of organodisulfide cathodes for storage batteries. *J. Electrochem. Soc.* **1990**, *137*, 750.
- (90) Liu, M.; Visco, S. J.; De Jonghe, L. C. Novel Solid Redox Polymerization Electrodes: All-Solid-State, Thin-Film, Rechargeable Lithium Batteries. *J. Electrochem. Soc.* **1991**, *138*, 1891.
- (91) Liu, M.; Visco, S. J.; De Jonghe, L. C. Novel solid redox polymerization electrodes: electrochemical properties. *J. Electrochem. Soc.* **1991**, *138*, 1896.
- (92) Sotomura, T.; Uemachi, H.; Takeyama, K.; Naoi, K.; Oyama, N. New organodisulfide—polyaniline composite cathode for secondary lithium battery. *Electrochim. Acta.* **1992**, *37*, 1851-1854.
- (93) Oyama, N.; Tatsuma, T.; Sato, T.; Sotomura, T. Dimercaptan—polyaniline composite electrodes for lithium batteries with high energy density. *Nature*, **1995**, *373*, 598-600.
- (94) Oyama, N.; Pope, J. M.; Sotomura, T. Effects of adding copper (II) salt to organosulfur cathodes for rechargeable lithium batteries. *J. Electrochem. Soc.* **1997**, *144*, L47.
- (95) Oyama, N.; Hatozaki, O. Lithium polymer battery with high energy density. *Macromol. Symp.* **2000**, *156*, 171-178.
- (96) Oyama, N. Development of polymer-based lithium secondary battery. *Macromol. Symp.* **2000**, *159*, 221-228.
- (97) Park, J. E.; Kim, S.; Mihashi, S.; Hatozaki, O.; Oyama, N. Roles of metal nanoparticles on organosulfur-conducting polymer composites for lithium battery with high energy density. *Macromol. Symp.* **2002**, *186*, 35-40.
- (98) Naoi, K.; Kawase, K. I.; Mori, M.; Komiyama, M. Electrochemistry of Poly (2, 2'-dithiodianiline): A New Class of High Energy Conducting Polymer Interconnected with S–S Bonds. *J. Electrochem. Soc.* **1997**, *144*, L173.
- (99) Deng, S. R.; Kong, L. B.; Hu, G. Q.; Wu, T.; Li, D.; Zhou, Y. H.; Li, Z. Y. Benzene-based polyorganodisulfide cathode materials for secondary lithium batteries. *Electrochim. Acta.* **2006**, *51*, 2589-2593.
- (100) Zhang, J. Y.; Kong, L. B.; Zhan, L. Z.; Tang, J.; Zhan, H.; Zhou, Y. H.; Zhan, C. M. Sulfides organic polymer: Novel cathode active material for rechargeable lithium batteries. *J. Power Sources.* **2007**, *168*, 278-281.

- (101) Tang, J.; Song, Z. P.; Shan, N.; Zhan, L. Z.; Zhang, J. Y.; Zhan, H.; Zhan, C. M. Poly [3, 4-(ethylenedithio) thiophene]: High specific capacity cathode active material for lithium rechargeable batteries. *J. Power Sources*. **2008**, *185*, 1434-1438.
- (102) Zhan, L.; Song, Z.; Zhang, J.; Tang, J.; Zhan, H.; Zhou, Y.; Zhan, C. PEDOT: Cathode active material with high specific capacity in novel electrolyte system. *Electrochim. Acta*. **2008**, *53*, 8319-8323.
- (103) Zhan, L.; Song, Z.; Shan, N.; Zhang, J.; Tang, J.; Zhan, H.; Zhan, C. Poly batteries. (tetrahydrobenzodithiophene): High discharge specific capacity as cathode material for lithium *J. Power Sources*. **2009**, *193*, 859-863.
- (104) Nakahara, K.; Iwasa, S.; Satoh, M.; Morioka, Y.; Iriyama, J.; Suguro, M.; Hasegawa, E. Rechargeable batteries with organic radical cathodes. *Chem. Phys. Lett.* **2002**, *359*, 351-354.
- (105) Suga, T.; Konishi, H.; Nishide, H. Photocrosslinked nitroxide polymer cathode-active materials for application in an organic-based paper battery. *Chem. Commun.* **2007**, 1730-1732.
- (106) Koshika, K.; Chikushi, N.; Sano, N.; Oyaizu, K.; Nishide, H. A TEMPO-substituted polyacrylamide as a new cathode material: an organic rechargeable device composed of polymer electrodes and aqueous electrolyte. *Green Chem.* **2010**, *12*, 1573-1575.
- (107) Oyaizu, K.; Kawamoto, T.; Suga, T.; Nishide, H. Synthesis and charge transport properties of redox-active nitroxide polyethers with large site density. *Macromolecules*, **2010**, *43*, 10382-10389.
- (108) Han, X.; Qing, G.; Sun, J. Sun, T. How Many Lithium Ions Can Be Inserted onto Fused C₆ Aromatic Ring Systems.? *Angew. Chem. Int. Ed.* **2012**, *51*, 5147-5151.
- (109) Wu, Y.; Zeng, R.; Nan, J.; Shu, D.; Qiu, Y.; Chou, S. L. Quinone electrode materials for rechargeable lithium/sodium ion batteries. *Adv. Energy Mater.* **2017**, *7*, 1700278.
- (110) Wang, H. G.; Zhang, X. B. Organic Carbonyl Compounds for Sodium-Ion Batteries: Recent Progress and Future Perspectives. *Chem. Eur. J.* **2018**, *24*, 18235-18245.
- (111) Zhao, Q.; Lu, Y.; Chen, J. Advanced organic electrode materials for rechargeable sodium-ion batteries. *Adv. Energy Mater.* **2017**, *7*, 1601792.
- (112) Xu, Y.; Zhou, M.; Lei, Y. Organic materials for rechargeable sodium-ion batteries. *Mater. Today*. **2018**, *21*, 60-78.
- (113) Williams, D. L.; Byrne, J. J.; Driscoll, J. S. **1969**, A high energy density lithium/dichloroisocyanuric acid battery system. *J. Electrochem. Soc.* **1969**, *116*, 2.

- (114) Alt, H.; Binder, H.; Köhling, A.; Sandstede, G. Investigation into the use of quinone compounds-for battery cathodes. *Electrochim. Acta.* **1972**, *17*, 873-887.
- (115) Bu, P.; Liu, S.; Lu, Y.; Zhuang, S.; Wang, H.; Tu, F. Effects of carbon black on the electrochemical performance of lithium-organic coordination compound batteries. *Int. J. Electrochem. Sci.* **2012**, *7*, 4617-4624.
- (116) Lei, Z.; Wei-kun, W.; An-bang, W.; Zhong-bao, Y.; Shi, C.; Yu-sheng, Y. A MC/AQ parasitic composite as cathode material for lithium battery. *Journal of the Electrochem. Soc.* **2011**, *158*, A991.
- (117) Genorio, B.; Pirnat, K.; Cerc-Korosec, R.; Dominko, R.; Gaberscek, M. Electroactive organic molecules immobilized onto solid nanoparticles as a cathode material for lithium-ion batteries. *Angew. Chem. Int. Ed.* **2010**, *49*, 7222-7224.
- (118) Boschi, T.; Pappa, R.; Pistoia, G.; Tocci, M. On the use of nonylbenzo-hexaquinone as a substitute for monomeric quinones in non-aqueous cells. *J. electroanal. Chem.* **1984**, *176*, 235-242.
- (119) Senoh, H.; Yao, M.; Sakaebe, H.; Yasuda, K.; Siroma, Z. A two-compartment cell for using soluble benzoquinone derivatives as active materials in lithium secondary batteries. *Electrochim. Acta.* **2011**, *56*, 10145-10150.
- (120) Hanyu, Y.; Ganbe, Y.; Honma, I. Application of quinonic cathode compounds for quasi-solid lithium batteries. *J. power sources.* **2013**, *221*, 186-190.
- (121) Suo, L.; Hu, Y. S.; Li, H.; Armand, M.; Chen, L. A new class of solvent-in-salt electrolyte for high-energy rechargeable metallic lithium batteries. *Nat. commun.* **2013**, *4*, 1481-1489.
- (122) Foos, J. S.; Erker, S. M.; & Rembetsy, L. M. Synthesis and Characterization of Semiconductive Poly-1, 4-Dimethoxybenzene and Its Derived Polyquinone. *J. Electrochem. Soc.* **1986**, *133*, 836.
- (123) Häringer, D.; Novák, P.; Haas, O.; Piro, B.; Pham, M. C. Poly (5-amino-1, 4-naphthoquinone), a Novel Lithium-Inserting Electroactive Polymer with High Specific Charge. *J. Electrochem. Soc.* **1999**, *146*, 2393.
- (124) Le Gall, T.; Reiman, K. H.; Grossel, M. C.; Owen, J. R. Poly (2, 5-dihydroxy-1, 4-benzoquinone-3, 6-methylene): a new organic polymer as positive electrode material for rechargeable lithium batteries. *J. power sources.* **2003**, *119*, 316-320.
- (125) Oyama, N.; Sarukawa, T.; Mochizuki, Y.; Shimomura, T.; Yamaguchi, S. Significant effects of poly (3, 4-ethylenedioxythiophene) additive on redox

- responses of poly (2, 5-dihydroxy-1, 4-benzoquinone-3, 6-methylene) cathode for rechargeable Li batteries. *J. Power Sources*. **2009**, 189, 230-239.
- (126) Song, Z.; Zhan, H.; Zhou, Y. Anthraquinone based polymer as high performance cathode material for rechargeable lithium batteries. *Chem. commun.* **2009**, 448-450.
- (127) Xu, W.; Read, A.; Koech, P. K.; Hu, D.; Wang, C.; Xiao, J.; Zhang, J. G. Factors affecting the battery performance of anthraquinone-based organic cathode materials. *J. Mater. Chem.* **2012**, 22, 4032-4039.
- (128) Choi, W.; Harada, D.; Oyaizu, K.; Nishide, H. Aqueous electrochemistry of poly (vinylanthraquinone) for anode-active materials in high-density and rechargeable polymer/air batteries. *J. Am. erican Chem. Soc.* **2011**, 133, 19839-19843.
- (129) Nokami, T.; Matsuo, T.; Inatomi, Y.; Hojo, N.; Tsukagoshi, T.; Yoshizawa, H.; Yoshida, J. I. Polymer-bound pyrene-4, 5, 9, 10-tetraone for fast-charge and-discharge lithium-ion batteries with high capacity. *J. Am. Chem. Soc.* **2012**, 134, 19694-19700.
- (130) Song, Z.; Zhan, H.; Zhou, Y. Polyimides: promising energy-storage materials. *Angew. Chem. Int. Ed.* **2010**, 49, 8444-8448.
- (131) Song, Z.; Xu, T.; Gordin, M. L.; Jiang, Y. B.; Bae, I. T.; Xiao, Q.; Wang, D. Polymer–graphene nanocomposites as ultrafast-charge and-discharge cathodes for rechargeable lithium batteries. *Nano Lett.* **2012**, 12, 2205-2211.
- (132) Armand, M.; Grugeon, S.; Vezin, H.; Laruelle, S.; Ribière, P.; Poizot, P.; Tarascon, J. M. Conjugated dicarboxylate anodes for Li-ion batteries. *Nat. Mater.* **2009**, 8, 120-125.
- (133) Zhao, L.; Zhao, J.; Hu, Y. S.; Li, H.; Zhou, Z.; Armand, M.; Chen, L. Disodium terephthalate (Na₂C₈H₄O₄) as high performance anode material for low-cost room-temperature sodium-ion battery. *Adv. Energy Mate.* **2012**, 2, 962-965.
- (134) Park, Y.; Shin, D. S.; Woo, S. H.; Choi, N. S.; Shin, K. H.; Oh, S. M.; Hong, S. Y. Sodium terephthalate as an organic anode material for sodium ion batteries. *Adv. Mater.* **2012**, 24, 3562-3567.
- (135) Abouimrane, A.; Weng, W.; Eltayeb, H.; Cui, Y.; Niklas, J.; Poluektov, O.; Amine, K. Sodium insertion in carboxylate based materials and their application in 3.6 V full sodium cells. *Energy Environ. Sci.* **2012**, 5(11), 9632-9638.
- (136) Walker, W.; Grugeon, S.; Vezin, H.; Laruelle, S.; Armand, M.; Wudl, F.; Tarascon, J. M. Electrochemical characterization of lithium 4, 4'-tolane-dicarboxylate for use as a negative electrode in Li-ion batteries. *J. Mater. Chem.* **2011**, 21(5), 1615-1620.

- (137) Chen, H.; Armand, M.; Courty, M.; Jiang, M.; Grey, C. P.; Dolhem, F.; Poizot, P. Lithium salt of tetrahydroxybenzoquinone: toward the development of a sustainable Li-ion battery. *J. Am. Chem. Soc.* **2009**, *131*, 8984-8988.
- (138) Zeng, R. H.; Li, X. P.; Qiu, Y. C.; Li, W. S.; Yi, J.; Lu, D. S.; Xu, M. Q. Synthesis and properties of a lithium-organic coordination compound as lithium-inserted material for lithium ion batteries. *Electrochem. commun.* **2010**, *12*, 1253-1256.
- (139) Xiang, J.; Chang, C.; Li, M.; Wu, S.; Yuan, L.; Sun, J. A novel coordination polymer as positive electrode material for lithium ion battery. *Crys. Growth and Des.* **2008**, *8*, 280-282.
- (140) Walker, W.; Grugeon, S.; Mentre, O.; Laruelle, S.; Tarascon, J. M.; Wudl, F. Ethoxycarbonyl-based organic electrode for Li-batteries. *J. Am. Chem. Soc.* **2010**, *132*, 6517-6523.
- (141) Renault, S.; Geng, J.; Dolhem, F.; Poizot, P. Evaluation of polyketones with N-cyclic structure as electrode material for electrochemical energy storage: case of pyromellitic diimide dilithium salt. *Chem. Commun.* **2011**, *47*, 2414-2416.
- (142) Kim, D. J.; Je, S. H.; Sampath, S.; Choi, J. W.; Coskun, A. Effect of N-substitution in naphthalenediimides on the electrochemical performance of organic rechargeable batteries. *RSC Adv.* **2012**, *2*, 7968-7970.

Type equation here.

CHAPTER 2

**Effect of Aromatic Rings and Substituent on the
Performance of Lithium Batteries with Rylene Imide
Cathodes.**

2.1 INTRODUCTION

Lithium-ion batteries (LIBs) find their wide use in portable electronic devices,¹⁻⁴, despite large efforts to use them for electrotraction and load leveling in electric grids.⁵ While inorganic intercalation compounds and carbon materials are routinely used as electrodes in LIB,⁶⁻¹¹ organic molecules are explored as active materials in LIBs due to their lightweight, flexibility, easy processability, and potentially unlimited availability (as compared to transition metal oxides). Among the tested classes of compounds are conjugated polymers, imides, quinones, triazines, corroles, triangulenes, and tetracyano quinodimethane.¹²⁻²⁰ Rylene imides are interesting due to the presence of carbonyl moieties that are attached to a conjugated backbone (Scheme 1). The LUMO energy levels of rylene imides vary as a function of the number of phenyl rings consist in the molecule. This variation in LUMO offers the possibility to vary the output voltage of the battery. Due to the advantageous properties of rylene imides. Perylene dianhydride was blended with sulfur and incorporated as an electrode in LIBs.²¹ A composite of perylene diimide (PDI) was prepared in the presence of CNT and was used in LIBs. The series of PDI polymers were prepared for utilization in LIBs.²²⁻²⁴ Polar functionalities attached to the PDI backbones were found to stabilize the battery performance.^{6,25,26} Naphthalenediimide (NDI) is an analogue of PDI with a smaller aromatic system. Naphthalenedianhydride (NDA) was polymerized with urea and diamino ethane.²⁷ The carbonyl moiety of the urea linker was found to enhance the specific capacity of LIBs based on NDI. The cycling stability and coulombic efficiency decreased to 150 charge-discharge cycles. NDA was also polymerized with hydrazine, and its utility in LIBs was studied. During the charge-discharge cycling, the N-N bond was cleaved, leading to a decrease in a specific capacity. An alkyl group was substituted on the imide nitrogen of NDI, and its performance was compared with that of Li substituted NDI.²⁸ In another set of experiments, NDA was polymerized with diamino ethane over graphene. Batteries were fabricated using lithium and sodium electrodes.²⁹ The lowest analogue in the rylene imide series is pyromellitic diimide (PyDI), which has been used in a sodium-ion battery.³⁰ LIBs of PyDI showed a specific capacity of 200 mAh/gover 25 cycles.³¹ Polymers of PyDI have been prepared and explored in LIBs.³² One of the issues in rylene imides-based LIBs is the decrease in specific capacity upon charge/discharge cycling. Simple rylene imides, as shown in Scheme 1, are usually insoluble in common organic solvents, hence they should have been the material of choice to fabricate LIBs with impressive efficiency. However, it has been shown that the lithium-ion insertion is precluded due to the close

packing of the molecules.²⁹ Thus, substituting the imide nitrogen is necessary to achieve a more open packing in the solid-state. However, the substitution can either increase the solubility of the material or further complicate the lithium-ion insertion process. Considering these issues, we have chosen triphenylamine (TPA) as a substituent on the imide nitrogen for the following reasons, (i) the absence of the redox process in the charge-discharge window of LIBs, (ii) the increased aromatic systems that are likely to decrease solubilities, and (iii) the propeller-type arrangement of phenyl rings in TPA is likely to disrupt the close packing of the molecules and facilitate lithium-ion insertion and desorption. Using the systematically varied compounds shown in Scheme 1, we were interested in identifying the relationship between molecular weight and performance as an organic battery material. Theoretically, a decrease in molecular weight should increase specific capacity. However, in rylene imides, the variation in molecular weight is accompanied by a variation in the number of aromatic units that may influence the redox properties, for which a systematic study is not available yet. To address all these issues, we have prepared TPA-substituted TPA-PDI, TPA-NDI, and TPA-Py and utilized them as electrodes in LIBs. Compounds TPA-PDI, TPA-NDI, and TPA-Py comprise four carbonyl moieties and two imide nitrogens as common structural motifs. They differ in the number of central aromatic rings, namely four, two, and one for molecules TPA-PDI, TPA-NDI, and TPA-Py, respectively. While our work was in progress, synthesis and electrochromic properties of compounds TPA-PDI, TPA-NDI, and TPA-Py were reported.³³

2.2 EXPERIMENTAL SECTION.

2.2.1 Chemicals and Materials.

Unless otherwise stated, all the chemicals and reagents were obtained commercially and used without further purification. Perylene-3,4,9,10-tetracarboxylic dianhydride, 1,4,5,8-naphthalene tetracarboxylic dianhydride, pyromellitic dianhydride, zinc acetate, copper (II) nitrate hydrate, imidazole, and triphenylamine were purchased from Sigma-Aldrich. Dimethylformamide (DMF), chloroform (CHCl₃), Tetrahydrofuran (THF), dichloromethane (DCM), ethyl acetate, hexane, and acetone were purchased from Merck Chemicals. Polyvinyl difluoride (PVDF, Kynar HSV900, Arkema Inc., USA) and N-Methyl-2-pyrrolidone (NMP, Merck AR grade). 1M LiPF₆ in ethylene carbonate and diethyl carbonate was purchased from BASF chemical company. All solvents used for battery performance tests were of HPLC grade and purchased from Merck chemical.

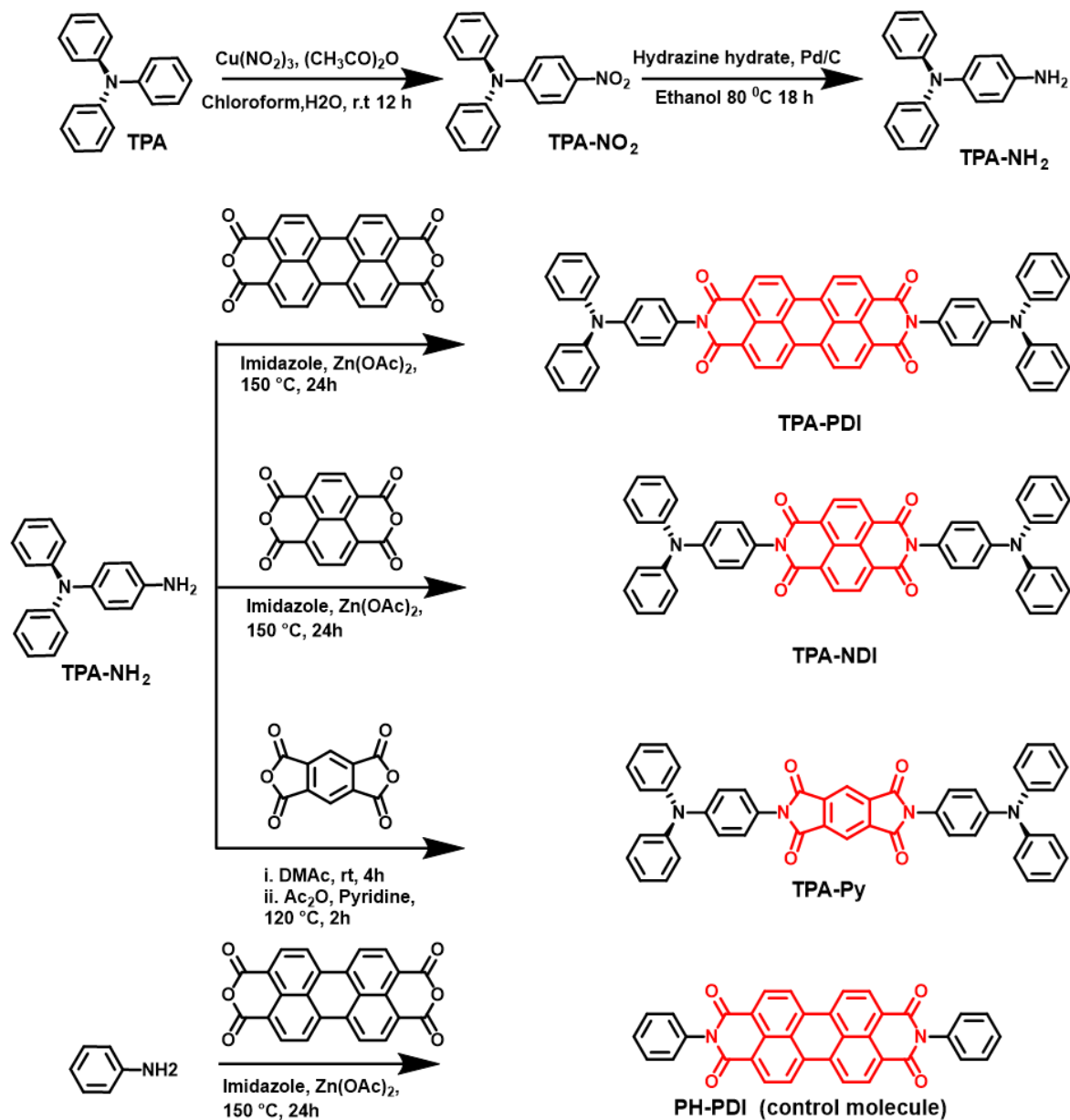
2.2.2 General Experimental Method and Instrumentation.

Analytical thin-layer chromatography was carried out on pre-coated silica gel plates (Kiesel gel 60F254, Merck). Column chromatography purification were performed with 60–120 mesh-sized silica gel. All ¹H NMR spectra were recorded in CDCl₃ and DMSO-d₆ on a Bruker arx AV 200 MHz, AV 400 MHz, and AV 500 MHz Bruker AVANS spectrometer. ¹³C NMR spectra were measured on a Bruker arx 200 MHz AVANS spectrometer. All chemical shifts are reported in δ ppm downfield to TMS, and peak multiplicities are referred to as singlet (s), doublet (d), triplet (t), quartet (q), pentet (p), and multiplet (m). UV-vis absorption spectra were recorded on SPECORD® 210/PLUS, a UV-visible spectrophotometer. An electrochemical analyzer CHI660 (CH Instruments) was used to record the cyclic voltammograms of the prepared molecules 0.1 M tetrabutylammonium perchlorate (TBAClO₄) in NMP (N-methyl-2-pyrrolidone) in a three-electrode setup with a Pt working electrode, Pt foil as the auxiliary electrode and an Ag/Ag⁺ reference electrode. TEM imaging was performed with a Jeol 1200 EX transmission electron microscope. The samples were prepared by drop-casting dispersed solution (In NMP) (5–10 μL of 5×10⁻⁴ M) of the sample on the carbon-coated copper grids (400 grids, Ted Pella) and dried at 80°C for 12 h. SEM imaging was done with a Helios Nanolab 600i system (FEI Company, Eindhoven, The Netherlands) at 10 kV accelerating voltage. The sample was prepared by drop-casting 5–10 μL of 5×10⁻⁴ M dispersed solution (in NMP) of the molecules on ZP-P4VP spun silicon wafers. Electrochemical Impedance Spectroscopy measurements were done in the frequency range of 10 MHz to 40 kHz using a Biologic instrument. The positive electrode consisted of either TPA-PDI or TPA-NDI, or TPA-Py as the electrochemically active material, PVDF (Kynar ADX 111) as a binder, and carbon black (TIMCAL ENSACO Super C 65) as a conductive additive. The composition of those components was TPA/PVDF/ carbon black=60%/10%/30% by mass. The compounds were mixed with NMP as a solvent, and a prepared slurry was coated on copper foil. Subsequently, electrodes with an area of 2×2 cm² were punched out after drying. Lithium was used as the negative electrode, 1 M LiPF₆ in EC: DEC (1:1, mass ratio) as the electrolyte, and Whatman® GF/A as a separator. All cells were assembled in a glove box under an argon atmosphere. Charge-discharge cycles were run with three replicates for each compound. After charge/discharge cycling, the separator was washed with NMP, and UV-vis absorption spectra were recorded.

2.2.3 Synthesis and Characterization.

The amine-substituted TPA and benzene substituted (control molecule) were condensed with rylene dianhydrides to prepare compounds TPA-PDI, TPA-PDI, 6 TPA-PDI, Ph-PDI

(Scheme 2.1). The detailed synthesis and characterization of small molecules and monomers can be found below.



Scheme 2.1: Synthesis of rylene imides TPA-PDI, TPA-NDI, TPA-Py and PH-PDI (control molecule)

a) Synthesis of TPA-NO₂

Procedure: This compound was synthesized by the following literature.³⁴ 100 mL round bottom flask equipped with a magnetic stirrer was charged with triphenylamine (Molecule 1) (2.5 g, 10.2 mmol) and acetic anhydride (50 mL). To this solution, copper (II) nitrate (1.9

g, 10.2 mmol) was added slowly with stirring. The solution was stirred at room temperature for 2 hours. After that water (100 mL) and chloroform (15 mL) were added to the reaction mixture and stirring was continued for 12 hours. The completion of the reaction was monitored by TLC. The layers were separated and the aqueous layer was extracted with 50 mL portions of chloroform. The combined organic layers were washed with 100 mL of water and dried over sodium sulfate. The organic layers were collected and concentrated under reduced pressure. A yellow solid compound was obtained after a silica gel column chromatography purification (ethyl acetate: pet ether = 1:9 as eluent) (yield = 50 %). ¹H NMR (200 MHz, CDCl₃, δ, ppm): 8.08 (d, J=9.3 Hz, 2H, 2-H), 7.42 (d, J=9.3 Hz, 2H, 3-H), 7.21-7.30 (m, 8H, 4-H, 5-H), 6.97 (d, J=9.2, Hz, 2H, 6-H). ¹³C NMR (200 MHz, CDCl₃, δ, ppm): 140.20 (C¹-NO₂), 118.15 (C²), 125.47 (C³), 153.53 (C⁴), 145.69 (C⁵), 126.56 (C⁶), 129.97 (C⁷), 125.78 (C⁸).

b) Synthesis of TPA-NH₂

Procedure: This compound was synthesized by the following literature.³⁵ A 100 mL round bottom flask equipped with a magnetic stirrer was charged with 4-nitro-triphenylamine (TPA-NO₂) (1.2 g, 4.15 mmol), Pd/C 10% (80 mg) in ethanol (20 mL), and the reaction mixture was refluxed for 10 min. Hydrazine hydrate (1.24 mL) was added dropwise to the hot solution. Afterward, the mixture was refluxed for 18 h. The completion of the reaction was monitored by TLC. The reaction mixture was cooled and passed over a celite pad. (Sigma Aldrich) The mixture was washed with dichloromethane and water. The organic layer was collected and concentrated under reduced pressure. A pale-yellow compound (yield = 80%) was obtain after a silica gel column chromatographic purification (ethyl acetate: pet ether = 2.5:7.5 as eluent). ¹H NMR (200 MHz, CDCl₃, δ, ppm): 3.42 (bs, NH₂), 6.57(d, J = 8.8 Hz, 2H, 2-H), 6.82-6.99 (m, 8H, 3-H, 4-H, 6-H), 7.15(m, 5-H), ¹³C NMR (200 MHz, CDCl₃, δ, ppm): 142.7 (C¹-NH₂), 117.20 (C²), 127.41 (C³), 138.90 (C⁴), 148.20 (C⁵), 122.80 (C⁶), 129.07 (C⁷), 121.72 (C⁸).

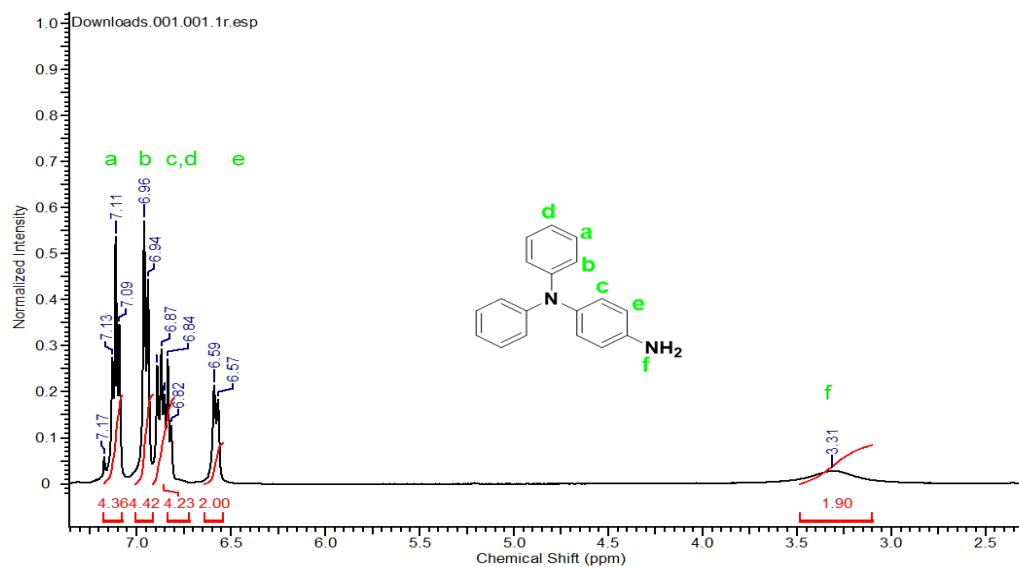


Figure 2.1: ^1H NMR of TPA-NH₂

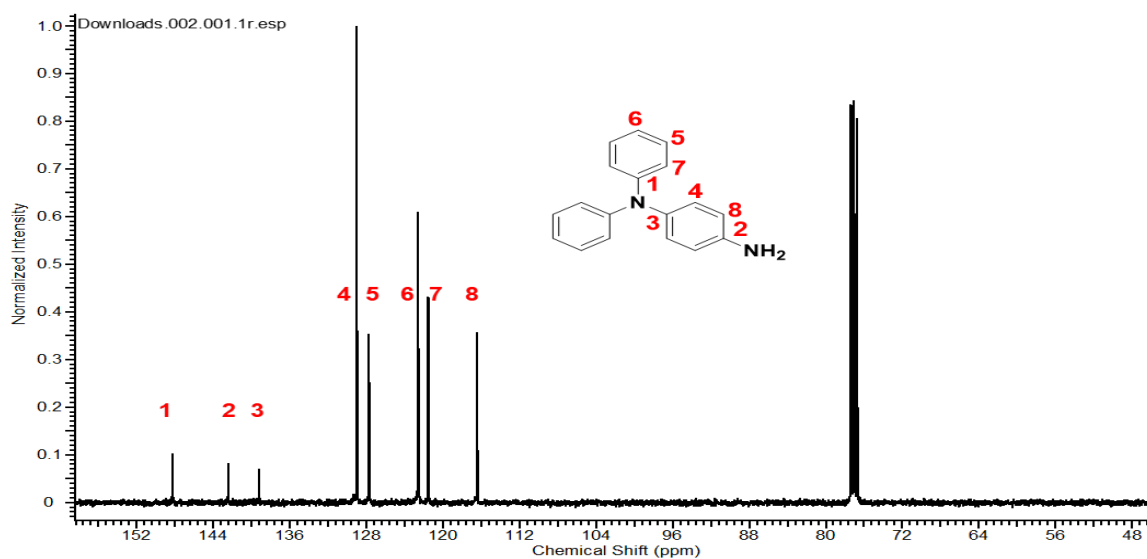


Figure 2.2: ^{13}C NMR of TPA-NH₂

c) Synthesis of TPA-PDI

Procedure: A 100 mL round bottom flask equipped with magnetic stirrer was charged with perylene-3,4,9,10-tetracarboxylic dianhydride (0.3 g, 0.76 mmol), 4-amino-triphenylamine (TPA-NH₂) (0.47 g, 1.8 mmol) and zinc acetate (0.09 g, 0.55 mmol) in imidazole (30 g). The resultant mixture was heated at 150 °C for 24 h under an argon atmosphere. The completion of the reaction was monitored by TLC. The reaction mixture was cooled down

to 60 °C. Then the product mixture was precipitated by adding 2 M HCl. The resultant crude product was washed with deionized water and methanol. A dark red solid (yield = 58 %) was obtained after a silica gel column chromatographic purification (hexane: CHCl₃ = 5:5 as eluent). ¹H NMR (500 MHz, CDCl₃, δ, ppm) 7.09 (t, *J* = 7.6 Hz, 4H, H_a), 7.21–7.29 (m, 16H, H_c + H_d + H_e), 7.30 (m, 8H, H_b), 8.67 (d, *J* = 7.6 Hz, 4H, H_g), 8.75 (d, *J* = 7.6 Hz, 4H, H_f). ¹³C NMR cannot be recorded because of low solubility.

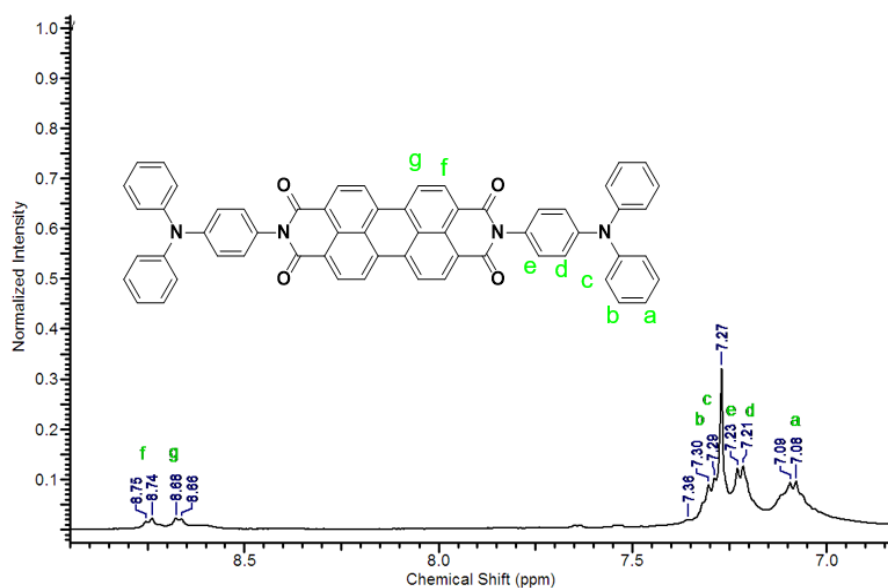


Figure 2.3: ¹H NMR of TPA-PDI

d) Synthesis of TPA-NDI

Procedure: The synthesis followed a similar procedure as used for compound **4** using 1,4,5,8-naphthalenetetracarboxylic dianhydride (0.3 g, 1.12 mmol), 4-amino-triphenylamine (TPA-NH₂) (0.64 g, 2.45 mmol) and zinc acetate (0.14 g, 0.7 mmol) in imidazole (30g). A purple coloured solid (yield = 60 %) was obtained after a silica gel column chromatographic purification (hexane: CHCl₃ = 6:4 as eluent). ¹H NMR (400 MHz, CDCl₃, δ, ppm): 7.09 (t, *J* = 7.5 Hz, 4H, H_a), 7.17 (m, *J* = 8 Hz, 4H, H_d), 7.23 (d, *J* = 7.9 Hz, 12H, H_c+ H_e), 7.32(t, *J* = 7.5 Hz, 8H, H_b), 8.85 (s, 4H, H_f). ¹³C NMR (200 MHz, CDCl₃, δ, ppm): 123.69 (C¹), 129.48 (C²), 125.25(C³), 147.33(C⁴), 148.48 (C⁵), 129.02(C⁶), 122.80 (C⁷), 128.97 (C⁸), 127.09 (C⁹), 131.47 (C¹⁰), 127.52 (C¹¹), 163.19 (C¹², imide carbonyl).

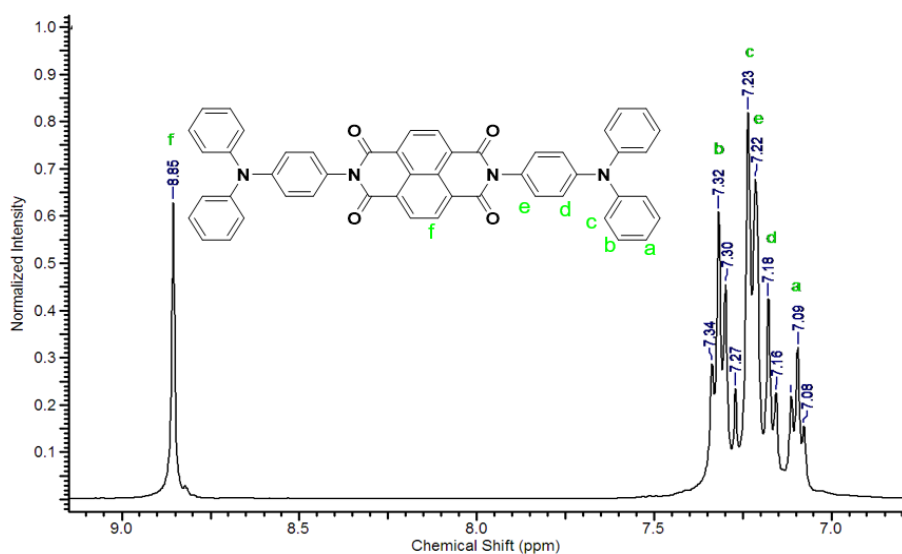


Figure 2.4: ^1H NMR of TPA-NDI

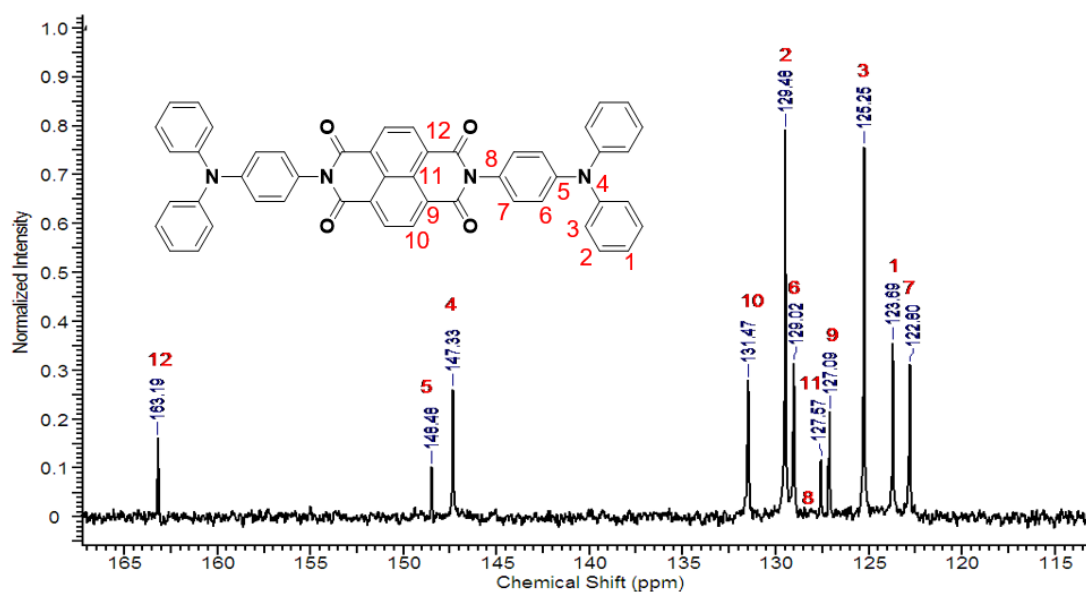


Figure 2.5: ^{13}C NMR of TPA-NDI

e) Synthesis of TPA-Py

Procedure: A 50 mL round bottom flask equipped with a magnetic stirrer was charged with pyromellitic dianhydride (0.3 g, 1.37 mmol), 4-amino-triphenylamine (TPA-NH₂) (0.8 g, 3.05 mmol) in DMAc (10 mL). The resultant reaction mixture was stirred at room temperature for 2 h, and then 2.5 mL acetic anhydride and 1.5 mL pyridine were added to the reaction mixture. After 2 h further stirring at 130 °C, the solution was poured into 100

mL methanol. The precipitated red solid was collected by filtration and dried (yield = 70 %). ^1H NMR (500 MHz, CDCl_3 , δ , ppm): 7.11 (t, $J = 7.2$ Hz, 4H, H_a), 7.28–7.32 (m, 12H, $\text{H}_b + \text{H}_e$), 7.19 (d, $J = 8.4$ Hz, 12H, $\text{H}_c + \text{H}_d$), 7.27–7.34 (m, 12H, $\text{H}_b + \text{H}_e$), 8.47 (s, 2H, H_f). ^{13}C NMR (200 MHz, CDCl_3 , δ , ppm): 123.75 (C^1), 129.49 (C^2), 125.49 (C^3), 147.22 (C^4), 148.22 (C^5), 122.70 (C^6), 127.06 (C^7), 124.16 (C^8), 137.19 (C^9), 119.06 (C^{10}), 165.40 (C^{11} , imide carbonyl).

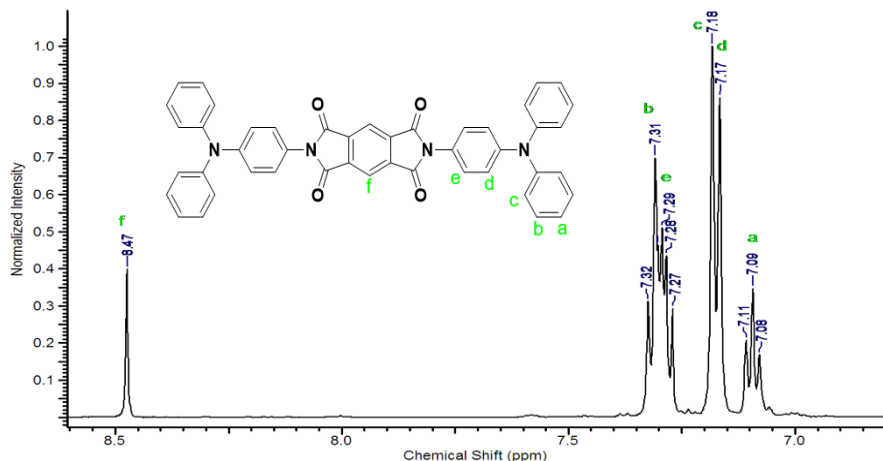


Figure 2.6: ^1H NMR of TPA-Py

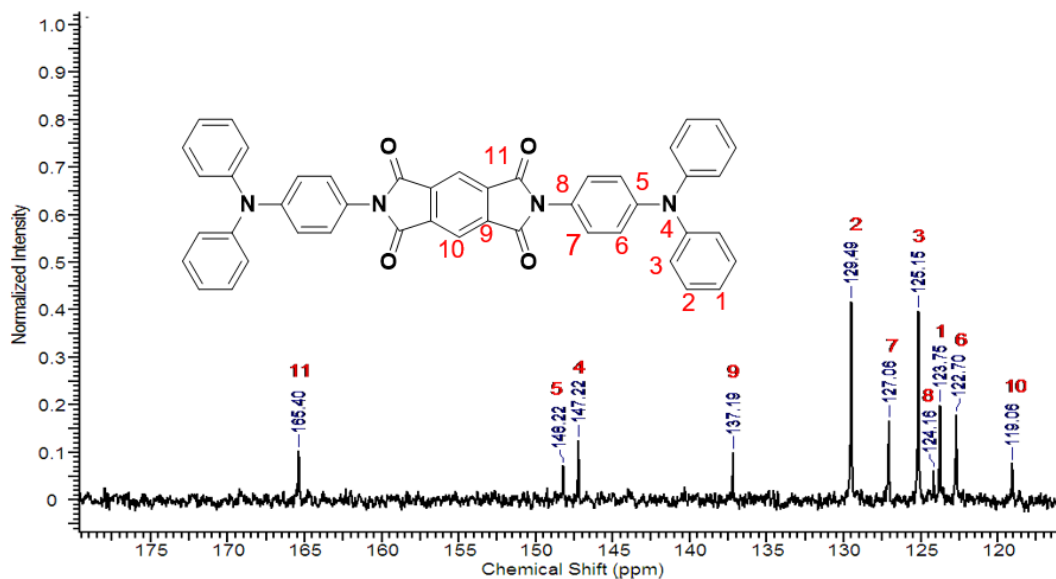


Figure 2.7: ^{13}C NMR of TPA-Py

f) Synthesis of PH-PDI

Procedure: This compound was synthesized by the following literature procedure.¹² A 100 mL round bottom flask equipped with a magnetic stirrer was charged with 0.5 g (1.27 mmol) of 3,4,9,10-perylene tetracarboxylic dianhydride, 0.296 g (3.18 mmol) of aniline, 20 g of

imidazole, and zinc acetate (0.1 g, 0.456 mmol) were heated at 100 °C for 2h. Further, the mixture was heated at 140 °C for 20 h under an argon atmosphere. Then the mixture was cooled to room temperature and acidified with 100 mL of 2 M hydrochloric acid. The precipitate was collected by filtration and washed with plenty of water and methanol to remove impurities and acid. The precipitate was finally dried under a vacuum at 100 °C in a vacuum oven. (yield = 50 %).

2.3 RESULT AND DISCUSSION.

2.3.1 UV-Visible absorption spectroscopy

The absorption spectra were recorded using a dilute solution of the molecules in N-methyl-2-pyrrolidone (NMP). Molecule TPA-PDI showed two sharp peaks at 527 nm and 491 nm and a hump at 460 nm. The frontier orbital difference was found to be 2.3 eV (Figure 2.8). Molecule TPA-NDI showed two peaks at 382 nm, 361 nm, and a hump at 341 nm with a frontier orbital difference of 3.19 eV (Figure 2.8). The frontier orbital difference was calculated to be 4.0 eV (Figure 2.8).

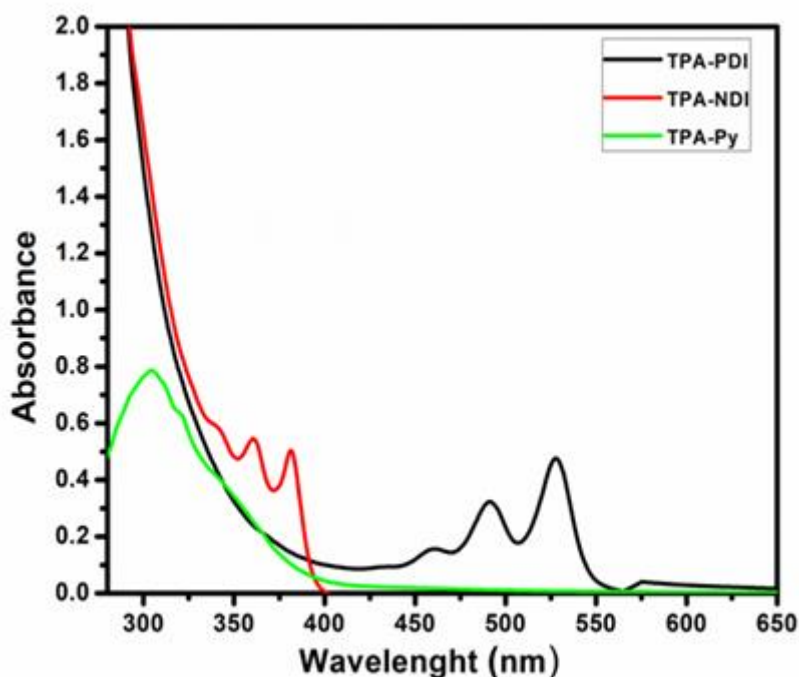


Figure. 2.8: UV-Visible Absorption spectra of molecules TPA-PDI, TPA-NDI and TPA-Py before battery cycling

2.3.2 Morphological study of molecules.

2.3.2.1 Scanning electron microscopy (SEM)

The morphology of the molecular crystals was studied by SEM. The samples were prepared using NMP because of the same solvent we used to measure battery performance. In the SEM image of molecule TPA-PDI, large crystals of rice husk-type morphology were found (Figure 2.9a). Whereas the molecule TPA-NDI and TPA-Py (Figure 2.8c and 2.8e). Show a long needle shape morphology.

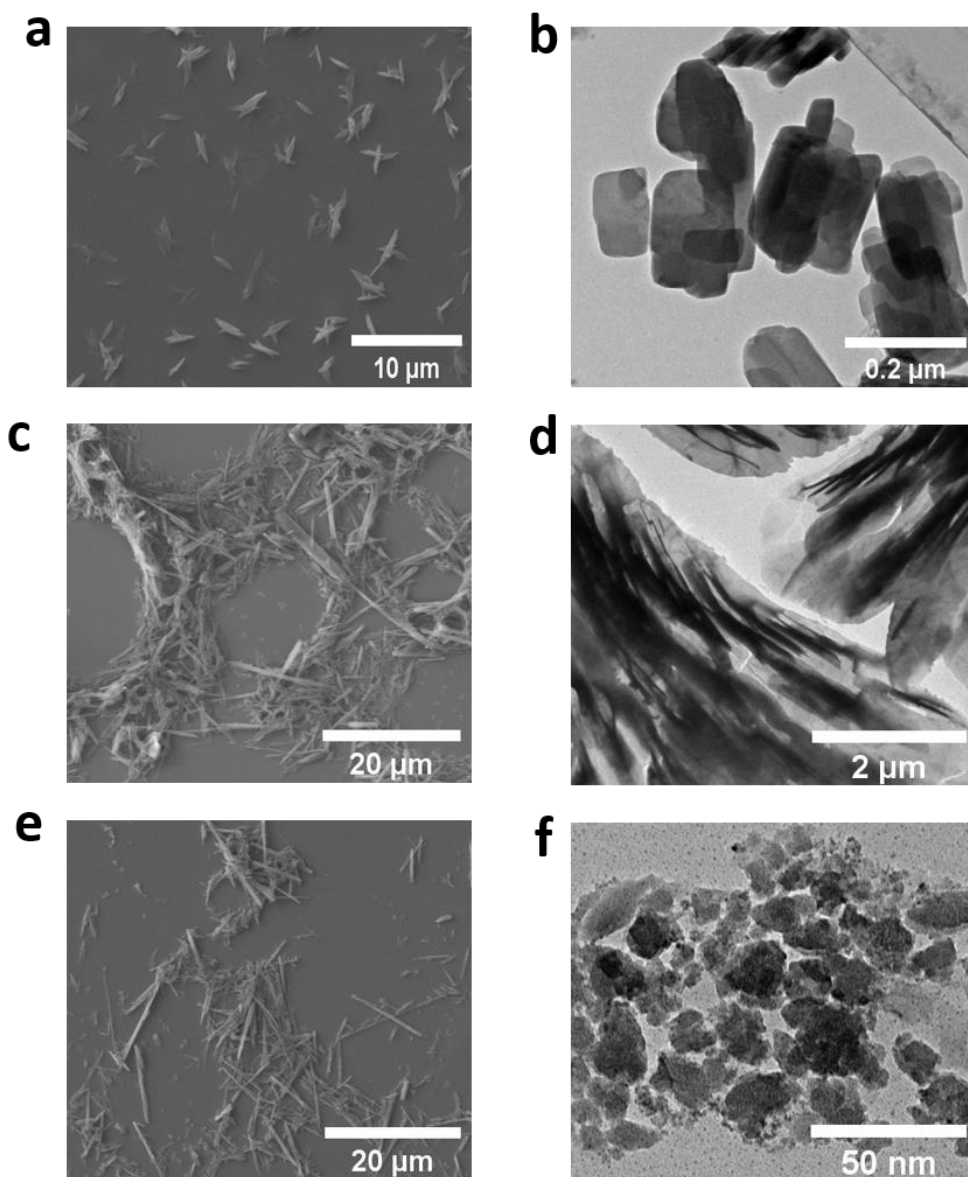


Figure 2.9: SEM image (a) and TEM image (b) of TPA-PDI, SEM image (c) and TEM image (d) of TPA-NDI, SEM image (e) and TEM image (f) of TPA-Py.

2.3.2.2 Transmission electron microscopy (TEM)

TEM images were also recorded in the same solvent, where the rice husk morphology was indeed found. Molecule TPA-PDI (Figure 2.9b) shows the same rice husk morphology. A

long needle shape morphology was retained in TEM for molecules TPA-NDI and TPA-Py. (Figures 2.9d and 2.9f).

2.3.3 Electrochemical performance of molecules.

2.3.3.1 Cyclic voltammetry

Cyclic voltammograms (CVs) of the compounds were recorded in 0.1 M tetrabutylammonium perchlorate (TBAClO₄) in NMP using a Pt wire, and Pt foil as working and auxiliary electrodes, respectively, whereas an Ag/Ag⁺ reference electrode. The potential of an electrode was cycled in the range 0 and -2 V. The CVs of molecule TPA-PDI exhibit two cathodic peaks at -0.82 V and -1.22 V, corresponding to the dianion formation. In the reverse scan, two peaks for the sequential re-oxidation of the dianion were observed (Figure 2.10a). Similarly, two reduction peaks were observed for molecule TPA-NDI during the potential sweep towards -2 V, indicating the formation of the dianion of TPA-NDI. (Figure 2.10a)

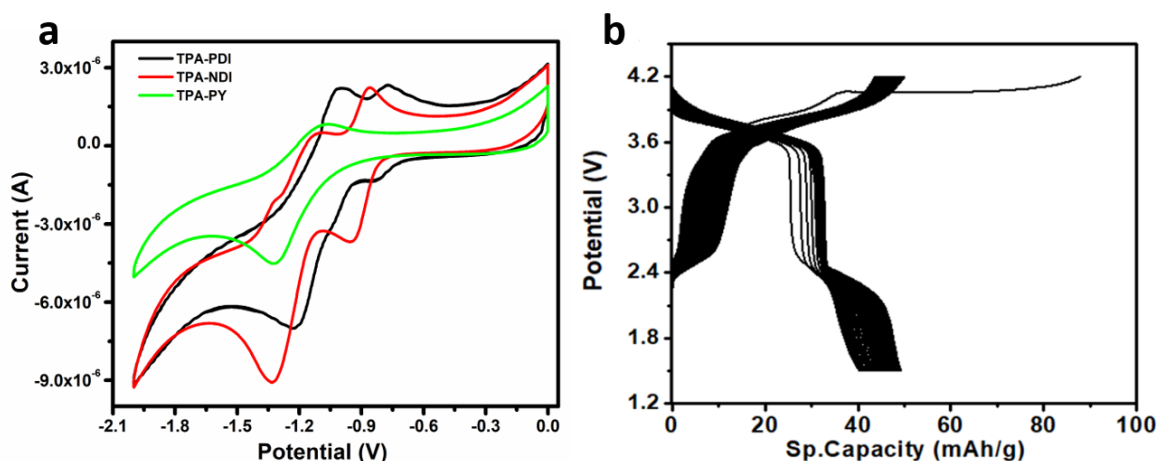


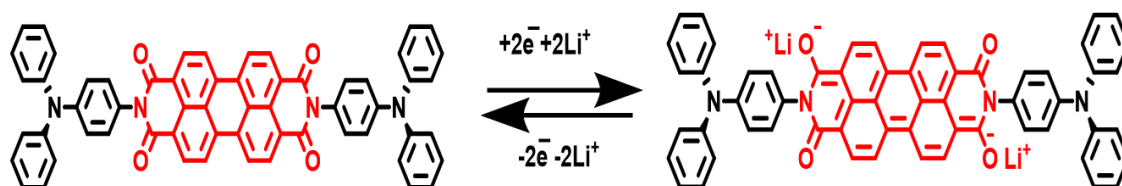
Figure 2.10: cyclic voltammograms (a) of molecules TPA-PDI, TPA-NDI and TPA-Py (b) Charge discharge curve of battery comprising molecule TPA-NDI as cathode, the C rate was 1 C.

Contrary to this, molecule TPA-Py showed only a single reduction peak, (Figure 2.10a) indicating the possibility of radical anion formation in the potential window.

2.3.3.2 Proposed electrochemical redox mechanism of molecules

All synthesized TPA substituted rylene imide derivatives in scheme 2.1 consist of four electrochemically active carbonyl groups, but only two of them participate in the enolate formation mechanism in order to avoid charge repulsion and maintain aromaticity of the

molecule. All these molecules undergo two-electron transfer during the redox reaction, which is the proposed mechanism given below.



2.3.3.3 Galvanostatic Charge/discharge experiments

With this information in hand, LIBs were fabricated in pouch cell configuration using a composite of molecule TPA-PDI or TPA-NDI or TPA-Py, PVDF as a binder, and carbon as conductive filler for one electrode, and lithium foil for the counter electrode.

Table 2.1: Battery metrics for molecules TPA-PDI, TPA-NDI and TPA-Py as a function of charge discharge cycles

Molecule	Charge/ discharge potential window vs Li/Li ⁺	Charge/ discharge C Rate	Sp. capacity at first discharge cycle	Sp. capacity 300th discharge cycle	Percentage decrease sp. capacity as Function of 300 Charge/ discharge Cycle
TPA-PDI	1.5-4.2 V	1C / 1C	55 mAhg ⁻¹	48 mAhg ⁻¹	13%
TPA-NDI	1.5-4.2 V	1C / 1C	63 mAhg ⁻¹	53 mAhg ⁻¹	16%
TPA-Py	1.5-4.2 V	1C / 1C	25 mAhg ⁻¹	20 mAhg ⁻¹	20%

Other details of preparation are provided in the general experimental method and instrumentation section. The charge/ discharge experiment was carried out at various C rates while sweeping the potential range 1.5 and 4.2 V vs. Li/Li⁺.

In the first set of experiments, the charging rate was the same as the discharge rate. The discharge curves of cells with molecule TPA-PDI showed two plateaus in the range 1.5 and 4.2 V vs. Li/Li⁺, indicating two-electron transfers (Figure 2.11a). Similar charge/discharge profiles were observed while using perylenebisimide^{37,38} and naphthalenebisimide³⁹ derivatives in LIBs. The first plateau changed into a slope upon continuous cycling. The specific capacity of the first cycle was 55 mAh/g, which decreased by 13% (Table 2.1) to 48 mAh/g after 300 cycles (Figure 2.11b). The C rate for this

experiment was 1 C. Subsequently, the C rate varied between 0.2 and 30 C, and the specific capacity was monitored. The specific capacity decreased gradually upon an increase in the C rate. At 30 C, the specific capacity was 38 mAh/g, which is ~30% less than that observed at 0.2 C (Figure 2.11c). In most batteries, a decrease in specific capacity is observed with increasing C rates. In all the experiments, the coulombic efficiency was 97%, which did not vary as a function of cycle number.

In the next set of experiments, the LIBs were charged at a slow C rate of 0.2 C, while different C rates between 0.2 C and 30 C were applied for discharge. This cell exhibits the specific capacity of 61 mAh/g when charged and discharged at 0.2 C. The specific capacity decreased to 49 mAh/g when the discharge rate was increased to 30 C (Figure 2.11c). The decrease is 20% compared to 30% observed for charge and discharge rate to 30 C. As expected, the performance of the tested LIBs increased by slowly charging the cell.

In the next set of experiments, molecule TPA-NDI was used to prepare the active cathode material. The discharge curves showed two plateaus, one between 4.2 and 3.6 V and the second between 2.4 to 2.1 V (Figure 2.10b). The two plateaus arise due to two-electron reductions of two carbonyl groups to two enolate groups. As shown in Table 2.1, the specific capacity decreased by 16% after 300 charge-discharge cycles. The decrease in specific capacity as a function of cycle number is comparable to that of molecule TPA-PDI. At a charging rate of 0.2 C and a discharge same rate, the specific capacity was 61 mAh/g. The specific capacity decreased by 75% to 15 mAh/g upon an increase in charging and discharging rates to 30 C (Figure 2.11d). Subsequently, the LIB was charged at 0.2 C, and the discharge experiment was conducted at C rates between 0.2 C and 30 C. At 0.2 C, the specific capacity was calculated to be 64 mAh/g, which decreased by 50% upon an increase in C rate to 30 C (Figure 2.11d). The 50% decrease in specific capacity for the LIB with compound TPA-NDI at charging/discharging rates of 0.2 C / 30 C is lower than the 75% loss when charging/discharging at 30 C / 30 C but significantly higher than the 20% observed for the LIB with molecule TPA-PDI upon charging/ discharging at 30 C / 30 C.

In the next set of experiments, molecule TPA-Py was tested in the battery. Unlike molecules TPA-PDI and TPA-NDI, only a single plateau was observed in the range 4.2 and 3.4 V vs. Li/Li⁺ for the LIB made from the compound TPA-Py (Figure 2.11e). It has been shown that two electrons are transferred for PyDI between 1.5 V to 3 V.³¹ A decrease of 20% in specific capacity was observed later 300 charge/discharge cycles (Table 2.1). At 0.2 C, a specific capacity was 29 mAh/g, which decreased by 99% to 0.06 mAh/g at 30 C (Figure 2.11f).

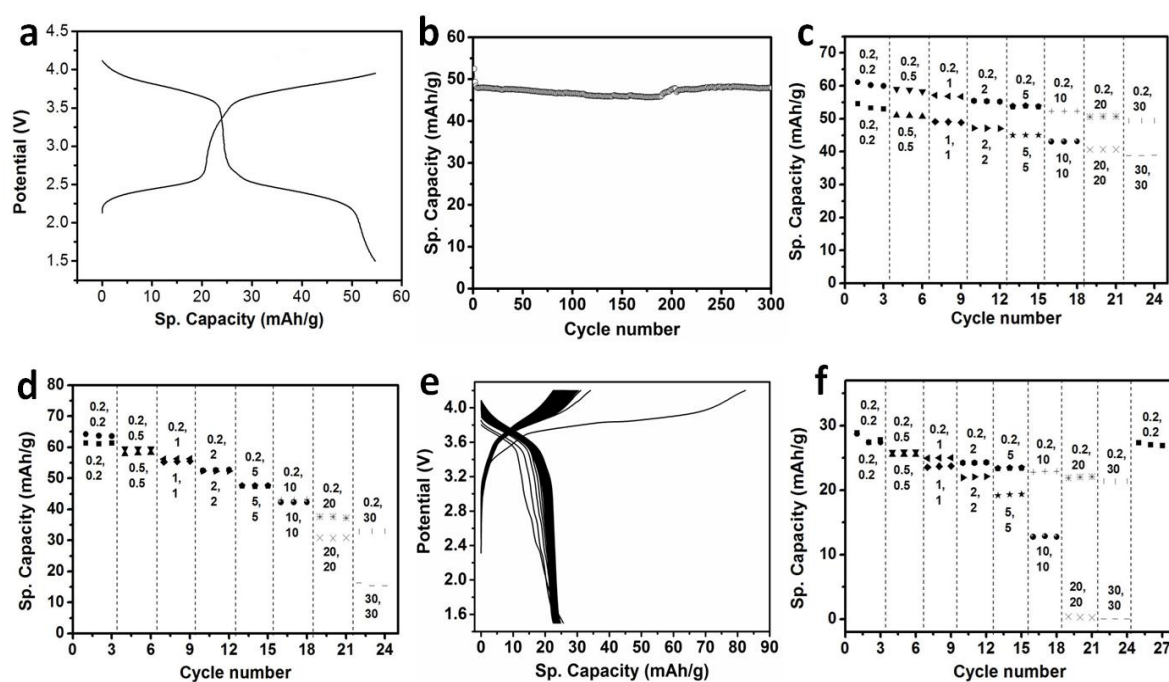
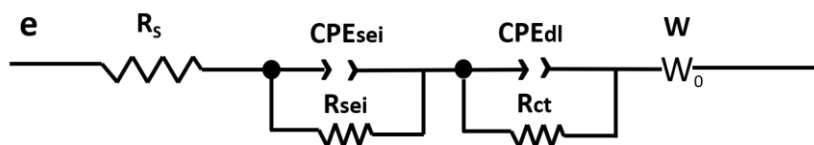


Figure 2.11: (a) Charge-discharge profile of molecule 4 at a C rate of 1 C. (b) Variation of specific capacity as a function of number of charge discharge cycles while using molecule TPA-PDI as cathode at a C rate of 1 C. (c) Specific capacity variation of a battery with molecule TPA-NDI as a function of C rate variation. (d) The effect of C rate variation on specific capacity while using molecule TPA-NDI as battery cathode. (e) Charge discharge curve of battery comprising molecule TPA-Py as cathode, the C rate was 1 C. (f) Specific capacity variation as a function of C rate for battery comprising molecule TPA-Py as cathode.

However, when subsequently charged and discharged at 0.2 C, the specific capacity bounced back to 27 mAh/g, which is quite close to the 29 mAh/g observed at the start of the charge-discharge experiments (Figure 2.11f). Therefore, the extremely small specific capacity observed at 30 C is not due to the degradation of the LIB. This is contrary to an earlier observation, wherein the experimentally observed decrease of the specific capacity to 23% was attributed to the dissolution of the PyDI molecules during battery cycling.³⁹ Finally, the LIB was charged at 0.2 C and discharged at C rates between 0.2 C and 30 C. A specific capacity of the LIBs discharged at 0.2 C (29 mAh/g) decreased by 28% to 21 mAh/g at 30 C (Figure 2.11f). Thus, the capacity is much less sensitive to high discharge rates (28% loss in specific capacity) than to high charging rates (99% loss in specific capacity).

2.3.3.4 Electrochemical impedance spectroscopy (EIS)

We hypothesize that TPA will facilitate lithium-ion diffusion. To measure the diffusion coefficient of lithium ions (DLi^+), impedance spectra were recorded, and a Nyquist plot was plotted for TPA-PDI, TPA-NDI, TPA-Py, and PH-PDI (figure 2.11 a, b, c, d). To fit Nyquist plots following equivalent circuit was used.



Equivalent circuit to fit Nyquist plot

The linear part of the EIS at the lower frequency present in the Nyquist plot is related to the Li^+ diffusion in the electrode, which can be calculated by using the following formula reported in the procedure.³⁵

$$D_{Li^+} = \frac{0.5R^2T^2}{F^4A^2C^2\sigma^2}$$

Where R is the gas constant, T is the temperature, F is the Faraday constant, A is the area of the electrode, n is the number of electrons involved in the reaction, and C is the concentration of Li^+ in the electrode, and σ is the Warburg factor. σ (Warburg factor) obtained from the slope of $1/\omega^{1/2}$ vs. Z' (ω is the angular frequency) in the Warburg plot Li^+ . From the Nyquist plot, the highest DLi^+ ($3.7 \times 10^{-13} \text{ cm}^2 \text{ s}^{-1}$) was observed for molecule TPA-Py, which is an order of magnitude higher than that observed for TPA-PDI ($3.7 \times 10^{-14} \text{ cm}^2 \text{ s}^{-1}$), (Table 2.2). Molecule TPA-Py has one aromatic unit that is attached to two TPA moieties, hence the closeness of the TPA precludes the close packing of TPA-Py. Thus, the lithium-ion diffusion is faster. On the other hand, the four aromatic units keep the TPA moieties apart in the molecule TPA-PDI. Therefore, close packing is still possible in TPA-PDI, leading to decreased lithium-ion diffusion (Table 2.2). Although molecule TPA-PDI exhibits the lowest DLi^+ among the series reported in this work, it still showed higher DLi^+ compared to control molecule PH-PDI with phenyl substituents (Scheme 2.1). This corroborates our hypothesis that TPA is likely to facilitate lithium-ion transport.

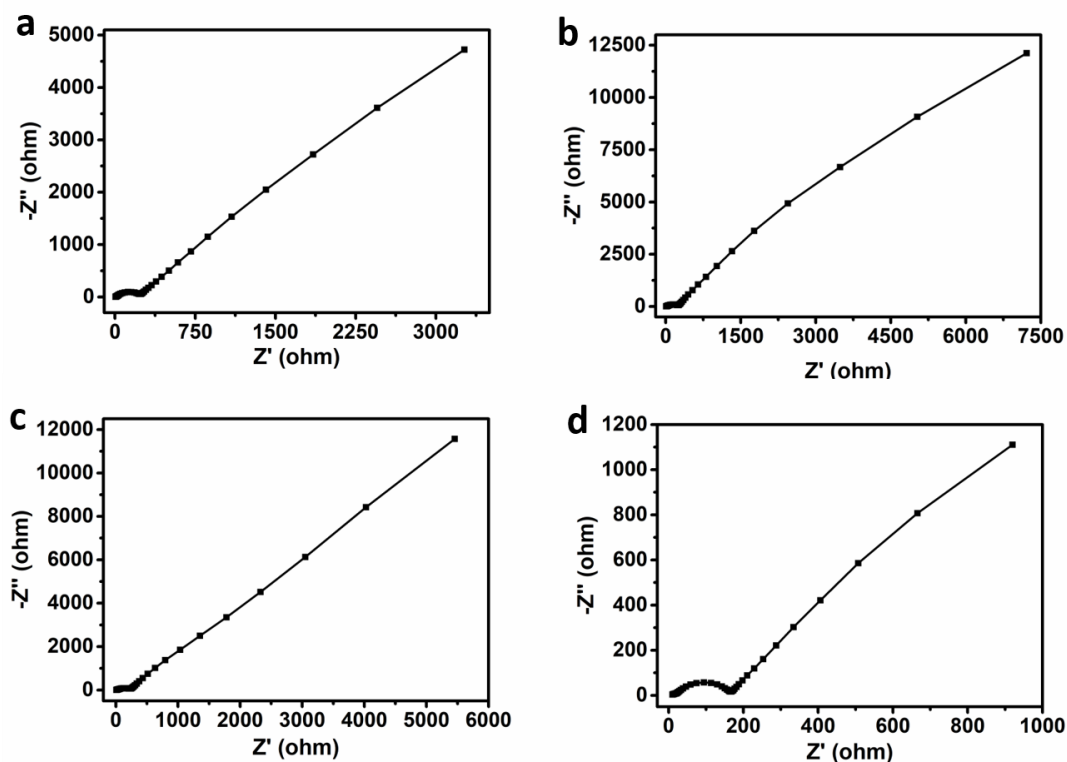


Figure 2.12: Nyquist plot of molecule (a) TPA-PDI, (b) TPA-NDI, (c) TPA-Py and (d)

Table 2.2: The Warburg factor and Diffusion co-efficient for the molecule TPA-PDI, TPA-NDI, TPA-Py and PH-PDI

Molecule	Warburg factor (σ) (Ohm s ^{-1/2})	Diffusion Coefficient (cm ² s ⁻¹)
TPA-PDI	706	2.28*10 ⁻¹⁴
TPA-NDI	372	8.21*10 ⁻¹⁴
TPA-Py	176	3.67*10 ⁻¹⁴
PH-PDI	1186	8.08*10 ⁻¹⁴

2.3.4 Effect of TPA substitution on solubility in the electrolyte.

2.3.4.1 Morphological study of molecules by SEM before and after batteries cycling.

In order to study the fate of the molecular crystal morphology during charge-discharge experiments (1.5 V to 4.2) over 300 cycles. The morphology was studied with the fabricated electrode before cycling, the LIB was opened, and the morphology was studied after 300 cycles by SEM. The SEM images indicated the retention of the rice husk morphology for fabricated electrodes before (Figure 2.13a) and after (Figure 2.13b). batteries cycling (300 Cycles) for TPA-PDI. The same experiment repeats for TPA-NDI and TPA-Py, where we found to be long needle morphologies of TPA-NDI fabricated electrodes before (Figure 2.13c) and after (Figure 2.13d) were retained in their blends. The morphology of the TPA-Py fabricated electrode before (Figure 2.13e) and after (Figure 2.13 f) does not seem to be an exact long needle. The charge-discharge cycling caused a change in the surface roughness, but we did not find significant changes in the morphologies of any molecules. This experiment indicates that molecules do not become soluble in electrolytes due to the exact morphology seems after the charge-discharge experimentation.

2.3.4.2 UV-Visible absorption spectroscopy

To check the existence of molecules after charge/discharge cycling, we analyzed the battery electrolyte to identify the presence of dissolved molecules. For this experiment, the battery was opened after 100 cycles. The electrolytes were mixed with fresh NMP, which dissolves molecules TPA-PDI, TPA-NDI, and TPA-Py. The absorption spectra were recorded between 250 and 700 nm. We observed all the peaks corresponding to molecules TPA-PDI, TPA-NDI, and TPA-Py (Figure 2.14), confirming the dissolution of molecules during the charge-discharge cycling. However, this data must be correlated with battery performance. It must be noted that the decrease in specific capacity of batteries comprising molecule 4 is 13% after 300 charge-discharge cycles. However, the decrease in specific capacity is 84% for the control molecule (PH-PDI) with phenyl moiety instead of TPA (Scheme 2.1).¹² Therefore, as hypothesized, the TPA decreases the solubility of rylene imide molecules in battery electrolytes. Due to the decreased solubility, the specific capacity fading is 13% (section charge-discharge performance) for molecule TPA-PDI, but the decrease is 84% for control molecule PH-PDI.¹²

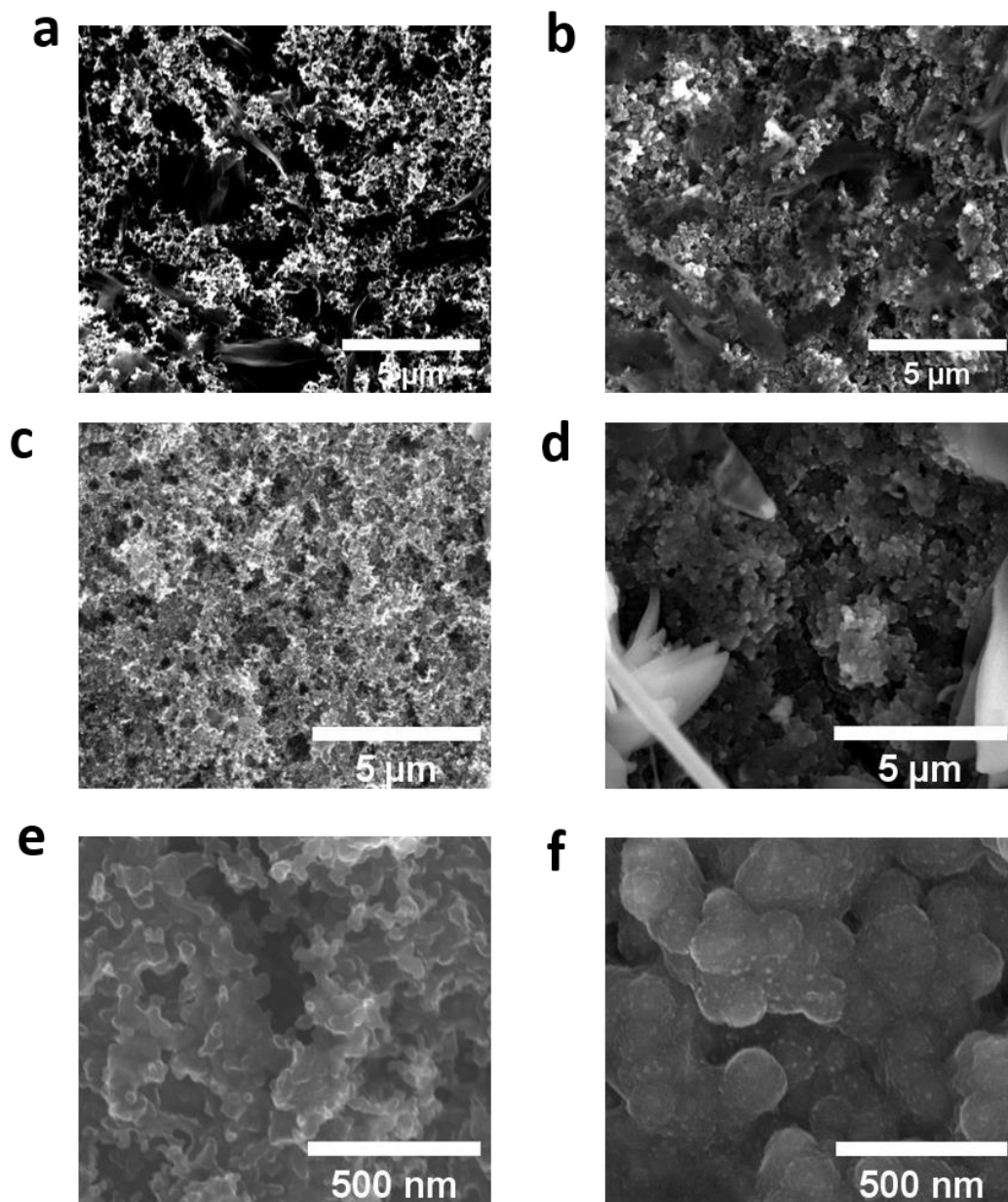


Figure 2.13: SEM images show that the battery electrodes before (a) and after 300 cycles (b) of TPA-PDI, SEM images show that the battery electrodes before (c) and after 300 cycles (d) of TPA-NDI SEM images show that the battery electrodes before (e) and after 300 cycles of TPA-Py. (f)

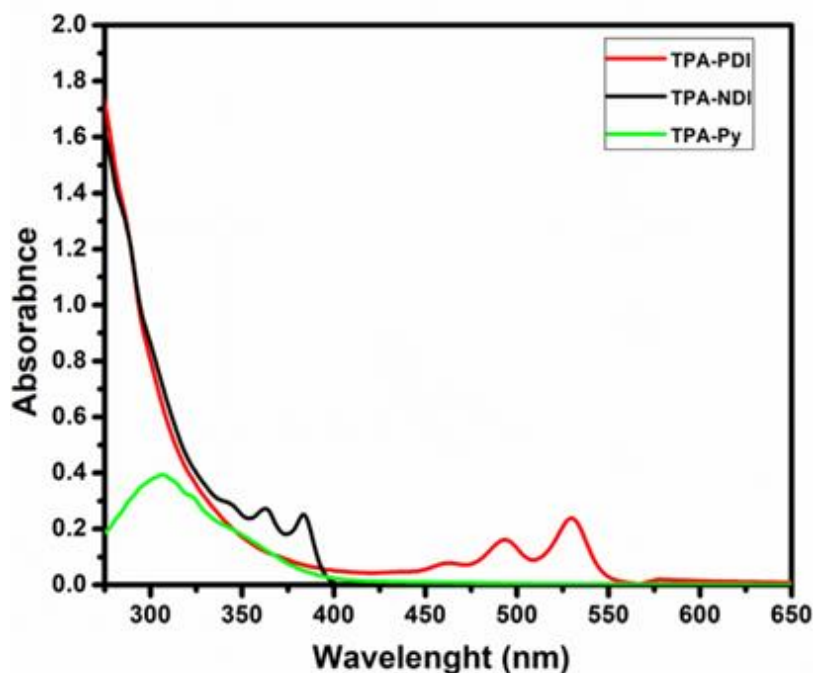


Figure. 2.14: UV-Visible Absorption spectra of molecules TPA-PDI, TPA-NDI and TPA-Py after battery cycling

2.4 CONCLUSION

TPA acts as an effective moiety to disrupt the aggregation of RIs without causing solubility of the molecule in battery electrolytes. The three molecules chosen from the RIs family have different numbers of aromatic units. The theoretical capacity of the RIs is expected to decrease with the number of aromatic rings in the rylene imides core of the molecule. Contrary to this, the experimental specific capacities varied with the number of aromatic units in the sequence $1 < 4 < 2$. Thus, decreasing the molecular weight alone does not impart improvement in battery performance. TPA is certainly a good motif to facilitate lithium-ion transport in solid RI molecules and improves crystal stability during charge-discharge experiments. All the RIs showed impressive cycling stability over 300 cycles. Molecules with few aromatic core units (TPA-Py) conjugated with redox functionality are not suitable for rapid charge-discharge experiments. Supporting to this, we found an extremely small specific capacity of 0.06 mAh/g for a molecule with one aromatic unit. Contrary to this, the specific capacity of the molecule with two aromatic rings showed a four order of magnitude higher specific capacity. From this study, we have identified that the TPA motif facilitates the design of efficient organic materials for LIBs.

2.5 REFERENCES

- (1) Armand, M.; Tarascon, J.-M. Issues and challenges facing rechargeable lithium batteries. *Nature* **2001**, *414*, 359-367.
- (2) Palacín, M. R. Recent advances in rechargeable battery materials: a chemist's perspective. *Chem. Soc. Rev.* **2009**, *38*, 2565-2575.
- (3) Deng, D. Li-ion batteries: basics, progress, and challenges. *Energy Sci. Eng.* **2015**, *3*, 385-418.
- (4) Bhosale, M. E.; Chae, S.; Kim, J. M.; Choi, J.-Y. Organic small molecules and polymers as an electrode material for rechargeable lithium ion batteries. *J. Mater. Chem. A* **2018**, *6*, 19885-19911.
- (5) Hesse, H. C.; Schimpe, M.; Kucevic, D.; Jossen, A. Lithium-Ion Battery Storage for the Grid-A Review of Stationary Battery Storage System Design Tailored for Applications in Modern Power Grids. *Energies* **2017**, *10*, 2107-2149.
- (6) Mizushima, K.; Jones, P.; Wiseman, P.; Goodenough, J. Li_xCoO_2 ($0 < x \leq 1$): A new cathode material for batteries of high energy density. *Solid State Ionics* **1981**, *3*, 171-174.
- (7) Zhang, W. M.; Wu, X. L.; Hu, J. S.; Guo, Y. G.; Wan, L. Carbon Coated Fe_3O_4 Nanospindles as a Superior Anode Material for Lithium-Ion Batteries. *J. Adv. Funct. Mater.* **2008**, *18*, 3941-3946.
- (8) Qie, L.; Chen, W. M.; Wang, Z. H.; Shao, Q. G.; Li, X.; Yuan, L. X.; Hu, X. L.; Zhang, W. X.; Huang, Y. H. Nitrogen-Doped Porous Carbon Nanofiber Webs as Anodes for Lithium Ion Batteries with a Superhigh Capacity and Rate Capability. *Adv. Mater.* **2012**, *24*, 2047-2050.
- (9) Flandrois, S.; Simon, B. Carbon materials for lithium-ion rechargeable batteries. *Carbon* **1999**, *37*, 165-180.
- (10) Endo, M.; Kim, C.; Nishimura, K.; Fujino, T.; Miyashita, K. Recent development of carbon materials for Li ion batteries. *Carbon* **2000**, *38*, 183-197.
- (11) Shia, Y.; Zhanga, M.; Qianb, D.; Meng, Y. S. Ultrathin Al_2O_3 Coatings for Improved Cycling Performance and Thermal Stability of $\text{LiNi}_{0.5}\text{Co}_{0.2}\text{Mn}_{0.3}\text{O}_2$ Cathode Material. *Electrochim. Acta* **2016**, *203*, 154-161.
- (12) Bhosale, M. E.; Krishnamoorthy, K. Chemically Reduced Organic Small-Molecule-Based Lithium Battery with Improved Efficiency. *Chem. Mater.* **2015**, *27*, 2121-2126.

- (13) Vadehra, G. S.; Maloney, R. P.; Garcia-Garibay, M. A.; Dunn, B. Naphthalene Diimide Based Materials with Adjustable Redox Potentials: Evaluation for Organic Lithium-Ion Batteries. *Chem.Mater.* **2014**, *26*, 7151-7157.
- (14) Guo, C. X.; Wang, M.; Chen, T.; Lou, X. W.; Li, C. M. Hierarchically Nanostructured Composite of MnO₂/Conjugated Polymer/Graphene for High-Performance Lithium Ion Batteries. *Adv. Energy Mater.* **2011**, *1*, 736-741.
- (15) Armand, M.; Tarascon, J.-M. Building Better Batteries. *Nature.* **2008**, *451*, 652-657.
- (16) Liang, Y.; Tao, Z.; Chen, J. Organic Electrode Materials for Rechargeable Lithium Batteries. *Adv. Energy Mater.* **2012**, *2*, 742-769.
- (17) Kurimoto, N.; Omoda, R.; Mizumo, T.; Ito, S; Aihara, Y.; Itoh, T. Four-electron transfer tandem tetracyanoquinodimethane for cathode-active material in lithium secondary battery. *J. Power Sources* **2018**, *377*, 12-17.
- (18) Wu, Y.; Zeng, R.; Nan, J.; Shu, D.; Qiu, Y.; Chou, S. L. Quinone Electrode Materials for Rechargeable Lithium/Sodium Ion Batteries. *Adv. Energy Mater.* **2017**, *7*, 1700278-1700304.
- (19) Kim, M. G.; Cho, J. Reversible and High-Capacity Nanostructured Electrode Materials for Li-Ion Batteries. *Adv. Funct. Mater.* **2009**, *19*, 1497-1514.
- (20) Morita, Y.; Nishida, S.; Murata, T.; Moriguchi, M.; Ueda, A.; Satoh, M.; Arifuku, K.; Sato, K.; Takui, T. Organic tailored batteries materials using stable open-shell molecules with degenerate frontier orbitals. *Nat. Mater.* **2011**, *10*, 947-951.
- (21) Han, X.; Chang, C.; Yuan, L.; Sun, T.; Sun, J. Aromatic Carbonyl Derivative Polymers as High-Performance Li-Ion Storage Materials. *Adv. Mater.* **2007**, *19*, 1616-1621
- (22) Wu, D.; Zhang, G.; Lu, D.; Ma, L.; Xu, Z.; Xi, X.; Liu, R.; Liu, P.; Su, Y. Perylene diimide-diamine/carbon black composites as high performance lithium/sodium ion battery cathodes. *J. Mater. Chem. A* **2018**, *6*, 13613-13618.
- (23) Wu, H.; Wang, K.; Meng, Y.; Lua, K.; Wei, Z. An organic cathode material based on a polyimide/CNT nanocomposite for lithium ion batteries. *J. Mater. Chem. A* **2013**, *1*, 6366-6372.
- (24) Sharma, P.; Damien, D.; Nagarajan, K.; Shaijumon, M. M.; Hariharan, M. Perylene-polyimide-Based Organic Electrode Materials for Rechargeable Lithium Batteries. *J. Phys. Chem. Lett.* **2013**, *4*, 3192-3197.

- (25) Veerababu, M.; Kothandaraman, R. Rational Functionalization of Perylene Diimide for Stable Capacity and Long-term Cycling Performance for Li-ion Batteries. *Electrochim. Acta* **2017**, *232*, 244-253.
- (26) Medabalmi, V.; Ramanujam, K. Glycination: A Simple Strategy to Enhance the Cycling Performance of Perylene Dianhydride for Secondary Li-Ion Battery Applications. *ChemistrySelect* **2018**, *3*, 10657-10662.
- (27) Chen, C.; Zhao, X.; Li, H.-B.; Gan, F.; Zhang, J.; Dong, J.; Zhang, Q. Naphthalene-based Polyimide Derivatives as Organic Electrode Materials for Lithium-ion Batteries. *Electrochim. Acta* **2017**, *229*, 387-395.
- (28) Shestakov, A.; Yarmolenko, O.; Ignatova, A.; Mumyatov, A.; Stevenson, K.; Troshin, P. Structural origins of capacity fading in lithium-polyimide batteries. *J. Mater. Chem. A* **2017**, *5*, 6532-6537.
- (29) Huang, Y.; Li, K.; Liu, J.; Zhong, X.; Duan, X.; Shakirc, I.; Xu, Y. Three-dimensional graphene/polyimide composite-derived flexible high-performance organic cathode for rechargeable lithium and sodium batteries. *J. Mater. Chem. A* **2017**, *5*, 2710-2716.
- (30) Renault, S.; Mihali, V. A.; Edström, K.; Brandell, D. Stability of organic Na-ion battery electrode materials: The case of disodium pyromellitic diimide. *Electrochem. Commun.* **2014**, *45*, 52-55.
- (31) Renault, S.; Geng, J.; Dolhem, F.; Poizot, P. Evaluation of polyketones with N-cyclic structure as electrode material for electrochemical energy storage: case of pyromellitic diimide dilithium salt. *Chem. Commun.* **2011**, *47*, 2414-2416.
- (32) Song, Z.; Zhan, H.; Zhou, Y. Polyimides: Promising Energy-Storage Materials. *Angew. Chem.* **2010**, *49*, 8444-8448.
- (33) Hsiao, S.-H.; Chen, Y.-Z. Electroactive and ambipolar electrochromic polyimides from arylene diimides with triphenylamine N-substituents *Dyes Pigm.* **2017**, *144*, 173-183.
- (34) Mayers, B. T.; Fry, A. J. Construction of Electrocatalytic Electrodes Bearing the Triphenylamine Nucleus Covalently Bound to Carbon. A Halogen Dance in Protonated Aminotriphenylamines. *Org. Lett.* **2006**, *8*, 411-414.
- (35) Hsiao, S.-H.; Chiu, Y.-T. Electrosynthesis and electrochromic properties of poly(amide-triarylamines) containing triptycene units. *RSC Adv.* **2015**, *5*, 90941-90951.

- (36) Li, L.; Gong, H.-X.; Chen, D.-Y.; Lin, M.-J. Stable Bifunctional Perylene Imide Radicals for High-Performance Organic–Lithium Redox-Flow Batteries. *Chem. Eur. J.* **2018**, *24*, 13188-13196.
- (37) Li, L.; Hong, Y.-J.; Chen, D.-Y.; Lin, M.-J. Molecular Engineering of Perylene Imides for High-Performance Lithium Batteries: Diels–Alder Extension and Chiral Dimerization. *Chem. Eur. J.* **2017**, *23*, 16612 -16620.
- (38) Chen, D.; Avestro, A.-J.; Chen, Z.; Sun, J.; Wang, S.; Xiao, M.; Erno, Z.; Algaradah, M. M.; Nassar, M. S.; Amine, K.; Meng, Y.; Stoddart, J. F.; A Rigid Naphthalenediimide Triangle for Organic Rechargeable Lithium-Ion Batteries. *Adv. Mater.* **2015**, *27*, 2907–2912.
- (39) Nalluri, S. K. M.; Liu, Z.; Wu, Y.; Hermann, K. R.; Samanta, A.; Kim, D. J.; Krzyaniak, M. D.; Wasielewski, M. R.; Stoddart, J. F. Chiral Redox-Active Isosceles Triangles. *J. Am. Chem. Soc.* **2016**, *138*, 5968–5977.

CHAPTER 3

**An Insoluble Naphthalic Anhydride Based Rylene
Imide Derivatives Cathode for Lithium-ion
Batteries.**

3.1 INTRODUCTION

Nowadays, energy storage technology is boosted because of depleting fossil fuel sources and plenty of available renewable energy sources. Energy Storage devices should not just provide the expected energy for the desired demand, again should provide the most adaptable, lighter, environmentally sustainable, and cheaper proposal.¹⁻⁶ However, advances in LIBs technologies execute a revelatory role in portable electronics and automobile technologies.⁷⁻⁹ Commercially available LIBs have graphite anode materials and oxides of lithium as cathode materials.¹⁰ Though these batteries provide long cycle life, energy densities are bounded by the number of redox-active position present, and capacities are often in the order of ~ 200 mAh/g.¹¹ Thus, the dependence is on classic inorganic intercalated cathodes,¹²⁻¹⁵ are not environmentally benign and not commercially feasible. Because nearly all inorganic-based cathode contains heavy metals such as Co, Mn, and Fe, thus the use of such toxic and geopolitical squabble materials in terms of environmental issues and supply chain risk. Hence, such materials force the development of alternatives, which can able to seek the understanding between performance and sustainability. However, alternative utilization of sustainable and eco-friendly organic cathode,¹⁶⁻¹⁸ will significantly reduce the use of inorganic materials. Organic material has an attractive prospect that is the tuneable molecular core and high structural versatility, which afford an advantage over inorganic counterparts.¹⁹⁻²⁸ these materials cover an entire range of structures, consisting of small molecules, polymers, and COF.^{29,30} Electrochemical activity is finely changed by a wise option of functional groups containing lighter elements and power groups which allow for large energy and flexibility. For instance, a synthesis of rylene dyes compounds by incorporating cyclic anhydride by oxidation of acenaphthene.³¹ this carbonyl group containing rylene dyes clears the probability of a cheaper cathode consisting of high theoretical capacity.⁴ A challenging obstacle and eventually the prime downside of the organic cathode at this stage is their solubility in liquid electrolytes. Along with Long-term cycling of charging/ discharging, organics materials result in solubilizing in the organic electrolyte, leading to an obvious capacity fading.

Due to the presence of the carbonyl group and extended aromatic structure, rylene dyes itself insoluble in liquid electrolytes. But it also comes up with the obstacle that is the substantial aggregation of these dyes slowing down the lithium-ion transport in the active organic materials.³² Rylene dyes without substitution may undergo cyclic anhydride bond opening during charging/discharging, which will lead to a decreased discharge potential.

Previously studied TPA (Triphenyl amine) substituent effect on rylene dyes, in terms of their electrochemical properties and solubility. It is found that TPA acts as an effective moiety to disrupt the aggregation of RIs (rylene imides) without compromising the solubility of the molecule in battery electrolytes.³³ However, TPA is not an electrochemical active; thus, even it helps disturb the aggregation and decrease the solubility due to their extended aromatic conjugation with parent rylene dyes but unnecessary increase in the molecular weight of the compound, which was getting down to decrease in theoretical capacity.

To resolve this problem, such as solubility in liquid electrolytes, aggregation, and theoretical capacity herein, we introduced naphthalene anhydride substituted rylene imide compounds, namely UN-PDI, UN-NDI, and UN-Py. (Scheme 3.1) For synthesizing this carbonyl-containing conjugated system, a simple imidization reaction did with amine-containing anhydride (UN-NH₂) and parental Rylene dyes. (PDA, NDA, and PMDA) After condensation reaction, the cyclic anhydride group becomes a cyclic imide that is very stable thermally and electrochemically. The arrangement of naphthalic anhydride in UN-PDI, UN-NDI, and UN-Py may be perpendicular to the parent rylene dyes; thus, it's useful for avoiding the aggregation of compounds. However, naphthalic anhydride also has an electrochemically active carbonyl group that participates in increasing the theoretical capacity of compounds. Even extended conjugation of naphthalic anhydride over rylene dyes will help resolve the solubility problem in liquid electrolytes. For long-term cycling, we have hypothesized that a large aromatic building block with an electrochemically active carbonyl group could enhance the stability of the organic electrode.³⁴

3.2 EXPERIMENTAL SECTION

3.2.1 Chemicals and Materials

The chemicals and reagents purchased commercially are used as such without further purification. Perylene-3,4,9,10-tetracarboxylic dianhydride, (PDA) 1,4,5,8-naphthalene (NDA) tetracarboxylic dianhydride, pyromellitic dianhydride, (PMDA) zinc acetate, and Imidazole were purchased from Sigma-Aldrich. Hydrazine hydrate and 1,8-Naphthalic anhydride were purchased from TCI chemical India. Dimethylformamide (DMF) chloroform (CHCl₃), Tetrahydrofuran (THF), dichloromethane (DCM), and acetone were purchased from Merck Chemicals. A battery-grade salt Bis(trifluoromethane)sulfonamide lithium salt (LiTFSI) and Polyvinyl difluoride (PVDF, Kynar HSV900, Arkema Inc., USA) was purchased from sigma Aldrich. 1,3-dioxolane (DOL), and 1,2 Dimethoxyethane (DME)

N-Methyl-2-pyrrolidone (NMP) solvent used for battery performance were purchased from Sigma Aldrich (HPLC grade).

3.2.2 Instrumentation and general Experiments method.

Structural characterization of molecules was done by recording their ^1H and ^{13}C NMR spectra at room temperature on Bruker-AVENS, 400 or 500 MHz NMR instruments. Deuterated Dimethyl sulfoxide (DMSO- d_6) and Sulfuric acid - d_2 solution (D_2SO_4) were used as a solvent in a trace amount of TMS as an internal reference. Chemical shifts of all compounds are reported in δ ppm downfield to TMS, and peak multiplicities are referred to as singlet (s), doublet (d), triplet (t), quartet (q), pentet (p), and multiplet (m). Analytical thin-layer chromatography was performed on pre-coated silica gel plates (Kiesel gel 60F254, Merck). UV-vis absorption spectra were recorded on SPECORD® 210/PLUS, a UV-visible spectrophotometer with deuterium and tungsten lamps as the source. The morphological characterizations of molecules were performed using FE-SEM with an FEI Nova Nano SEM 450. Infrared spectra (IR) were recorded on a Bruker α -T spectrophotometer with sample pellets prepared by mixing with 5% w/w in KBr and dried under a vacuum before spectra were recorded. Thermogravimetric analysis (TGA) was recorded by using PerkinElmer STA 6000 Thermogravimetric Analyzer. Samples were scanned from 50 °C to 800 °C with a heating rate of 10 °C/ min under an inert nitrogen atmosphere. The cyclic voltammetry experiments were performed in a multi-channel auto lab MAC 80038 instrument with a potential range of 1- 4 V vs. Li/Li $^+$. Electrochemical Impedance Spectroscopy measurements were done in the frequency range of 10 MHz to 40 kHz using a Biologic instrument. The galvanostatic charging/discharging experiments were carried out by using CR 2032-type coin cells on a Neware battery testing system (BTS7.5.6, Shenzhen, China) in the potential range of 1-4 V vs. Li/Li $^+$.

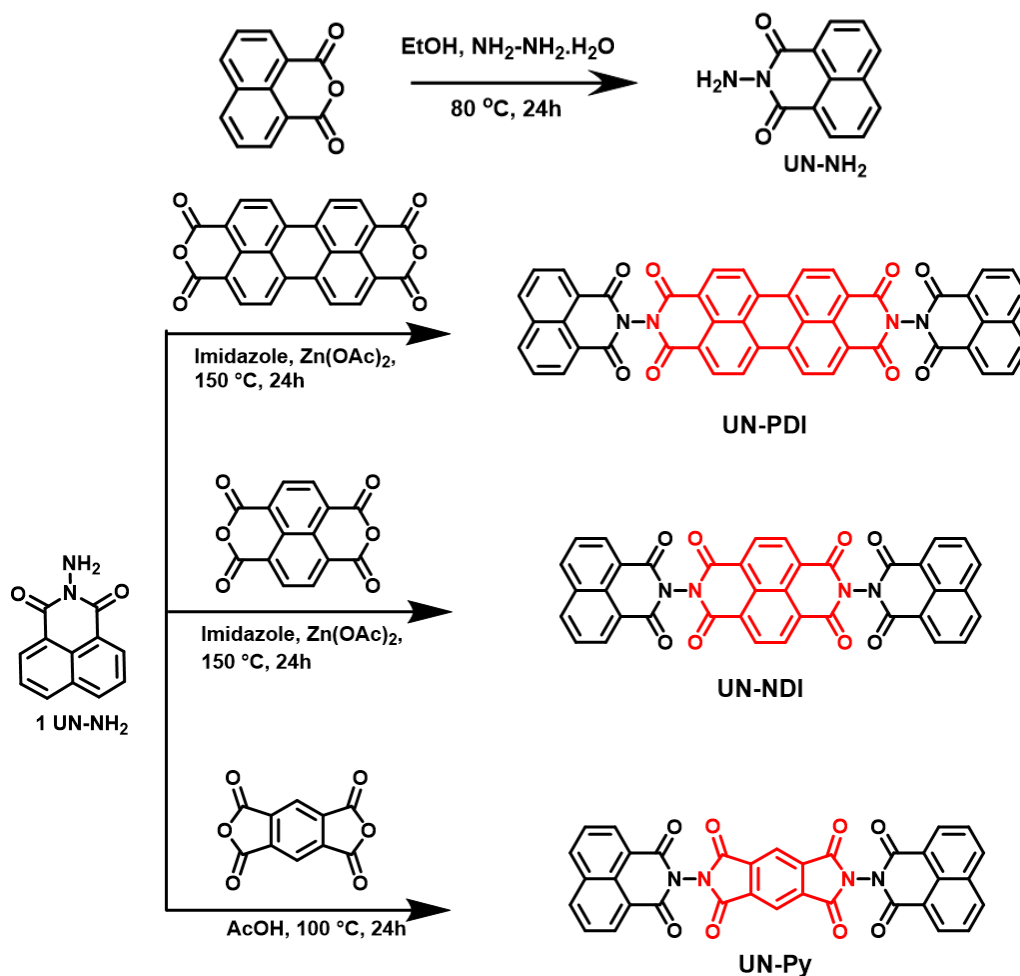
Electrode preparation (cathode)

All the electrochemical measurements were conducted using prepared CR 2032-type coin cells assembled in an Ar-filled glovebox. The cathode electrode consisted of 50% wt active material (UN-PDI, UN-NDI, and UN-Py), 40% wt carbon black, and 10% wt polyvinylidene fluoride (PVDF) as a binder. The mixture was put up in a grinder and N-methyl-2-pyrrolidinone (NMP) and thoroughly mixed to form a uniform slurry, which was further coated onto a carbon-coated aluminum foil. The electrodes were dried under a vacuum at 90 °C overnight. The coin cells for lithium-ion batteries were assembled by using lithium metal

foil as the counter electrode, electrolyte as 1 M LiTFSI in a mixture of DOL/DME (1:1 by volume), and Celgard (2325) as the separator.

3.2.3 Synthesis and Characterization.

The -NH₂ group of naphthalic anhydride (UN-NH₂) was condensed with rylene dianhydrides dyes to prepare compounds (UN-PDI), (UN-NDI), and (UN-Py) (Scheme 3.1). The detailed synthesis and characterization of compounds can be found below.



Scheme 3.1: Synthesis of UN-NH₂, UN-PDI, UN-NDI and UN-PY

a) Synthesis of UN-NH₂

Procedure: To a 500 mL round bottom flask equipped with a magnetic stirrer and 1,8-Naphthalic anhydride (5g, 25.25 mmol) in ethanol (300 mL), and the mixture is allowed to be stirred at 80 °C for 1h. After that, slow addition of hydrazine hydrate (2.5 mL 75.75 mol) was done in the reaction mixture and stirred further for 16 h at the same temperature. The completion of the reaction is monitored by TLC. After completion of the reaction, the

ethanol was evaporated by a vacuum evaporator, and the purification of the compound was done by recrystallization in DMF and H₂O. yield 80 % ¹H NMR (400 MHz, DMSO D₆, δ, ppm): 8.50 (d, 2-H, J- 7.1, H_a), 8.45 (d, J-8.1 2-H, H_b), 7.87 (t, J-7.6, 2-H, H_c), 5.81 (bs, , 2-H, H_d), ¹³C NMR (400 MHz, DMSO D₆, δ, ppm): 160.94 (C¹ imide carbonyl), 134.95 (C²), 131.71 (C³), 131.23 (C⁴), 127.76 (C⁵), 126.44 (C⁶), 122.13 (C⁷).

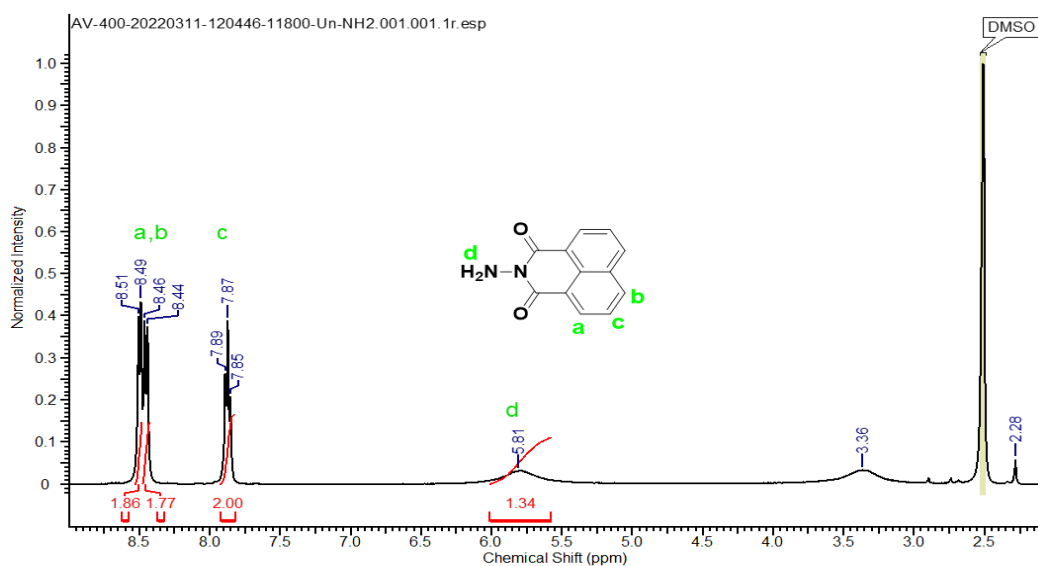
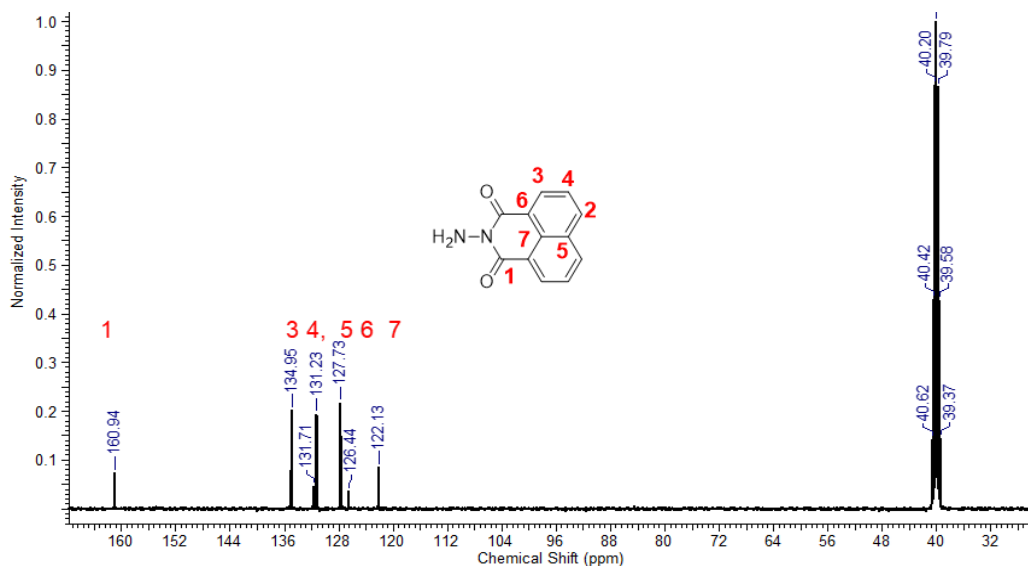


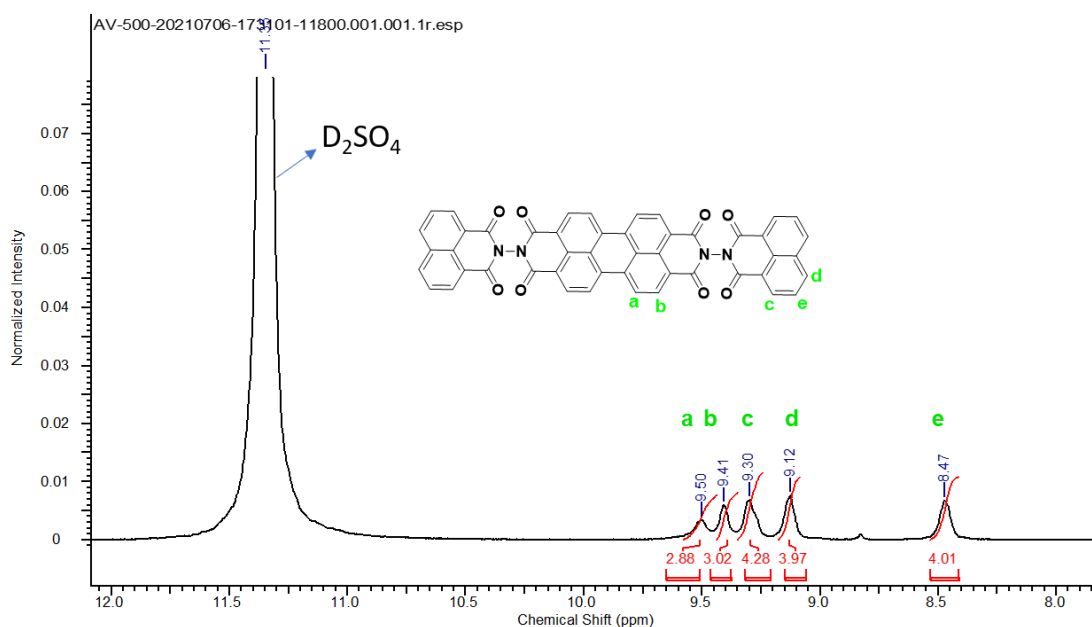
Figure 3.1: ¹H NMR Spectrum of UN-NH₂

Figure 3.2: ¹³C NMR Spectrum of UN-NH₂



b) Synthesis of UN-PDI

Procedure- A 100 mL round bottom flask equipped with a magnetic stirrer was charged with PDA (200 mg, 0.51 mmol), UN-NH₂ (432 mg, 2.04 mmol), and zinc acetate (catalytic amount) taken in imidazole 10 g). The resultant mixture was heated at 150 °C for 24 h under an argon atmosphere. After completion of the reaction, the reaction mixture was cooled down to 60 °C. Then the product mixture was precipitated by adding 1 N HCl (100 mL). The resultant crude product was washed with deionized water until the eluant get neutral. The obtained product is washed with chloroform and Acetone to remove excess UN-NH₂. A sufficient amount of THF washing was given to remove the unreacted PDA (Yield 95 %).¹H NMR (500 MHz, D₂SO₄, δ, ppm): 9.50 (m, 4-H, H_a), 9.41 (m, 4-H, H_b), 9.30 (m, 4-H, H_c), 9.12 (m, 4-H, H_d), 8.47 (m, 4-H, H_e).



c) Synthesis of UN-NDI

Procedure- A 100 mL round bottom flask equipped with a magnetic stirrer was charged with NDA (200 mg, 0.74 mmol), UN-NH₂ (627mg, 2.96 mmol), and zinc acetate (catalytic amount) taken in imidazole 15 g. The resultant mixture was heated at 150 °C for 24 h under an argon atmosphere. After completion of the reaction, the reaction mixture was cooled down to 60 °C. Then the product mixture was precipitated by adding 1N HCl (100 mL). The resultant crude product was filtered and obtained precipitated was washed with deionized water and methanol for several until the filtrate became neutral. The obtained product was thoroughly washed with chloroform and Acetone to remove excess UN-NH₂. Further, the

mixture was washed with DMSO to remove the unreacted NDA. (Yield 75 %). ^1H NMR (500 MHz, D_2SO_4 , δ , ppm): 9.60 (s, 4-H, H_a), 9.47 (d, $J=6.3$ 4-H, H_b), 9.29 (d, $J=7.3$, 4-H, H_b), 8.62 (m, 4-H, H_d)

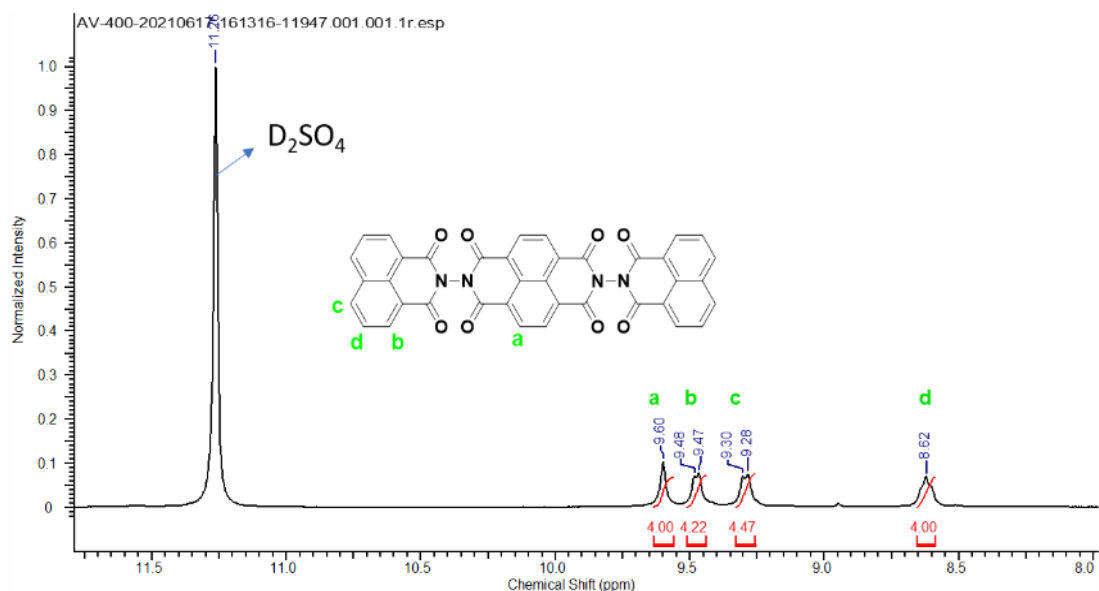
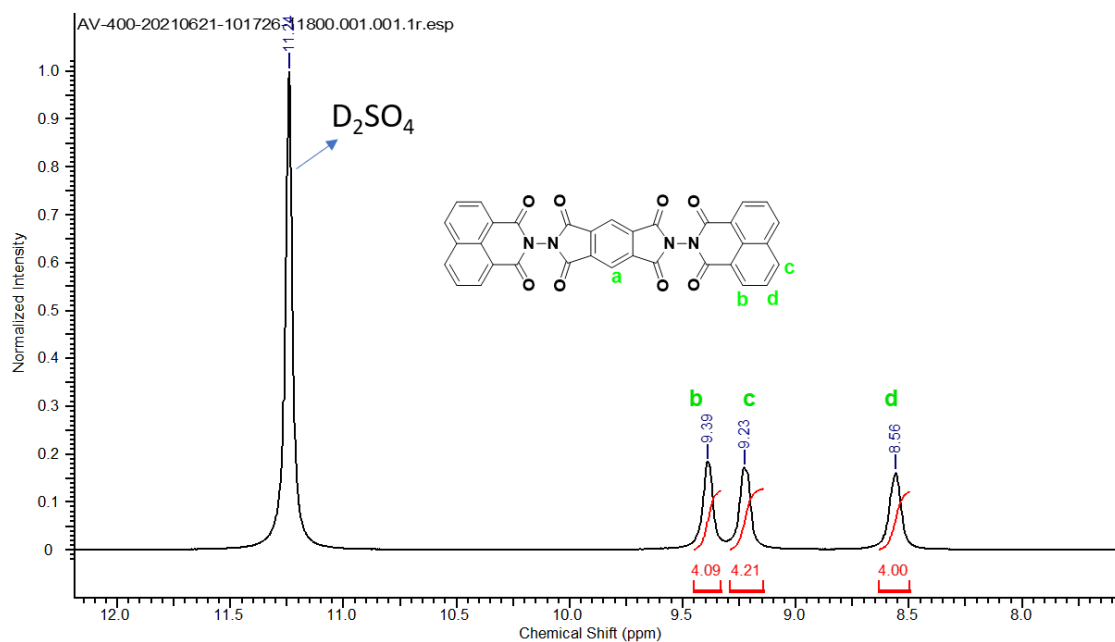


Figure 3.4: ^1H NMR Spectrum of UN-NDI

d) Synthesis of UN-Py

Procedure- A 100 mL round bottom flask equipped with a magnetic stirrer was charged with PMDA (200 mg, 0.917 mmol), UN- NH_2 (781 mg, 3.668 mmol), and zinc acetate (catalytic amount) taken in imidazole 15 g. The resultant mixture was heated at 150 $^\circ\text{C}$ for 24 h under an argon atmosphere. After completion of the reaction, the reaction mixture was cooled down to 60 $^\circ\text{C}$. Then the product mixture was precipitated by adding 1 N HCl (100 mL). The resultant crude product was washed with deionized water and methanol. The obtained product is washed with chloroform and Acetone to remove excess UN- NH_2 . Further, the mixture was washed with DMSO to remove the unreacted PMDA (Yield 60 %). ^1H NMR (500 MHz, D_2SO_4 , δ , ppm): (H_a -proton undergo deuterium exchange), 9.39 (bs, 4-H, H_b), 9.23 (bs, 4-H, H_c), 8.56 (m, 4-H, H_d).

Figure 3.5: ^1H NMR Spectrum of UN-Py

3.3 RESULTS AND DISCUSSION.

3.3.1 UV-Visible absorption spectroscopy

The optical properties of UN-PDI, UN-NDI, and UN-Py have been explored by UV-Visible spectroscopy. At room temperature, a dilute solution of compounds (UN-PDI, UN-NDI, and UN-Py) in NMP (N-methyl-2-pyrrolidone) was used to record the UV-Visible spectrum. The UN-PDI showed two pairs of sharp peaks, one at 339 nm and 353 nm and the second at 491 nm and 528 nm, with a calculated frontier orbital difference found to be 2.28 eV (Figure 3.6). Whereas for UN-NDI and UN-PDI, the sharp peak hypsochromically shifted to 354 nm, 378 nm, and 339 nm, 354 nm, respectively (Figure 3.6). The frontier orbital difference for UN-NDI and UN-Py was recognized as 3.08 eV and 3.37 eV, respectively. Such noticeable hypsochromic shifts may be correlated with a fusion of the electron-withdrawing group (naphthalic anhydride) with PDA, NDA, and PMDA, leading to a decline in HOMO energies in the order of UN-PDI < UN-NDI < UN-Py.

3.3.2 Fourier transform infrared spectroscopy (FT-IR)

To confirm functional group presence, the FTIR spectra were recorded for molecules UN-PDI, UN-NDI, UN-Py, and their parental substituent UN-NH₂. As shown in figure 3.7. UN-PDI, UN-NDI, UN-Py, and UN-NH₂ all these compounds show characteristics strong absorption peaks at 1692, 1700, 1690, and 1680 cm⁻¹, respectively, on account of

unsymmetric stretching vibration of the -C=O- bond of cyclic imide. The further detailed starching and

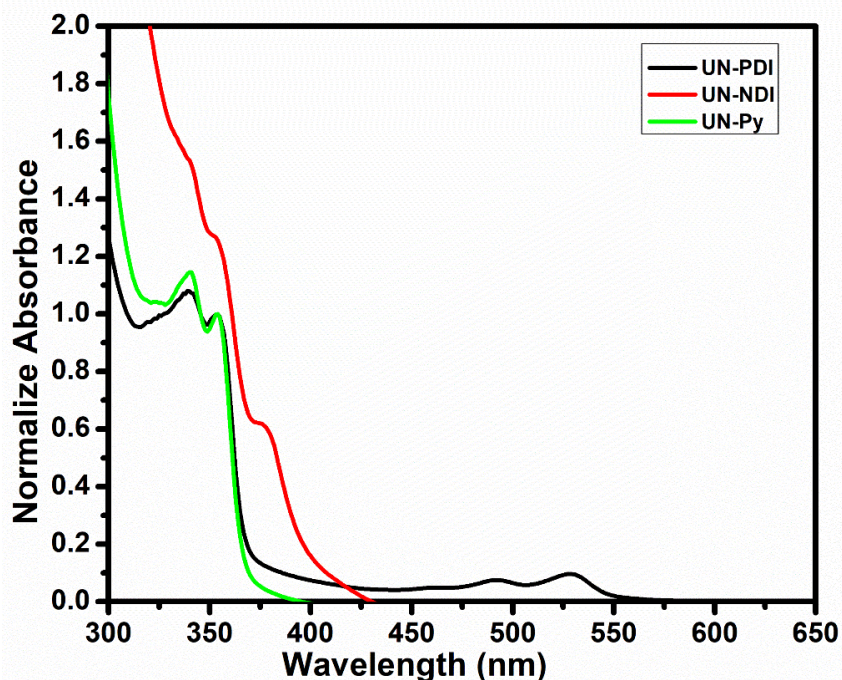


Figure 3.6: UV-Visible Absorption spectra of molecules UN-PDI, UN-NDI and UN-Py before battery cycling

Bending vibrations are shown in table 3.1. To differentiate and confirm the synthesis of the compound (UN-PDI, UN-NDI, UN-Py) done by the presence of two -NH₂- starching peaks at 3213 and 3326 cm⁻¹ for UN-NH₂ (Primary amine), which become disappear in the final compound (UN-PDI, UN-NDI, UN-Py).

Table 3.1: FTIR data of UN-PDI, UN-NDI, UN-Py and UN-NH₂

Molecule	Imide C=O Vas	Aromatic C=C Str. Mode.	Imide C=O Bending Mode	Imide C-N Str.	-N-H Str. Mode
UN-NH ₂	1680cm ⁻¹	1582 cm ⁻¹	761 cm ⁻¹	1340 cm ⁻¹	3213,3326 cm ⁻¹
UN-PDI	1692 cm ⁻¹	1585 cm ⁻¹	770 cm ⁻¹	1331 cm ⁻¹	-----
UN-NDI	1700 cm ⁻¹	1590 cm ⁻¹	770 cm ⁻¹	1331 cm ⁻¹	-----
UN-Py	1690 cm ⁻¹	1588 cm ⁻¹	765 cm ⁻¹	1332 cm ⁻¹	-----

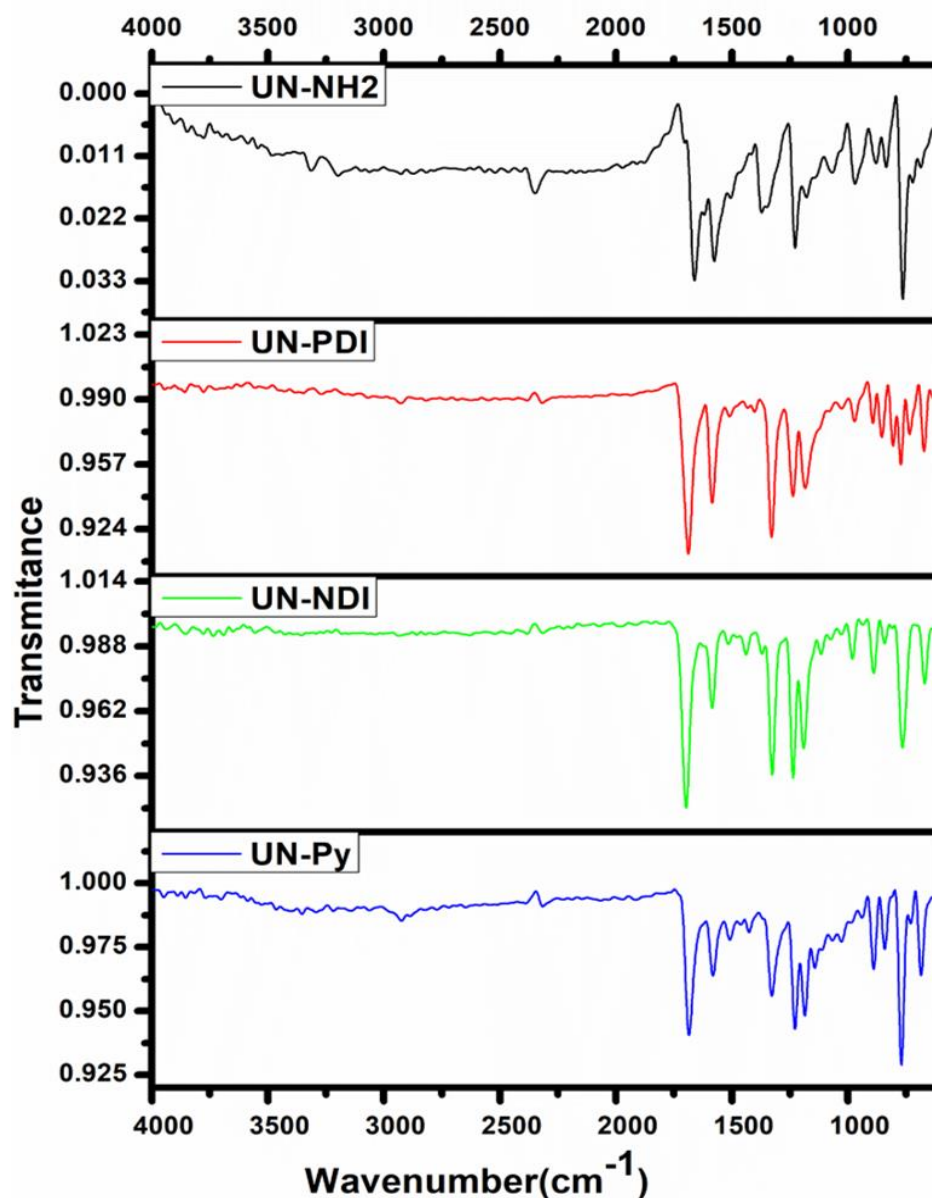


Figure 3.7: FTIR Spectra of UN-NH₂, UN-PDI, UN-NDI, and UN-Py.

3.3.3 Morphological study of molecules before and after battery cycling by Field emission scanning electron microscope (FE-SEM)

As synthesized UN-PDI, UN-NDI, and UN-Py molecules, morphologies were studied by FE-SEM. The sample was prepared by dispersing a sample of about 1 mg in 2 mL N-methyl-2-pyrrolidone (NMP). After that, 5–10 μL of the dispersed solution was drop-casted on ZP-P4VP spun silicon wafers. All three molecules have morphologies of the smooth surface sheet (figure 3.8 a,c,e). Generally, the organic molecule is soluble in the electrolyte, which results in a remarkable loss of active materials in the electrolyte, and a change in the crystal

morphology of molecules is also observed. To know the solubility in electrolytes and to know the fate of the sheet morphology after cycling, morphology was subsequently measured for all three molecules after the 200th cycle. For that, after a 200th charge/discharge cycle, a coin cell was disassembled, and the sample coated aluminum foil cathode electrodes were washed with acetonitrile and ethanol to wash out the electrolyte and dissolved binder (PVDF). After that, the coated electrode materials crashed, and powder was dispersed in NMP. A dispersed solution of the sample was drop cast on ZP-P4VP spun silicon wafers, and FE-SEM images were recorded. An UN-PDI shows the same smooth sheet morphology after the 200th charge/discharge cycle (Figure 3.8 b), whereas UN-NDI also persists with the same sheet morphology. (Figure 3.8 d)

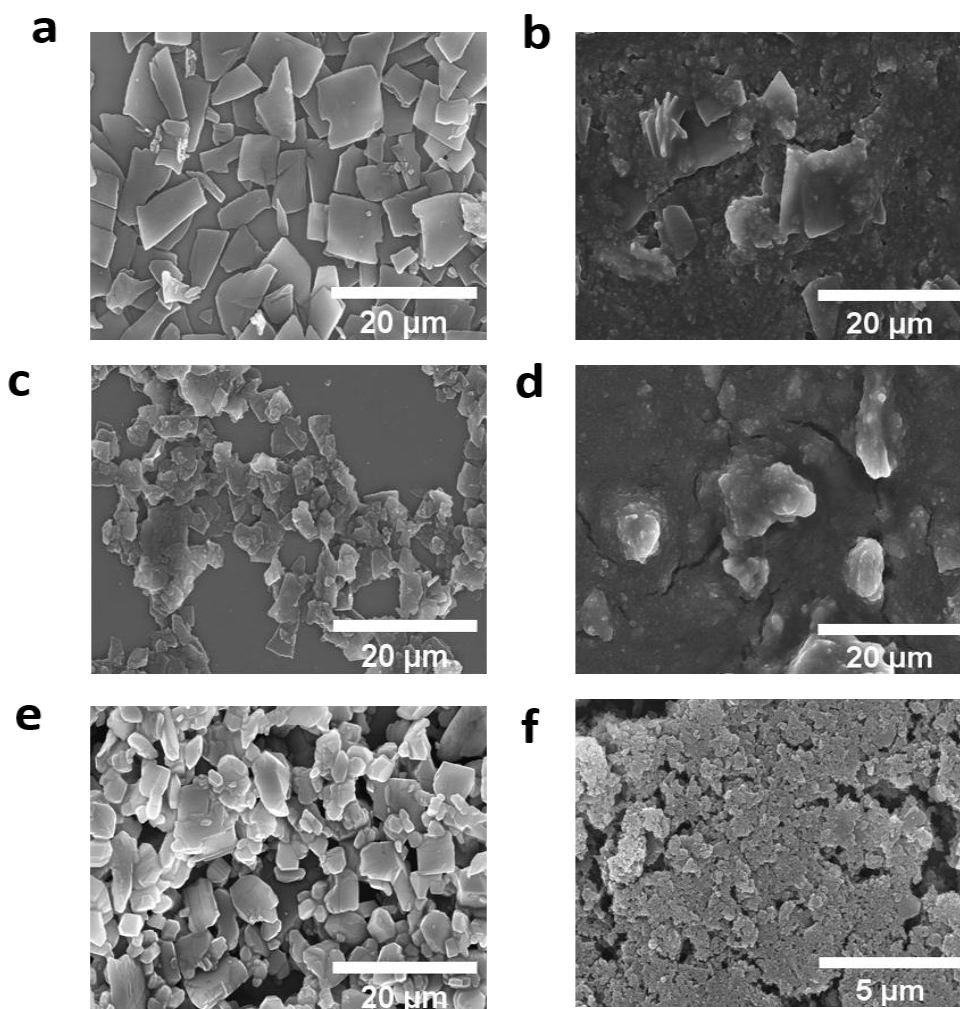


Figure 3.8: FE-SEM images of UN-PDI molecule before (a) and after 200 cycles (b) FE-SEM images of UN-NDI molecule before (c) and after 200 cycles (d) FE-SEM images of UN-Py molecule before (e) and after 200 cycles (f)

In the case of UN-py, the sheet morphology was still there, but little increase in surface roughness (Figure 3.8 f) of UN-Py. It may be due to the significant interaction of lithium with active materials. This experiment indicates no significant change in the morphology of any molecules after the 200th cycle. Thus, none of the molecules (UN-PDI, UN-NDI, and UN-Py) will be soluble in the electrolyte during charge /discharge experiments.

3.3.4 Thermogravimetric Analysis (TGA)

The structure characteristics of UN-PDI, UN-NDI, and UN-Py were further studied by TGA. As appears in Figure 3.9 d, all three compounds exhibit good thermal stability in the presence nitrogen atmosphere in the temperature of range 50 °C to 800 °C, with a scanning rate of 10 °C /min. The results show a much more enhanced inherent stability of three large aromatic compounds (UN-PDI, UN-NDI, and UN-Py) as compared with single PDA, NDA, and PMDA^{33,34} units. Exhaustively, among series, A lower aromatic unit containing UN-Py starts to decompose at a temperature of approximately 265 °C. In comparison, UN-NDI start decomposing at 360 °C, and A higher aromatic unit containing UN-PDI start decomposing at 430 °C. (Figure 3.9 d) It is concluded that the thermal stability increases with a backbone having a higher aromatic unit (UN-PDI>UN-NDI>UN-Py)

3.3.5 Electrochemical performance of molecules.

3.3.5.1 Cyclic voltammetry (CV)

Cyclic voltammetry studies were performed by using UN-PDI, UN-NDI, and UN-Py as working electrodes, whereas lithium chips as counter and reference electrodes. A potential range had been kept between 1V to 4V at a 1 mV/s scan rate. More than two small redox peaks were observed in all these molecules. But the data are following to the CV of previously NDA, PDA, and PMDA synthesized cathode materials,³⁵⁻³⁸ which are generally demonstrated by the presence of reversible two-electron transfer throughout the redox mechanism respectively. Thus, we have evaluated only two pairs of prominent oxidation and reduction large hump here, which further ideally helps to show the possible two-step mechanism of lithium intercalation and deintercalation. (In section 3.3.5.3) In detail, UN-PDI displayed two pairs of redox peaks. The first pair was 2.715 V & 2.38 V, representing the intercalation/deintercalation of the first two Li-ions. In contrast, the other two Li-ion insertion/deinsertion happens at 1.92 V & 1.73 V (Figure 3.9 a). However, for UN-NDI (figure 3.9 b) and UN-Py (figure 3.9 c), the first lithiation/delithiation^{39,40} process was observed at 2.60 V/2.26 V and 3.04 V /2.5 V, respectively, whereas second

lithiation/delithiation process observed at 1.91 V/1.70V and 2.16 V/1.59 V respectively. Moreover, all these redox of UN-PDI, UN-NDI, and UN-Py corresponding to enolization

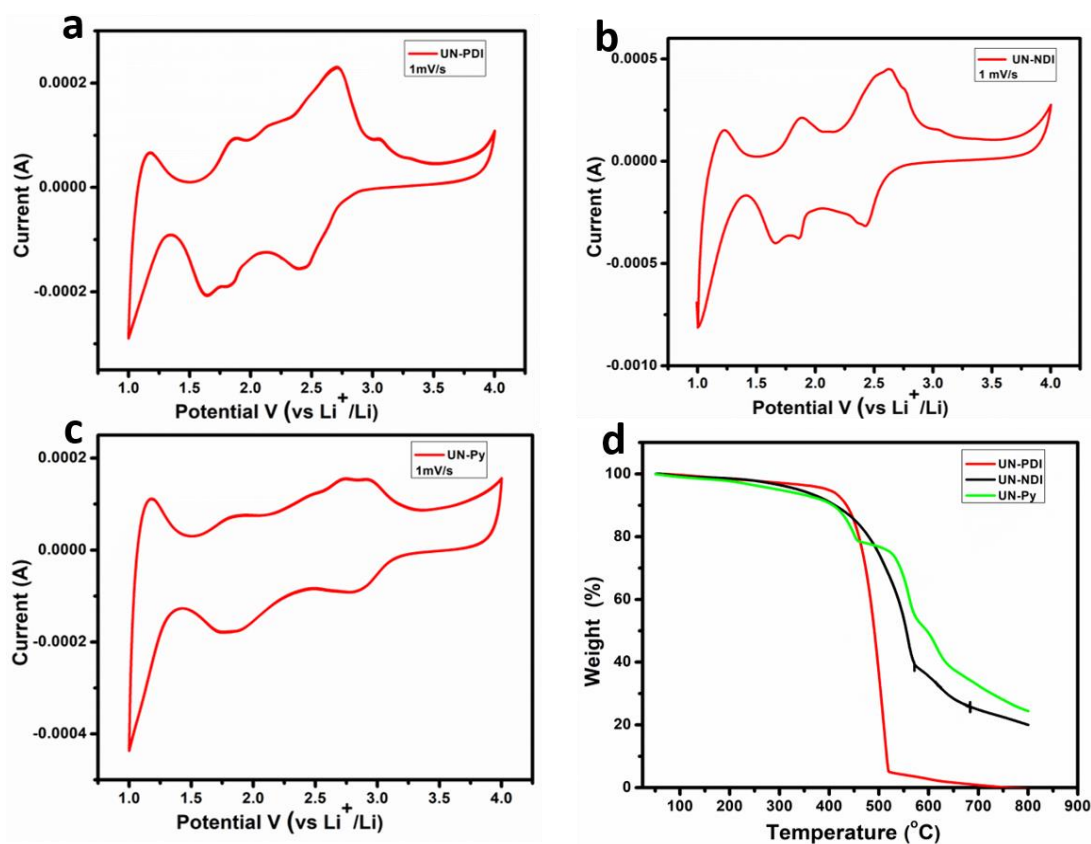


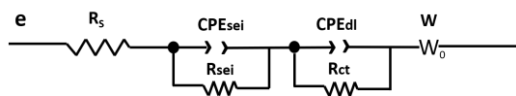
Figure 3.9: cyclic voltammograms (a) of molecules TPA-PDI, (b) TPA-NDI, (b) and (c) TPA-Py (d) TGA profile of UN-PDI, UN-NDI and UN-Py.

processes at the carbonyl moieties are following the plateaus present in their charge/discharge curve.

3.3.5.2 Electrochemical Impedance Spectroscopy (EIS) Study.

EIS measurements were recorded by a Biologic instrument considering a signal amplitude of 5 mV in the frequency between 40 kHz to 10 MHz. To study additional factors that can probably outcome, the comparative study of rate performance of UN-PDI, UN-NDI, and UN-Py Impedance spectroscopy was used. Impedance spectroscopy was done even to evaluate any changes in charge transfer of UN-PDI, UN-NDI, and UN-Py, which generally represents the kinetics process of reaction. However, the examinations were conducted by taking a fully prepared battery cell with the organic cathode materials (scheme 3.1) and

anode and lithium chip. An obtained Nyquist plot was fitted using the following equivalent circuit.



It appears that UN-PDI, UN-NDI, and UN-Py exhibit similar characteristics in that every profile consists of a semi-circle at a high-frequency and a tail low-frequency range. In (Figure 3.10 a) appeared EIS diagram before battery cycling, for UN-PDI, UN-NDI, and UN-Py have the same electrolyte resistance with a nominal number of approximately 3.7Ω . In the Nyquist plots before battery cycling, at high-frequency region consist of well-defined semi-circles corresponding to charge transfer resistance (R_{ct}) of UN PDI, UN-NDI, and UN-Py. However, the linear line at low frequencies was associated with a Warburg impedance. It can be distinctly compared that UN-PDI shows a charge transfer resistance of 79Ω . Further, it was observed to be decreased for compound UN-NDI (70Ω) and UN-Py (50Ω). (Figure 3.10 a) The charge transfer resistance reveals that a better kinetics reaction and electronic conductivity is possible between the UN-Py electrode and the electrolyte as compared to UN-PDI and UN-NDI. To know the electronic conductivity after battery cycling same cell, impedance was measured after 20 charge/discharge cycles. It is found that there is no significant change observed for

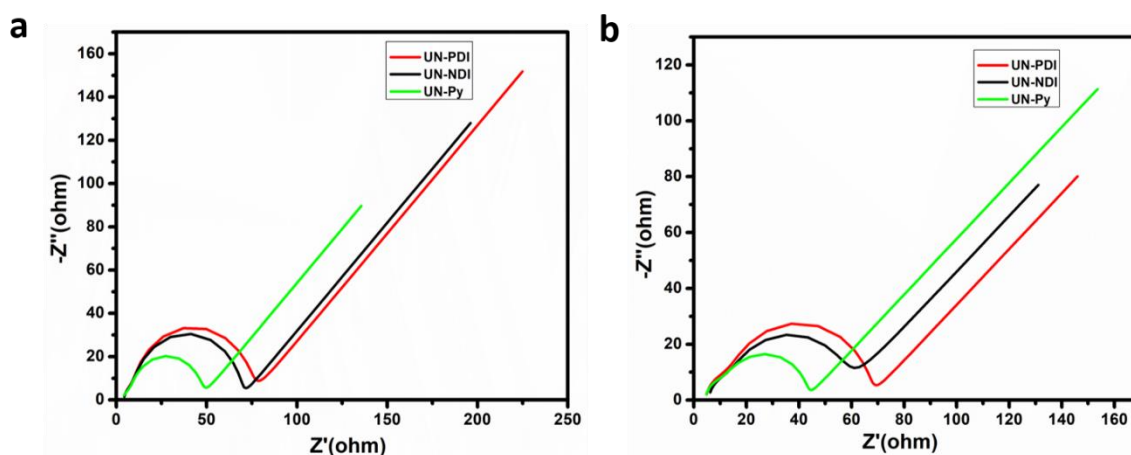


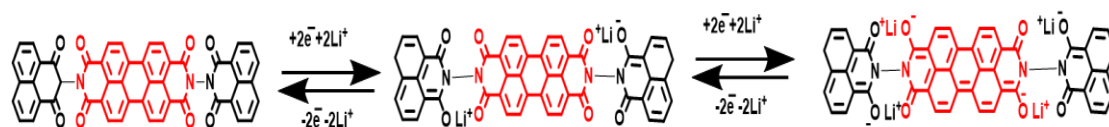
Figure 3.10: Nyquist plots of fresh UN-PDI, UN-NDI, and UN-Py electrode cell (a) and (b) Nyquist plots of after 20th the galvanostatic charge/discharge cycling.

the electrolyte resistance (4Ω) but charge transfer resistance was decreased subsequently for compound UN-PDI (68Ω), UN-NDI (60Ω), and UN-Py (43Ω). (Figure 3.10 b) The

obtained charge transfer resistance after the 20th cycle is less than their respective fresh cell charge transfer resistance; a probable reason for decreased charge transfer resistance (R_{ct}) value may be because of the wetting of the electrodes by the electrolyte throughout the battery cycling. It is observed that there is increased conductivity for all molecules after cycling, even it not only persists during the process of charge-discharge cycling but also slightly increases in the number.

3.3.5.3 Proposed electrochemical redox mechanism of molecules.

All synthesized naphthalene anhydride substituted rylene imide UN-PDI, UN-NDI, and UN-Py. It consists of six electrochemically active carbonyl groups, but only two from the Main core and one carbonyl from naphthalic anhydride moieties participate in the enolate formation mechanism in order to avoid charge repulsion and maintain the aromaticity of the molecule. All these molecules undergo four-electron transfer during the redox reaction, which consists of the following two-step mechanism.



3.3.5.4 Galvanostatic charge/discharge experiment

The galvanostatic charge/discharge profile for molecules UN-PDI, UN-NDI, and UN-Py is shown in figures 3.10 a, b, and c. all compounds measure at a 0.2 C rate at potential windows 1 to 4 V (vs. Li^+/Li). In the first charge cycle, UN-PDI, UN-NDI, and UN-Py exhibit a specific capacity of 198, 297, and 239 mAh/g, respectively, whereas the first discharge capacity for this molecule was found to be 186, 250, and 216 mAh/g respectively which was much larger than their theoretical specific capacity (Table 3.2). This is because of the generation of the SEI layer on the surface of the electrode. In the charge/discharge profile, the discharge curve for UN-PDI found two plateaus centered at 2.41 V and 1.57 V. (Figure 3.11 a), whereas UN-NDI and UN-Py discharge curves also exhibit two plateaus at 2.4 V, 1.57 V, and 2.3V, 1.50 V respectively. (Figure 3.11 b, c). This may be due to the two-step reaction of lithiation and dilithiation. These results are nearly coinciding with the results obtained from CV. Notably, the curve of charge/discharge voltage profiles was well

maintained from the 10th cycle to the 200th cycle, which is clearly indicating the good reaction reversibility of all these three cathode materials.

Table 3.2: Battery metrics for molecules UN-PDI, UN-NDI and UN-Py as a function of charge discharge cycles

Molecule	Charge/ discharge potential window vs Li/Li ⁺	Charge/ discharge C Rate	Theoretical specific capacity	Sp. capacity at first Discharge cycle	Sp. capacity 200 th discharge cycle	Percentage decrease sp. capacity as Function of 200 th Charge/ Discharge Cycle
UN-PDI	1-4 V	0.2 C / 0.2 C	137.3 mAhg ⁻¹	186 mAhg ⁻¹	89 mAhg ⁻¹	36 %
UN-NDI	1-4 V	0.2 C / 0.2 C	163.3 mAhg ⁻¹	247 mAhg ⁻¹	60 mAhg ⁻¹	63 %
UN-Py	1-4 V	0.2 C / 0.2C	176.7 mAhg ⁻¹	213 mAhg ⁻¹	70 mAhg ⁻¹	60.4 %

In a long-term cycling experiment, the cycling activity was measured until the 200th cycle for each molecule at 0.2 C and 2 C. All these molecules show stable capacity up to the 200th cycle. In detail, UN-PDI shows 89 mAh/g discharge capacity after the 200th cycle at 0.2C with an average Coulombic efficiency is 99%. (Figure 3.11 d) whereas for UN-NDI and UN-Py, discharge capacity was 60 mAh/g and 70 mAh/g, respectively, at 0.2 C, while maintaining excellent Coulombic efficiency of nearly 99 % for both molecules. (Figure 3.11 e,f) All these molecules show excellent coulombic efficiency, which is very near to 100%, which confirms the good reaction reversibility possible for these molecules. The % decrease after the 200th cycle at 0.2 C from its theoretical capacity was found to be 36 %, 63 %, and 60.4% for molecules UN-PDI, UN-NDI, and UN-Py, respectively. (Table 3.2) This supports our hypothesis that long-term cycling stability increases by changing more aromatic conjugated systems such as NDA or PMDA to PDA.

In this set of experiments, we tested all molecules for long-term cycling (200 Cycles) at a fast charge and discharge rate (2 C) to know the stability of the fast reaction kinetics of the molecules. UN-PDI shows the initial discharge capacity of 130 mAh/g which is decreased to 85 mAh/g after the 200th cycle with very fluctuating coulombic efficiency (90-105%) (Figure 3.12 a). Whereas molecules UN-NDI show an initial discharge capacity of 160 mAh/g, which is become 85 mAh/g after the 200th cycle with coulombic efficiency between 95-105 %. (Figure 3.12 b). In the case of UN-Py, the initial discharge capacity was 200 mAh/g, which decreased to 60 mAh/g after the 200th cycle; in this case, up to the 40th

cycle, the coulombic efficiency very much fluctuated, but after the 40th cycle, the coulombic efficiency was almost near two 99 %. (Figure 3.12 c).

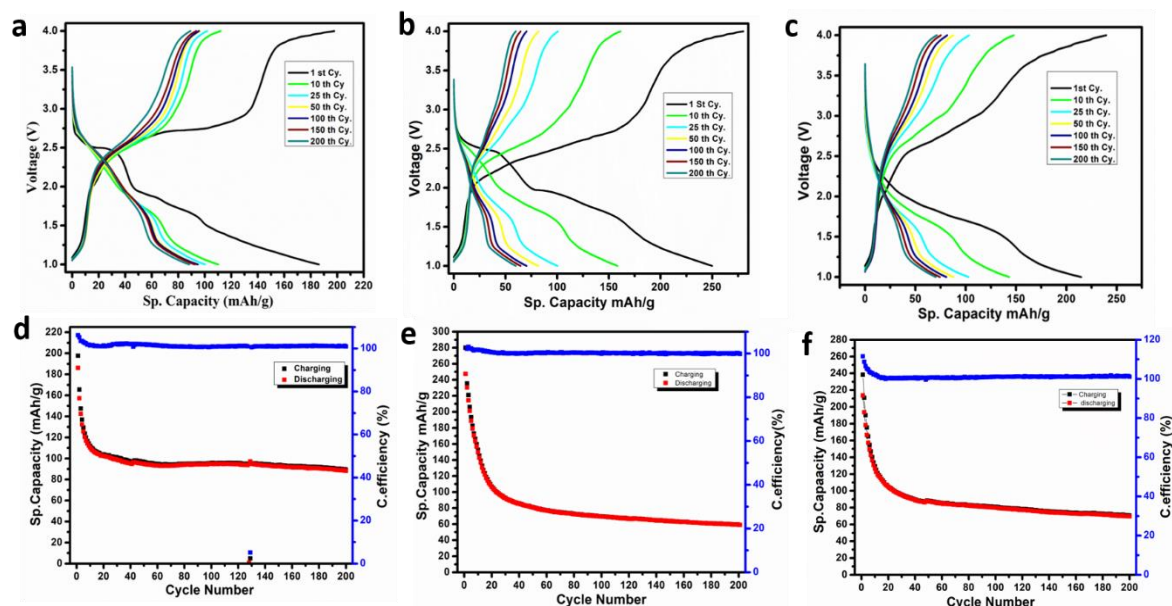


Figure 3.11: Galvanostatic charge/discharge profile curve of (a) UN-PDI (b) UN-NDI and (c) UN-Py. Cycling stability at 0.2 C for (d) UN-PDI, (e) UN-NDI, and (f) UN-Py

The above result reveals that the fast reaction kinetics increases for molecules in the order of UN-PDI < UN-NDI < UN-Py, which is further confirmed by their impedance R_{ct} (Charge transfer resistance value).

Rate study.

High-rate stability electrode materials are mostly advantageous for the growth of quick charge/discharge batteries. In this study, knowing the stabilities of molecules (UN-PDI, UN-NDI, and UN-Py) at the different C rates. Various C rates were applied. Each C rate was applied for five consecutive charge-discharge cycles. The C rate was varied between 0.2 to 30 C, and specific capacity was monitored. For all molecules, the specific capacity was found to decrease gradually with increasing C rates (Figure 3.12 d,e f) which are maybe due to an increase in the internal temperature of batteries. For UN-PDI at a 0.2 C rate, the discharge capacity was 139 mAh/g, which gets reduced to 26 mAh/g at 30 C. (Figure 3.12 d). When we charge-discharge the same cell at a low C rate (0.2 C), the discharge-specific capacity bounced back 132 mAh/g, which was almost near to initial charge-discharge rates (0.2 C). (Figure 3.12 d) For UN-NDI at a 0.2 C rate, the discharge specific capacity was 162

mAh/g which gets reduced to 15 mAh/g at 30 C. (Figure 3.12 e) which was almost negligible; the specific capacity was bounced back to 147 mAh/g when we again charge-

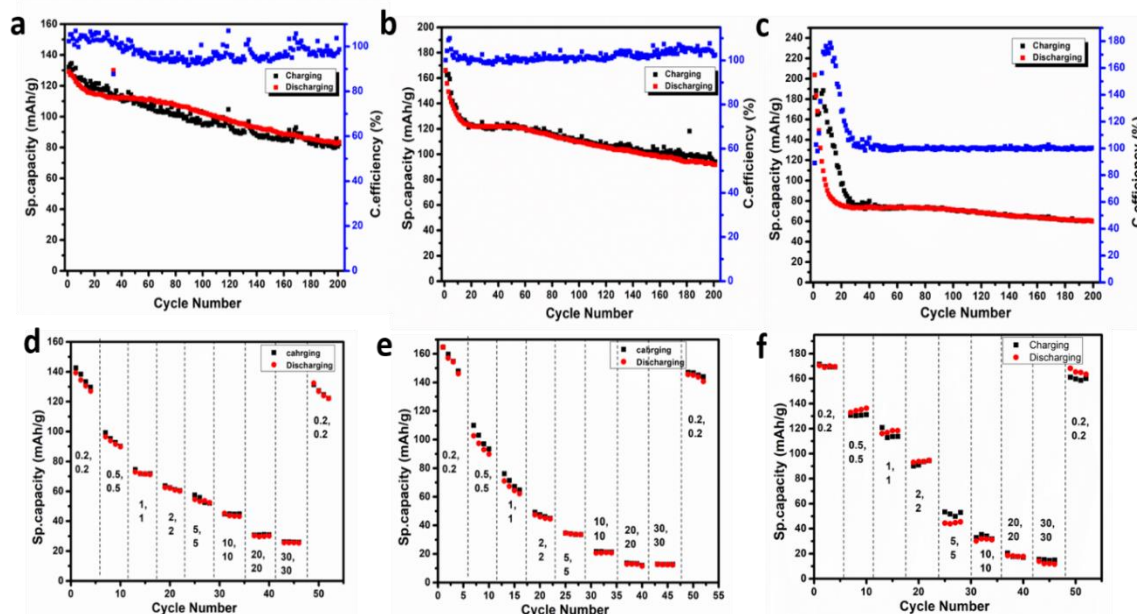


Figure 3.12: Cycling stability at 2 C for (a) UN-PDI (b) UN-NDI and (c) UN-Py. Rate capability for (d) UN-PDI (e) UN-NDI and (f) UN-Py at different C rate.

discharge the same cell at a low C rate (0.2 C). (Figure 3.12 e) whereas UN-Py at a 0.2 C rate, the discharge specific capacity shows 170 mAh/g, which gets reduced to 12 mAh/g at 30 C. (Figure 3.12 f). Same cells at a low C rate (0.2 C), the discharge specific capacity bounced back to 168 mAh g⁻¹, which is almost initial charge-discharge rates (0.2 C). (Figure 3.12 f) from these studies it's concluded that none of the above molecules are able to show the desired discharge capacity to a high C (10,20,30 C) rate.

3.3.6 Solubility study of molecules in liquid electrolytes.

3.3.6.1 Electrode Soaking experiment

For monitoring the effect of naphthalic anhydride substitution on the solubility of the synthesized molecule (Scheme 3.1) in battery liquid electrolyte (LiTFSI in DOL: DME 1:1), we have taken the prepared electrode of the sample and put it into a battery electrolyte for soaking and observed change in colored of an electrode-soaked molecule with respect to the pristine electrolyte. As the soaking time changed from 0 days to 7 days, the sample's color remained unchanged (Figure 3.13), which clearly indicates the insolubility of UN-PDI, UN-NDI, and UN-Py in liquid electrolyte.

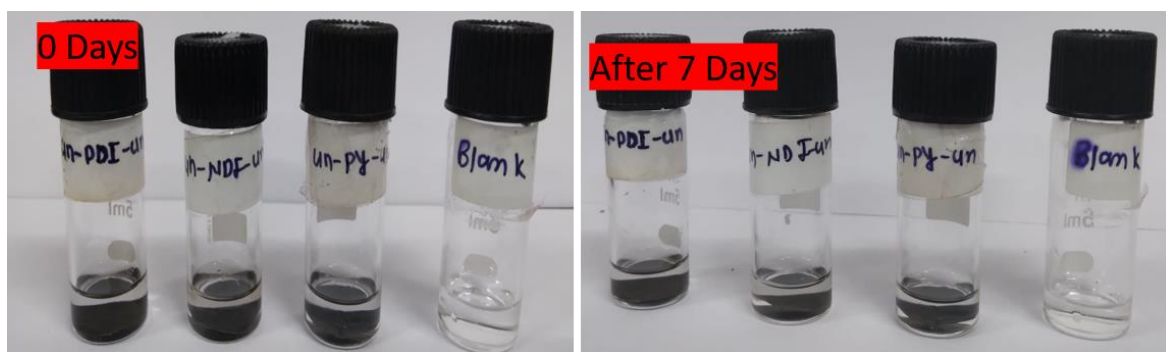


Figure 3.13: Photographs of the blank electrolyte and UN-PDI, UN-NDI and UN-Py soaked active electrode at 0 days and 7 days respectively.

3.3.6.2 UV-Visible Absorption Spectroscopy after 200th Cycle

In this experiment, to check the existence of molecules (UN-PDI, UN-NDI, and UN-Py) after the 200th charge/discharge cycling, we analyzed the battery cathode electrode by opening the cell after the 200th cycle. For removal, the electrolytes and PVDF (Polyvinyl difluoride) were washed with acetonitrile. The crushed powder of the positive electrode was mixed in fresh NMP, and UV-Visible absorption spectra were recorded between 250 and 700 nm. We identified all the peaks corresponding to molecules UN-PDI, UN-NDI, and UN-Py (Figure 3.14), which exactly match the peak observed before battery cycling. (Figure 3.6)

Confirming that dissolution molecules do not happen in electrolytes during the charge-discharge cycling.

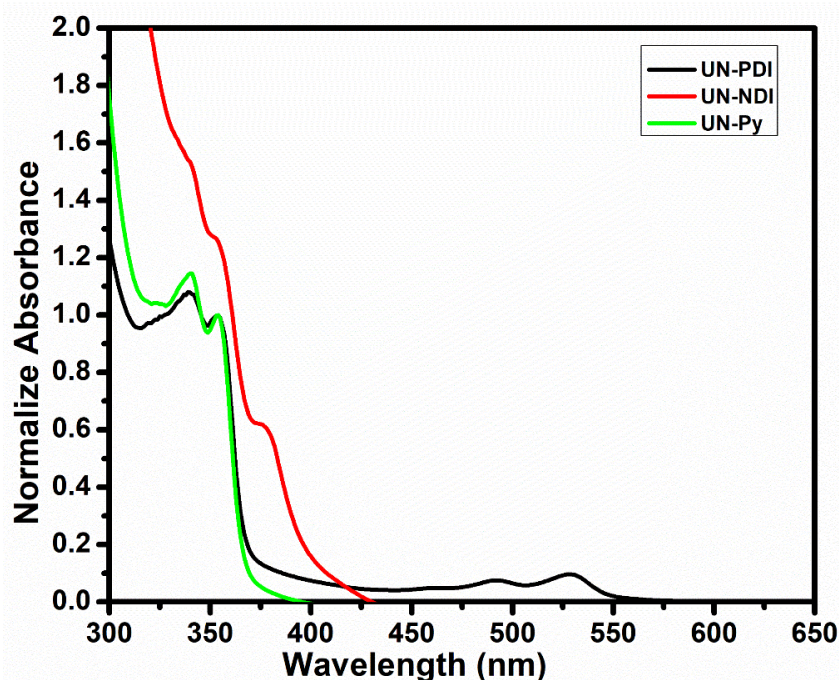


Figure 3.14: UV-Visible Absorption spectra of molecules UN-PDI, UN-NDI and UN-Py After 200th battery cycling

3.4 CONCLUSION

A simple strategic naphthalene anhydride substituted molecules (UN-PDI, UN-NDI, and UN-Py) were synthesized, and their electrochemical performance was tested successfully. A naphthalene anhydride substitution was not only helpful in taking part in electrochemical reactions, but also it is a valuable moiety for making molecules insoluble in liquid electrolytes. Long-term cycling stability (in %) at a 0.2 C rate for these rylene imide series (schemes 3.1) following an order UN-PDI>UN>NDI>UN-Py. All these molecules achieved specific capacity to their theoretical capacity, confirming that the proposed reaction mechanism was successfully followed during the charging/discharging experiment. UN-Py can show fast reaction kinetics compared to UN-PDI and UN-NDI, supported by their small charge transfer resistance value and stable coulombic efficiency during high charge/discharge rates (2 C).

3.5 REFERENCES

- (1) Borah, R.; Hughson, F. R.; Johnston, J.; Nann, T. On battery materials and methods. *Mater. Today Adv.* **2020**, *6*, 100046.
- (2) Chu, S.; Cui, Y.; Liu, N. The Path towards Sustainable Energy. *Nat. Mater.* **2016**, *16*, 16–22.
- (3) Larcher, D.; Tarascon, J.-M. Towards Greener and More Sustainable Batteries for Electrical Energy Storage. *Nat. Chem.* **2015**, *7*, 19–29.
- (4) Lu, Y.; Chen, J. Prospects of Organic Electrode Materials for Practical Lithium Batteries. *Nat. Rev. Chem.* **2020**, *4*, 127–142.
- (5) Winter, M.; Barnett, B.; Xu, K. Before Li-Ion Batteries. *Chem. Rev.* **2018**, *118*, 11433–11456.
- (6) Goodenough, J. B. Energy Storage Materials: A Perspective. *Energy Storage Mater.* **2015**, *1*, 158–161
- (7) Goodenough, J. B.; Park, K. S. The Li-ion rechargeable battery: a perspective. *J. Am. Chem. Soc.* **2013**, *135*, 1167-1176.
- (8) Cheng, F.; Liang, J.; Tao, Z.; Chen, J. Functional Materials for Rechargeable Batteries. *Adv. Mater.* **2011**, *23*, 1695–1715.
- (9) Thackeray, M. M.; Wolverton, C.; Isaacs, E. D. Electrical energy storage for transportation—approaching the limits of, and going beyond, lithium-ion batteries. *Energy Environ. Sci.* **2012**, *5*, 7854–7863.
- (10) Lee, J.; Kim, H.; Park, M. J. Long-life, high-rate lithium-organic batteries based on naphthoquinone derivatives. *Chem. of Mater.* **2016**, *28*, 2408-2416.
- (11) Wilkinson, D.; Bhosale, M.; Amores, M.; Naresh, G.; Cussen, S. A.; Cooke, G. A quinone-based cathode material for high-performance organic lithium and sodium batteries. *ACS Appl. Energy Mater.* **2021**, *4*, 12084-12090.
- (12) Manthiram, A. A. Reflection on Lithium-Ion Battery Cathode Chemistry. *Nat. Commun.* **2020**, *11*, 1550.
- (13) Chen, Z.; Zhang, W.; Yang, Z. A Review on Cathode Materials for Advanced Lithium Ion Batteries: Microstructure Designs and Performance Regulations. *Nanotechnology* **2019**, *31*, 12001.
- (14) Kraytsberg, A.; Ein-Eli, Y. Higher, Stronger, Better... A Review of 5 Volt Cathode Materials for Advanced Lithium-Ion Batteries. *Adv. Energy Mater.* **2012**, *2*, 922–939.

- (15) Shanmukaraj, D.; Ranque, P.; Ben Youcef, H.; Rojo, T.; Poizot, P.; Grugeon, S.; Laruelle, S.; Guyomard, D. Review—Towards Efficient Energy Storage Materials: Lithium Intercalation/Organic Electrodes to Polymer Electrolytes—A Road Map (Tribute to Michel Armand). *J. Electrochem. Soc.* **2020**, *167*, 70530.
- (16) Cariello, M.; Johnston, B.; Bhosale, M.; Amores, M.; Wilson, E.; McCarron, L. J.; Wilson, C.; Corr, S. A.; Cooke, G. Benzo-Diptyridine Derivatives as Organic Cathodes for Li- and Na-Ion Batteries. *ACS Appl. Energy Mater.* **2020**, *3*, 8302–8308.
- (17) Qin, K.; Huang, J.; Holguin, K.; Luo, C. Recent Advances in Developing Organic Electrode Materials for Multivalent Rechargeable Batteries. *Energy Environ. Sci.* **2020**, *13*, 3950–3992.
- (18) Gannett, C. N.; Melecio-Zambrano, L.; Theibault, M. J.; Peterson, B. M.; Fors, B. P.; Abruña, H. D. Organic Electrode Materials for Fast-Rate, High-Power Battery Applications. *Mater. Rep. Energy* **2021**, *1*, 100008.
- (19) Luo, W.; Allen, M.; Raju, V.; Ji, X. An Organic Pigment as a High-Performance Cathode for Sodium-Ion Batteries. *Adv. Energy Mater.* **2014**, *4*, No. 1400554.
- (20) Shi, R.; Liu, L.; Lu, Y.; Wang, C.; Li, Y.; Li, L.; Yan, Z.; Chen, J. Nitrogen-Rich Covalent Organic Frameworks with Multiple Carbonyls for High-Performance Sodium Batteries. *Nat. Commun.* **2020**, *11*, 178.
- (21) Vitaku, E.; Gannett, C. N.; Carpenter, K. L.; Shen, L.; Abruña, H. D.; Dichtel, W. R. Phenazine-Based Covalent Organic Framework Cathode Materials with High Energy and Power Densities. *J. Am. Chem. Soc.* **2019**, *142*, 16–20.
- (22) Acker, P.; Speer, M. E.; Wössner, J. S.; Esser, B. Azine-Based Polymers with a Two-Electron Redox Process as Cathode Materials for Organic Batteries. *J. Mater. Chem. A* **2020**, *8*, 11195–11201.
- (23) Li, Q.; Li, D.; Wang, H.; Wang, H.; Li, Y.; Si, Z.; Duan, Q. Conjugated Carbonyl Polymer-Based Flexible Cathode for Superior Lithium-Organic Batteries. *ACS Appl. Mater. Interfaces* **2019**, *11*, 28801–28808.
- (24) Zhu, L. M.; Lei, A. W.; Cao, Y. L.; Ai, X. P.; Yang, H. X. An All-Organic Rechargeable Battery Using Bipolar Polyparaphenylene as a Redox-Active Cathode and Anode. *Chem. Commun.* **2013**, *49*, 567–569.
- (25) Gospodinova, N.; Terlemezyan, L. Conducting Polymers Prepared by Oxidative Polymerization: Polyaniline. *Prog. Polym. Sci.* **1998**, *23*, 1443–1484.

- (26) Xie, J.; Wang, Z.; Xu, Z. J.; Zhang, Q. Toward a High-Performance All-Plastic Full Battery with a' Single Organic Polymer as Both Cathode and Anode. *Adv. Energy Mater.* **2018**, *8*, 1703509.
- (27) Deng, S.-R.; Kong, L.-B.; Hu, G.-Q.; Wu, T.; Li, D.; Zhou, Y.-H.; Li, Z.-Y. Benzene-Based Polyorganodisulfide Cathode Materials for Secondary Lithium Batteries. *Electrochim. Acta* **2006**, *51*, 2589–2593.
- (28) Koshika, K.; Chikushi, N.; Sano, N.; Oyaizu, K.; Nishide, H. A TEMPO-Substituted Polyacrylamide as a New Cathode Material: An Organic Rechargeable Device Composed of Polymer Electrodes and Aqueous Electrolyte. *Green Chem.* **2010**, *12*, 1573.
- (29) Mauger, A.; Julien, C.; Paoletta, A.; Armand, M.; Zaghbi, K. Recent Progress on Organic Electrodes Materials for Rechargeable Batteries and Supercapacitors. *Materials* **2019**, *12*, 1770.
- (30) Kong, L.; Liu, M.; Huang, H.; Xu, Y.; Bu, X. H. Metal/covalent-organic framework based cathodes for metal-ion batteries. *Advanced Energy Mater.* **2022**, *12*, 2100172.
- (31) Huang, C.; Barlow, S.; & Marder, S. R. Perylene-3, 4, 9, 10-tetracarboxylic acid diimides: synthesis, physical properties, and use in organic electronics. *J. Org. Chem.* **2011**, *76*, 2386-2407.
- (32) Huang, Y.; Li, K.; Liu, J.; Zhong, X.; Duan, X.; Shakirc, I.; Xu, Y. Three-dimensional graphene/polyimide composite-derived flexible high-performance organic cathode for rechargeable lithium and sodium batteries. *J. Mater. Chem. A* **2017**, *5*, 2710-2716.
- (33) Aher, J.; Graefenstein, A.; Deshmukh, G.; Subramani, K.; Krueger, B.; Haensch, M.; Wittstock, G. Effect of aromatic rings and substituent on the performance of lithium batteries with rylene imide cathodes. *ChemElectroChem.* **2020**, *7*, 1160-1165.
- (34) Xie, J.; Chen, W.; Wang, Z.; Jie, K. C. W.; Liu, M.; Zhang, Q. Synthesis and Exploration of Ladder-Structured Large Aromatic Dianhydrides as Organic Cathodes for Rechargeable Lithium-Ion Batteries. *Chem. Asian J.* **2017**, *12*, 868-876.
- (35) Xu, F.; Wang, H.; Lin, J.; Luo, X.; Cao, S. A.; Yang, H. Poly (anthraquinonyl imide) as a high capacity organic cathode material for Na-ion batteries. *J. Mater.Chem. A.* **2016**, *4*, 11491-11497.

- (36) Pan, L.; Lu, S.; Xiao, X.; He, Z.; Zeng, C.; Gao, J.; Yu, J. Enhanced mechanical and thermal properties of epoxy with hyperbranched polyester grafted perylene diimide. *RSC advances*, **2015**, *5*, 3177-3186.
- (37) Iordache, A.; Delhorbe, V.; Bardet, M.; Dubois, L.; Gutel, T.; Picard, L. Perylene-based all-organic redox battery with excellent cycling stability. *ACS Appl. Mater. Interfaces*. **2016**, *8*, 22762-22767.
- (38) Sharma, P.; Damien, D.; Nagarajan, K.; Shaijumon, M. M.; Hariharan, M. Perylene-polyimide-based organic electrode materials for rechargeable lithium batteries. *J. Phys. Chem. Lett.* **2013**, *4*, 3192-3197.
- (39) Song, Z.; Zhan, H.; Zhou, Y. Polyimides: promising energy-storage materials. *Angew. Chem. Int. Ed.* **2010**, *49*, 8444-8448.
- (40) Lv, M.; Zhang, F.; Wu, Y.; Chen, M.; Yao, C.; Nan, J.; Chou, S. L. Heteroaromatic organic compound with conjugated multi-carbonyl as cathode material for rechargeable lithium batteries. *Sci. rep.* **2016**, *6*, 1-8.

CHAPTER 4

**An Anthraquinone Based Rylene Imide Derivatives
Cathode for Organic Lithium-ion Batteries.**

4.1 INTRODUCTION

The energy is created using conventional renewable energy sources, e.g. solar, water, wind, and waste energy,¹ which can be stockpiled by using fuel cells, supercapacitors, and rechargeable batteries.² Among these all-energy storage systems, rechargeable LIBs have emerging popularity because of their high energy density, stable and long cycle life, and less ecological footprint.³ even so, LIBs have significant drawbacks such as the addressable low theoretical capacity of anode material, which is only 372 mAh/g⁴⁻⁶ Even one of the leading drawbacks need to be addressed that is poisonous metal present in LIBs which brings massive energy implementation and pollution, specifically in bulk energy storage application.⁷⁻⁹ Despite, inorganic origin electrode is used for industrial purposes. It is hazardous and scanty, which brings on the sustainability issue.¹⁰ However, advances in the organic cathode are modest compared to inorganic ones.¹¹⁻¹³ Due to the unique properties of organic cathode materials such as simplistic molecular engineering,^{4,14} cheap, plenty of availability, eco-friendly, and high theoretical capacity.¹³ organic molecules have one more attentional advantage: their chemical diversity.¹⁵ Till now, widely explored organic materials for LIBs are radical organic polymers,¹³ conjugated polymers,^{16,17} C=O and C/N-based compounds, and^{18,19} organosulfur compounds.^{13,17-19} A unfortunate solubility in an organic liquid electrolyte, capacity decay, and less cycle stability were often observed in these compounds, limiting their applicability.^{4, 20} To overcome the solubility issue, many attempts have been made, consisting of conductive carbon additives to ensure solidified structures^{4,21} and molecular polymerization of different molecules.^{22,23}

However, to overcome such problems, a creative and challenging approach needs to be addressed in the present day to enhance the capacities of electrode materials. Diversified redox-active molecules were investigated as active materials, including functional groups such as C=O, nitroxyl, and, phenoxy; among all, quinone (specific anthraquinone) was widely used as active cathode materials due to their adjustable redox potential, large theoretical capacities (due to putting on $2e^-/2Li^+$ per quinone unit), structural diversities, high rate of redox reaction and ecofriendliness.²⁴⁻³³

In this work, we have initially opened the molecular engineering doors and synthesized anthraquinone substituted rylene Imides AQ-PDI, AQ-NDI, and AQ-Py (Scheme 4.1) by simple imidization reaction of commercially available AQ-NH₂ and Rylene dyes (PDA, NDA, and PMDA). When our work was in progress, molecule AQ-PDI synthesis and their use in potassium ion batteries were reported.³⁴ Due to extended

conjugation of two anthraquinone substitutions over PDA, NDI, and PMDA synthesized molecule, the solubility in the liquid electrolyte will decrease. Most importantly, the core containing AQ-NH₂, PDA, NDA, and PMDA has a redox-active carbonyl group. Thus, after imidization, the theoretical specific capacity will not be sacrificed for compound AQ-PDI, AQ-NDI, and AQ-Py. The increased theoretical specific capacity is 200 mAh/g, 236.9 mAh/g, and 255.8 mAh/g, respectively, achieved by each molecule considering 6 electrons transfer redox mechanism. Anthraquinone arrangement on the rylene dyes (PDA, NDA, and PMDA) is expected to be perpendicular which helps facilitate the lithium-ion transfer by avoiding the aggregation of molecules.³⁵ However, molecule AQ-PDI shows a 40 % loss at 0.2 C from its theoretical capacity. In comparison, AQ-NDI and AQ-Py losses were 56% and 60% after 150 cycles at 0.2 C. Table 2.2 suggests that highly aromatic conjugated compounds containing active carbonyl group highly stable capacity retention for long-term cycling.

4.2 EXPERIMENTAL SECTION

4.2.1 Chemicals and Materials

All chemicals and reagents commercially available were used as received without further purification. Perylene-3,4,9,10-tetracarboxylic dianhydride, (PDA) 1,4,5,8-naphthalene tetracarboxylic dianhydride, (NDA) pyromellitic dianhydride, (PMDA) zinc acetate, 2-amino anthraquinone (AQ-NH₂) and Imidazole were purchased from Sigma-Aldrich. Dimethylformamide (DMF), chloroform (CHCl₃), Tetrahydrofuran (THF), dichloromethane (DCM), and acetone were purchased from Merck Chemicals. A battery-grade salt Bis(trifluoromethane)sulfonamide lithium salt (LiTFSI) and Polyvinyl difluoride (PVDF, Kynar HSV900, Arkema Inc., USA) was purchased from sigma Aldrich. 1,3-dioxolane (DOL), and 1,2 Dimethoxyethane (DME) N-Methyl-2-pyrrolidone (NMP) solvent used for battery performance were purchased from Sigma Aldrich (HPLC grade).

4.2.2 Instrumentation and General Experiments Method.

Structural characterization of molecules was done by recording their ¹H and spectra at room temperature on Bruker-AVENS, 400 or 500 MHz NMR instruments. Deuterated Sulfuric acid -d₂ solution (D₂SO₄) was used as a solvent in a trace amount of TMS as an internal reference. all compounds' chemical shift was reported in δ ppm downfield to TMS. In contrast, peak multiplicities are referred to as singlet (s), doublet (d), triplet (t), quartet (q), pentet (p), and multiplet (m). UV-vis absorption spectra were recorded on SPECORD®

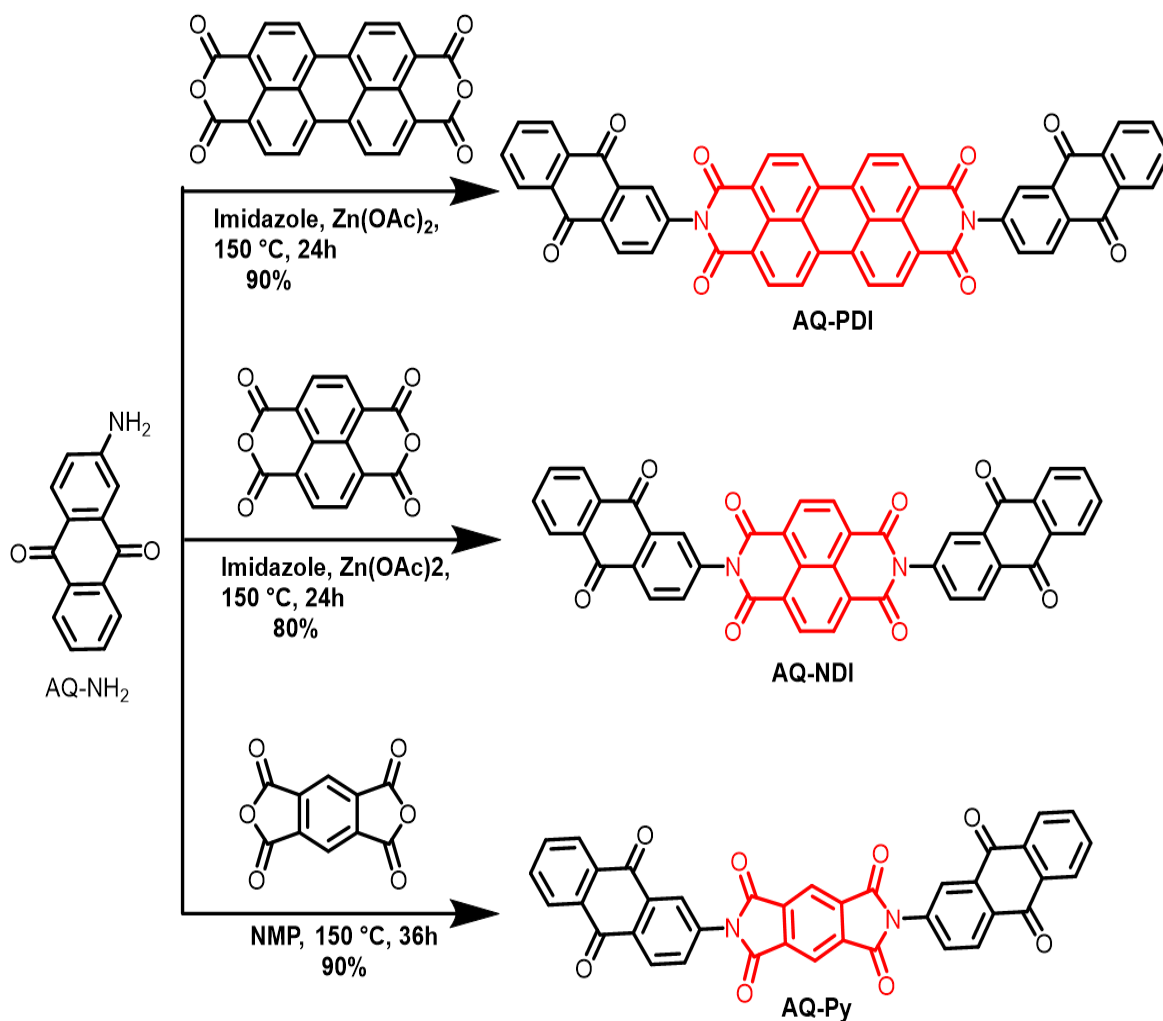
210/PLUS, a UV-visible spectrophotometer with deuterium and tungsten lamps as the source. The morphological characterizations of molecules were performed using FE-SEM with an instrument FEI Nova Nano SEM 450. Infrared spectra (IR) were recorded on a Bruker α -T spectrophotometer with sample pellets prepared by mixing with 5% w/w in KBr and dried under a vacuum before spectra were recorded. Thermogravimetric analysis (TGA) was recorded using Perkin Elmer STA 6000 Thermogravimetric Analyzer. Samples were scanned from 50 °C to 800 °C with a heating rate of 10 °C/ min under an inert nitrogen atmosphere. The cyclic voltammetry experiments were performed in a multi-channel auto lab MAC 80038 instrument with a potential range of 1 to 4 V vs. Li/Li⁺. Electrochemical Impedance Spectroscopy measurements (EIS) were done using a Biologic instrument in the frequency range of 40 kHz to 10 MHz. The galvanostatic charging/discharging experiments were carried out by using CR 2032-type coin cells on a Neware battery testing system (BTS7.5.6, Shenzhen, China) in the potential range of 1-4 V vs. Li/Li⁺.

Electrode preparation. (Cathode)

Working electrode (positive electrode) slurries were prepared by mixing 50% wt. active material AQ-PDI, AQ-NDI, and AQ-Py 40 % wt. Carbon black, and 10% wt. polyvinylidene fluoride (PVDF) as a binder. The mixture was put up in a grinder with N-methyl-2-pyrrolidinone (NMP). The mixture was thoroughly mixed to form a uniform slurry; the prepared slurry was uniformly coated on aluminum foil and then dried at 90 °C for 12 h in a vacuum oven. A circular shape electrode was punched by an electrode puncture machine, and a further electrode was transferred to an argon-filled glove box. CR 2032-type coin cells were fabricated by using Li-foil as a counter electrode, working electrode as an above organic compound, electrolyte as 1 M LiTFSI in a mixture of DOL/DME (1:1 by volume), and Celgard (2325) as the separator.

4.2.3 Synthesis and Characterization.

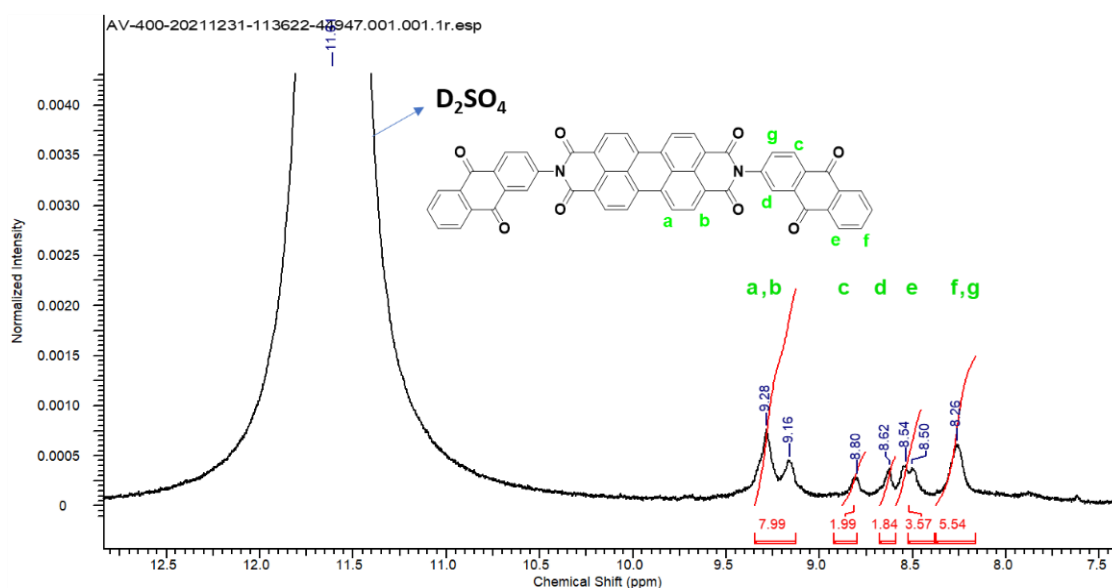
The -NH₂ group of anthraquinone (AQ-NH₂) was condensed with rylene dianhydrides dyes (PDA, NDA, and PMDA) to prepare compounds (AQ-PDI), (AQ-NDI), (AQ-Py), (Ph-PDI), (Scheme 4.1). The detailed synthesis and characterization of compounds can be found below.



Scheme 3.1: Synthesis of AQ-PDI, AQ-NDI and AQ-PY

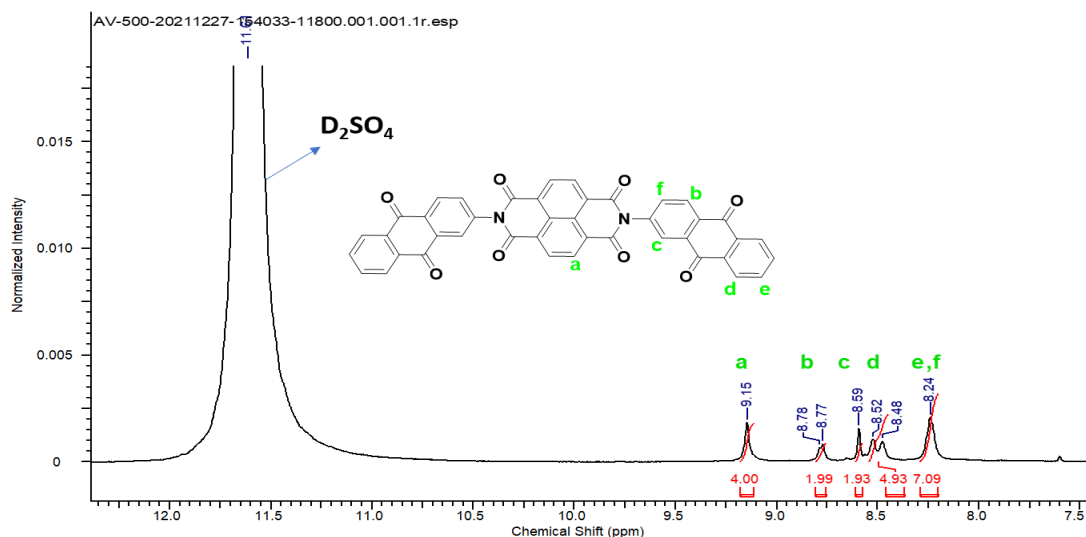
a) Synthesis of AQ-PDI

Procedure- A 100 mL two-neck round bottom flask equipped with a magnetic stirrer was charged with PDA (Perylene-3,4,9,10-tetracarboxylic dianhydride) (200 mg, 0.51 mmol), AQ-NH₂ (454 mg, 2.04 mmol), and zinc acetate (catalytic amount) taken in imidazole (15 g). The resultant mixture was heated at 150 °C for 24 h under an argon atmosphere. After completion of the reaction, the reaction mixture was cooled down to 70 °C. Then the product mixture was precipitated by adding 1 N HCl (100 ml). The resultant crude product was washed with deionized water until the eluant got neutral. The obtained product is washed with Acetone to remove excess AQ-NH₂. A sufficient amount of THF has been used to remove the unreacted PDA. The final product is a dark red solid (Yield 90 %). ¹H NMR (500 MHz, D₂SO₄, δ, ppm): 9.28 (m, 4-H, H_a), 9.16 (m, 4-H, H_b), 8.80 (m, 2-H, H_c), 8.62 (s, 2-H, H_d), 8.52 (m, 4-H, H_e), 8.26 (m, 6-H, H_f + H_g).

Figure 4.1: ^1H NMR spectra of AQ-PDI

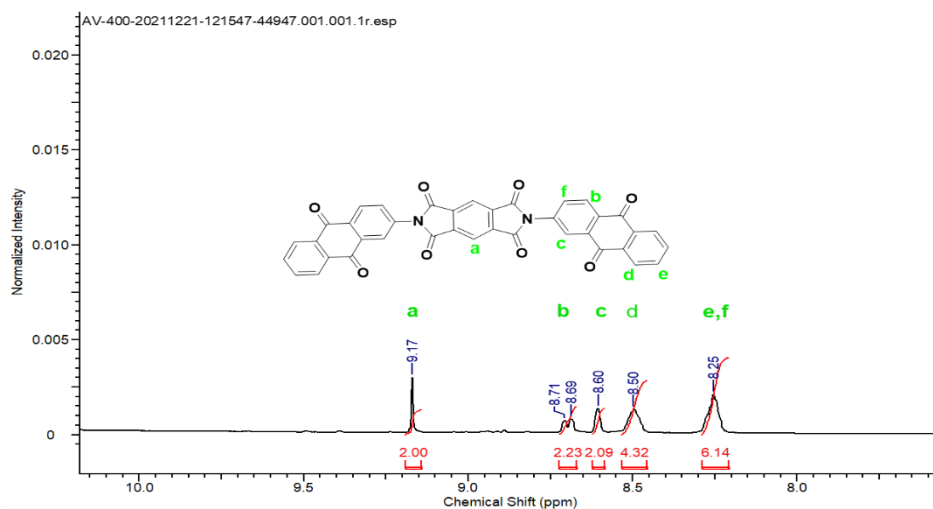
b) Synthesis of AQ-NDI

Procedure- In A 100 mL two-neck round bottom flask equipped with a magnetic stirrer was charged with NDA (1,4,5,8-naphthalene tetracarboxylic dianhydride), (200 mg, 0.74 mmol), AQ-NH₂ (577 mg, 2.59 mmol), and zinc acetate (catalytic amount) taken in imidazole (12 g). The resultant mixture was heated at 150 °C for 24 h under an argon atmosphere. After completion of the reaction, the reaction mixture was cooled down to 70 °C. Then the product mixture was precipitated by adding 1 N HCl (100 ml). The resultant crude product was washed with deionized water until the eluant get became neutral. The obtained product is washed with Acetone to remove excess AQ-NH₂. Further, the mixture was recrystallized in dimethyl sulfoxide (DMSO) and water to remove the unreacted NDA and get the purified product (Yield 80 %). ^1H NMR (500 MHz, D₂SO₄, δ , ppm): 9.15 (bs, 4-H, H_a), 8.78 (m, 2-H, H_b), 8.59 (s, 2-H, H_c), 8.50 (m, 4-H, H_d), 8.24 (m, 6-H, H_e + H_f).

Figure 4.2: ^1H NMR spectra of AQ-NDI

c) Synthesis of AQ-Py

Procedure- In A 100 mL two-neck round bottom flask equipped with a magnetic stirrer was charged with PMDA (pyromellitic dianhydride) (200 mg, 0.91 mmol), AQ-NH₂ (709 mg, 3.18 mmol), and zinc acetate (catalytic amount) taken in NMP (30 g). The resultant mixture was heated at 150 °C for 24 h under an argon atmosphere. After completion of the reaction, the reaction mixture was cooled down to room temperature. Then the product mixture was precipitated by adding deionized water. The obtained product is washed with Acetone to remove excess AQ-NH₂. Further, purification is done by recrystallizing in dimethyl sulfoxide (DMSO) water and removing the unreacted PMDA (Yield 90 %). ^1H NMR (500 MHz, D₂SO₄, δ , ppm): 9.17 (s, 2-H, H_a), 8.70 (d, 2-H, H_b), 8.60 (s, 2-H, H_c), 8.50 (m, 4-H, H_d), 8.26 (m, 6-H, H_e + H_f).

Figure 4.3: ^1H NMR spectra of AQ-Py

4.3 RESULT AND DISCUSSION

4.3.1 Fourier transform infrared spectroscopy (FT-IR)

Furthermore, structural information could be evaluated by FT-IR. Detail of functional group presence at respective wavenumber for molecule AQ-PDI, AQ-NDI, AQ-Py, and their parental substituent AQ-NH₂ are shown in figure 4.4. all these compounds show characteristics of strong absorption peaks at 1675, 1680, and 1675 cm⁻¹ for AQ-PDI, AQ-NDI, and AQ-Py, respectively, due to the unsymmetric stretching vibration of the C=O bond of cyclic imide. The further detailed stretching and bending vibrations are shown in table 4.1. To differentiate and confirm the synthesis of the compound (AQ-PDI, AQ-NDI, and AQ-Py) done by the presence of two -NH₂- vibration peaks at 3613 and 3685 cm⁻¹ in AQ-NH₂ (Primary amine), which become disappear in the final compound (AQ-PDI, AQ-NDI, AQ-Py) after imidization. The presence of ketonic C=O vibrational peak at 1740 cm⁻¹ for AQ-NH₂, which become appears for compound AQ-PDI, AQ-NDI, and AQ-Py at 1711, 1716, and 1720 cm⁻¹ respectively.

Table 4.1: FTIR data of AQ-NH₂, AQ-PDI, AQ-NDI, and AQ-Py

Molecule	Imide C=O Vas	Aromatic C=C Str. Mode	Imide C=O Bending Mode	Imide C-N Str. Mode	Ketonic C=O Str. Mode	-N-H. Str. Mode
AQ-NH ₂	1550 cm ⁻¹	----	----	1740 cm ⁻¹	3213,3326 cm ⁻¹
AQ-PDI	1675 cm ⁻¹	1590 cm ⁻¹	711 cm ⁻¹	1345 cm ⁻¹	1716 cm ⁻¹	-----
AQ-NDI	1680 cm ⁻¹	1590 cm ⁻¹	711 cm ⁻¹	1336 cm ⁻¹	1736 cm ⁻¹	-----
AQ-Py	1675 cm ⁻¹	1595 cm ⁻¹	711 cm ⁻¹	1380 cm ⁻¹	1780 cm ⁻¹	-----

4.3.2 UV-Visible absorption spectroscopy

The UV-Vis. absorption spectra were recorded at room temperature by taking a dilute solution of compounds AQ-PDI, AQ-NDI, and AQ-Py in N-methyl-2-pyrrolidone (NMP). AQ-PDI molecules show a sharp absorption peak at 526 nm, and 488 nm, and one hump at 450 nm with a calculated frontier orbital difference was 2.27 eV (Figure 4.5). Whereas for AQ-NDI and AQ-Py sharp peak was hypsochromically shifted to 377 nm, 357 nm, and 339 nm, 355 nm, respectively (Figure 4.5). The calculated frontier orbital difference for AQ-NDI and AQ-Py was observed to be 3.14 eV and 3.36 eV, respectively. Such noticeable hypsochromic shifting of the peak is due to the changing core of the rylene dyes from PDA to NDA and PMDA. Thus, more aromatic conjugation in AQ-PDI increases the energy of

HOMO, whereas compared to AQ-PDI, the less aromatic conjugation in AQ-NDI and AQ-Py decreases the energy level of HOMO, which results in an observed peak in the blue shift.

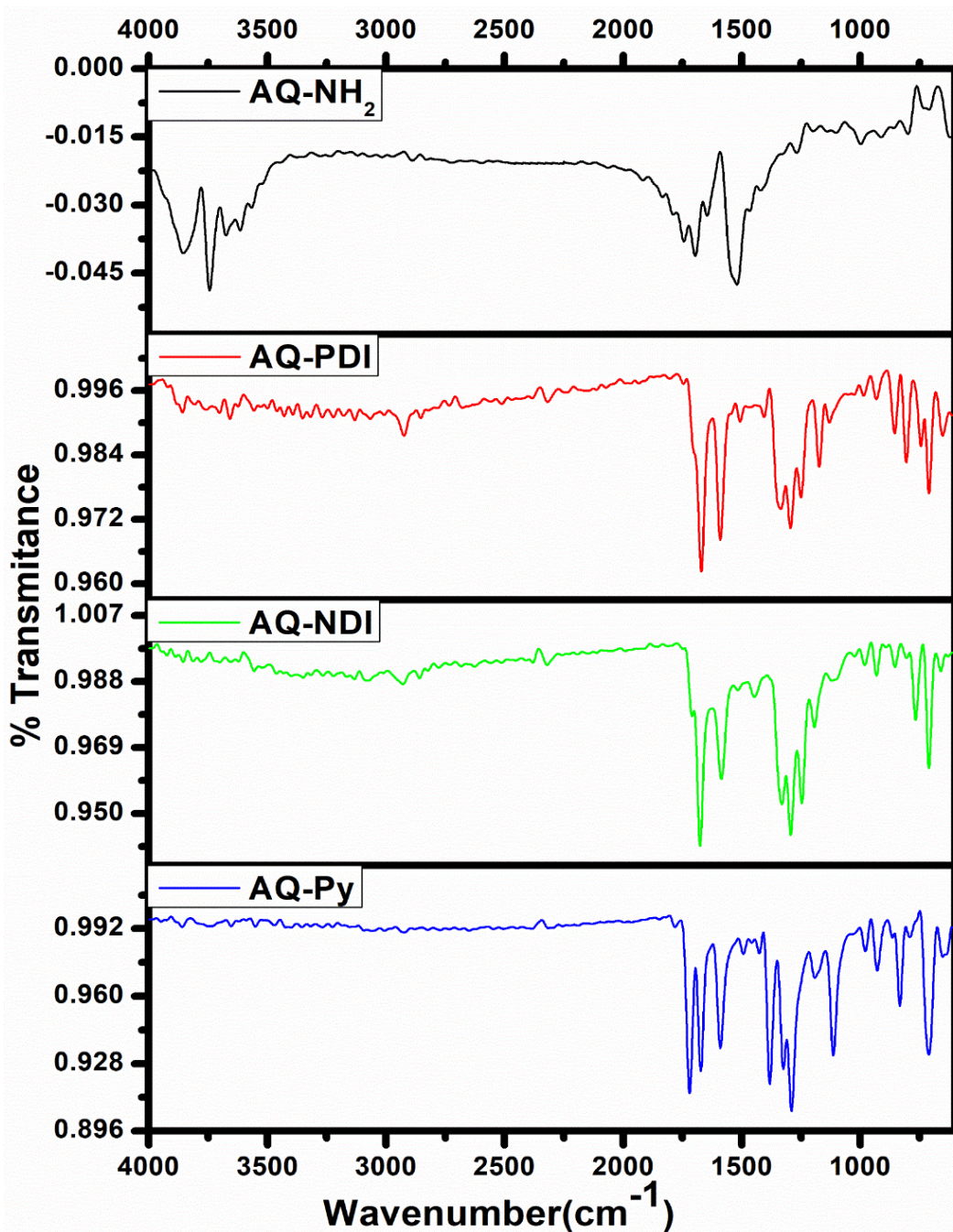


Figure 4.4: FTIR Spectra of AQ-NH₂, AQ-PDI, AQ-NDI, and AQ-Py

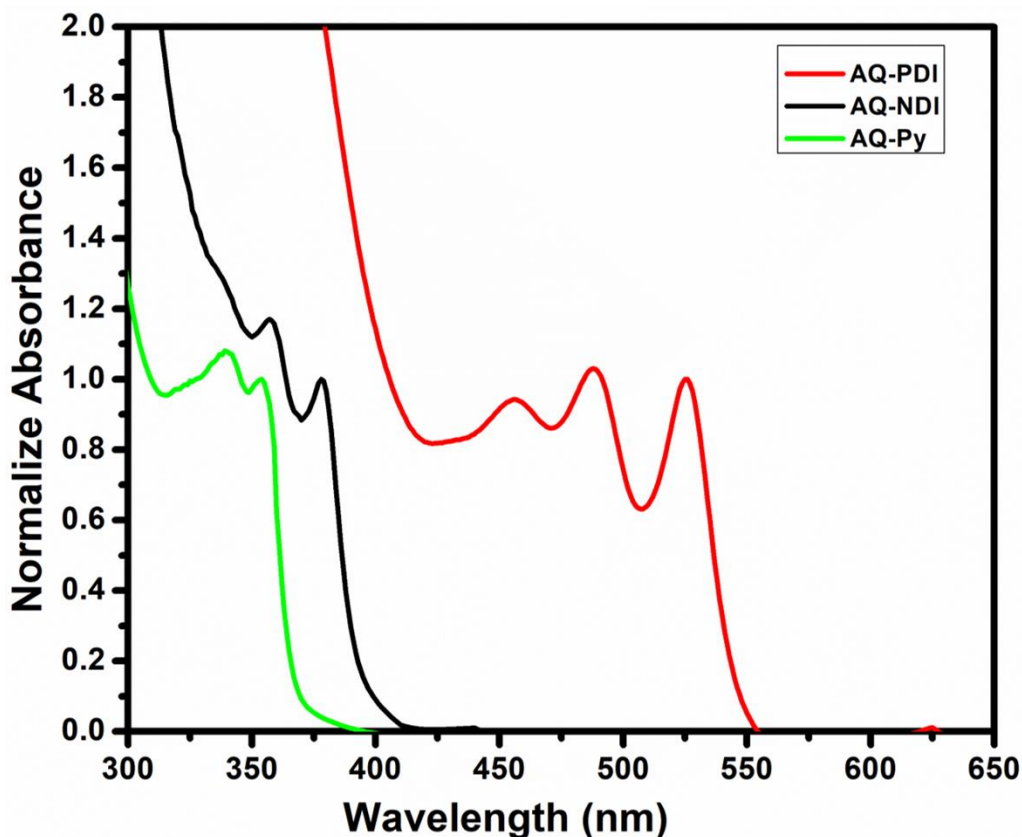


Figure 4.5: UV-Visible Absorption spectra of molecules AQ-PDI, AQ-NDI and AQ-Py before battery cycling

4.3.3 A morphological study of molecules by Field emission scanning electron microscope (FE-SEM) before and after battery cycling.

The morphological study was done by taking FE-SEM images of AQ-PDI, AQ-NDI, and AQ-Py as-synthesized and after the 150th charge/discharge cycle. The sample was prepared by dispersing a sample of about 1 mg in 2 ml N-methyl-2-pyrrolidone (NMP). After that, 5–10 μL of the dispersed solution was drop-casted on ZP-P4VP spun silicon wafers. It can be seen from figure 4.6a that AQ-PDI shows sheet-type morphology (20 μm) with a smooth surface. Whereas AQ-NDI morphology (20 μm) seemed to be a flappy sheet (Figure 4.6c), the morphology becomes a long sheet with a smooth surface in AQ-Py. (Figure 4.6e). Generally, solubility in liquid electrolytes of active organic materials results in a notable loss of active mass in the electrolyte. The change in the crystal morphology of molecules is also observed. To know the solubility in liquid electrolytes and the fate of the obtained morphology of AQ-PDI, AQ-NDI, and AQ-Py after charge/discharge cycling,

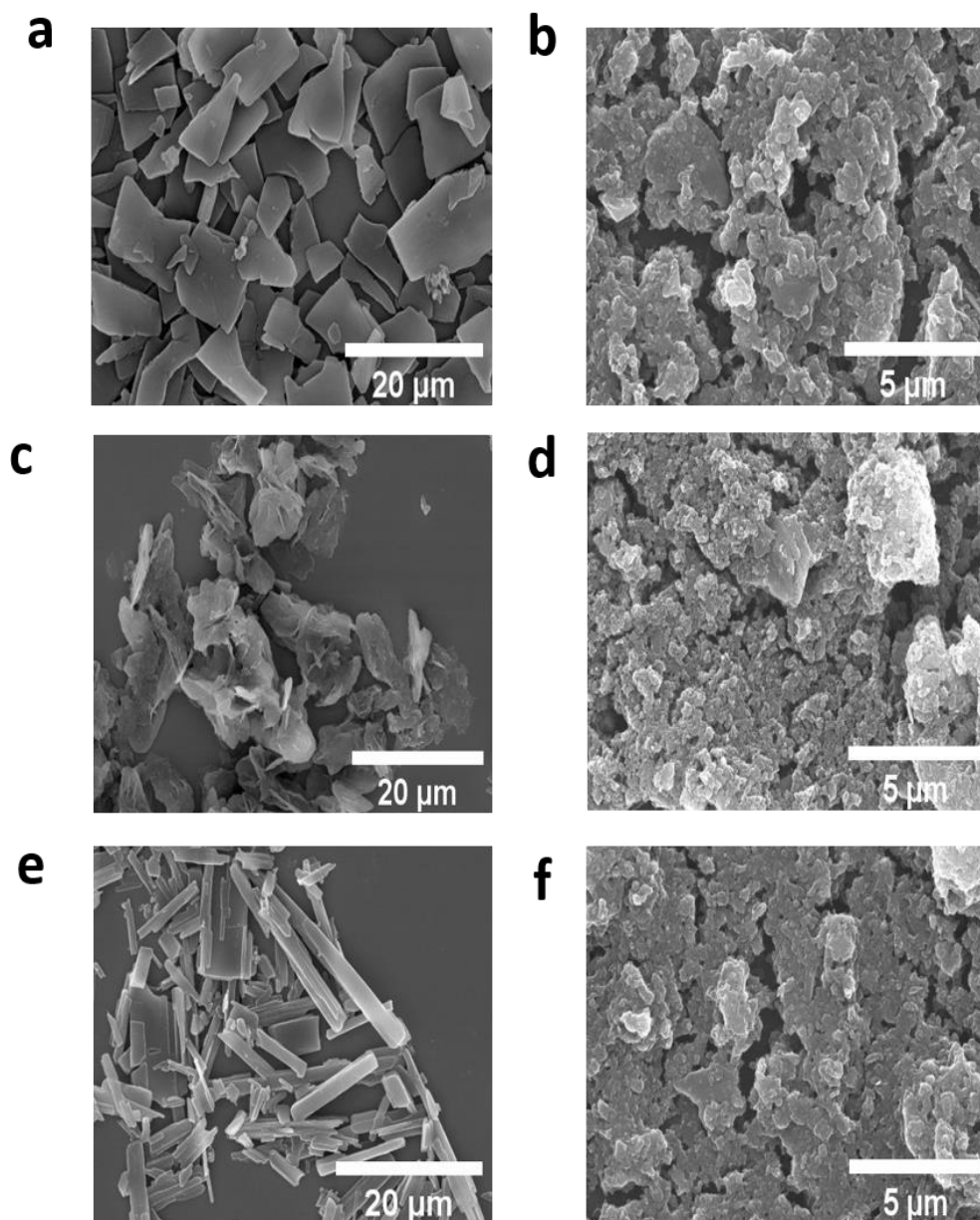


Figure 4.6: FE-SEM images of AQ-PDI molecule before (a) and after 150th cycles (b) FE-SEM images of AQ-NDI molecule before (c) and after 150th cycles (d) FE-SEM images of AQ-Py molecule before (e) and after 150th cycles (f)

morphology was measured by FE-SEM for all three molecules after the 150th cycle. The sample was collected after a 150th charge/ discharge cycle. For that, a coin cell was dissembled, and the sample-coated aluminum foil cathode electrode was washed with acetonitrile and ethanol to wash out the electrolyte and dissolved binder (PVDF). After that, the coated electrode materials crashed, and powder was dispersed in NMP. A dispersed solution of the sample was drop cast on ZP-P4VP spun silicon wafers, and FE-SEM images were recorded. An AQ-PDI shows the same sheet morphology was observed with a powder

mark of carbon black after the 150th charge/ discharge cycle (Figure 4.6b). However, a sheet morphology for AQ-NDI and long sheet morphology of AQ-Py still persisted after the 150th cycle. (Figure 4.6d, f) Generally, long-term insertion and deinsertion of lithium-ion in active materials lead to the form of a crack in the active materials. A change in surface roughness was also observed, but here we did not find any significant difference in the surface of active molecules. However, all molecule's morphology shows an intact presence after the 150th cycle indicating molecules AQ-PDI, AQ-NDI and AQ-Py will not be soluble in a liquid electrolyte. It does present as such on the electrode.

4.3.4 Thermogravimetric analysis (TGA)

The thermal stability of all three molecules (AQ-PDI, AQ-NDI, and AQ-Py) was carried out by TGA. As shown in figure 4.7d, the thermogram of all compounds offers good stability while experimenting with a nitrogen environment in the temperature between 50 °C to 800 °C while keeping a scanning rate of 10 °C /min. In detail, AQ-PDI start decomposing at 526 °C (Figure 4.7d), whereas AQ-NDI and AQ-Py start decomposing at 346 °C and 253 °C, respectively (Figure 4.7d). This result indicates a much more increase in thermal stability than their parental compound, namely PDA, NDA, and PMDA^{36,37} units.

4.3.5 Electrochemical performance of molecules.

4.3.5.1 Cyclic voltammetry

Cyclic voltammetry studies were performed using coin cells with AQ-PDI, AQ-NDI, and AQ-Py as working electrodes, whereas counter and reference electrodes as lithium foil. The redox potential of these molecules was analyzed vs. Li/Li⁺ through cyclic voltammetry while sweeping potential between 1V to 4V (scan rate 1 mV/s). Even though many oxidations and reduction peaks were observed in the CV scan here, we have evaluated only two pairs of prominent oxidation and reduction large hump here, which further ideally helps to show the possible two-step mechanism of lithium intercalation and deintercalation. (In section 4.3.5.3). AQ-PDI displayed two reduction humps centered at 2.29 and 2.10 V and two oxidation humps centered at 2.38 and 2.38 V. (Figure 4.7a) AQ-NDI displayed two reduction peaks centered at 2.25, 1.98 V; two oxidation hump centered 2.47, 2.27 V. (Figure 4.7b). In contrast, AQ-Py also shows two reduction humps centered at 2.14 and 1.95 V and two oxidation humps centered at 2.50 and 2.27 V. (Figure 4.7c). For all three molecules, ideally, six carbonyl groups take part in the redox process.³⁸ while the first redox peaks, four carbonyl groups from two anthraquinone units undergo lithiation/dilithiation, and the second

redox peaks represent the two-carbonyl group of the core backbone undergoes lithiation/delithiation.³⁹

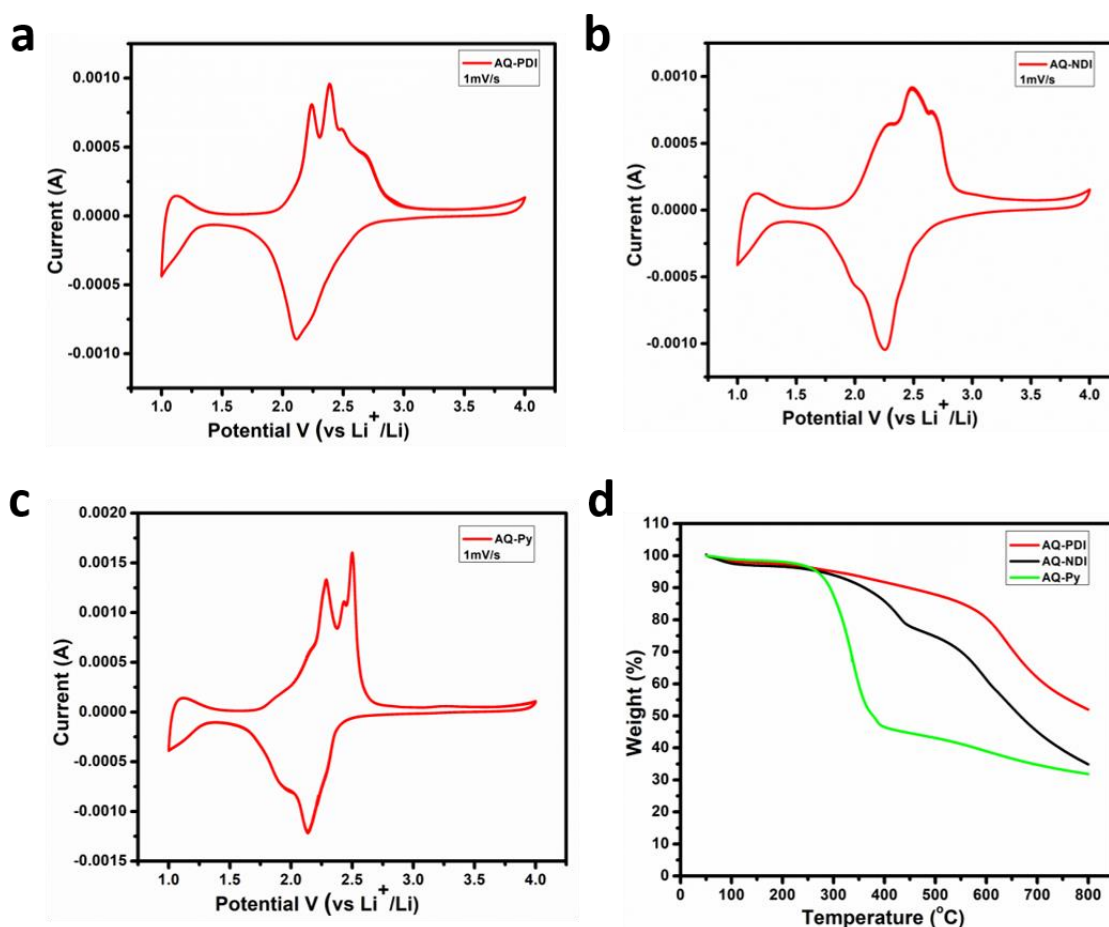


Figure 4.7: cyclic voltammograms (a) of molecules AQ-PDI, (b) AQ-NDI, (b) and (c) AQ-Py (d) TGA profile of AQ-PDI, AQ-NDI and AQ-Py.

4.3.5.2 Electrochemical Impedance Spectroscopy (EIS) Measurement.

Impedance spectroscopy was done to evaluate a detailed and comparative study of the kinetic process and internal resistance of electrochemical cells^{40,41} of molecules AQ-PDI, AQ-NDI, and AQ-Py. A Biologic instrument was used to measure the electrochemical impedance spectroscopy at a frequency between 40 kHz to 10 MHz and signal amplitude of 5 mV. However, examinations were conducted using the fully prepared battery cell with the organic compounds' cathode and (scheme 4.1) the Li-chip as an anode. The equivalent circuits were shown in the inset figure 4.8a for evaluating the value of electrolyte resistance (R_s), charge-transfer resistance (R_{ct}), and Warburg impedance (W). It appears that AQ-PDI,

AQ-NDI, and AQ-Py exhibit similar characteristics, in that every profile consists of a semi-circle at a high frequency and a tail low-frequency range. Before battery cycling, the EIS profile of AQ-PDI, AQ-NDI, and AQ-Py have the same R_s value of approximately 3.2Ω . (Figure 4.8 a). However, all the tested electrode materials of fresh cell R_{ct} value gradually decreased from AQ-PDI (95Ω), AQ-NDI (73Ω) to AQ-Py (58Ω) (Figure 4.8 a), indicating the rate of lithium-ion transport increases in the order of AQ-PDI < AQ-NDI < AQ-Py. On the other hand, it suggests that high fast reaction kinetics are possible for AQ-Py than AQ-PDI and AQ-NDI. The impedance of the same cells was measured after the 20th charge/discharge cycle. It was observed that there was no significant change in electrolytic resistance (4.3Ω). (Figure 4.8 b) But charge transfer resistance was decreased gradually for compound AQ-PDI (77Ω) to AQ-NDI (63Ω) and AQ-Py (51Ω). (Figure 4.8 b) The R_{ct} value after the 20th charge/discharge cycle was less than their respective fresh cell R_c value. It's because of wetting of the electrode by electrolyte throughout charge/discharge cycling.

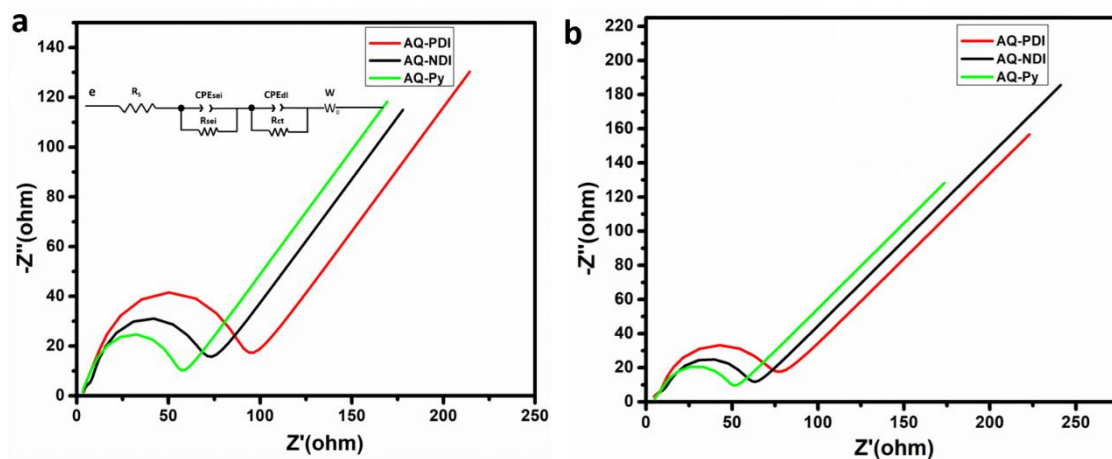
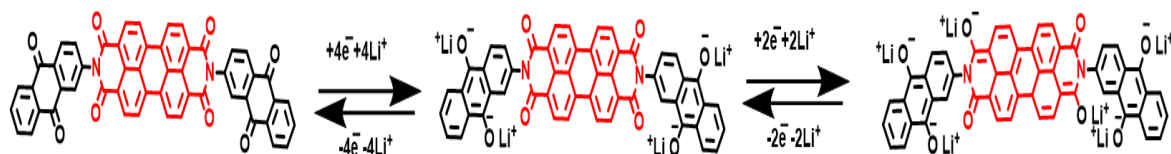


Figure 4.8: Nyquist plots of fresh AQ-PDI, AQ-NDI, and AQ-Py electrode cell. The inset shows the equivalent circuit. (a) and (b) Nyquist plots of after 20th the galvanostatic charge/discharge cycling.

4.3.5.3 Proposed electrochemical redox mechanism of molecules.

All synthesized Anthraquinone substituted rylene imide AQ-PDI, AQ-NDI, and AQ-Py; it consists of six electrochemically active carbonyl groups. Two anthraquinone carbonyl moieties consist of four reductions centered, whereas two reduction-centered carbonyl moieties are present at the central organic core. All these molecules undergo six electron transfers during the redox reaction, consisting of the following two-step mechanism.



4.3.5.4 Galvanostatic charge/discharge experiment

A fabricated CR-2032 type coin cell was used for the galvanostatic charge/discharge experiment. Figures 3.9 a, b, and c shows galvanostatic charge/discharge profile for molecules AQ-PDI, AQ-NDI, and AQ-Py. All compounds were measured at a 0.2 C rate in the voltage window 1 to 4 V (vs. Li^+/Li). A first charge cycle for AQ-PDI, AQ-NDI, and AQ-Py exhibit a specific capacity of 214, 240, and 278 mAh/g, respectively, whereas the first discharge capacity for this molecule was observed at 209, 235, and 290 mAh/g, respectively that was much larger than their theoretical specific capacity (Table 4.2). This is maybe because of the generation SEI layer over the surface of the electrode. In the charge/discharge profile, A discharge curve for AQ-PDI found one well-defined plateau centered at 1.89 V (figure 4.9 a), whereas AQ-NDI and AQ-Py discharge curves also exhibit only one well-defined plateau at 1.96 V, and 1.856 V, respectively. (figure 4.9 b,c). significantly, the shape of the charge-discharge voltage profiles was finely conserved fro

Table 4.2: Battery metrics for molecules AQ-PDI, AQ-NDI and AQ-Py as a function of charge discharge cycles

Molecule	Charge/ discharge potential window vs Li/Li^+	Charge/ discharge C Rate	Theoretical sp. capacity	Sp. capacity at first Discharge Cycle	Sp. capacity 150 th discharge Cycle	Percentage decrease sp. capacity as Function of 150 th Charge/ Discharge Cycle
AQ-PDI	1-4 V	0.2 C / 0.2 C	200 mAhg^{-1}	208 mAhg^{-1}	120 mAhg^{-1}	40 %
AQ-NDI	1-4 V	0.2 C / 0.2 C	236.9 mAhg^{-1}	235 mAhg^{-1}	103 mAhg^{-1}	56 %
AQ-Py	1-4 V	0.2 C / 0.2 C	255 mAhg^{-1}	291 mAhg^{-1}	97 mAhg^{-1}	60 %

1st to the 150th cycle, clearly indicating the good reaction reversibility of all these three cathodes.

In the long-term cycling experiment, the cycle stability was measured till the 150th cycle for each molecule at 0.2 C and 2 C. All these molecules show stable capacity up to

150th cycles. In detail, the discharge capacity of AQ-PDI shows 120 mAh/g after the 150th charge /discharge cycle at a 0.2 C rate consisting average Coulombic efficiency is 99%. (Figure 4.9 d) AQ-NDI exhibits a discharge capacity of 103 mAh/g, whereas AQ-Py shows 97 mAh/g discharge capacity after the 150th cycle at 0.2 C with excellent Coulombic efficiency between 97-100 % for both molecules. (Figure 4.9 e,f) All these molecules show excellent coulombic efficiency between 97-100 %, which confirms that these all molecules show good reaction reversibility throughout the 150th charge/discharge cycle. The % decrease after the 150th cycle from its theoretical capacity was found to be 40 %, 56 %, and 60 % for molecules AQ-PDI, AQ-NDI, and AQ-Py, respectively. (Table 4.2) This confirms that the long-term cycling stability increases as a function of the increased conjugated aromatic unit, such as the stability order for molecules, which is AQ-PDI>AQ-NDI>AQ-Py, consisting of 4, 2, and 1 Aromatic unit, respectively, in their parent moiety (PDA, NDA, and PMDA).

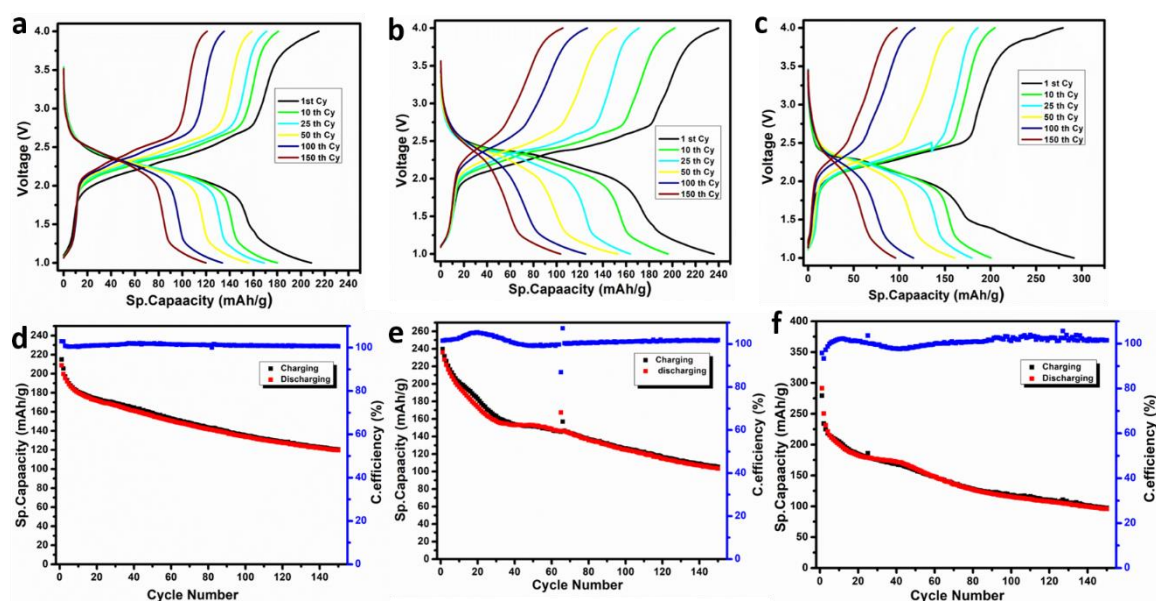


Figure 4.9: Galvanostatic charge/discharge profile curve of (a) AQ-PDI (b) AQ-NDI and (c) AQ-Py. Cycling stability at 0.2 C for (d) AQ-PDI, (e) AQ-NDI, and (f) AQ-Py

In this set of experiments, we tested all molecules for long-term cycling (150th Cycle) at a fast charge and discharge rate (2 C) to know the stability of the fast reaction kinetics of the molecules. AQ-PDI shows the first cycle discharge capacity of 168 mAh/g that was decreased to 105 mAh/g after the 150th cycle with coulombic efficiency between 94-100% (Figure 4.10 a). Whereas molecules AQ-NDI show an initial discharge capacity of 150 mAh/g, which became 66 mAh/g after the 150th cycle with coulombic efficiency between 95-105 %. (Figure 4.10 b). A molecule AQ-Py shows a first cycle discharge capacity of 149

mAh/g that was decreased to 85 mAh/g after the 150th cycle with very fluctuating coulombic efficiency between 95-105% (Figure 4.10 c). the above study confirms that the AQ-PDI is stable even at a high charge/discharge C (2 C) rate. The decrease in capacity for AQ-NDI and AQ-Py at a high C rate may be because of the solubility of molecules in liquid electrolyte because battery temperature will increase at a high C rate, and it may be making molecules soluble at high temperature.

Rate study

To understand the stability of molecules at different C rates, the rate capability was studied for molecules AQ-PDI, AQ-NDI, and AQ-Py. The C rate was varied between 0.2 to 30 C, and specific capacity was monitored. Each C rate was tested for five consecutive charge-discharge cycles. For all molecules, the specific capacity was found to decrease gradually with increasing C rates (Figure 4.10 d,e f) which are maybe due to an increase in the internal

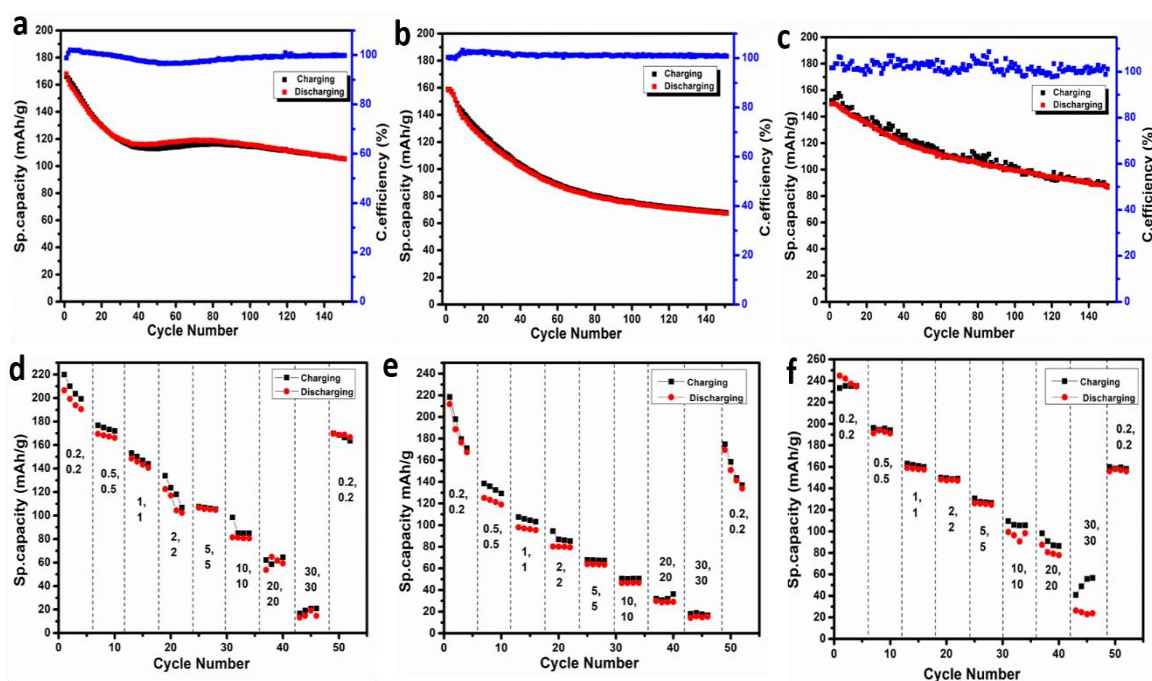


Figure 4.10: Cycling stability at 2 C for (a) AQ-PDI (b) AQ-NDI and (c) AQ-Py. Rate capability for (d) AQ-PDI (e) AQ-NDI and (f) AQ-Py at different C rate.

temperature of batteries. For AQ-PDI at a 0.2 C rate, the discharge capacity was 207 mAh/g, which gets reduced to 13 mAh/g at 30 C (Figure 4.10d), which is significantly less than the theoretical capacity (200 mAh/g) of the molecule AQ-PDI. When we charge-discharge the same cell at a low C rate (0.2 C), the discharge-specific capacity bounces back to 168 mAh/g, which was almost near to the initial charge-discharge rate (0.2 C). (Figure 4.10d) For AQ-NDI at a 0.2 C rate, the discharge specific capacity was 211 mAh/g which gets reduced to

14 mAh/g at 30 C. which is almost negligible; the specific capacity was bounced back to 147 mAh/g when we again charge-discharge the same cell at a low C rate (0.2 C). (Figure 4.10 e) whereas AQ-Py at a 0.2 C rate, the discharge capacity was 243 mAh/g, which gets reduced to 25 mAh/g at 30 C. (Figure 4.10 f). Same cells at a low C rate (0.2 C), the discharge-specific capacity bounced back at 153 mAh/g (Figure 4.10 f), which was observed to be less than the initial C rate (0.2 C); this contradictory result may be due to the dissolution of active masses in the liquid electrolyte at high C rate. The molecules AQ-Py show a discharge capacity of 85 mAh/g at a 20 C rate, which was significantly better compared to AQ-NDI (27 mAh/g) and even than AQ-PDI (53 mAh/g). This indicates that superior rate behavior is possible for AQ-Py than AQ-NDI and AQ-PDI, which is further confirmed by their low R_{ct} values (figure 4.8a). At an ultra-high C rate (30 C), none of the molecules can show a desired specific capacity.

4.3.6 Solubility study of molecules in liquid electrolytes.

4.3.6.2 UV-Visible Spectroscopy after 150th Cycle

The battery working electrode was identified further for the existence of molecules (AQ-PDI, AQ-NDI, and AQ-Py) after the 150th charge/discharge cycling. The battery cell was disassembled after the 150th cycle, and the cathode materials were washed with acetonitrile and ethanol to remove the electrolyte and binder (PVDF). The working electrode was crashed, and the powder was collected in fresh NMP, and UV-Visible Spectra were recorded. The peak corresponds to AQ-PDI, AQ-NDI, and AQ-Py, which were observed in figure 4.5, are intact after the 150th charge/discharge cycle (Figure 4.11). This indicates the molecule is still there on the electrode after the 150th cycle without dissolving in the electrolyte.

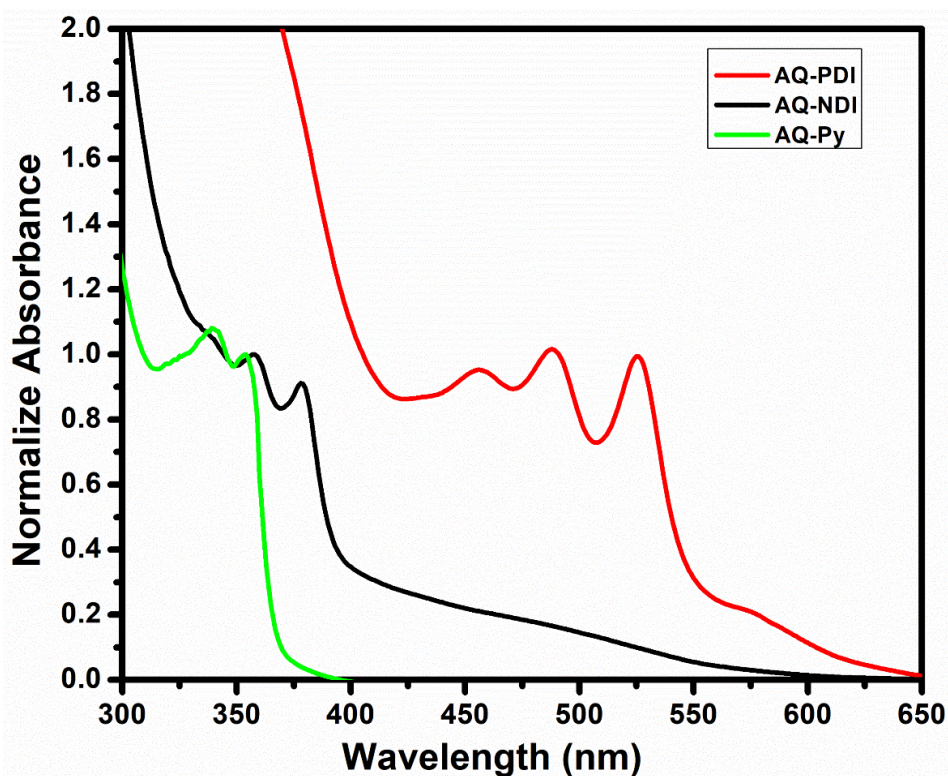


Figure 4.11: UV-Visible Absorption spectra of molecules AQ-PDI, AQ-NDI, and AQ-Py After 150th battery cycling

4.3.6.2 Electrode soaking experiments.

To monitor the effect of Anthraquinone substitution over solubility of the synthesized molecule (Scheme 4.1) in battery liquid electrolyte (LiTFSI in DOL: DME 1:1), we have taken the prepared electrode of the sample and put it into a battery electrolyte for soaking and observed change in colored of an electrode-soaked molecule with respect to the without any electrode (Blank) electrolyte. As the soaking time changed from 0 days to 7 days, the sample's color remained unchanged (Figure 4.12), which clearly indicates the insolubility of AQ-PDI, AQ-NDI, and AQ-Py in liquid electrolyte.

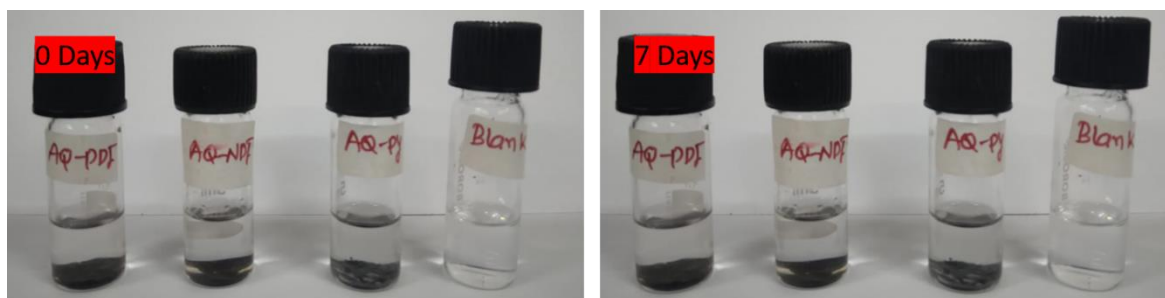


Figure 4.12: Photographs of the blank electrolyte and AQ-PDI, AQ-NDI and AQ-Py soaked active electrode at 0 days and 7 days respectively.

4.4 CONCLUSION

We have successfully designed and synthesized anthraquinone substituted, high theoretical capacity containing rylene imides derivatives such as AQ-PDI, AQ-NDI, and AQ-Py. We have investigated the chemical structure, structural properties, thermal properties, and morphological study before applying organic cathode in LIBs. All these cathode materials exhibit a first discharge capacity that is higher or near to their theoretical specific capacity (Table 4.2), which confirms a stable six electron transfer for each molecule. When we applied AQ-PDI, AQ-NDI, and AQ-Py as cathode materials, the LIBs cell showed a discharge capacity of 120, 103, and 97 mAh/g at 0.2 C, respectively. This capacity follows long-term cycling stability as a function of an increase in aromatic conjugation in the central organic core. Poor solubility in liquid electrolyte high-rate capability was achieved due to the anthraquinone perpendicular substitution on PDA, NDA, and PMDA. At 20 C, the discharge capacity of AQ-Py was 85 mAh/g, indicating that high reaction kinetics are possible for the AQ-Py molecules, further confirmed by their low R_{ct} value (58 Ω).

4.5 REFERENCES

- (1) Armand, M.; Tarascon, J. M. Building better batteries. *nature*. **2008**, *451*, 652-657.
- (2) Winter, M.; Brodd, R. J. (2004). What are batteries, fuel cells, and supercapacitors?. *Chem. Rev.* **2004**, *104*, 4245-4270.
- (3) Mohamed, M.G.; Sharma, S.U.; Yang, C.H.; Samy, M.M.; Mohammed, A.A.; Chaganti, S.V.; Lee, J.T.; Wei-Kuo, S. Anthraquinone-Enriched Conjugated Microporous Polymers as Organic Cathode Materials for High-Performance Lithium-Ion Batteries. *ACS Appl. Energy Mater.* **2021**, *4*, 14628–14639
- (4) Xue, X.; Luo, J.; Kong, L.; Zhao, J.; Zhang, Y.; Du, H.; Chen, S.; Xie, Y. The synthesis of triazine–thiophene–thiophene conjugated porous polymers and their composites with carbon as anode materials in lithium-ion batteries. *RSC Adv.* **2021**, *11*, 10688–10698.
- (5) Zhang, C.; He, Y.; Mu, P.; Wang, X.; He, Q.; Chen, Y.; Zeng, J.; Wang, F.; Xu, Y.; Xing, J. Toward High Performance Thiophene-Containing Conjugated Microporous Polymer Anodes for Lithium-Ion Batteries through Structure Design. *Adv. Funct. Mater.* **2018**, *28*, No. 1705432.
- (6) Zhang, S.; Huang, W.; Hu, P.; Huang, C.; Shang, C.; Zhang, C.; Yang, R.; Cui, G. Conjugated microporous polymers with excellent electrochemical performance for lithium and sodium storage. *J. Mater. Chem. A* **2015**, *3*, 1896–1901.
- (7) Li, M.; Lu, J.; Chen, Z.; Amine, K. 30 Years of Lithium-Ion Batteries. *Adv. Mater.* **2018**, *30*, No. 1800561.
- (8) Liu, W.; Song, M. S.; Kong, B.; Cui, Y. Flexible and Stretchable Energy Storage: Recent Advances and Future Perspectives. *Adv. Mater.* **2017**, *29*, No. 1603436.
- (9) Schmuch, R.; Wagner, R.; Hörpel, G.; Placke, T.; Winter, M. Performance and cost of materials for lithium-based rechargeable automotive batteries. *Nat. Energy.* **2018**, *3*, 267–278.
- (10) De, A.; Das, S.; Samanta, A. Hot Hole Transfer Dynamics from CsPbBr₃ Perovskite Nanocrystals. *ACS Energy Lett.* **2020**, *5*, 2246–2252.
- (11) Larcher, D.; Tarascon, J. M. Towards greener and more sustainable batteries for electrical energy storage. *Nat. Chem.* **2015**, *7*, 19–29.
- (12) Liu, Y. C.; Yeh, L. H.; Zheng, M. J.; Wu, K. C. W. Highly selective and high-performance osmotic power generators in sub nano channel membranes enabled by metal-organic frameworks. *Sci. Adv.* **2021**, *7*, No. eabe9924.

- (13) Wang, J.; Chen, C. S.; Zhang, Y. Hexaazatrinaphthylene-Based Porous Organic as Organic Cathode Materials for Polymers Lithium- Ion Batteries. *ACS Sustainable Chem. Eng.* **2018**, *6*, 1772–1779.
- (14) Armand, M.; Grugeon, S.; Vezin, H.; Laruelle, S.; Ribi re, P.; Poizot, P.; Tarascon, J. M. Conjugated dicarboxylate anodes for Li-ion batteries. *Nat. Mater.* **2009**, *8*, 120–125.
- (15) Wang, H. G.; Li, Q.; Wu, Q.; Si, Z.; Lv, X.; Liang, X.; Wang, H.; Sun, L.; Shi, W.; Song, S. Conjugated Microporous Polymers with Bipolar and Double Redox-Active Centers for High-Performance Dual-Ion, Organic Symmetric Battery. *Adv. Energy Mater.* **2021**, *11*, No. 2100381.
- (16) Shi, Y.; Zhou, X.; Zhang, J.; Bruck, A. M.; Bond, A. C.; Marschilok, A. C.; Takeuchi, K. J.; Takeuchi, E. S.; Yu, G. Nanostructured Conductive Polymer Gels as a General Framework Material To Improve Electrochemical Performance of Cathode Materials in Li-Ion Batteries. *Nano Lett.* **2017**, *17*, 1906–1914.
- (17) Xu, N.; Mei, S.; Chen, Z.; Dong, Y.; Li, W.; Zhang, C. Highperformance Li-organic battery based on thiophene-containing porous organic polymers with different morphology and surface area as the anode materials. *Chem. Eng. J.* **2020**, *395*, No. 124975.
- (18) Hong, J.; Lee, M.; Lee, B.; Seo, D. H.; Park, C. B.; Kang, K. Biologically inspired pteridine redox centres for rechargeable batteries. *Nat. Commun.* **2014**, *5*, No. 5335.
- (19) Schon, T. B.; Tilley, A. J.; Bridges, C. R.; Miltenburg, M. B.; Seferos, D. S. Bio-Derived Polymers for Sustainable Lithium-Ion Batteries. *Adv. Funct. Mater.* **2016**, *26*, 6896–6903.
- (20) Peng, C.; Ning, G. H.; Su, J.; Zhong, G.; Tang, W.; Tian, B.; Su, C.; Yu, D.; Zu, L.; Yang, J. M.; Ng, F.; Hu, Y. S.; Yang, Y.; Armand, M.; Loh, K. P. Reversible multi-electron redox chemistry of π -conjugated N-containing heteroaromatic molecule-based organic cathodes. *Nat. Energy* **2017**, *2*, No. 17074.
- (21) Jaffe, A.; Valdes, A. S.; Karunadasa, H. I. Quinone-Functionalized Carbon Black Cathodes for Lithium Batteries with High Power Densities. *Chem. Mater.* **2015**, *27*, 3568–3571.
- (22) Oyaizu, K.; Choi, W.; Nishide, H. Functionalization of poly (4-chloromethylstyrene) with anthraquinone pendants for organic anode-active materials. *Polym. Adv. Technol.* **2011**, *22*, 1242–1247.

- (23) Samy, M. M.; Mohamed, M. G.; Mansoure, T. H.; Meng, T. S.; Khan, M. A. R.; Liaw, C. C.; Kuo, S. W. Solid state chemical transformations through ring-opening polymerization of ferrocene-based conjugated microporous polymers in host–guest complexes with benzoxazine-linked cyclodextrin. *J. Taiwan Inst. Chem. Eng.* **2022**, *132*, 104110
- (24) Häupler, B.; Wild, A.; Schubert, U. S. Carbonyls: Powerful Organic Materials for Secondary Batteries. *Adv. Energy Mater.* **2015**, *5*, No. 1402034.
- (25) Kim, K. C.; Liu, T.; Lee, S. W.; Jang, S. S. First-Principles Density Functional Theory Modeling of Li Binding: Thermodynamics and Redox Properties of Quinone Derivatives for Lithium-Ion Batteries. *J. Am. Chem. Soc.* **2016**, *138*, 2374–2382.
- (26) Liang, Y.; Tao, Z.; Chen, J. Organic Electrode Materials for Rechargeable Lithium Batteries. *Adv. Energy Mater.* **2012**, *2*, 742–769.
- (27) Mohamed, M. G.; Mnanoure, T. H.; Takashi, Y.; Samy, M. M.; Chen, T.; Kuo, S. W. Ultrastable Porous Organic/Inorganic Polymers Based on Polyhedral Oligomeric Silsesquioxane (POSS) Hybrids Exhibiting High Performance for Thermal Property and Energy Storage. *Microporous Mesoporous Mater.* **2021**, *328*, No. 111505.
- (28) Molina, A.; Patil, N.; Ventosa, E.; Liras, M.; Palma, J.; Marcilla, R. New Anthraquinone-Based Conjugated Microporous Polymer Cathode with Ultrahigh Specific Surface Area for High-Performance Lithium-Ion Batteries. *Adv. Funct. Mater.* **2020**, *30*, 1908074.
- (29) Rasheev, H. G.; Araujo, R. B.; Tadjer, A.; Johansson, P. Fundamental promise of anthraquinone functionalized graphene based next generation battery electrodes: a DFT study. *J. Mater. Chem. A* **2020**, *8*, 14152–14161.
- (30) Son, E. J.; Kim, J. H.; Kima, K.; Park, C. B. Quinone and its derivatives for energy harvesting and storage materials. *J. Mater. Chem. A* **2016**, *4*, 11179–11202.
- (31) Sotomura, T.; Uemachi, H.; Takeyama, K.; Naoi, K.; Oyama, N. New organodisulfide-polyaniline composite cathode for secondary lithium battery. *Electrochim. Acta.* **1992**, *37*, 1851–1854.
- (32) Wu, Y.; Zeng, R.; Nan, J.; Shu, D.; Qiu, Y.; Chou, S. L. Quinone Electrode Materials for Rechargeable Lithium/Sodium Ion Batteries. *Adv. Energy Mater.* **2017**, *7*, 1700278.
- (33) Zhao, Q.; Zhu, Z.; Chen, J. Molecular Engineering with Organic Carbonyl Electrode Materials for Advanced Stationary and Redox Flow Rechargeable Batteries. *Adv. Mater.* **2017**, *29*, 1607007.

- (34) Hu, Y.; Tang, W.; Yu, Q.; Wang, X.; Liu, W.; Hu, J.; Fan, C. Novel insoluble organic cathodes for advanced organic K-ion batteries. *Adv. Funct. Mater.* **2020**, *30*, 2000675.
- (35) Aher, J.; Graefenstein, A.; Deshmukh, G.; Subramani, K.; Krueger, B.; Haensch, M.; Schwenzel, J.; Krishnamoorthy, K.; Wittstock, G. Effect of aromatic rings and substituent on the performance of lithium batteries with rylene imide cathodes. *ChemElectroChem.* **2020**, *7*, 1160-1165.
- (36) Xu, F.; Wang, H.; Lin, J.; Luo, X.; Cao, S. A.; Yang, H. Poly (anthraquinonyl imide) as a high capacity organic cathode material for Na-ion batteries. *J. Mater.Chem. A.* **2016**, *4*, 11491-11497.
- (37) Pan, L.; Lu, S.; Xiao, X.; He, Z.; Zeng, C.; Gao, J.; Yu, J. Enhanced mechanical and thermal properties of epoxy with hyperbranched polyester grafted perylene diimide. *RSC advances.* **2015**, *5*, 3177-3186.
- (38) Wilkinson, D.; Bhosale, M.; Amores, M.; Naresh, G.; Cussen, S. A.; Cooke, G. A quinone-based cathode material for high-performance organic lithium and sodium batteries. *ACS appl. energy mater.* **2021**, *4*, 12084-12090.
- (39) Song, Z.; Qian, Y.; Gordin, M. L.; Tang, D.; Xu, T.; Otani, M.; Zhan, H.; Zhou, H.; Wang, D. Polyanthraquinone as a Reliable Organic Electrode for Stable and Fast Lithium Storage. *Angew. Chem., Int. Ed.* **2015**, *127*, 13947–14157.
- (40) Z.; Zhu, Z.; Cheng, F.; Zhang, K.; Wang, J.; Chen, C.; Chen, J. Pyrite FeS₂ for high-rate and long-life rechargeable sodium batteries. *Energy Environ. Sci.* **2015**, *8*, 1309–1316.
- (41) Diard, J.-P.; Le Gorrec, B.; Montella, C. EIS study of electrochemical battery discharge on constant load. *J. Power Sources* **1998**, *70*, 78–84.

CHAPTER 5

A Star-Shaped Conjugated Carbonyl Imides Cathode for Lithium-ion Batteries.

5.1 INTRODUCTION

Rechargeable organic lithium-ion batteries (OLBs), consisting of electro-active organic electrodes, appear as future energy harvesting devices.¹ due to their inherent features for instance tunable specific capacity, abundant availability, and sustainability.²⁻⁷ Aromatic conjugated imide is deserved to be a favorable grade of electrode materials due to its capacity to hold multiple electrons per molecule. Still, it has suffered from several serious problems.⁸⁻¹¹ first, low practical capacity was observed due to the low utilization rate of the carbonyl site.¹² Second, the relatively low operating potentials (< 2.5 V vs. Li/Li^+) than the latest inorganic electrode (>3 V vs. Li/Li^+),¹³⁻¹⁵ which are responsible for limiting their energy density. Third, molecular compact π - π staking in the solid-state decreases the lithium-ion diffusion coefficient.¹⁶⁻¹⁸ Forth, low electronic conductivity and most aromatic imides dissolution in the traditional aprotic electrolyte, resulting in self-discharge rate and less cyclability.^{19,20} The above disadvantages and unfavorable outcome, the progress of OLBs consisting of small aromatic imides impede continuously.

Chemists try to solve these problems through molecular engineering strategy.²¹⁻²⁴ From a molecular structural design and synthesis point of view, adding more redox-active groups could enhance the specific capacity. At the same time, the operating voltage could be modified by adding an electron-withdrawing substituent. The more aromatic conjugated structure will help increase electronic conductivity, which also helps decrease solubility in an organic liquid electrolyte and increase charge/discharge rate, and affect redox potential. The solubility problem can be solved by synthesizing polymer with a redox-active imides group; it will be able to solve the solubility problem but dramatically decrease the discharge potential due to the polarization of charges.^{25,26}

The design for high energy density batteries should have positive electrode materials with relatively high average potentials vs. Li/Li^+ . Wittstock et al. reported that PDA, NDA, and PMDA could be modified by substituent triphenylamine (TPA), which helps to disrupt their aggregation as well as simultaneously maintain a low solubility.²⁷ More importantly, this extended aromatic conjugation of compound TPA-PDI, TPA-NDI, and TPA-Py shows a high first discharge voltage plateau at 3.85 V, 3.75 V, and 3.70 V, respectively. Jun C. and et al. synthesized four phthalimide groups connected to benzoquinone (TPB), in which the presence of four rigid phthalimide groups lowers the energy of the LUMO, assigning an extended delocalized conjugated structure that not only reduces solubility but also resulting from that much higher first discharge potential plateau was found at 3.05.²⁸

By following the literature, we have addressed two main obstacles for OLBs, i.e., solubility in liquid electrolytes and low discharge potential of cathodic materials. We designed and synthesized two star-shaped molecules (UN-4 and NDI-4) and used them as positive electrodes for LIBs. The high discharge voltage batteries are very demanding because they directly affect the energy density of batteries. The expected electrochemical outcome of these two molecules was they should increase discharge potential as well as decrease the solubility in liquid electrolytes. This hypothesis was supported by our molecular design in which molecule UN-4 consist of four naphthalic anhydride group connected to benzoquinone, whereas molecule NDI-4 consist of four naphthalic diamides (NDI-BA). Both of these molecules consist of extended aromatic conjugation, which will help to decrease the solubility in liquid electrolytes, and the extended conjugation is also expected to reduce the energy of LUMO²⁹ energy level of molecules, which directly affects the discharge potential or reduction potential of batteries.

5.2 EXPERIMENTAL SECTION

5.2.1 Chemicals and Materials

All starting chemicals and reagents provided by the commercial supplier are used as received without further purification. 1,8 Naphthalic anhydride, Naphthalene tetracarboxylic dianhydride, (NDA) zinc acetate, Tetrachloro-p-benzoquinone, Hydrazine hydrate (80% solution), potassium phthalimide, Butylamine, and Imidazole were purchased from Sigma-Aldrich. Dimethylformamide (DMF), chloroform (CHCl₃), Tetrahydrofuran (THF), dichloromethane (DCM), and acetone were purchased from Merck Chemicals. A battery-grade salt Bis(trifluoromethane)sulfonamide lithium salt (LiTFSI) and Polyvinyl difluoride (PVDF, Kynar HSV900, Arkema Inc., USA) was purchased from sigma Aldrich. 1,3-dioxolane (DOL), and 1,2 Dimethoxyethane (DME) N-Methyl-2-pyrrolidone (NMP) solvent used for battery performance were purchased from Sigma Aldrich (HPLC grade).

5.2.2 Instrumentation and General Experimental method.

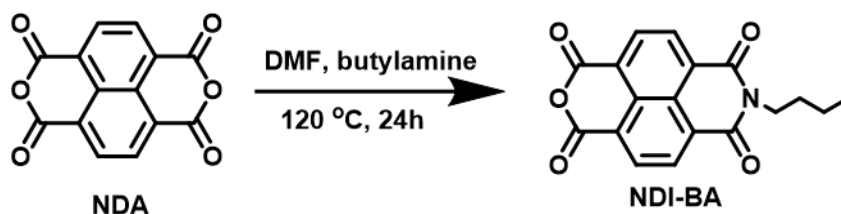
Structural characterization of molecules was done by recording their ¹H and spectra at room temperature on Bruker-AVENS, 400 or 500 MHz NMR instruments. Deuterated Sulfuric acid -d₂ solution (D₂SO₄), Deuterated chloroform (CDCl₃), and Deuterated dimethyl sulfoxide (DMSO) were used as a solvent in a trace amount of TMS as an internal reference. all compound's chemical shift was reported in δ ppm downfield to TMS whereas peak multiplicities are referred to as singlet (s), doublet (d), triplet (t), quartet (q), pentet (p), and

multiplet (m). UV-vis absorption spectra were recorded on SPECORD® 210/PLUS, a UV-visible spectrophotometer with deuterium and tungsten lamps as the source. The morphological characterizations of molecules were performed using FE-SEM with an instrument FEI Nova Nano SEM 450. Infrared spectra (IR) were recorded on a Bruker α -T spectrophotometer with sample pellets prepared by mixing with 5% w/w in KBr and dried under a vacuum before spectra were recorded. Thermogravimetric analysis (TGA) was recorded using Perkin Elmer STA 6000 Thermogravimetric Analyzer. Samples were scanned from 50 °C to 800 °C with a heating rate of 10 °C/ min under an inert nitrogen atmosphere. The cyclic voltammetry experiments were performed in a multi-channel auto lab MAC 80038 instrument with a potential range of 1 to 4 V vs. Li/Li⁺. Electrochemical Impedance Spectroscopy measurements (EIS) were done using a Biologic instrument in the frequency range of 40 kHz to 10 MHz. The galvanostatic charging/discharging experiments were carried out using CR 2032-type coin cells on a Neware battery testing system (BTS7.5.6, Shenzhen, China) in the potential range of 1-4 V vs. Li./Li⁺.

5.2.3 Synthesis and Characterization.

The general synthesis of starting compound and their condensed product (UN-4, NDI-4) synthesis scheme is shown below.

a) Synthesis of NDI-BA



Procedure: To a 100 ml two neck round bottom flask containing magnetic stirred and Naphthalene tetracarboxylic dianhydride NDA (2 g 7.46 mmol), in DMF (50 ml). Allow this mixture to be stirred for 10 min at 120 °C. After forming a clear and uniform solution, the dropwise addition of butylamine (0.5 ml 7.46 mmol) was done for 20 min. and the reaction mixture continues to stir for 24 h at 120 °C. the reaction is monitored by TLC, and the final product is purified by column chromatography in DCM: PET Ether 80:20 solvent system. (Yield 30%). ¹H NMR (400 MHz, CDCl₃, δ , ppm): 8.82 (s, 4-H, H_a), 4.21 (t, 2-H, H_b), 1.73 (m, 2-H, H_c), 1.47 (m, 2-H, H_d), 0.99 (t, 2-H, H_e). ¹³C NMR (400 MHz, CDCl₃, δ , ppm):

162.23 (C¹ imide carbonyl), 158.86 (C²), 133.14 (C³), 131.20 (C⁴), 128 (C⁵), 127.93 (C⁶), 126.65 (C⁷), 122.81 (C⁸), 40.96 (C⁹), 30.92 (C¹⁰), 20.30 (C¹¹), 13.76 (C¹²).

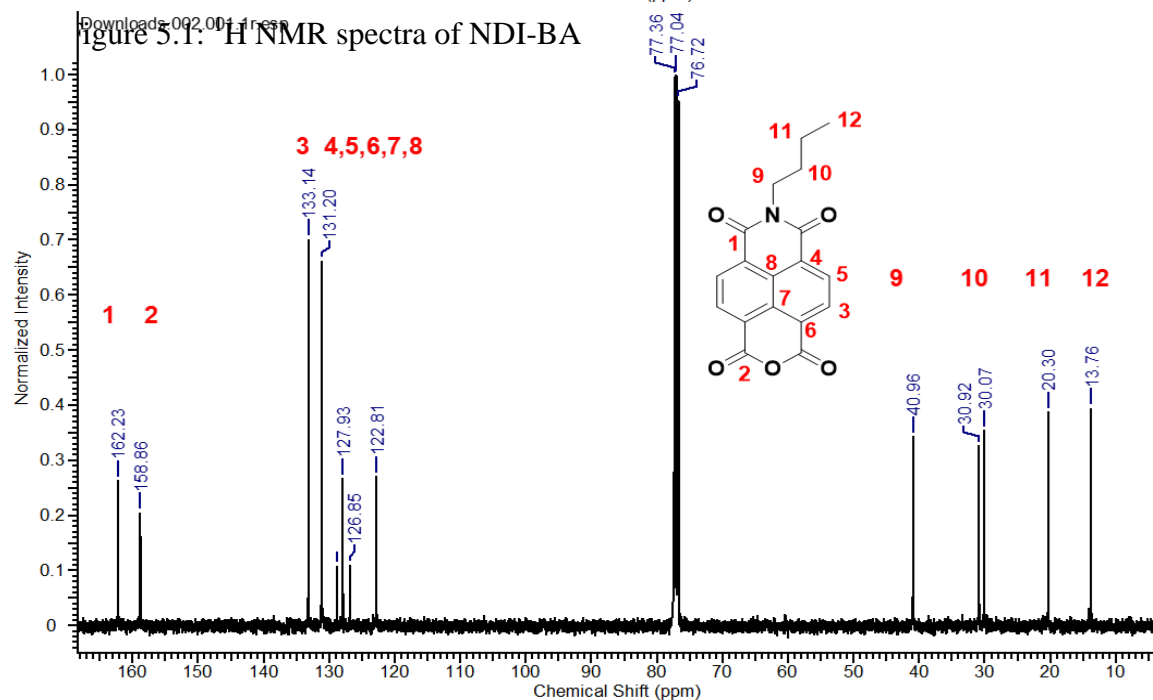
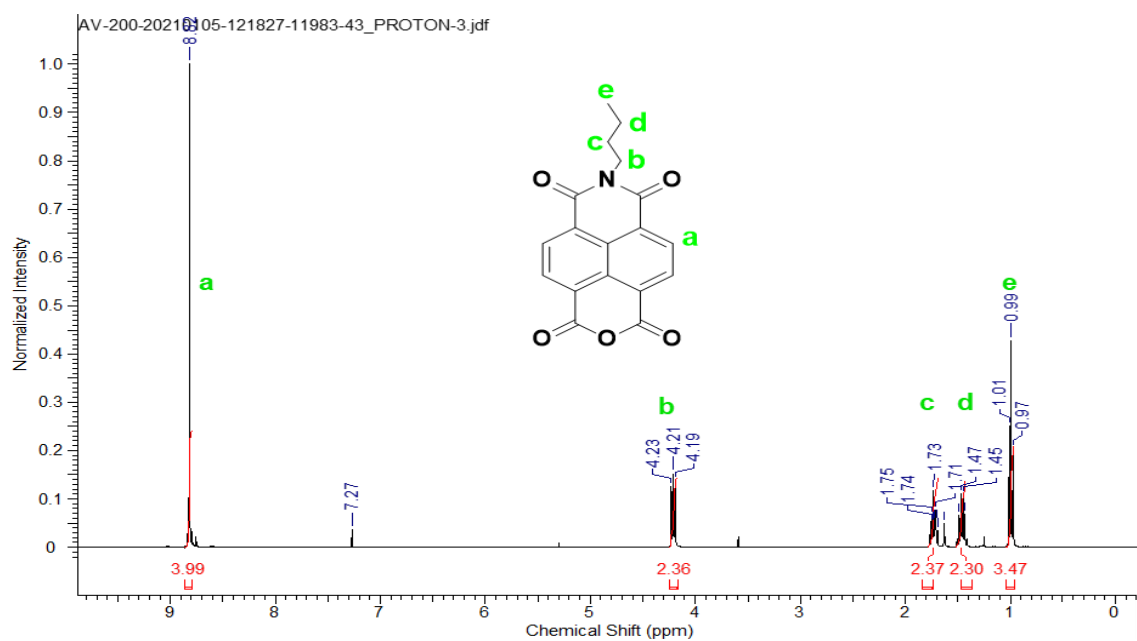
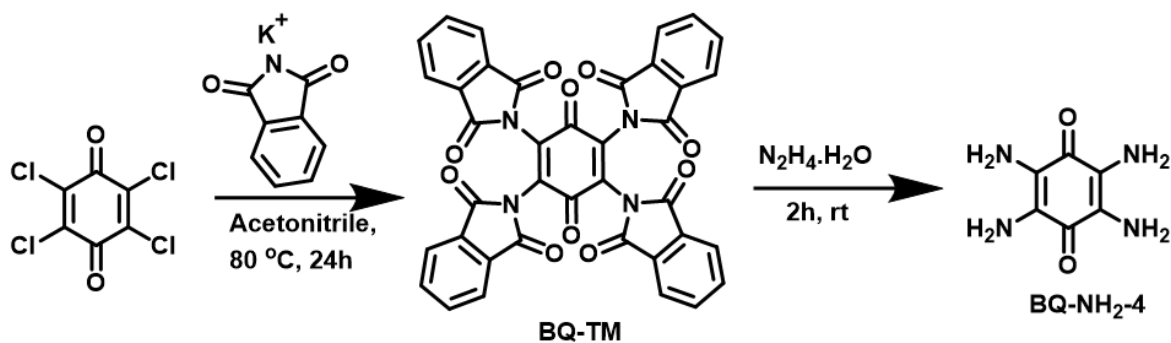


Figure 5.2: ¹³C NMR spectra of NDI-BA

b) Synthesis of Tetra(phthalimido)-benzoquinone (BQ-TM)



Procedure: This compound was synthesized by the following literature procedure.²⁸ Under a nitrogen atmosphere, tetrachloro-p-benzoquinone (12.5 g) and potassium phthalimide (37.5 g) was added to 125 mL of acetonitrile in a 250 ml round bottom flask, and the reaction mixture was stirred for 12h at 80 °C. After cooling to room temperature, the products were filtered and washed with N, N-Dimethylformamide, and hot deionized water (100 °C), several times. Finally, the obtained samples were suspended in 50 mL of ethanol and heated to the boiling temperature, and the final product precipitated was obtained by vacuum filtered. It was then dried in a vacuum oven at 105 °C for 12h. tetra(phthalimido)-benzoquinone (BQ-TM) (brown-yellow powder) was used as such for the next step.

c) Synthesis of 2,3,5,6-tetraaminocyclohexa-2,5-diene-1,4-dione (BQ-NH₂-4)

Procedure: This compound was synthesized by the following literature procedure.³⁰ The synthesized tetra(phthalimido)-benzoquinone was transferred into a 100 mL round bottom flask, into which 120 mL of hydrazine hydrate (80.0 wt%) was added. After being kept at 65 °C for 2 h. After completion of reaction reaction mixture was cooled and filtered to obtained purple 2,3,5,6-tetraaminocyclohexa-2,5-diene-1,4-dione (BQ-NH₂-4) (Yield 28 %) ¹H NMR (500 MHz, DMSO-D₆, δ, ppm): 4.55 (s, 8-H, H_a). ¹³C NMR (500 MHz, DMSO-D₆, δ, ppm): 179.32 (C¹ Ketone), 121.86 (C²).

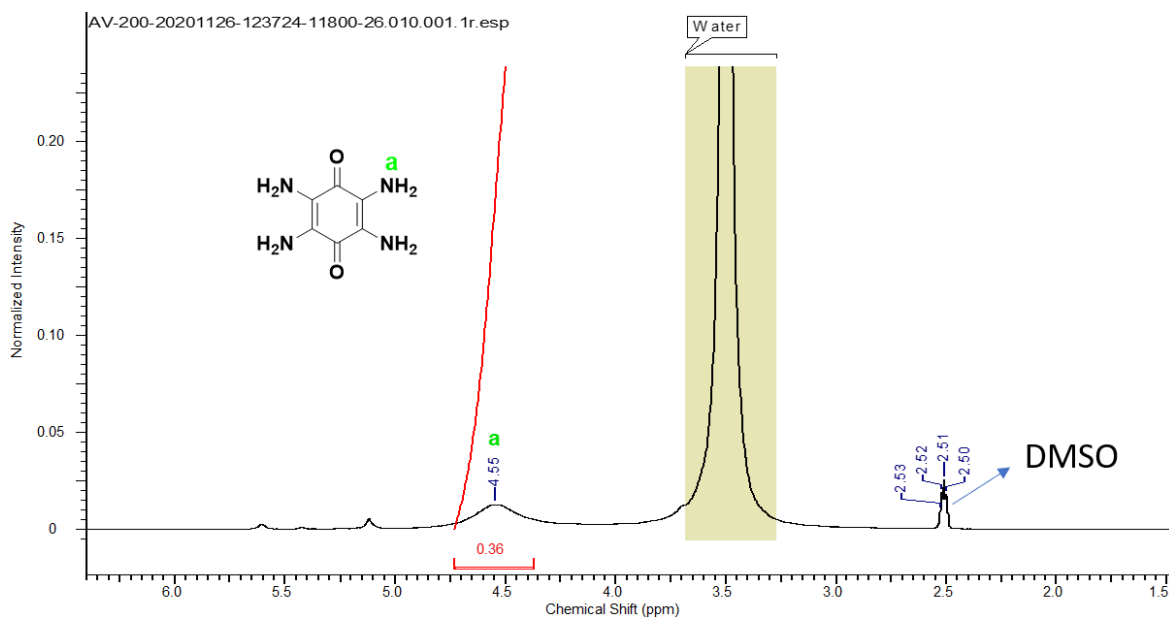


Figure 5.3: ¹H NMR spectra of BQ-NH₂-4

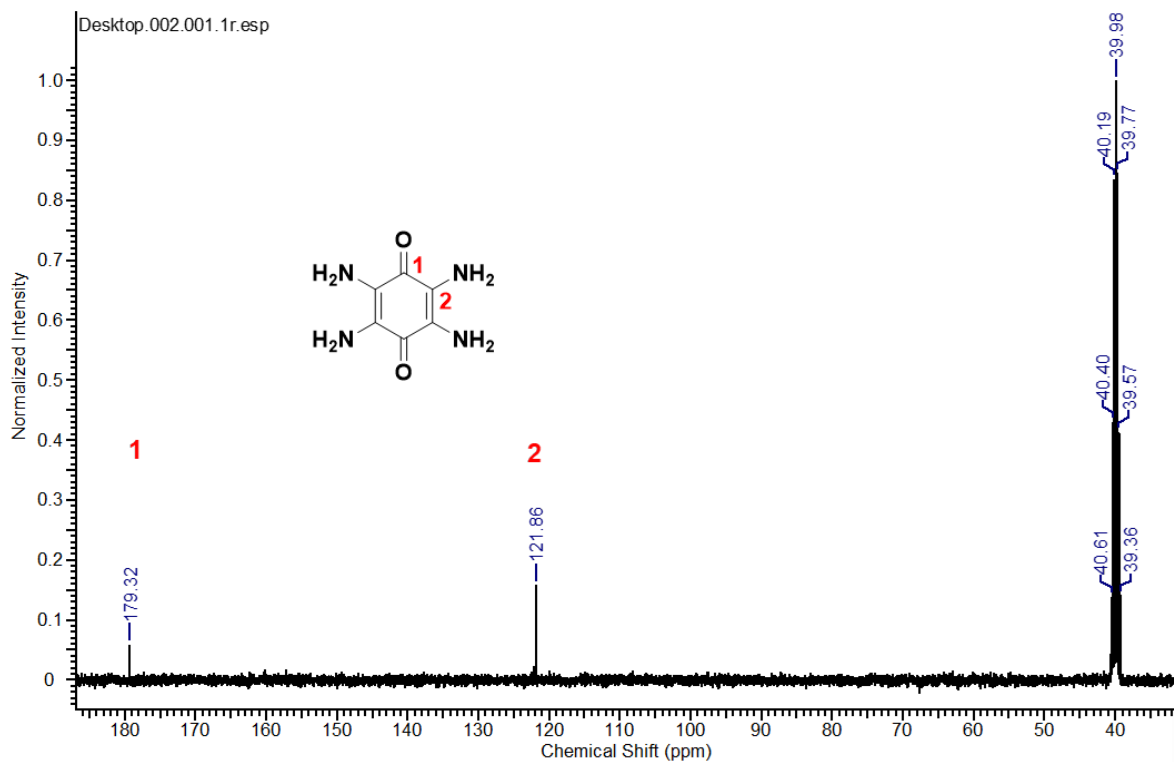
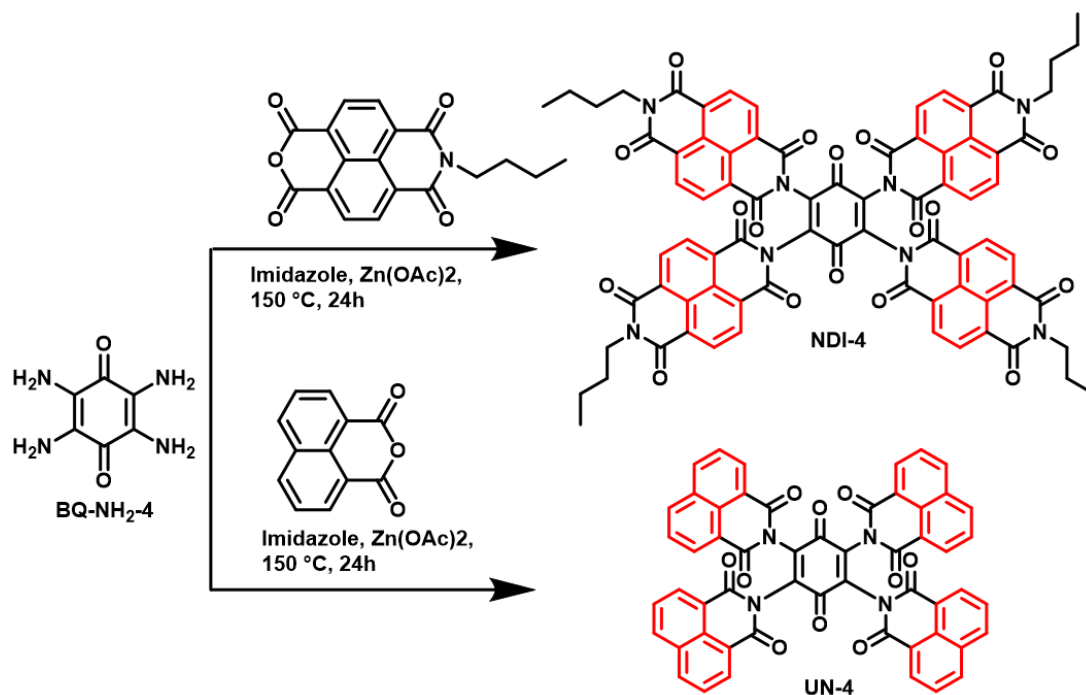


Figure 5.4: ¹³C NMR spectra of BQ-NH₂-4



Scheme 5.1: Synthesis of UN-4, and NDI-4

d) Synthesis of NDI-4

Procedure for molecule 1: A 50 mL two neck round bottom flask consisting of a magnetic stirrer, BQ-NH₂-4 (100 mg, 0.59 mmol), NDI-BA (1143 mg, 3.54 mmol), and zinc acetate (0.09 g, 0.59 mmol) in imidazole (15 g). The resultant reaction mixture was heated at 150 °C for 24 h under an argon atmosphere. After completion of the reaction, the reaction mixture was cooled down to 60 °C. The product mixture was precipitated by adding 2 M HCl. The mixture was filtered through suction filtration, and the resultant crude product was washed with deionized water and methanol until the eluant became neutral. The obtained product was added to chloroform (200ml) and stirred for hours, and a dissolve NDI-BA was removed through filtration. After that, the crude product recrystallizes in DMF and water for the obtained final product (Yield 70 %) ¹H NMR (400 MHz, CDCl₃, δ, ppm): 8.57 (bs, 16-H, H_a), 4.03 (m, 8-H, H_b), 1.62 (m, 8-H, H_c), 1.38 (m, 8-H, H_d), 0.93 (t, 12-H, H_e).

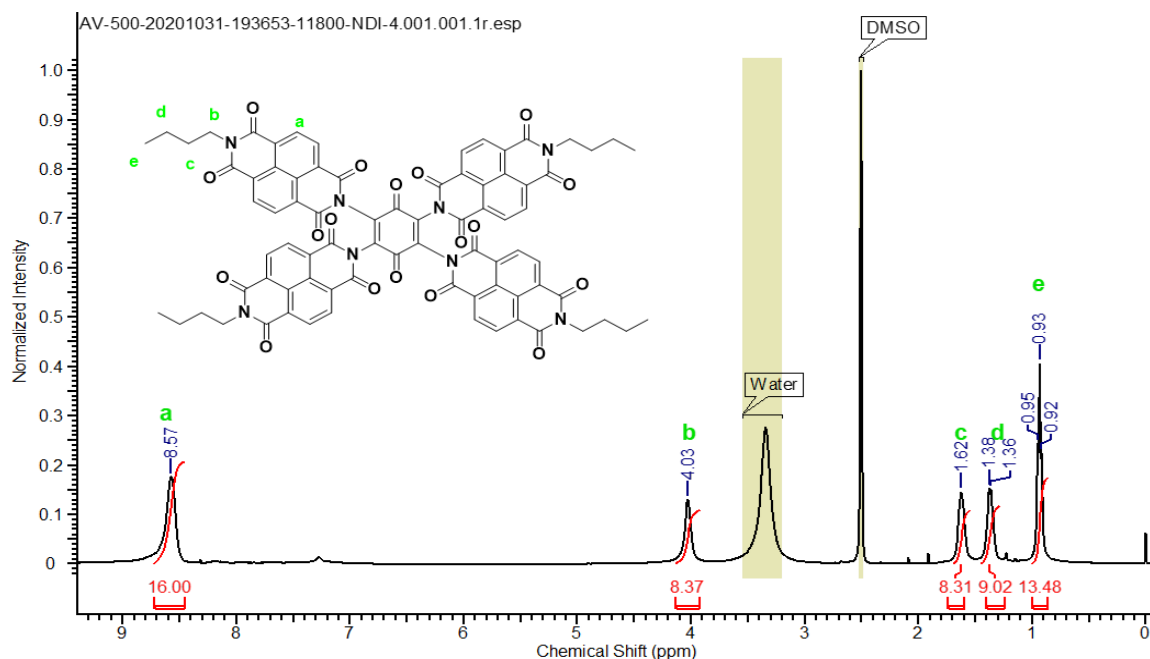
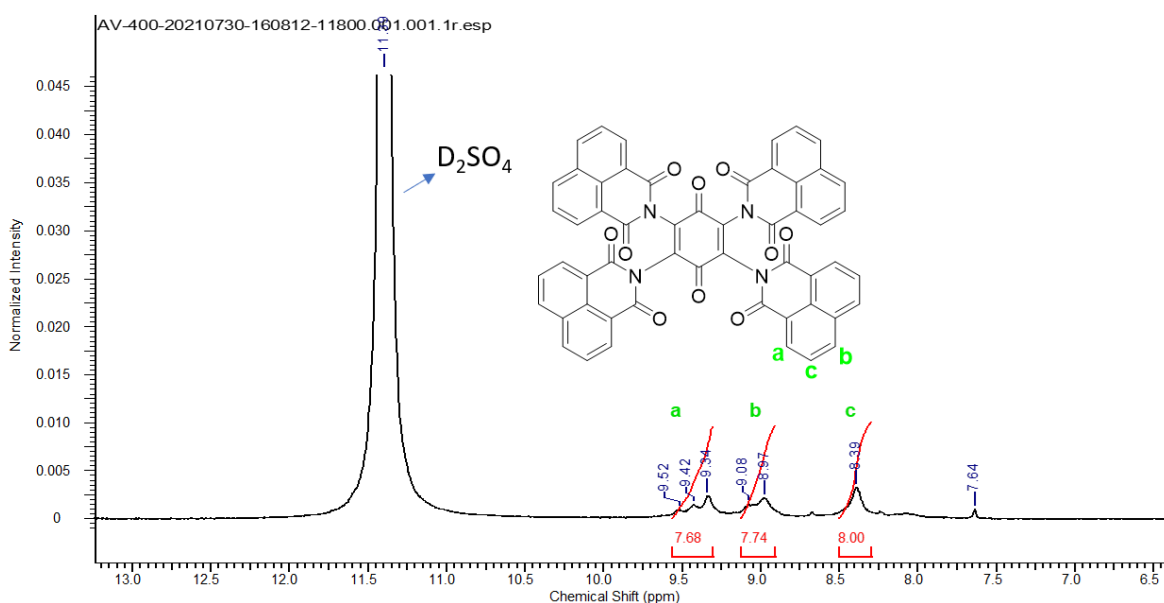


Figure 5.5: ^1H NMR spectra of NDI-4

e) Synthesis of UN-4

Procedure for molecule 2: A 50 mL two neck round bottom flask equipped with a magnetic stirrer was charged with BQ-NH₂-4 (100 mg, 0.59 mmol), 1,8 Naphthalic anhydride (N-AN) (700 mg, 3.54 mmol), and zinc acetate (0.09 g, 0.59 mmol) in imidazole 15 g). The resultant mixture was heated at 150 °C for 24 h under an argon atmosphere. After completion of the reaction, the reaction mixture was cooled down to 60 °C. Then the product mixture was precipitated by adding 2 M HCl. The obtained precipitated was filtered through suction filtration, and the resultant crude product was washed with deionized water and methanol until the eluant became neutral. The obtained product is stirred in acetone to remove excess 1,8 Naphthalic anhydride (N-AN). The crude product was finally recrystallized in DMF water to get UN-4 (Yield 80 %) ^1H NMR (400 MHz, D₂SO₄, δ , ppm): 9.42 (m, 8-H, H_a), 9.02 (m, 8-H, H_b), 8.39 (m, 8-H, H_c).

Figure 5.6: ^1H NMR spectra of UN-4

5.3 RESULT AND DISCUSSION

5.3.1 Fourier transform infrared spectroscopy (FT-IR)

Molecular structural analysis was further done by FT-IR. The details of functional group presence at respective wavenumber for molecules UN-4 and NDI-4 are shown in the FT-IR spectrum. (Figure 5.7) Both these compounds show characteristics of strong absorption humps at 1660, and 1658 cm^{-1} , due to unsymmetric stretching vibration of the $-\text{C}=\text{O}-$ bond cyclic imide of UN-4, and NDI-4, respectively. An asymmetric stretching vibration of a ketonic group of molecule UN-4 and NDI-4 were noticed at 1711, and 1702 cm^{-1} respectively. (Figure 5.7) The further detailed stretching and bending vibrations of molecules UN-4, and NDI-4 are shown in table 5.1.

5.3.2 UV-Visible absorption spectroscopy

The UV-Visible absorption spectra of UN-4 and NDI-4 were explored in NMP as solvent. In NMP the molecule NDI-4 typical absorption feature with peaks at 380 nm, 360 nm, and one hump at 340 nm with a calculated frontier orbital difference was 3.17 eV (Figure 5.8). Whereas for UN-4 absorption peak was observed at 356 nm, and 334 nm with a 3.34 eV frontier orbital difference (Figure 5.8). More extended conjugation in NDI-4 is expected to increase the energy level of HOMO which results in a redshift of peak compared to UN-4.

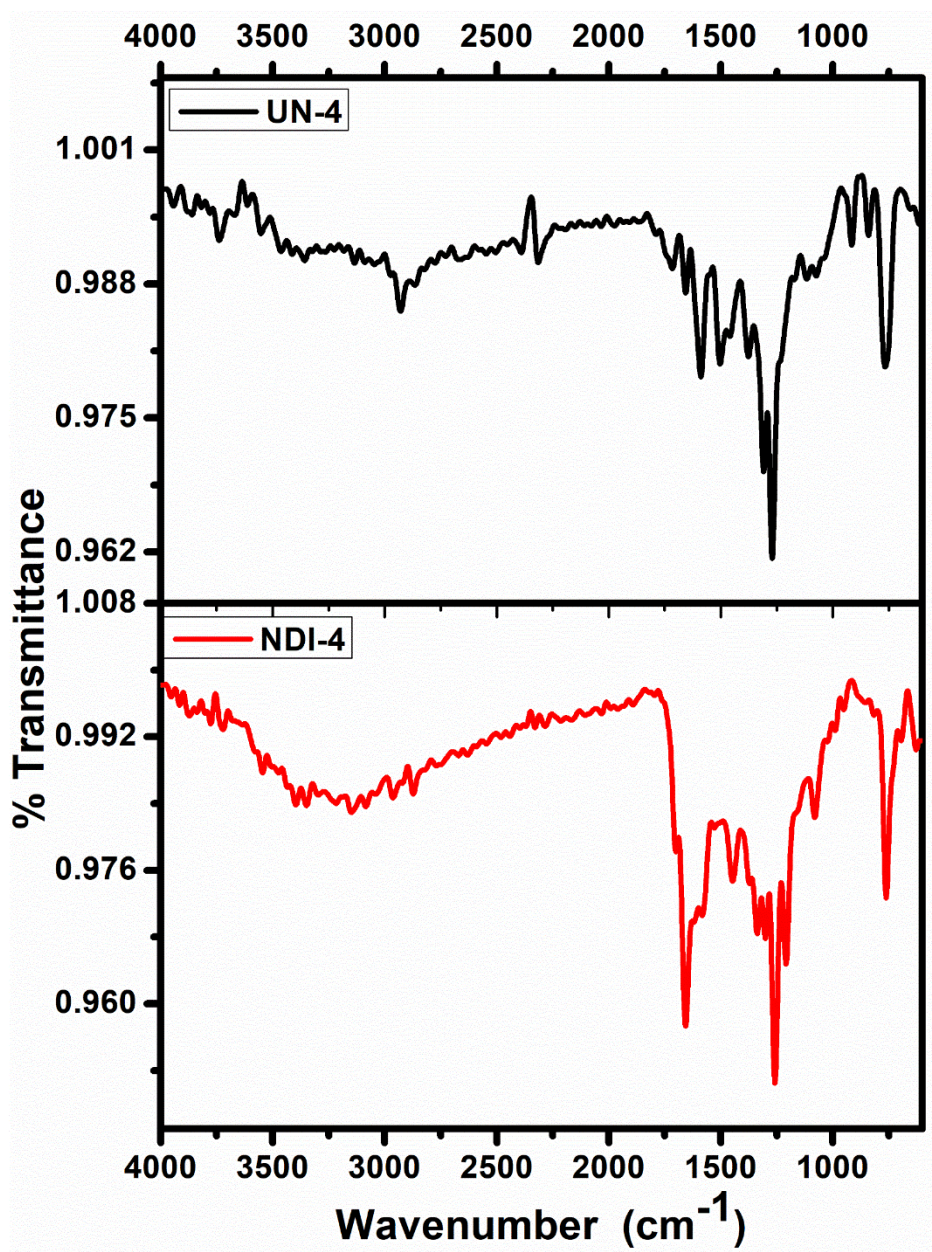


Figure 5.7: FTIR Spectra of UN-4, and NDI-4

Table 5.1: FTIR data of UN-4, and NDI-4

Molecule	Imide C=O Vas	Aromatic C=C Str. Mode.	Imide C=O Bending Mode	Imide C-N Str.	Ketone Str. Mode.
UN-4	1660 cm ⁻¹	1580 cm ⁻¹	760 cm ⁻¹	1370 cm ⁻¹	1711 cm ⁻¹
NDI-4	1658 cm ⁻¹	1585 cm ⁻¹	760 cm ⁻¹	1340 cm ⁻¹	1702 cm ⁻¹

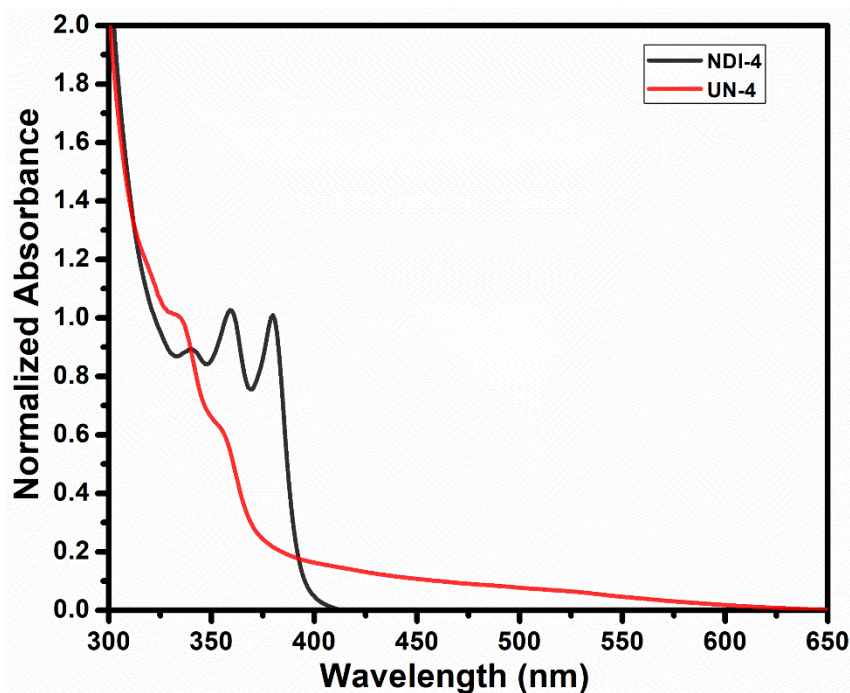


Figure 5.8: UV-Visible Absorption spectra of molecules NDI-4 and UN-4

5.3.3 Morphological study by Field emission scanning electron microscope (FE-SEM) before and after battery cycling.

The morphological study of compounds UN-4 and NDI-4 was done by taking FE-SEM images as-synthesized and after the 150th charge/discharge cycle. The sample was prepared by dispersing a molecule of about 1 mg in 2 ml N-methyl-2-pyrrolidone (NMP). After that, 5–10 μL of the dispersed solution was drop-casted on ZP-P4VP spun silicon wafers and dried at 80 $^{\circ}\text{C}$ overnight before recording images. Rough sheet type morphology (1 μm) was observed for molecule UN-4. (Figure 5.9 a) Whereas the molecules NDI-4 were quickly soluble in NMP, thus, the drop cast solution of NDI-4 observed smooth crystalline sheet agglomerates (20 μm) in FE-SEM images. (Figure 5.9 b) The morphology fate was checked after the 150th charge/discharge cycle at 0.2 C, generally due to the fast insertion and deinsertion of lithium-ion the surface roughness and the surface cracking will observe in morphology. To know the significant changes, we have disassembled the coin cell, the cathode electrode of the molecule UN-4 seemed intact, with a very slightly brown colored electrolyte was seems to stick on the separator. the cathode electrode of Molecule UN-4 was crashed and dispersed in fresh NMP. The dispersed solution was drop cast on a silicon wafer

and FE-SEM images were recorded. The Morphology of UN-4 seemed intact (as before the 150th cycle) with embedded in powder spots of carbon black, (Figures 5.9 e) without any significant change in surface roughness. After opening the coin cell of molecule NDI-4 after the 150th cycle the separator seemed finely colored (reddish-brown) and the coated materials on the aluminium foil also seems to be disturbed. We have deep the separator in fresh NMP and FE-SEM was recorded. The morphology of the molecule found the same crystalline agglomerates, (Figures 5.9 d) indicating that NDI-4 shows significant solubility in the electrolyte (1M LiTFSI in DOL: DME 1:1).

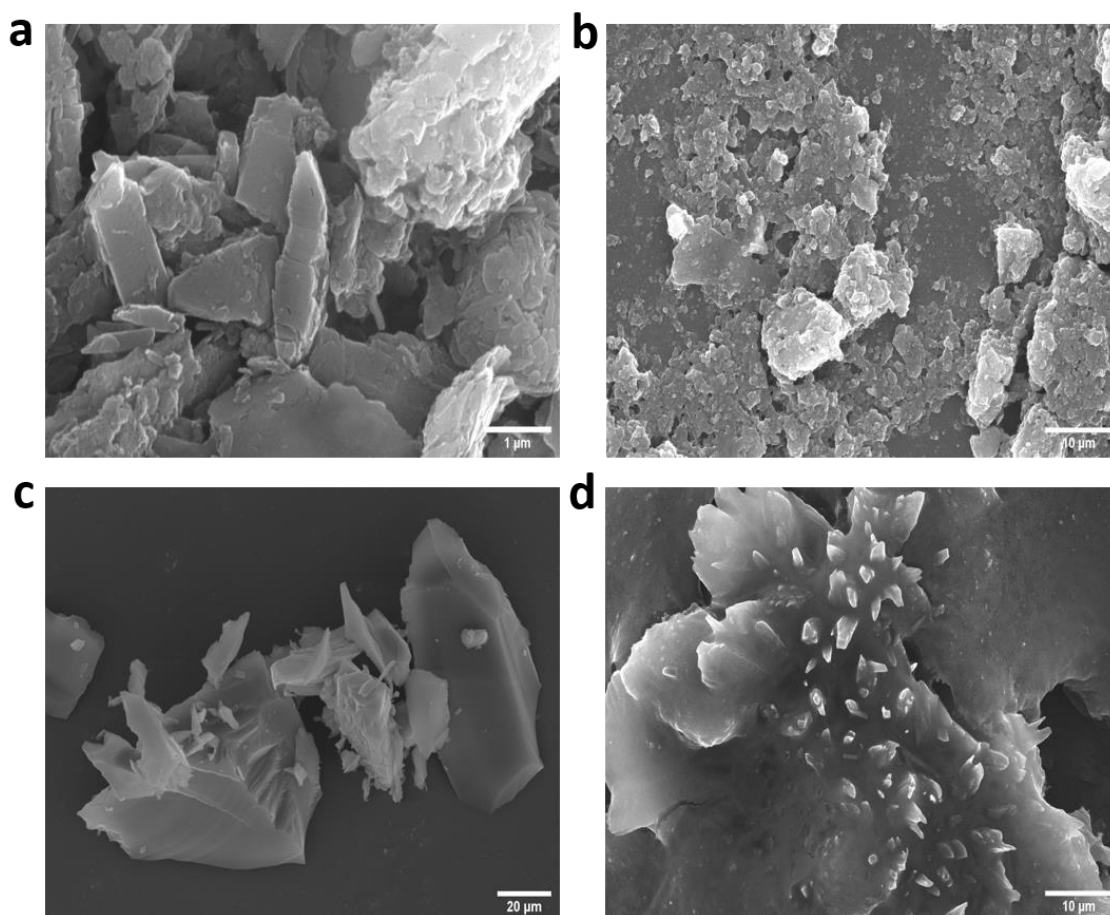


Figure 5.9: FE-SEM images of UN-4 molecule before (a) and after 150th cycles (b) FE-SEM images of NDI-4 molecule before (c) and after 150th cycles (d)

5.3.4 Thermogravimetric analysis (TGA)

The thermal stability of both these compounds (UN-4, and NDI-4) was recorded by TGA. As appears in figure 5.10 a, a thermogram of both compounds offers good stability while experimenting in a nitrogen environment between a temperature range of 50 °C to 800 °C

while keeping a scanning rate of 10 °C /min. In detail, UN-4 start decomposing at 400 °C, whereas NDI-4 initiate decomposing at approximately 502 °C (Figure 5.10 a). The thermal stability of NDI-4 is high compared to UN-4 due to the presence of four extended aromatic NDA-BA groups. The high-temperature stability of these molecules indicates the battery prepared from such materials can be operated at a much high temperature.

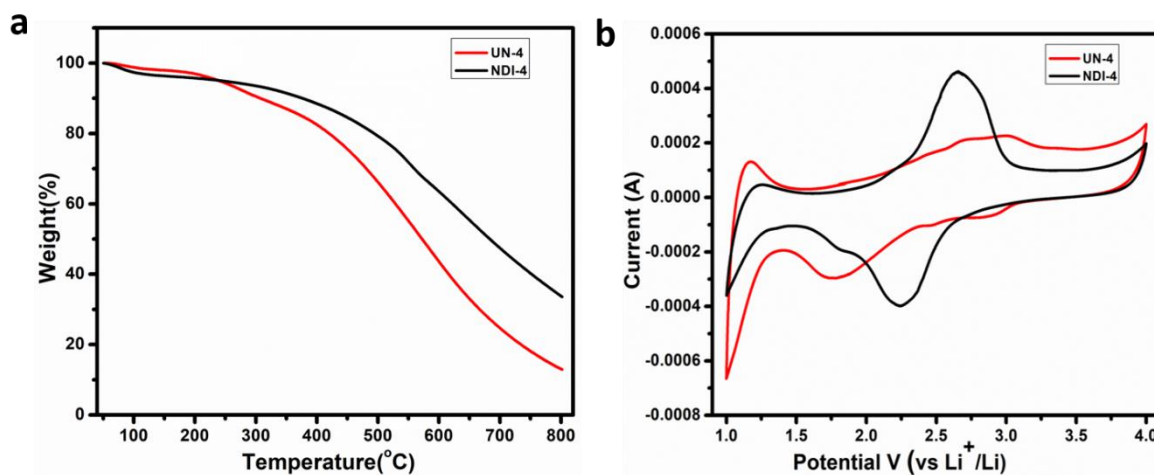


Figure 5.10: TGA profile of UN-4, and NDI-4, (a) cyclic voltammograms of molecules UN-4, and NDI-4 (b)

5.3.5 Electrochemical performance of molecules.

5.3.5.1 Cyclic voltammetry

Cyclic voltammetry studies were performed using CR 2032-type coin with UN-4, and NDI-4 as working electrodes (cathode), while, reference electrodes (anode) were thin lithium chips. A redox potential of these molecules was analyzed vs. Li/Li⁺ while sweeping potential between 1V to 4V at a scan rate of 1 mV/s. For NDI-4 large reduction peaks were observed at 2.6 V and one small reduction hump at 2.03 V whereas, two oxidation hump was noticed at 2.3 and 2.38 V (Figure 5.10 b). UN-4 displayed two reduction hump at 3.08, and 2.3 V, and two oxidation humps at 2.33 and 2.66 V. (Figure 5.10 b). Here we expected the increase in first reduction voltage beyond 3 V. the logic behind the increased reduction potential was due to the giant aromatic conjugated delocalized structure of molecules UN-4 and NDI-4. The observed first reduction potential for NDI-4 was only 2.6 volts whereas the increase in reduction potential was observed for molecules UN-4 (3.08 V) which seems to be high than four phthalimide groups connected to benzoquinone (TPB).²⁸

5.3.5.2 Galvanostatic charge/discharge experiment

Electrode preparation.

Working electrode slurries were prepared by mixing 50% wt. active material (NDI-4, UN-4), 40% wt. Carbon black and 10% wt. polyvinylidene fluoride (PVDF) as a binder. The mixture was put up in a grinder and N-methyl-2-pyrrolidinone (NMP). The mixture was thoroughly mixed to form a uniform slurry; the prepared slurry was uniformly coated on aluminium foil and then dried at 90 °C for 12 h in a vacuum oven. A circular shape electrode was punched by an electrode puncture machine and it was further transferred to an argon-filled glove box. CR 2032-type coin cells were fabricated by using Li-foil as a counter electrode, electrolyte as 1 M LiTFSI in a mixture of DOL/DME (1:1 by volume), and Celgard (2325) as the separator.

A fabricated CR-2032 type coin cell was used for the galvanostatic charge/discharge experiment. Figures 5.11 a, c, shows galvanostatic charge/discharge profile for molecules UN-4 and NDI-4. UN-4 electrode cell was measured at 0.2 C rate between potential window 1 to 4 V (vs. Li⁺/Li) whereas the NDI-4 electrode cell was measured at 0.2 C rate while sweeping potential between 1.5 to 4 V. A first charge cycle for NDI-4, and UN-4 noticed a specific capacity at 133 mAh/g, and 193 mAh/g respectively, whereas the first discharge capacity for this molecule was found to be 134 mAh/g, and 201 mAh/g, (Figures 5.11 a, c) respectively. The increase in the first cycle observed specific capacity for molecule UN-4 than their theoretical capacity (calculated by considering six electrons transfer 180.9 mAh/g) is because of the generation of an SEI layer over surface of the electrode. Very less observed specific capacity first discharge for molecule NDI-4 than their theoretical capacity (calculated by considering ten electrons transfer 192.9 mAh/g) is due to significant dissolution of molecule in liquid electrolyte. In the charge/discharge profile, the discharge curve plateau for UN-4 was found at 3.05 and 1.9 V (Figure 5.11 a) which is in good agreement with the CV reduction potential of molecule UN-4. In Figure 5.11a the first reduction plateau is may due to the middle benzoquinone group lithiation, whereas the second lithiation of four naphthalic carbonyl groups, resulting in the second reduction plateau in the charge/discharge profile of UN-4. for molecule NDI-4 two discharge plateaus were observed, approximately 2.5 V, and 2.33 V figure 5.11 c which is nearly equal to the CV reduction voltage curve in figure 5.10 b. The first reduction plateau may be due to the

formation of lithium enolate of the middle benzoquinone group whereas the second reduction plateau represents lithiation of four NDA-BA carbonyl groups of NDI-4.

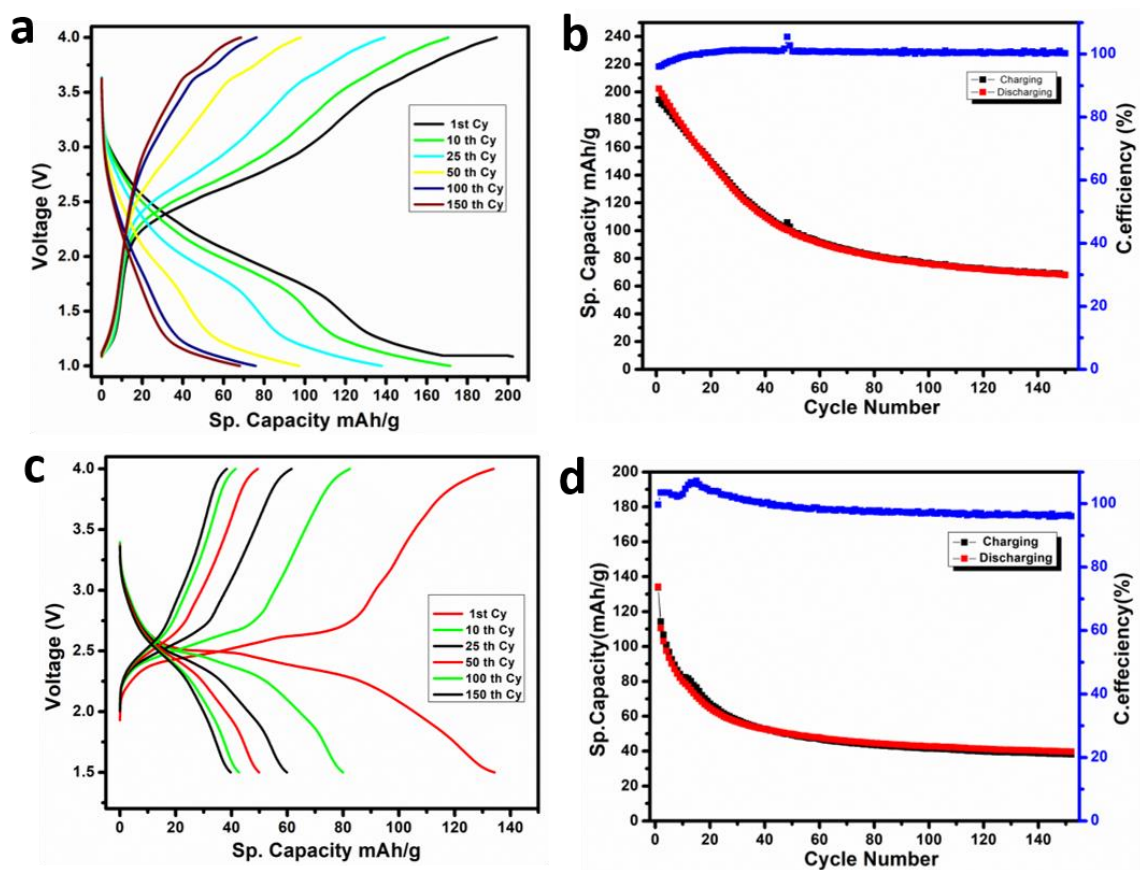


Figure 5.11: Galvanostatic charge/discharge profile curve of (a) UN-4, Cycling stability at 0.2 C for UN-4 (b) Galvanostatic charge/discharge profile curve of (C) for NDI-4, Cycling stability at 0.2 C for NDI-4 (d)

In a long-term cycling experiment, the cycle stability was measured until 150th cycle for each molecule at 0.2 C. Molecule UN-4 has shown the specific capacity of 68 mAh/g after complete 150th cycle with coulombic efficiency between 95-100 %. (Figure 5.11 b) A percentage decrease from the theoretical capacity (180.9 mAh/g) to the 150th cycle was 67.42 %. For molecule NDI-4 the discharge-specific capacity after the 150th cycle was observed at 40 mAh/g with average coulombic efficiency of 95 %. (Figure 5.11 d) A percentage decrease in specific capacity after the 150th cycle is 80 % from its theoretical specific capacity (192.9 mAh/g) indicating a critical dissolution of molecules in electrolyte leads to capacity fading.

Rate study

We have further compared the electrochemical activity of molecules UN-4, and NDI-4. Figure 5.12 a, b presents the rate capability of both molecule electrodes at different C rates. The discharge capacity of both these molecules decreases as the C rate increases from 0.2 to 30 C whereas the UN-4 electrode exhibits a high discharge capacity between 0.2 C to 30 C than NDI-4. A molecule UN-4 displayed first discharge capacity at a 0.2 C rate was 188 mAh/g which is decreased to 20 mAh/g at a 30 C rate. (Figure 5.12 a) When same cell were charged/discharged at a 0.2 C rate the repeated discharge capacity was found to be 170 mAh/g that was very near to the starting charge/discharge C rates (0.2 C). the result indicates the molecule does not stable much at high C rate (10, 20, and 30C) but significantly stable at slow charge/discharge rate. The first discharge capacity for molecule NDI-4 at 0.2 C rate was 124 mAh/g which decrease further to only 14 mAh/g at 30 C. (Figure 5.12 b) when the same cell charge/ discharge at 0.2 C rate the specific capacity rebounded to only 80 mAh/g. Indicating, that even though the NDI-4 presence a more extended conjugated structure and high theoretical capacity than UN-4 still unable to attend specific capacity near to their theoretical capacity, even at a slow C rate (0.2 C) due to the presence of alkyl chain in the molecule, it causes solubility of the molecule in the electrolyte. Due to the solubility of the molecule (NDI-4) in a liquid electrolyte, it shows much high-capacity fading.

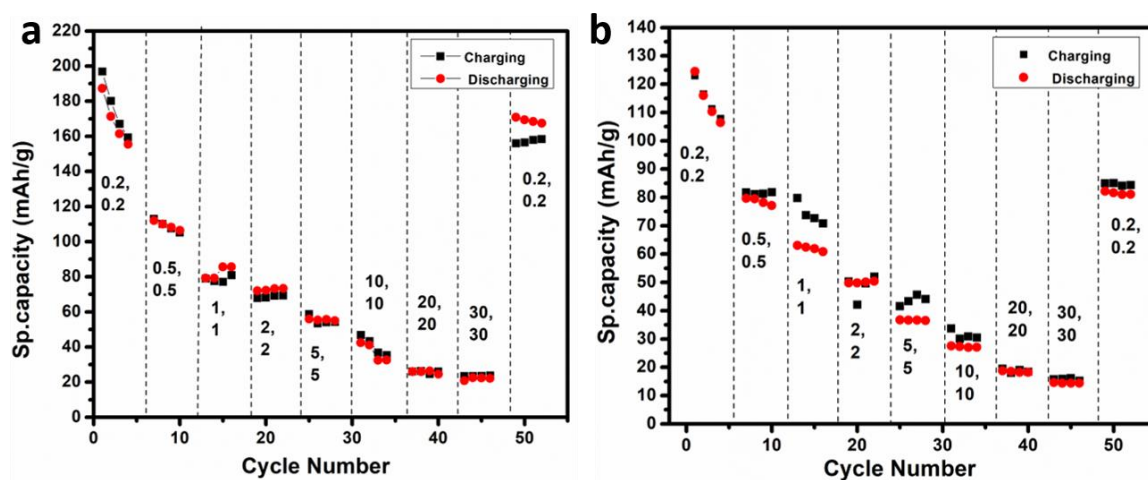


Figure 5.12: Rate capability for (a) UN-4, and (b) NDI-4 at different C rate

5.4 CONCLUSION

we have successfully addressed two main problems associated with organic carbonyl conjugated cathode materials i.e., solubility in liquid electrolyte and low discharge voltage of cathode materials. UN-4 and NDI-4 compounds formed by the four rigid naphthalic anhydrides and NDA-4 group coordination to middle benzoquinone group, thus the structure UN-4 was found to be remarkably very less soluble in liquid electrolyte. However, NDI-4 was found to be dramatically high soluble in liquid electrolytes even presence of aromatic extended conjugated structure. Benefiting from this distinctive, application UN-4 cathode in rechargeable LIBs build starting discharge capacity of 201 mAh/g at a 0.2 C rate and a high initial reduction potential at 3.08 V. On the whole, designing an easy synthetic method provided such conjugated carbonyl imide cathode for high energy density LIBs.

5.5 REFERENCES.

- (1) Li, L.; Hong, Y. J.; Chen, D. Y.; Lin, M. J. Molecular Engineering of Perylene Imides for High-Performance Lithium Batteries: Diels–Alder Extension and Chiral Dimerization. *Chem. Eur. J.* **2017**, *23*, 16612-16620.
- (2) Oyama, N.; Tatsuma, T.; Sato, T.; Sotomura, T. Dimercaptan–polyaniline composite electrodes for lithium batteries with high energy density. *Nature.* **1995**, *373*, 598-600.
- (3) Milczarek, G.; Inganäs, O. Renewable cathode materials from biopolymer/conjugated polymer interpenetrating networks. *Science*, **2012**, *335*, 1468-1471.
- (4) Schon, T. B.; McAllister, B. T.; Li, P. F.; Seferos, D. S. The rise of organic electrode materials for energy storage. *Chem. Soc. Rev.* **2016**, *45*, 6345-6404.
- (5) Muench, S.; Wild, A.; Friebe, C.; Häupler, B.; Janoschka, T.; Schubert, U. S. Polymer-based organic batteries. *Chem. Rev.* **2016**, *116*, 9438-9484.
- (6) Sun, T.; Li, Z. J.; Wang, H. G.; Bao, D.; Meng, F. L.; Zhang, X. B. A biodegradable polydopamine-derived electrode material for high-capacity and long-life lithium-ion and sodium-ion batteries. *Angew. Chem. Int. Ed.* **2016**, *55*, 10662-10666.
- (7) Wang, H. G.; Yuan, S.; Si, Z.; Zhang, X. B. Multi-ring aromatic carbonyl compounds enabling high capacity and stable performance of sodium-organic batteries. *Energy Environ. Sci.* **2015**, *8* 3160-3165.
- (8) Renault, S.; Geng, J.; Dolhem, F.; Poizot, P. Evaluation of polyketones with N-cyclic structure as electrode material for electrochemical energy storage: case of pyromellitic diimide dilithium salt. *Chem. Commun.* **2011**, *47*, 2414-2416.
- (9) Kim, D. J.; Jung, Y. H.; Bharathi, K. K.; Je, S. H.; Kim, D. K.; Coskun, A.; Choi, J. W. An aqueous sodium ion hybrid battery incorporating an organic compound and a Prussian blue derivative. *Adv. Energy Mater.* **2014**, *4*, 1400133.
- (10) Meng, Y.; Wu, H.; Zhang, Y.; Wei, Z. A flexible electrode based on a three-dimensional graphene network-supported polyimide for lithium-ion batteries. *J. Mater. Chem. A.* **2014**, *2*, 10842-10846.
- (11) Wu, Y. L.; Horwitz, N. E.; Chen, K. S.; Gomez-Gualdron, D. A.; Luu, N. S.; Ma, L.; Wang, T. C.; Hersam, M. C.; Hupp, J. T.; Farha, O. K.; Snurr, R. Q.; Wasielewski, M. R. G-quadruplex organic frameworks. *Nat. chem.* **2017**, *9*, 466-472.
- (12) Leedy, D. W.; Muck, D. L. Cathodic reduction of phthalimide systems in nonaqueous solutions. *J. Am. Chem. Soc.* **1971**, *93*, 4264-4270.

- (13) Song, Z.; Zhan, H.; Zhou, Y. Polyimides: promising energy-storage materials. *Angew. Chem. Int. Ed.* **2010**, *122*, 8622-8626.
- (14) Wang, H. G.; Yuan, S.; Ma, D. L.; Huang, X. L.; Meng, F. L.; Zhang, X. B. Tailored aromatic carbonyl derivative polyimides for high-power and long-cycle sodium-organic batteries. *Adv. Energy Mater.* **2014**, *4*, 1301651.
- (15) Yuan, S.; Liu, Y.B.; Xu, D.; Ma, D.L.; Wang, S.; Yang, X.H.; Cao, Z.Y. Zhang, X.B. Pure Single-Crystalline Na₁.1V₃O₇.9 Nanobelts as Superior Cathode Materials for Rechargeable Sodium-Ion Batteries. *Adv. Sci.* **2015**, *2*, 1400018.
- (16) Zhao, R. R.; Cao, Y. L.; Ai, X. P.; Yang, H. X. Reversible Li and Na storage behaviors of perylenetetracarboxylates as organic anodes for Li-and Na-ion batteries. *J. Electroanal. Chem.* **2013**, *688*, 93-97.
- (17) Fédèle, L.; Sauvage, F.; Bécuwe, M. Hyper-conjugated lithium carboxylate based on a perylene unit for high-rate organic lithium-ion batteries. *J. Mater. Chem. A*, **2014**, *2*, 18225-18288.
- (18) Veerababu, M.; Varadaraju, U. V.; Kothandaraman, R. Improved electrochemical performance of lithium/sodium perylene-3, 4, 9, 10-tetracarboxylate as an anode material for secondary rechargeable batteries. *Int. J. Hydrogen Energy.* **2015**, *40*, 14925-14931.
- (19) Häupler, B.; Wild, A.; Schubert, U. S. Carbonyls: powerful organic materials for secondary batteries. *Adv. Energy Mater.* **2014**, *4*, 1402034.
- (20) Xu, F.; Jin, S.; Zhong, H.; Wu, D.; Yang, X.; Chen, X.; Wei, H.; Fu, R. Jiang, D. Electrochemically active, crystalline, mesoporous covalent organic frameworks on carbon nanotubes for synergistic lithium-ion battery energy storage. *Sci. Rep.* **2015**, *5*, 8225.
- (21) Milton, R. D.; Hickey, D. P.; Abdellaoui, S.; Lim, K.; Wu, F.; Tan, B.; Minter, S. D. Rational design of quinones for high power density biofuel cells. *Chem. Sci.*, **2015**, *6*, 4867-4875.
- (22) Liang, Y.; Zhang, P.; Chen, J. Function-oriented design of conjugated carbonyl compound electrodes for high energy lithium batteries. *Chem. Sci.* **2013**, *4*, 1330-1337.
- (23) Vadehra, G. S.; Maloney, R. P.; Garcia-Garibay, M. A.; Dunn, B. Naphthalene diimide based materials with adjustable redox potentials: Evaluation for organic lithium-ion batteries. *Chem. Mater.*, **2014**, *26*, 7151-7157.

- (24) Zhao, Q.; Zhu, Z.; Chen, J. Molecular engineering with organic carbonyl electrode materials for advanced stationary and redox flow rechargeable batteries. *Adv. Mater.* **2017**, *29*, 1607007.
- (25) Oyaizu, K.; Choi, W.; Nishide, H. Functionalization of Poly(4-Chloromethylstyrene) with Anthraquinone Pendants for Organic Anode-Active Materials. *Polym. Adv. Technol.* **2011**, *22*, 1242–1247.
- (26) Yao, M.; Yamazaki, S.-i.; Senoh, H.; Sakai, T.; Kiyobayashi, T. Crystalline Polycyclic Quinone Derivatives as Organic Positive- Electrode Materials for Use in Rechargeable Lithium Batteries. *Mater. Sci. Eng. B.* **2012**, *177*, 483–487.
- (27) Aher, J.; Graefenstein, A.; Deshmukh, G.; Subramani, K.; Krueger, B.; Haensch, M.; Schwenzel, J.; Krishnamoorthy, K.; Wittstock, G. Effect of aromatic rings and substituent on the performance of lithium batteries with rylene imide cathodes. *ChemElectroChem.* **2020**, *7*, 1160-1165.
- (28) Luo, Z.; Liu, L.; Zhao, Q.; Li, F.; Chen, J. An Insoluble Benzoquinone-Based Organic Cathode for Use in Rechargeable Lithium-Ion Batteries. *Angew. Chem. Int. Ed.* **2017**, *56*, 12561 –12565.
- (29) Zhu, L.; Ding, G.; Xie, L.; Cao, X.; Liu, J.; Lei, X.; Ma, J. Conjugated carbonyl compounds as high-performance cathode materials for rechargeable batteries. *Chem. Mater.* **2019**, *31*, 8582–8612.
- (30) Luo, Z.; Liu, L.; Ning, J.; Lei, K.; Lu, Y.; Li, F.; Chen, J. A microporous covalent–organic framework with abundant accessible carbonyl groups for lithium-ion batteries. *Angew. Chem. Int. Ed.* **2018**, *57*, 9443-9446.

CHAPTER 6

Conclusion and Future Perspectives

CONCLUSION AND FUTURE PERSPECTIVES

6.1 Conclusion

A thesis entitled “Conjugated carbonyl molecules for lithium-ionthe batteries” highlighted A design and synthesis of different rylene substituted conjugated carbonyl imides derivatives as the cathode (positive electrode) for LIBs. In the present thesis, the electrochemical performance, fast reaction kinetics, solubility issue in the electrolyte, and increase in discharge voltage. All these respective parameters for developing ideal lithium batteries were tried to achieve by increasing aromatic conjugation of rylene dyes with different electrochemically active carbonyl moieties. However, we also successfully studied the comparatively effect of various substitutions over rylene dyes and their electrochemical performance on lithium-ion batteries.

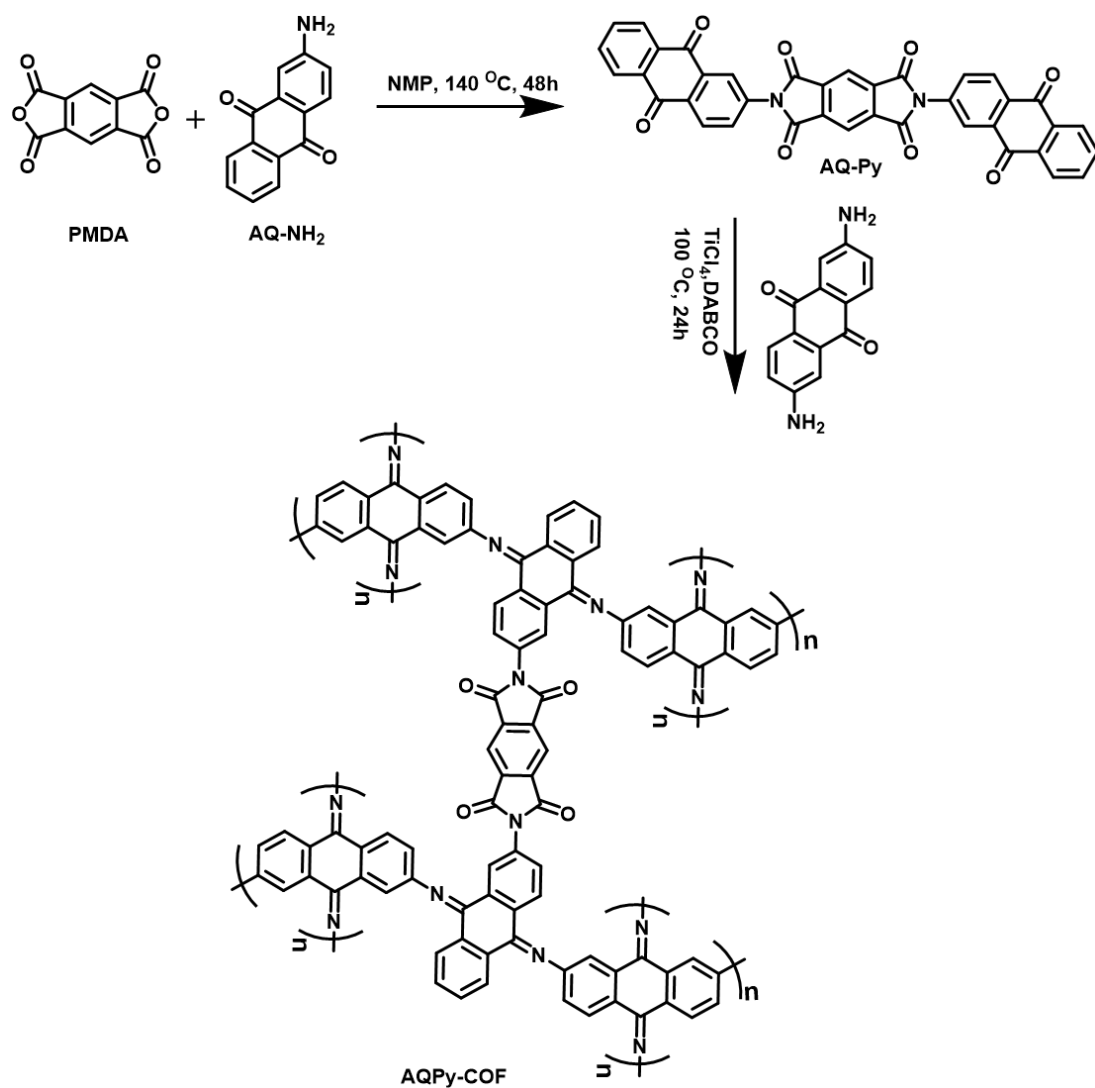
In the first working chapter, we synthesized TPA substituted three rylene Imides (TPA-PDI, TPA-NDI, and TPA-Py) and utilized them as electrodes (cathode) in LIBs. Triphenyl TPA substitution act as effective moieties for disturbing the aggregation due to their propellent type arrangement over rylene dyes. It is also responsible for decreased solubility in liquid electrolytes due to the extended aromatic conjugation over rylene dyes. However, the molecular weight of molecules is inversely proportional to theoretical specific capacity; thus, the molecular weight of the molecules increases in the sequence TPA-PY<TPA-NDI<TPA-PDI. Though experimental specific capacity also expected the same sequence but the observed specific capacity varied in the sequence TPA-NDI<TPA-PDI<TPA-Py having the 2, 4, and 1 aromatic unit in the central core, respectively. Indicating that only molecular weight decrease alone does not impact the enhancement of battery performance. All of them exhibit stable specific capacity until 300th charge-discharge cycle at a 1 C rate. However, maximum specific energy and specific powers were found to be 197 mWhg⁻¹ and 37 mWhg⁻¹, respectively.

In the second working chapter, we synthesized naphthalic anhydride substituted rylene dyes derivatives (UN-PDI, UN-NDI, and UN-Py) by simple imidization reaction and comparatively studied the electrochemical performance and solubility in liquid electrolyte. All molecule was found insoluble in liquid electrolyte even after seven days of soaking time. All molecule was able to achieve specific capacity to their theoretical capacity. Long-term cycling stability up to 200th charge/discharge at a 0.2 C rate following an order U-PDI>UN>NDI>UN-Py. In the third working chapter, we have extended the theme of the

second working chapter. The anthraquinone substituted, high theoretical capacity containing rylene imides derivatives such as AQ-PDI, AQ-NDI, and AQ-Py was synthesized, and their comparative electrochemical performance was studied. The specific capacity of these insoluble anthraquinones substituted rylene imide was found to be 120 mAh/g (AQ-PDI), 103 mAh/g (AQ-NDI), and 97 mAh/g (AQ-Py), at 0.2 C after 150th charge /discharge cycle. Among the series, high stability for long term cycling was achieved for AQ-PDI due to their extended aromatic conjugated structure. In A fourth working chapter, the high discharge voltage was able to achieve for molecule UN-4 compared to molecule NDI-4. The first discharge voltage found for molecule UN-4 was 3.08 V which is expected to be high among the literature as per our knowledge. The solubility of NDI-4 increases in liquid electrolytes due to the alkyl chain present in the molecule, which is further confirmed by less specific capacity than UN-4.

6.2 Future Perspective

Developing a cathode electrode for LIBs using a simple and cost-effective method and materials has great commercial interest due to the growing demand for energy worldwide. Most of the imine and carbonyl Imide compounds are soluble in commercially available electrolytes, as well as the compact structure of these electrochemical active imine and carbonyl imide structures hinder lithium-ion transport. Thus, here we have an idea for the synthesis of a three-dimensional porous covalent organic framework containing plenty of electrochemically active imide carbonyl and imine carbonyl (AQPy-COF). Their robust covalent polymeric structure will definitely be insoluble in commercial electrolytes, and their three-dimensional structure will facilitate lithium smoothly. This will help us develop high-energy and power density for LIBs. The synthetic scheme for AQPy-COF as per shown below.



ABSTRACT

Name of the Student: Jagadish Dhanaji Aher **Registration No.:** 10CC17J26045
Faculty of Study: Chemical Science **Year of Submission:** 2022
AcSIR academic center/CSIR Lab: **Name of the Supervisor:**
CSIR-National Chemical Laboratory, Pune Dr. Krishnamoorthy
Title of the thesis: Conjugated carbonyl molecules for lithium ion batteries.

While searching for new and different cathode materials for lithium-ion batteries, it seems that organic cathode materials are expected to be an auspicious candidate for next-generation organic batteries because of their easy synthesis, high theoretical capacity, and diversified structural modification possible. New demand for rechargeable lithium-ion batteries, such as natural abundance, environmentally friendly, and low production cost, precludes us from emphasizing heavy toxic metal-based materials; thus, it still imposes cost and resources limitation. Significantly, the organic conjugated carbonyl compounds highlight reaction reversibility, and multielectron reactions are absolutely suitable for meeting this requirement. This thesis aims to develop a cost-effective different organic conjugated carbonyl compound as the cathode (positive electrode) for lithium-ion battery application. **Chapter 1** discussed the recent effort to develop different organic electrode materials for LIBs, along with the highlighted significance of organic conjugated compound electrode materials over other organic electrode materials. Here mainly emphasizes the main problems associated with this organic electrode materials dissolution in an organic electrolyte, low electronic conductivity, slow reaction kinetics, and low discharge potentials. In **chapter 2**, we have prepared TPA-substituted TPA-PDI, TPA-NDI, and TPA-Py and utilized them as electrodes in LIBs. Here, we have successfully identified the relationship between molecular weight and performance as an organic battery material. In **chapter 3**, We have synthesized the naphthalene substituted rylene dyes compound, namely UN-PDI, UN-NDI, and UN-Py, to address the issue of solubility and reaction kinetics and comparative study of electrochemical performance in LIBs. In **chapter 4**, we have extended the same analogy as in chapter 3 with an increase in theoretical capacity by six electron transfers in molecule AQ-PDI, AQ-NDI, and AQ-Py. In **chapter 5**, we emphasized the low reduction potential problem and solubility associated with organic carbonyl imide and tried to resolve it by synthesizing UN-4 and NDI-4-star shaped imide cathode.

List of Publications Emanating from the Thesis Work

- (1) **Jagdish D. Aher**, Graefenstein A, Deshmukh G, Subramani K, Krueger B, Haensch, M, Schwenzel J, Krishnamoorthy K, Wittstock G. Effect of aromatic rings and substituent on the performance of lithium batteries with rylene imide cathodes. *ChemElectroChem*. **2020**, 7, 1160-1165.

DOI: 10.1002/celec.202000118

- (2) **Jagdish D. Aher**, Krishnamoorthy K. An Insoluble Naphthalic Anhydride Based Rylene Imide Derivatives Cathode for Lithium-ion Batteries. (*Manuscript under preparation*)

- (3) **Jagdish D. Aher**, Krishnamoorthy K. An anthraquinone based rylene imide derivatives cathode for organic lithium-ion Batteries. (*Manuscript under preparation*)

List of Publications Non-Emanating from the Thesis Work

- (1) Kanetkar, M. V., **J. D. Aher**, Kakde, G. K, Puyad, A., Kalalawe, V. G., Dharmapurikar, S. Synthesis and characterization of urethane side chain substituted Diketopyrrolopyrrole, *J. Sci. Res.* **2021**, 13, 635-642.

List of posters Presented with details

SPSI MACRO 2018 Poster Presentation at International Conference on Polymers Science and Technology Pune, (India). (December **2018**)

Title: Effect of Aromatic Rings and Substituent on the Performance of Lithium-ion Batteries with Rylene Imide as Cathodes.

Abstract: Rylene imides (RIs) are attractive organic battery materials because of the inherently present modularity in the molecule. Strong aggregation of RIs is disadvantageous for fast lithium-ion transport but also beneficial because it decreases the solubility of RIs in typical organic battery electrolytes. Balancing both trends renders the design and synthesis of RIs for lithium batteries a non-trivial task. We have chosen triphenylamine (TPA) as a substituent that disrupts the aggregation, but due to the increased aromaticity of TPA, the solubility is also decreased. We have synthesized three RIs with 1, 2, and 4 aromatic units in the core. All of them showed stable specific capacity over 300 charge-discharge cycles. The batteries also showed specific capacity close to their theoretical capacity with 97-99% coulombic efficiency. Maximum energy density and power density were found to be 197 mWh g⁻¹ and 37 mW g⁻¹, respectively.

National Science Day 2021 Poster presentation at CSIR-National Chemical Laboratory, Pune, (India). (February **2021**)

Title: Effect of Aromatic Rings and Substituent on the Performance of Lithium Batteries with Rylene Imide Cathodes

Abstract: Rylene imides (RIs) are attractive organic battery materials because of the inherent modularity of the molecules. While strong aggregation of RIs is disadvantageous for fast lithium-ion transport in the organic active material, decreasing the solubility of the RIs in battery electrolytes is essential to avoid performance fading. Therefore, the design and synthesis of RIs for lithium batteries is a non-trivial task that must, among other considerations, balance lithium-ion transport in the solid material vs. low solubility by controlling aggregation and packing. We have chosen triphenylamine (TPA) as a substituent that disrupts the aggregation but maintains a low solubility due to the increased aromaticity

List of Posters with details.....

of TPA. We have synthesized three RIs with one, two, and four aromatic units in the core. All of them showed stable specific capacity over 300 charge-discharge cycles. The batteries also showed specific capacities close to their theoretical capacities with 97–99% coulombic efficiency. The maximum specific energy and specific powers were 197 mWhg⁻¹ and 37 mWhg⁻¹, respectively.

List of Conferences Attended with Details

- (1) **SPSI MACRO** International Conference on Polymers Science and Technology IISER Pune, (India). **2018**
- (2) **NCL-RF annual students' Conference** at CSIR-National Chemical Laboratory, Pune, (India). (November **2018**)

ABOUT THE AUTHOR



Mr. Jagadish was born to Shri. Dhanajirao and Smt. Taramati Aher in 1990 at Pimpalgaon, a small village in the Washim district of Maharashtra (India). The author started his primary schooling at Z. P school in the same village. In the same village, he extended his secondary schooling at Vidhrbha Vidyalaya Pimpalgaon. He completed his higher secondary education in 2008 from P.D. Jaine College Ansing. (Washim, Maharashtra) He completed his graduation from R.A. College, Washim (Maharashtra) (2012). The author pursued his master's degree in Chemistry from the Post Graduate Teaching Department of Chemistry, SGB Amaravati University, Amravati (Maharashtra). After qualifying CSIR-UGC National Eligibility Test (NET-JRF) examination with AIR 84, he joined the Polymer Science and Engineering (PSE) Division of CSIR-National Chemical Laboratory, Pune, India, as a Junior Research Fellow (JRF) to pursue his Ph.D. degree under the supervision of Dr. K. Krishnamoorthy (January 2017). He has received a research fellowship (JRF and SRF) from the University Grand Commission (UGC) under the UGC fellowship scheme, New Delhi, India, to carry out his Ph.D. thesis work.

Effect of Aromatic Rings and Substituent on the Performance of Lithium Batteries with Rylene Imide Cathodes

Jagdish Aher,^[a, b] Alexander Graefenstein,^[c] Guntavt Deshmukh,^[a, b] Kumar Subramani,^[a, b] Bastian Krueger,^[d] Mareike Haensch,^[d] Julian Schwenzel,^{*,[c]} Kothandam Krishnamoorthy,^{*,[a, b]} and Gunther Wittstock^{*,[d]}

Rylene imides (RIs) are attractive organic battery materials because of the inherent modularity of the molecules. While strong aggregation of RIs is disadvantageous for fast lithium-ion transport in the organic active material, decreasing the solubility of the RIs in battery electrolytes is essential to avoid performance fading. Therefore, the design and synthesis of RIs for lithium batteries is a non-trivial task that must, among other considerations, balance lithium-ion transport in the solid material vs. low solubility by controlling aggregation and

packing. We have chosen triphenylamine (TPA) as a substituent which disrupts the aggregation but maintains a low solubility due to increased aromaticity of TPA. We have synthesized three RIs with one, two, and four aromatic units in the core. All of them showed stable specific capacity over 300 charge-discharge cycles. The batteries also showed specific capacities close to their theoretical capacities with 97–99% coulombic efficiency. The maximum specific energy and specific power were 197 mWh g⁻¹ and 37 mW g⁻¹, respectively.

1. Introduction

Lithium-ion batteries (LIBs) find their wide use in portable electronic devices,^[1–4] despite large efforts to use them for electrotraction and load levelling in electric grids.^[5] While inorganic intercalation compounds and carbon materials are routinely used as electrodes in LIB,^[6–11] organic molecules are

explored as active materials in LIB due to their light weight, flexibility, easy processability and potentially unlimited availability (as compared to transition metal oxides). Among the tested classes of compounds are conjugated polymers, imides, quinones, triazines, corroles, triangulenes, tetracyanoquinodimethane.^[12–20] Rylene imides are interesting due to the presence of carbonyl moieties that are attached to a conjugated backbone (Scheme 1). The lowest unoccupied molecular orbital (LUMO) energy levels of rylene imides vary as a function of the number of phenyl rings present in the molecule. This variation in LUMO offers the possibility to vary the output voltage of the battery. Due to the advantageous properties of rylene imides,

[a] J. Aher, G. Deshmukh, K. Subramani, Prof. Dr. K. Krishnamoorthy
Polymer Science and Engineering Division
CSIR-National Chemical Laboratory
Dr. Homi Bhabha Road, Pashan Road, Pune 411008
E-mail: jd.aher@ncl.res.in
gr.deshmukh@ncl.res.in
k.subramani@ncl.res.in
k.krishnamoorthy@ncl.res.in

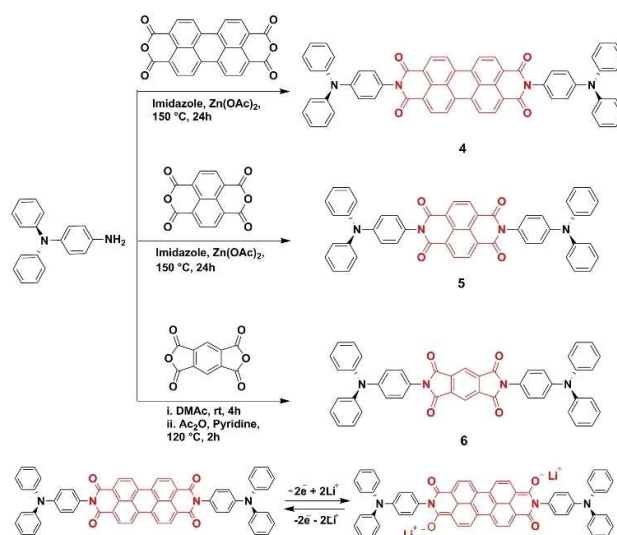
[b] J. Aher, G. Deshmukh, K. Subramani, Prof. Dr. K. Krishnamoorthy
Academy of Scientific and Innovative Research (AcSIR)
Ghaziabad-201002, India

[c] A. Graefenstein, Dr. J. Schwenzel
Department Electrical Energy Storage
Fraunhofer Institute for Manufacturing Technology and Advanced Materials IFAM
D-26129, Oldenburg, Germany
E-mail: alexander.graefenstein@ifam.fraunhofer.de
julian.schwenzel@ifam.fraunhofer.de

[d] B. Krueger, Dr. M. Haensch, Prof. Dr. G. Wittstock
School of Mathematics and Science, Chemistry Department
Carl von Ossietzky University of Oldenburg
D-26111, Oldenburg, Germany
E-mail: bastian.krueger@uni-oldenburg.de
mareike@familie-haensch.de
wittstock@uol.de

Supporting information for this article is available on the WWW under <https://doi.org/10.1002/celc.202000118>

© 2020 The Authors. Published by Wiley-VCH Verlag GmbH & Co. KGaA. This is an open access article under the terms of the Creative Commons Attribution Non-Commercial License, which permits use, distribution and reproduction in any medium, provided the original work is properly cited and is not used for commercial purposes.



Scheme 1. Synthesis of rylene imides 4 (PDI), 5 (NDI) and 6 (PyDI), and the redox reaction during charge/discharge experiment.

perylene dianhydride was blended with sulfur and incorporated as an electrode in LIBs.^[21] A composite of perylene diimide (PDI) was prepared in the presence of carbon nanotubes and was used in LIBs. A series of PDI polymers were prepared for utilization in LIBs.^[22–24] Polar functionalities attached to the PDI backbones were found to stabilize the battery performance.^[6,25,26] Naphthalenediimide (NDI) is an analogue of PDI with a smaller aromatic system. Naphthalenedianhydride (NDA) was polymerized with urea and diamino ethane.^[27] The carbonyl moiety of the urea linker was found to increase the specific capacity of LIBs based on NDI. The cycling stability and coulombic efficiency decreased over 150 charge-discharge cycles. NDA was also polymerized with hydrazine and its utility in LIBs was studied. During the charge-discharge cycling, the N–N bond was cleaved, leading to a decrease in specific capacity. An alkyl group was substituted on the imide nitrogen of NDI and its performance was compared with that of Li-substituted NDI.^[28] In another set of experiments, NDA was polymerized with diamino ethane over graphene. Batteries were fabricated using lithium and sodium electrodes.^[29] The lowest analogue in the rylene imide series is pyromellitic diimide (PyDI), which has been used in a sodium-ion battery.^[30] LIBs of PyDI showed a specific capacity of 200 mAhg⁻¹ over 25 cycles.^[31] Polymers of PyDI have been prepared and explored in LIBs.^[32]

One of the issues in rylene imides-based LIBs is the decrease in specific capacity upon charge-discharge cycling. Simple rylene imides as shown in Scheme 1 are usually insoluble in common organic solvents, hence they should have been the material of choice to fabricate LIBs with impressive efficiency.

However, it has been shown that the lithium-ion insertion is precluded due to close packing of the molecules.^[29] Thus, a substitution at the imide nitrogen is necessary to achieve a more open packing in the solid state. However, the substitution can either increase solubility of the material or further complicate the lithium-ion insertion process. Considering these issues, we have chosen triphenylamine (TPA) as a substituent on the imide nitrogen for the following reasons, (i) the absence of redox process in the charge-discharge window of LIBs, (ii) the increased aromatic systems that are likely to decrease solubilities, and (iii) the propeller-type arrangement of phenyl rings in TPA is likely to disrupt the close packing of the molecules and facilitate lithium-ion insertion and desorption. Using the systematically varied compounds shown in Scheme 1, we were interested in identifying the relation between molecular weight and performance as an organic battery material. Theoretically, a decrease in molecular weight should increase specific capacity. However, in rylene imides, the variation in molecular weight is accompanied by a variation in the number of aromatic units that may influence the redox properties for which a systematic study is not available yet. To address all these issues, we have prepared TPA-substituted PDI (4), NDI (5) and PyDI (6) and utilized them as electrodes in LIBs. Compounds 4, 5 and 6 comprise four carbonyl moieties and two imide nitrogens as common structural motifs. They differ in the number of central aromatic rings, namely four, two and one for molecules 4, 5 and 6, respectively. While our work was in progress, synthesis and

electrochromic properties of compounds 4, 5 and 6 were reported.^[33]

2. Results and Discussion

The amine-substituted TPA was condensed with rylene dianhydrides to prepare compounds 4, 5 and 6 (Scheme 1). The absorption spectra were recorded using dilute solution of the molecules in N-methyl-2-pyrrolidone (NMP). Molecule 4 showed two sharp peaks at 527 nm, 491 nm and a hump at 460 nm. The frontier orbital difference was found to be 2.3 eV (Figure 1a). Molecule 5 showed two peaks at 382 nm, 361 nm and a hump at 341 nm with a frontier orbital difference of 3.19 eV (Figure 1a).

The frontier orbital difference was calculated to be 4.0 eV (Figure 1a). Cyclic voltammograms (CVs) of the compounds were recorded in 0.1 M tetrabutylammonium perchlorate (TBAClO₄) in NMP using a Pt wire as the working electrode, at Pt foil as the auxiliary electrode and a Ag/Ag⁺ reference electrode. The potential of the electrode was cycled between 0 and –2 V. The CVs of molecule 4 showed two reduction peaks at –0.82 V and –1.22 V corresponding to the dianion formation. In the reverse scan, two peaks for the sequential re-oxidation of the dianion were observed (Figure 1b). Similarly, two reduction peaks were observed for molecule 5 during the potential sweep towards –2 V indicating the formation of the dianion of 5. Contrary to this, molecule 6 showed only a single reduction peak indicating the possibility of anion radical formation in the potential window.

The morphology of the molecular crystals was studied by SEM and TEM. The samples were prepared using NMP because this solvent is used to prepare battery electrodes. In the SEM image of 4, large crystals of rice husk type morphology were found (Figure 1c). A similar morphology was also in TEM (Figure 1d). It is necessary to look at the morphology of 4 in the blends that are used as electrodes in LIB, where the rice husk

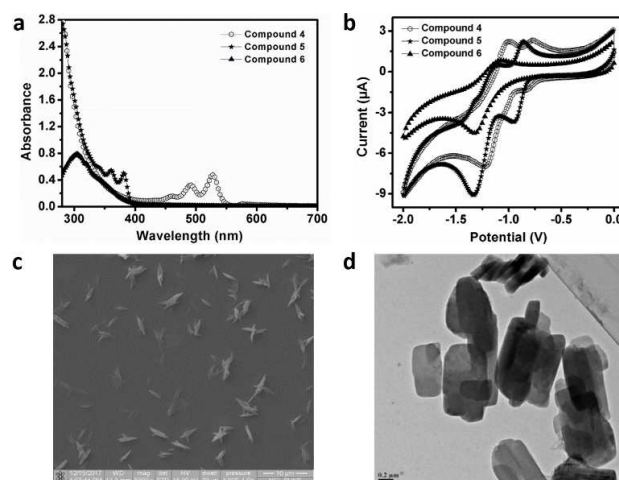


Figure 1. Absorption spectra (a) and cyclic voltammograms (b) of molecules 4, 5 and 6. SEM image (c) and TEM image (d) of molecule 4. The scale bars in (c) and (d) have a length of 10 μm and 0.2 μm , respectively.

morphology was indeed found (Figure 2a). In order to study the fate of the rice husk crystal morphology during charge-discharge experiments (1.5 V to 4.2 V vs Li/Li⁺) over 300 cycles, the LIB was opened and the morphology was studied by SEM. The SEM images indicated the retention of the rice husk morphology (Figure 2b). The morphologies of **5** and **6** were found to be long needles (Figure 2c and Figure 2d). The morphologies of **5** (Figure 2e) and **6** (Supporting Information, Figure S6a) were retained in their blends. The charge-discharge cycling caused a change in the surface roughness, but we did not find significant changes in the morphologies of **5** (Figure 2f) or **6** (Supporting Information, Figure S6b).

With this information in hand, LIBs were fabricated in pouch cell configuration using a composite of molecule **4** or **5** or **6**, PVDF as binder and carbon as conductive filler as one electrode and lithium foil as the counter electrode. Other details of the cells are provided in the Experimental Section. The charge-discharge experiment was carried out at various C rates while sweeping the potential between 1.5 and 4.2 V vs. Li/Li⁺.

In the first set of experiments, the charging rate was the same as the discharge rate. The discharge curves of cells with molecule **4** showed two plateaus between 1.5 V and 4.2 V vs. Li/Li⁺ indicating two electron transfers (Figure 3a). Similar charge-discharge profiles were observed while using perylenebisimide^[34,35] and naphthalenebisimide^[36] derivatives in LIBs. The first plateau changed into a slope upon continuous cycling. The specific capacity of the first cycle was 55 mAh/g, which decreased by 13% to 48 mAh/g after 300 cycles (Figure 3b). The C rate for this experiment was 1 h⁻¹. Subsequently, the C rate was varied between 0.2 and 30 h⁻¹ and the specific

capacity was monitored. The specific capacity decreased gradually upon increase in C rate. At 30 h⁻¹, the specific capacity was 38 mAh/g, which is ~30% less than that observed at 0.2 h⁻¹ (Figure 3c). In most batteries, a decrease in specific capacity is observed with increasing C rates. In all the experiments, the coulombic efficiency was 97%, which did not vary as a function of cycle number.

In the next set of experiments, the LIB was charged at slow C rate of 0.2 h⁻¹, while different C rates between 0.2 h⁻¹ and 30 h⁻¹ were applied for discharge. This cell showed a specific capacity of 61 mAh/g when charged and discharged at 0.2 h⁻¹. The specific capacity decreased to 49 mAh/g, when the discharge rate was increased to 30 h⁻¹ (Figure 3c). The decrease is 20% compared to 30% observed for charge and discharge rate to 30 h⁻¹. As expected, the performance of the tested LIBs increased by slowly charging the cell.

In the next set of experiments, molecule **5** was used to prepare the active cathode material. The discharge curves showed two plateaus, one between 4.2 and 3.6 V vs. Li/Li⁺ and the second between 2.4 to 2.1 V vs. Li/Li⁺ (Supporting Information, Figure S8). The two plateaus arise due to two-electron reductions of two carbonyl groups to two enolate groups. As shown in Table 1, the specific capacity decreased by 16% after 300 charge-discharge cycles. The decrease in specific capacity as a function of cycle number is comparable to that of molecule **4**. At charging rate of 0.2 h⁻¹ and a discharge at the same rate, the specific capacity was 61 mAh/g. The specific capacity decreased by 75% to 15 mAh/g upon increase in charging and discharging rates to 30 h⁻¹ (Figure 3d). Subsequently, the LIB was charged at 0.2 h⁻¹ and the discharge

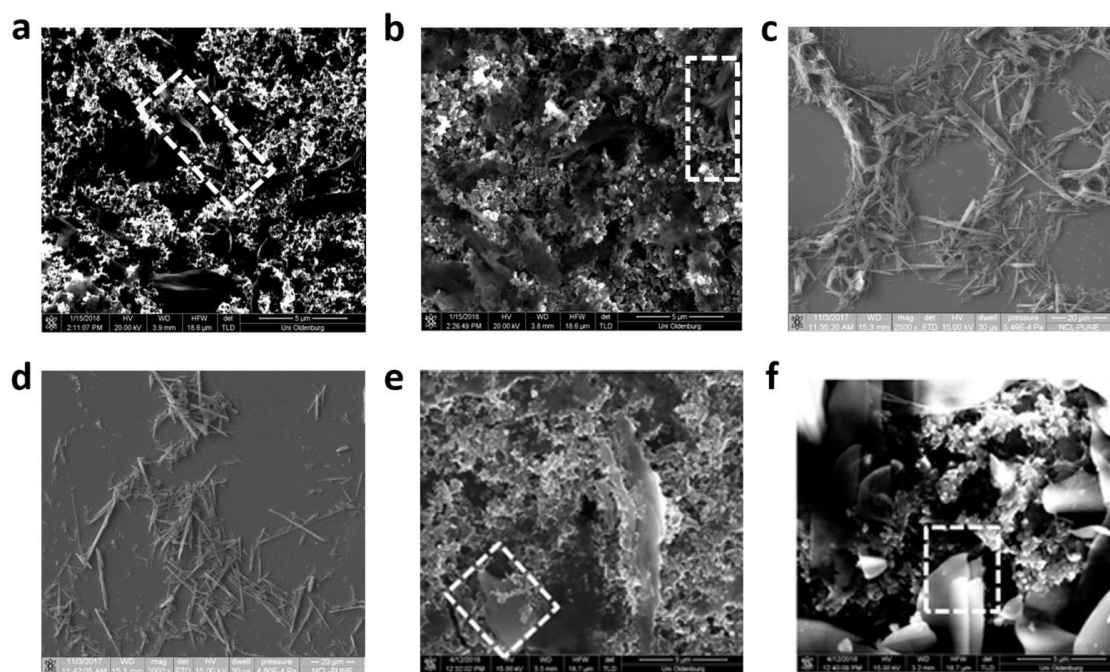


Figure 2. SEM image showing the presence of rice husk morphology of molecule **4** in the blends before (a) and after (b) 300 charge-discharge cycles between 1.5 V and 4.2 V. SEM images show the needle-type morphologies of molecule **5** (c) and **6** (d). SEM images show that the battery electrodes do have the compound **5** before (e) and after (f) 300 charge-discharge cycles between 1.5 V and 4.2 V.

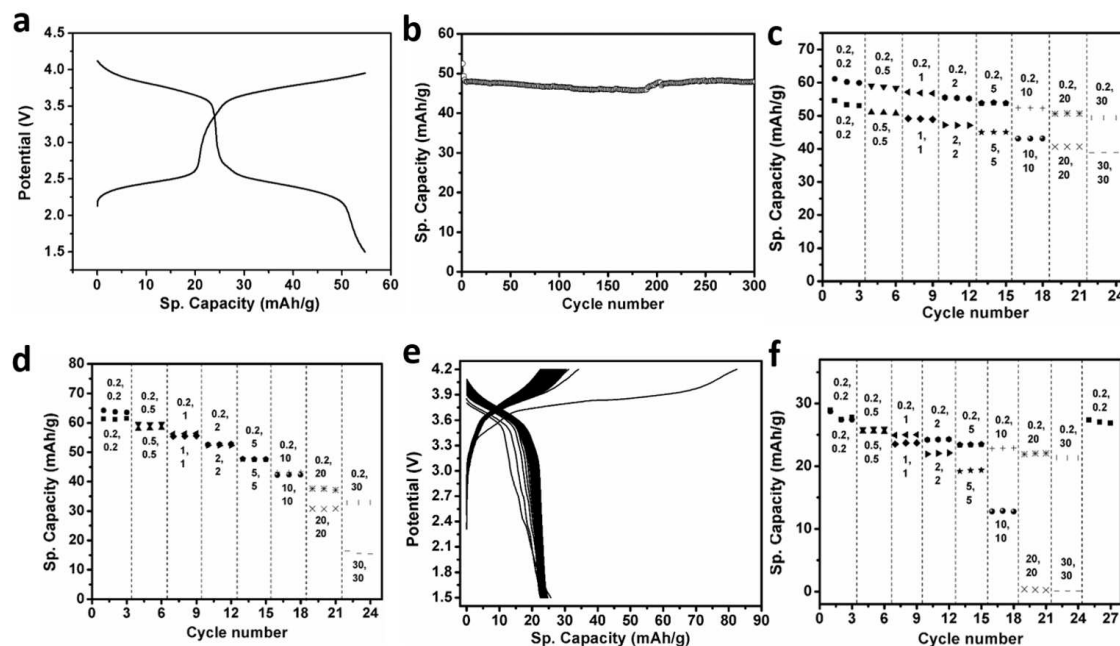


Figure 3. a) Charge-discharge profile of molecule **4** at a C rate of 1 h^{-1} ; b) variation of specific capacity with the number of charge-discharge cycles using molecule **4** as cathode material at a C rate of 1 h^{-1} ; c) specific capacity of a battery with molecule **4** as a function of C rate; d) effect of C rate on the specific capacity using molecule **5** as cathode material; e) charge-discharge curve of a battery with molecule **6** as cathode material, the C rate was 1 h^{-1} ; and f) specific capacity as a function of C rate for a battery using molecule **6** as cathode material.

Table 1. Battery metrics for molecules **4**, **5** and **6** as a function of charge discharge cycles).

Molecule	Charge/discharge potential window vs. Li/Li^+	Charge/discharge C Rate	Specific capacity in first discharge cycle	Specific capacity in 300th discharge cycle	Relative decrease in specific capacity 300 charge-discharge cycles compared to the initial cycle
4	1.5–4.2 V	$1 \text{ h}^{-1}/1 \text{ h}^{-1}$	55 mAh g^{-1}	48 mAh g^{-1}	13%
5	1.5–4.2 V	$1 \text{ h}^{-1}/1 \text{ h}^{-1}$	63 mAh g^{-1}	53 mAh g^{-1}	16%
6	1.5–4.2 V	$1 \text{ h}^{-1}/1 \text{ h}^{-1}$	25 mAh g^{-1}	20 mAh g^{-1}	20%

experiment was conducted at C rates between 0.2 h^{-1} and 30 h^{-1} . At 0.2 h^{-1} , the specific capacity was calculated to be 64 mAh/g , which decreased by 50% upon increase in C rate to 30 h^{-1} (Figure 3d). The 50% decrease in specific capacity for the LIB with compound **5** at charging/discharging rates of $0.2 \text{ h}^{-1}/30 \text{ h}^{-1}$ is lower than the 75% loss when charging/discharging at $30 \text{ h}^{-1}/30 \text{ h}^{-1}$, but significantly higher than 20% observed for the LIB with molecule **4** upon charging/ discharging at $30 \text{ h}^{-1}/30 \text{ h}^{-1}$.

In the next set of experiments, molecule **6** was tested in the battery. Unlike molecules **4** and **5**, only a single plateau was observed between 4.2 and 3.4 V vs. Li/Li^+ for the LIB made from compound **6** (Figure 3e). It has been shown that two electrons are transferred for PyDI between 1.5 V to 3 V vs. Li/Li^+ .^[31] A decrease of 20% in specific capacity was observed after 300 charge-discharge cycles (Table 1). At 0.2 C, the specific capacity was 29 mAh/g which decreased by 99% to 0.06 mAh/g at 30 h^{-1} (Figure 3f). However, when subsequently charged and discharged at 0.2 h^{-1} , the specific capacity bounced back to 27 mAh/g , which is quite close to the 29 mAh/g observed at the start of the charge-discharge experiments (Figure 3f). There-

fore, the extremely small specific capacity observed at 30 h^{-1} is not due to degradation of the LIB. In fact, this is contrary to an earlier observation, wherein the experimentally observed decrease of the specific capacity to 23% was attributed to dissolution of the PyDI molecules during battery cycling.^[37] Finally, the LIB was charged at 0.2 h^{-1} and discharged at C rates between 0.2 h^{-1} and 30 h^{-1} . The specific capacity of the LIBs discharged at 0.2 h^{-1} (29 mAh/g) decreased by 28% to 21 mAh/g at 30 h^{-1} (Figure 3f). Thus, the capacity is much less sensitive to high discharge rates (28% loss in specific capacity) than to high charging rates (99% loss in specific capacity).

We hypothesize that TPA will facilitate lithium-ion diffusion. To measure the diffusion coefficient of lithium ions (D_{Li^+}), impedance spectra were recorded and evaluated using the equivalent circuit in Supporting Information, Figure S9 following the reported procedure.^[35] From the Nyquist plot (Supporting Information, Figure S10), a plot of $1/\omega^{1/2}$ vs. Z' was computed. The slope of this plot is the Warburg factor, which was used to calculate D_{Li^+} (Supporting Information, Figure S11).^[35] The highest D_{Li^+} ($3.7 \times 10^{-13} \text{ cm}^2 \text{ s}^{-1}$) was observed for molecule **6**, which is an order of magnitude higher than that

observed for **4** ($2.3 \times 10^{-14} \text{ cm}^2 \text{ s}^{-1}$, Supporting Information, Table S1). Molecule **6** has one aromatic unit that is attached to two TPA moieties, hence the closeness of the TPA precludes the close packing of **6**. Thus, the lithium-ion diffusion is faster. On the other hand, the four aromatic units keep the TPA moieties apart in molecule **4**. Therefore, close packing is still possible in **4** leading to decreased lithium-ion diffusion (Table S1). Although molecule **4** exhibits the lowest D_{Li^+} among the series reported in this work, it still showed higher D_{Li^+} compared to control molecule **7** with phenyl substituents (Scheme S1). This corroborates our hypothesis that TPA is likely to facilitate lithium-ion transport.

In the final set of experiments, we analyzed the battery electrolyte to identify the presence of dissolved molecules. For this experiment, the battery was opened after 100 cycles. The electrolytes were mixed with fresh NMP, which dissolves molecules **4**, **5** and **6**. The absorption spectra were recorded between 250 and 700 nm. We observed all the peaks corresponding to molecules **4**, **5** and **6** (Supporting Information, Figure S12) confirming the dissolution of molecules during the charge-discharge cycling. However, this data must be correlated with battery performance. It must be noted that the decrease in specific capacity of batteries comprising molecule **4** is 13% after 300 charge-discharge cycles. However, the decrease in specific capacity is 84% for the control molecule **7** with phenyl moiety instead of TPA (Scheme S1).^[12] Therefore, as hypothesized, the TPA decrease the solubility of rylene imide molecules in battery electrolyte. Due to the decreased solubility, the specific capacity fading is 13% for molecule **4**, but the decrease is 84% for control molecule **7**.^[12]

3. Conclusion

TPA acts as an effective moiety to disrupt the aggregation of RIs without causing solubility of the molecule in battery electrolytes. The three molecules chosen from the RIs family have different numbers of aromatic units. The theoretical capacity of the RIs is expected to decrease with the number of aromatic rings in the rylene imides core of the molecule. Contrary to this, the experimental specific capacities varied with the number of aromatic units in the sequence $1 < 4 < 2$. Thus, decreasing the molecular weight alone does not impart improvement in battery performance. TPA is certainly a good motif to facilitate lithium ion transport in solid RI molecules and improves the crystal stability during the charge-discharge experiments. All the RIs showed impressive cycling stability over 300 cycles. Molecules with few aromatic core units conjugated with redox functionality are not suitable for rapid charge-discharge experiments. In fact, we found extremely small specific capacity of 0.06 mAh/g for a molecule with one aromatic unit. Contrary to this, the specific capacity of the molecule with two aromatic rings showed a four order of magnitude higher specific capacity. From this study, we have identified that the TPA motif facilitates the design of efficient organic materials for lithium-ion battery.

Experimental Section

Chemicals and Materials

Unless otherwise stated, all the chemicals and reagents were obtained commercially and used without further purification. Perylene-3,4,9,10-tetracarboxylic dianhydride, 1,4,5,8-naphthalene-tetracarboxylic dianhydride, pyromellitic dianhydride, zinc acetate, copper(II) nitrate hydrate and triphenylamine were purchased from Sigma-Aldrich. All solvents were purchased from Merck Chemicals. All solvents used for battery performance tests were of HPLC grade.

General Experimental Method and Instruments

Analytical thin layer chromatography was carried out on pre-coated silica gel plates (Kiesel gel 60F254, Merck). Column chromatographic purifications were performed with 60–120 mesh sized silica gel. All ^1H NMR spectra were recorded in CDCl_3 and DMSO-d_6 on a Bruker arx AV 200 MHz, AV 400 MHz and AV 500 MHz Bruker AVANS spectrometer. ^{13}C NMR spectra were measured on a Bruker arx 200 MHz AVANS spectrometer. All chemical shifts are reported in δ ppm downfield to TMS and peak multiplicities are referred to as singlet (s), doublet (d), triplet (t), quartet (q), pentet (p), and multiplet (m). UV-vis absorption spectra were recorded on SPECORD® 210/PLUS, UV-visible spectrophotometer. LC-HRMS analysis was carried out on a Thermo Fisher instrument. An electrochemical analyzer CHI660 (CH Instruments) was used to record the cyclic voltammograms of the prepared molecules 0.1 M tetrabutylammonium perchlorate (TBAClO_4) in NMP in a three-electrode setup with a Pt working electrode, Pt foil as the auxiliary electrode and a Ag/Ag^+ reference electrode. TEM imaging was performed with a Jeol 1200 EX transmission electron microscope. The samples were prepared by drop casting (5–10 μL of 5×10^{-4} M) of the sample on the carbon-coated copper grids (400 grids, Ted Pella) and dried at 50°C for 12 h. SEM imaging was done with a Helios Nanolab 600i system (FEI Company, Eindhoven, The Netherlands) at 10 kV accelerating voltage. The sample was prepared by drop casting 5–10 μL of 5×10^{-4} M solution of the molecules on ZP-P4VP spun silicon wafers.

The positive electrode consisted of either **4** or **5** or **6** as the electrochemically active material, PVDF (Kynar ADX 111) as a binder and carbon black (TIMCAL ENSACO Super C 65) as a conductive additive. The composition of those components was TPA/PVDF/carbon black = 60%/10%/30% by mass. The compounds were mixed with N-methyl-2-pyrrolidone (NMP) as solvent and coated on copper foil. Subsequently, electrodes with an area of $2 \times 2 \text{ cm}^2$ were punched out after drying. Lithium was used as the negative electrode, 1 M LiPF_6 in EC:DEC (1:1, mass ratio) as the electrolyte and Whatman® GF/A as separator. All cells were assembled in a glove box under argon atmosphere. Charge-discharge cycles were run with three replicates for each compound. After charge-discharge cycling, the separator was washed with NMP and UV-vis absorption spectra were recorded.

Acknowledgements

K.K. thanks Alexander von Humboldt Foundation for an Experienced Researcher Fellowship. K.K. also thanks SERB for funding. J.A. and G.D. thank UGC for fellowship. K.S. thanks DST India for fellowship. M.H. was supported by Deutsche Forschungsgemeinschaft grant Wi1617/21.

Keywords: rylene imides · organic cathode material · triphenylamine · solubility · lithium-ion batteries

- [1] M. Armand, J.-M. Tarascon, *Nature* **2001**, *414*, 359–367.
 [2] M. R. Palacin, *Chem. Soc. Rev.* **2009**, *38*, 2565–2575.
 [3] D. Deng, *Energy Sci. Eng.* **2015**, *3*, 385–418.
 [4] M. E. Bhosale, S. Chae, J. M. Kim, J.-Y. Choi, *J. Mater. Chem. A* **2018**, *6*, 19885–19911.
 [5] H. C. Hesse, M. Schimpe, D. Kucevic, A. Jossen, *Energies* **2017**, *10*, 2107–2149.
 [6] K. Mizushima, P. Jones, P. Wiseman, J. Goodenough, *Solid Stat Ion.* **1981**, *3*, 171–174.
 [7] W. M. Zhang, X. L. Wu, J. S. Hu, Y. G. Guo, L. Wan, *J. Adv. Funct. Mater.* **2008**, *18*, 3941–3946.
 [8] L. Qie, W. M. Chen, Z. H. Wang, Q. G. Shao, X. Li, L. X. Yuan, X. L. Hu, W. X. Zhang, Y. H. Huang, *Adv. Mater.* **2012**, *24*, 2047–2050.
 [9] S. Flandrois, B. Simon, *Carbon* **1999**, *37*, 165–180.
 [10] M. Endo, C. Kim, K. Nishimura, T. Fujino, K. Miyashita, *Carbon* **2000**, *38*, 183–197.
 [11] Y. Shia, M. Zhanga, D. Qianb, Y. S. Meng, *Electrochim. Acta.* **2016**, *203*, 154–161.
 [12] M. E. Bhosale, K. Krishnamoorthy, *Chem. Mater.* **2015**, *27*, 2121–2126.
 [13] G. S. Vadehra, R. P. Maloney, M. A. Garcia-Garibay, B. Dunn, *Chem. Mater.* **2014**, *26*, 7151–7157.
 [14] C. X. Guo, M. Wang, T. Chen, X. W. Lou, C. M. Li, *Adv. Energy Mater.* **2011**, *1*, 736–741.
 [15] M. Armand, J.-M. Tarascon, *Nature* **2008**, *451*, 652–657.
 [16] Y. Liang, Z. Tao, J. Chen, *Adv. Energy Mater.* **2012**, *2*, 742–769.
 [17] N. Kurimoto, R. Omoda, T. Mizumo, S. Ito, Y. Aihara, T. Itoh, *J. Power Sources* **2018**, *377*, 12–17.
 [18] Y. Wu, R. Zeng, J. Nan, D. Shu, Y. Qiu, S. L. Chou, *Adv. Energy Mater.* **2017**, *7*, 1700278–1700304.
 [19] M. G. Kim, J. Cho, *Adv. Funct. Mater.* **2009**, *19*, 1497–1514.
 [20] Y. Morita, S. Nishida, T. Murata, M. Moriguchi, A. Ueda, M. Satoh, K. Arifuku, K. Sato, T. Takui, *Nat. Mater.* **2011**, *10*, 947–951.
 [21] X. Han, C. Chang, L. Yuan, T. Sun, J. Sun, *Adv. Mater.* **2007**, *19*, 1616–1621.
 [22] D. Wu, G. Zhang, D. Lu, L. Ma, Z. Xu, X. Xi, R. Liu, P. Liu, Y. Su, *J. Mater. Chem. A* **2018**, *6*, 13613–13618.
 [23] H. Wu, K. Wang, Y. Meng, K. Lua, Z. Wei, *J. Mater. Chem. A* **2013**, *1*, 6366–6372.
 [24] P. Sharma, D. Damien, K. Nagarajan, M. M. Shaijumon, M. Hariharan, *J. Phys. Chem. Lett.* **2013**, *4*, 3192–3197.
 [25] M. Veerababu, R. Kothandaraman, *Electrochim. Acta.* **2017**, *232*, 244–253.
 [26] V. Medabalmi, K. Ramanujam, *ChemistrySelect* **2018**, *3*, 10657–10662.
 [27] C. Chen, X. Zhao, H.-B. Li, F. Gan, J. Zhang, J. Dong, Q. Zhang, *Electrochim. Acta* **2017**, *229*, 387–395.
 [28] A. Shestakov, O. Yarmolenko, A. Ignatova, A. Mumyatov, K. Stevenson, P. Troshin, *J. Mater. Chem. A* **2017**, *5*, 6532–6537.
 [29] Y. Huang, K. Li, J. Liu, X. Zhong, X. Duan, I. Shakirc, Y. Xu, *J. Mater. Chem. A* **2017**, *5*, 2710–2716.
 [30] S. Renault, V. A. Mihali, K. Edström, D. Brandell, *Electrochem. Commun.* **2014**, *45*, 52–55.
 [31] S. Renault, J. Geng, F. Dolhem, P. Poizat, *Chem. Commun.* **2011**, *47*, 2414–2416.
 [32] Z. Song, H. Zhan, Y. Zhou, *Angew. Chem.* **2010**, *49*, 8444–8448.
 [33] S.-H. Hsiao, Y.-Z. Chen, *Dyes Pigm.* **2017**, *144*, 173–183.
 [34] L. Li, H.-X. Gong, D.-Y. Chen, M.-J. Lin, *Chem. Eur. J.* **2018**, *24*, 13188–13196.
 [35] L. Li, Y.-J. Hong, D.-Y. Chen, M.-J. Lin, *Chem. Eur. J.* **2017**, *23*, 16612–16620.
 [36] D. Chen, A.-J. Avestro, Z. Chen, J. Sun, S. Wang, M. Xiao, Z. M. Algaradah, M. S. Nassar, K. Amine, Y. Meng, J. F. Stoddart, *Adv. Mater.* **2015**, *27*, 2907–2912.
 [37] S. K. M. Nalluri, Z. Liu, Y. Wu, K. R. Hermann, A. Kim, D. J. M. D. Krzyaniak, M. R. Wasielewski, J. F. Stoddart, *J. Am. Chem. Soc.* **2016**, *138*, 5968–5977.

Manuscript received: January 21, 2020

Revised manuscript received: February 13, 2020

Accepted manuscript online: February 14, 2020

Erratum